

CONTENTS

<p><b>S. Maneein, J.J. Milledge, P.J. Harvey and B.V. Nielsen</b> Methane production from <i>Sargassum muticum</i>: effects of seasonality and of freshwater washes</p>	<p>235</p>	<p><b>E. Bellos and C. Tzivanidis</b> Parametric analysis of a solar-driven trigeneration system with an organic Rankine cycle and a vapor compression cycle</p>	<p>278</p>
<p><b>V. Prakash, K.C. Sharma and R. Bhakar</b> Optimal generation mix for frequency response adequacy in future power system</p>	<p>243</p>	<p><b>C. Camarasa, L.K. Kalahasthi and L. Rosado</b> Drivers and barriers to energy-efficient technologies (EETs) in EU residential buildings</p>	<p>290</p>
<p><b>M. Hu, Suhendri, B. Zhao, X. Ao, J. Cao, Q. Wang, S. Riffat, Y. Su and G. Pei</b> Effect of the spectrally selective features of the cover and emitter combination on radiative cooling performance</p>	<p>251</p>	<p><b>W.P. Akanmu, S.S. Nunayon and U.C. Eboson</b> Indoor environmental quality (IEQ) assessment of Nigerian university libraries: A pilot study</p>	<p>302</p>
<p><b>B. Yang, X. Ding, F. Wang and A. Li</b> A review of intensified conditioning of personal micro-environments: Moving closer to the human body</p>	<p>260</p>	<p><b>A.M. Mohammed, A. Elnokaly and A.M.M. Aly</b> Empirical investigation to explore potential gains from the amalgamation of phase changing materials (PCMs) and wood shavings</p>	<p>315</p>
<p><b>A.K. Pandey, M. George, N.A. Rahim, V.V. Tyagi, S. Shahabuddin and R. Saidur</b> Preparation, characterization and thermophysical properties investigation of A70/polyaniline nanocomposite phase change material for medium temperature solar applications</p>	<p>271</p>	<p><b>Y. Huang, S. Wang, Y. Ji and Z. Liu</b> Study of the automotive aerodynamic performance affected by entrance structure of forecabin</p>	<p>327</p>

INDEXED/ABSTRACTED IN:  
 Energy and Built Environment, Compendex, Architectural Periodicals Index, Cambridge Scientific Abstracts, Current Contents - Engineering, Technology & Applied Sciences, Current Energy Information, Energy Abstracts, EIC/Intelligence (Energy Index), Environmental Periodicals Bibliography, Focus On: Global Change, Fuel and Energy Abstracts, Scopus, Science Citation Index Expanded, INSPEC, Also covered in the abstract and citation database SCOPUS®. Full text available on ScienceDirect®.



2666-1233(202106)2:3;1-A

ISSN 2666-1233

# Energy and Built Environment

Volume 2 • Issue 3 • July 2021



ScienceDirect

Available online at [www.sciencedirect.com](http://www.sciencedirect.com)

## Aims and Scope:

*Energy and Built Environment* (EBE) is an international journal disseminating original research articles on energy harvest and utilization in built environment. The aim is to present new research results focused on promoting energy efficiency, clean energy utilization, and environment quality in built environment related to buildings and transportation.

We encourage submissions in the following areas

- Energy conservation and balances in built environment

- Energy storage technologies and their applications in built environment
- Application and integration of renewable energy technologies in built environment
- Evaluation and control of indoor environment quality (acoustic, visual, thermal and air quality)
- Impact of climate change on built environment performance
- Modelling and prediction technologies for built environment

## Energy and Built Environment

---

### Editors-in-Chief

#### Yanping Yuan

Southwest Jiaotong University, China

### Editorial Board

#### Alireza Afshari

University of Aalborg, Denmark

#### Patrice Blondeau

La Rochele University, France

#### Maher Chaabene

Digital Reasearch Center of Sfax, Tunis

#### Haisheng Chen

Institute of Engineering Thermophysics, Chinese Academy of Sciences, China

#### YanJun Dai

Shanghai Jiao Tong University, China

#### Claudio Del Pero

Politecnico Di Milano, Italy

#### Yulong Ding

University of Birmingham, UK

#### Mohamed El Mankibi

University of Lyon, France

#### Weijun Gao

The University of Kitakyushu, Japan; Qingdao University of Technology, China

#### Jun Gao

Tongji University, China

#### Karel Kabele

Czech Technical University, Czech Republic

#### Risto Kosonen

Aalto University, Finland

#### Mingjia Li

Xi'an Jiaotong University, China

#### Zhiwei Lian

Shanghai Jiao Tong University, China

#### Xiaohua Liu

Tsinghua University, China

#### Lin Lu

Hong Kong Polytechnic University, China

#### Isaac A. Meir

Ben-Gurion University of the Negev, Israel

#### Tingzhen Ming

Wuhan University of Technology, China

### Assistant Editors

#### Zhengtao Ai

Hunan University, China

#### Xiaoling Cao

Southwest Jiaotong University, China

#### Wenhui Ji

Southwest Jiaotong University, China

#### Fariborz Haghighat

Concordia University, Canada

#### Jinhan Mo

Tsinghua University, China

#### Fuzhan Nasiri

Concordia University, Canada

#### Meng Ni

Hong Kong Polytechnic University, China

#### Halime Paksoy

Cukurova University, Turkey

#### Jinqing Peng

Hunan University, China

#### Marco Perino

Politecnico di Torino, Italy

#### Dusan Petras

Slovak University of Technology in Bratislava, Slovakia

#### Saffa B. Riffat

The University of Nottingham, United Kingdom

#### Zhe Tian

Tianjin University, China

#### Jun Wang

Beihang University, China

#### Yi Wang

Xi'an University of Architecture and Technology, China

#### Kwang Woo Kim

Seoul National University, South Korea

#### Da Yan

Tsinghua University, China

#### Hiroshi Yoshino

Tohoku University, Japan; Tsinghua University, China

#### Zhiqiang Zhai

University of Colorado, United States

#### Dan Zhao

the University of Canterbury, New Zealand

#### Xudong Zhao

University of Hull, United Kingdom

#### Yang Zhao

Zhejiang University, China

#### Wei Wu

City University of Hong Kong, China

#### JinZhi Zhou

Southwest Jiaotong University, China

# Energy and Built Environment

Volume 2 (2021)



ELSEVIER

Amsterdam • Boston • London • New York • Oxford • Paris • Philadelphia • San Diego • St Louis

# Energy and Built Environment

---

## Editors-in-Chief

### Yanping Yuan

Southwest Jiaotong University, China

### Fariborz Haghighat

Concordia University, Canada

## Editorial Board

### Alireza Afshari

University of Aalborg, Denmark

### Patrice Blondeau

La Rochele University, France

### Maher Chaabene

Digital Reasearch Center of Sfax, Tunis

### Haisheng Chen

Institute of Engineering Thermophysics, Chinese Academy of Sciences, China

### Yanjun Dai

Shanghai Jiao Tong University, China

### Claudio Del Pero

Politecnico Di Milano, Italy

### Yulong Ding

University of Birmingham, UK

### Mohamed El Mankibi

University of Lyon, France

### Weijun Gao

The University of Kitakyushu, Japan; Qingdao University of Technology, China

### Jun Gao

Tongji University, China

### Karel Kabele

Czech Technical University, Czech Republic

### Risto Kosonen

Aalto University, Finland

### Mingjia Li

Xi'an Jiaotong University, China

### Zhiwei Lian

Shanghai Jiao Tong University, China

### Xiaohua Liu

Tsinghua University, China

### Lin Lu

Hong Kong Polytechnic University, China

### Isaac A. Meir

Ben-Gurion University of the Negev, Israel

### Tingzhen Ming

Wuhan University of Technology, China

## Assistant Editors

### Zhengtao Ai

Hunan University, China

### Xiaoling Cao

Southwest Jiaotong University, China

### Wenhui Ji

Southwest Jiaotong University, China

### Jinhan Mo

Tsinghua University, China

### Fuzhan Nasiri

Concordia University, Canada

### Meng Ni

Hong Kong Polytechnic University, China

### Halime Paksoy

Cukurova University, Turkey

### Jinqing Peng

Hunan University, China

### Marco Perino

Politecnico di Torino, Italy

### Dusan Petras

Slovak University of Technology in Bratislava, Slovakia

### Saffa B. Riffat

The University of Nottingham, United Kingdom

### Zhe Tian

Tianjin University, China

### Jun Wang

Beihang University, China

### Yi Wang

Xi'an University of Architecture and Technology, China

### Kwang Woo Kim

Seoul National University, South Korea

### Da Yan

Tsinghua University, China

### Hiroshi Yoshino

Tohoku University, Japan; Tsinghua University, China

### Zhiqiang Zhai

University of Colorado, United States

### Dan Zhao

the University of Canterbury, New Zealand

### Xudong Zhao

University of Hull, United Kingdom

### Yang Zhao

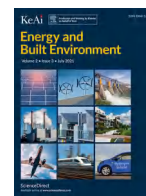
Zhejiang University, China

### Wei Wu

City University of Hong Kong, China

### Jinzhi Zhou

Southwest Jiaotong University, China



## Methane production from *Sargassum muticum*: effects of seasonality and of freshwater washes

Supattra Maneein\*, John J. Milledge, Patricia J. Harvey, Birthe V. Nielsen

Algae Biotechnology, University of Greenwich, Chatham Maritime, ME4 4TB, UK

### ARTICLE INFO

#### Keywords:

Seaweed  
Biogas  
Biofuels  
Seasonality  
Washing

### ABSTRACT

Biogas production from *Sargassum muticum*, an invasive seaweed species to Europe, is hampered by low methane (CH<sub>4</sub>) yields during anaerobic digestion (AD), but causes are unclear. This research is the first to demonstrate the impact of extensive freshwater washing of spring- and summer-harvested *S. muticum* on the CH<sub>4</sub> production rates and the biochemical methane potential (BMP). The findings reveal that the rate profile of CH<sub>4</sub> production is affected by extensively washing the seaweed and is dependent on seasonality. Spring-harvested *S. muticum* had higher initial CH<sub>4</sub> production rates compared to summer-harvested *S. muticum*. For spring-harvested *S. muticum*, the initial rate of CH<sub>4</sub> production was lowered by extensive washing. In contrast, extensively washed summer-harvested *S. muticum* had a higher degradation rate and CH<sub>4</sub> production rate relative to its non-extensively washed counterpart. The highest CH<sub>4</sub> potentials accumulated by the treated and non-treated *S. muticum* are, however, statistically similar and not influenced by seasonality or extensive washing ( $p > 0.05$ ). Potential causes for differences in the rate of CH<sub>4</sub> production between summer- and spring-harvested *S. muticum* are discussed. The differences in CH<sub>4</sub> production from treated summer- and spring-harvested *S. muticum* acts as a stepping stone to understanding the causes for low CH<sub>4</sub> yields, which could allow for further enhancements in CH<sub>4</sub> production from *S. muticum*.

### 1. Introduction

*Sargassum muticum* is a brown seaweed species that is invasive to Europe and poses economic and environmental challenges [1]. Seaweeds are known to contain substances that can serve as high-value products, such as polysaccharides and polyphenols with pharmacological value, as well as possessing biofuel production potential [2,3]. Hence, the valorisation of this seaweed could have positive implications.

Anaerobic digestion (AD) for biofuel production is a versatile and suitable method of obtaining biofuels from wet biomass such as seaweed [1]. However, methane (CH<sub>4</sub>) yields currently obtained from *S. muticum* are ~17% of the theoretical CH<sub>4</sub> yield [1]. This could be due to the recalcitrance of seaweed to hydrolysis during AD and/or possible inhibitors of AD present in seaweed, including high polyphenol, protein, and sulphur contents; the removal of these components was associated with increased CH<sub>4</sub> yields [4,5].

Several pre-treatment methods have been employed to enhance CH<sub>4</sub> production yields from different types of seaweeds [6]. Washing seaweeds prior to AD showed mixed results: an increase in CH<sub>4</sub> production was recorded for washed *Gracilaria vermiculophylla* and *Laminaria*

*digitata* relative to the unwashed counterpart [7,8]; no significant difference was shown in CH<sub>4</sub> yields after washing *S. muticum* [9]; while lower volumes of CH<sub>4</sub> were produced during the AD of washed and macerated *Ulva lactuca* compared to its unwashed and macerated counterpart [10]. Reasons for enhancements in CH<sub>4</sub> yields were associated with a reduction in salt content [8]. The authors also suggested that removing potential AD inhibitors, such as polyphenols and epiphytes with antimicrobial activity, could contribute to increases in CH<sub>4</sub> yields [8]. However, the reasons for differences in the effect of washing on CH<sub>4</sub> yield between different seaweed types are not fully understood, and the removal of components other than salts has not been shown.

This study explores the effect of removing water-soluble components from *S. muticum* on CH<sub>4</sub> production by AD. Rather than rinsing as achieved by previous authors, the effects of sequentially washing freeze-dried seaweed, referred to as extensive washing, was investigated. Sequential extraction was shown to extract higher yields, and potentially more novel compounds, otherwise not extracted by single extractions [11,12]. Sequentially washing the seaweed, therefore, attempts to remove as many water-soluble components as possible while minimising energy costs associated with heating or continuous stirring; thereby, po-

**Abbreviations:** AD, Anaerobic digestion; AMPTS II, Automatic Methane Potential Test System II; BMP, Biochemical methane potential; C: N ratio, Carbon-to-nitrogen ratio; DW, Dry weight; FD, Freeze-dried; VS, Volatile solids; WW, Wet weight.

\* Corresponding author.

E-mail address: [sm8149w@gre.ac.uk](mailto:sm8149w@gre.ac.uk) (S. Maneein).

<https://doi.org/10.1016/j.enbenv.2020.06.011>

Available online 6 July 2020

2666-1233/Copyright © 2020 Southwest Jiatong University. Publishing services by Elsevier B.V. on behalf of KeAi Communication Co. Ltd. This is an open access article under the CC BY-NC-ND license (<http://creativecommons.org/licenses/by-nc-nd/4.0/>)

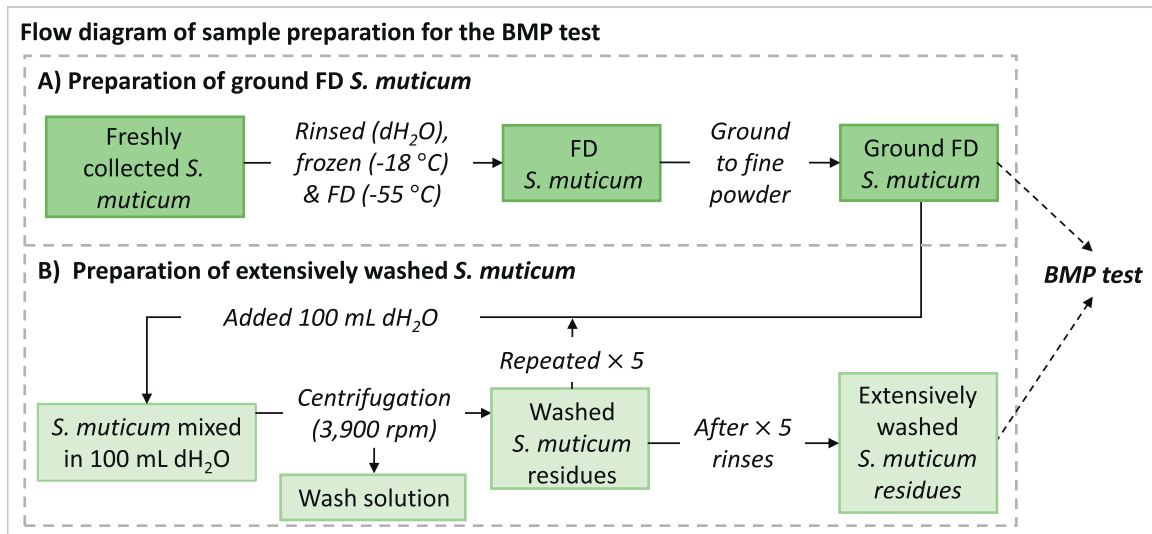


Fig. 1. Methodology for the preparation of ground freeze-dried (FD) *S. muticum* and extensively washed *S. muticum* residues. Biochemical methane potential (BMP) test was performed on the samples to determine the CH<sub>4</sub> production profile and yield.

tentially maximising net energy production from the CH<sub>4</sub> produced. To the authors' knowledge, this study is the first to evaluate the impact of removing water-soluble components from ground, freeze-dried, *S. muticum* collected in two seasons (spring- and summer-collected) on CH<sub>4</sub> yields. The recovery of high-value products (polyphenolics) in the water-soluble fraction is also demonstrated. It may increase the economic viability of this process in a biorefinery approach, with water being an ideal solvent for food-grade purposes [13,14].

## 2. Experimental method

### 2.1. Seaweed collection and treatment

Spring *S. muticum* was collected from the Coast in April 2018 (Ramsgate, UK; TR372640) and summer *S. muticum* was collected in July 2018 (Broadstairs, UK; TR399675). Freshly collected samples were treated according to Fig. 1. Samples of *S. muticum* from both seasons were lightly washed, herein referred to as rinsed, with deionised water (dH<sub>2</sub>O) to remove sand and any residues from the seawater, stored at  $-18^{\circ}\text{C}$ , and freeze-dried (FD) ( $-55^{\circ}\text{C}$ , 48 h).

FD samples were ground (Lloytron®, Kitchen Perfected coffee grinder) to a fine powder. 10 g of ground, FD summer and spring *S. muticum* was mixed in 100 mL deionised water (dH<sub>2</sub>O) and centrifuged (Eppendorf, Centrifuge 5810R) (3900 rpm, 20 min). The procedure was repeated on the remaining residues five times to ensure a thorough wash. The residues herein are referred to as extensively washed or washed spring and summer *S. muticum*, and their properties were compared with FD samples that were not extensively washed. These latter samples are referred to as FD samples.

### 2.2. Biochemical methane potential (BMP) determination

The inoculum was collected from an anaerobic digester treating paper-making waste at Smurfit Kappa Townsend Hook Paper Makers, Kent, United Kingdom. The inoculum was 'degassed' in a water bath ( $37^{\circ}\text{C}$ , 7 days) to minimise its contribution to the CH<sub>4</sub> yields during the BMP test [15], and then homogenised using a handheld blender (Philips™) before use.

The Automatic Methane Potential Test System II (AMPTS II, Bioprocess Control Sweden AB) was used to measure CH<sub>4</sub> production. This system contains fifteen 500 mL reactors in a temperature-controlled water bath, each with a CO<sub>2</sub> capturing unit using 3 M sodium hydroxide,

and a gas measuring device. Three replicates were made containing 1 g volatile solids (VS) content of each biomass type (FD summer, washed summer, FD spring, and washed spring *S. muticum*). Inoculum was added to make an inoculum-to-substrate ratio of 5, and made up with water to 400 g. Blanks with only inoculum and water were made to calculate the net CH<sub>4</sub> production from the *S. muticum* biomass, removing the CH<sub>4</sub> contribution by the inoculum. Reactors were mixed continuously at 75% power (150 rpm) and incubated at  $37^{\circ}\text{C}$ . CH<sub>4</sub> volumes were recorded daily over 36 days and corrected for water vapour, temperature ( $0^{\circ}\text{C}$ ), and pressure (101.325 kPa).

### 2.3. Dry weight and ash content

All biomass types were dried in a vacuum oven at  $105^{\circ}\text{C}$  overnight to determine its dry weight (DW) and moisture content (wet weight (WW)) [16]. Ash and VS content were determined using the muffle furnace at  $250^{\circ}\text{C}$  for 1 h, followed by  $550^{\circ}\text{C}$  for 2 h [17].

### 2.4. CHNS analysis

Flash dynamic combustion (Flash EA1112 CHNS Elemental Analyser, Thermo Scientific) was used to determine the proportion of carbon, nitrogen, hydrogen, and sulphur in the freeze-dried samples. Sulphanilamide was used as the standard. The means of a minimum of duplicates are reported. As drying may affect the elemental composition of the samples, values were adjusted for moisture content rather than oven drying before the analysis. Oxygen content was calculated by difference.

The empirical formula, derived from the elemental analysis, was used in the Buswell equation to calculate the maximum theoretical CH<sub>4</sub> yield for each biomass type [18]. The biodegradability index, expressed as a percentage, was calculated by dividing the highest net cumulative CH<sub>4</sub> yield after 36 days of each biomass by its theoretical yield [19].

### 2.5. Total polyphenolic content

Polyphenolic extraction and quantification were performed on all samples in triplicates using 30% aqueous EtOH as the extracting solvent (solid-solvent ratio of 1: 200) [20]. Extracts were incubated in a shaking incubator (New Brunswick Scientific, Innova® 43) (250 rpm, 1 h,  $40^{\circ}\text{C}$ ), then centrifuged ( $21,000 \times g$ ,  $4^{\circ}\text{C}$ , 20 min). Once the supernatants were collected, the process was repeated on the pellets (obtained from the centrifugation process) three times.

Polyphenolic quantification was conducted according to a modified protocol of the Folin–Ciocalteu (FC) method performed at room temperature [21], using 2 min incubation of FC reagent rather than 1 min. The absorbance was measured at 750 nm in a UV–visible spectrophotometer (Jenway 6305). Phloroglucinol was used as the standard to generate a calibration curve to determine the polyphenolic concentration, reporting total polyphenolic content as a percentage DW of the samples.

## 2.6. Total protein content of residues

Protein quantification using the Lowry method overestimated protein content more than those calculated using the nitrogen-to-protein factor of 4.56 (found by Angell et al. (2016) [22]) for brown seaweeds (unpublished data). Therefore, protein content was calculated by multiplying the nitrogen content by 4.56.

## 2.7. Data analysis

### 2.7.1. Mass balance for specific CH<sub>4</sub> yield calculation

The mass of the washed residues were calculated by the difference in the DW mass of the FD samples and the DW mass of the dried wash solutions (Fig. 1B). DW of the rinsed freshly collected spring and summer *S. muticum* samples (not freeze-dried) and of the aliquots of the wash solutions were dried and ashed according to Section 2.3. The total DW yield of the wash solution was calculated using the total volume of the wash solution.

### 2.7.2. Analysis of process dynamics

Analysis of the process dynamics during AD was conducted to elucidate differences in the biodegradability of the substrate as well as its rate [23]. IBM SPSS version 25 was used to model the second-order kinetics (the modified Gompertz equation) (Eq. 1) to the net cumulative CH<sub>4</sub> production obtained from summer samples, while first-order kinetics (Eq. 2) was used for the spring samples [24,25]. FD spring samples appeared to produce CH<sub>4</sub> in two phases (from days 1 to 10 (P1) and days 11 to 36 (P2)) and were modelled separately. P1 was modelled using first-order kinetics while P2 was modelled using the second-order kinetics. Two models were used due to the better fit of the models to the net cumulative CH<sub>4</sub> production results. Lower residual sum of squared errors and R<sup>2</sup> values closer to 1 (indicating the fit of the model) were found when using the respective models for the net cumulative CH<sub>4</sub> production from the two different seasons and for P2. Except for P2 of the FD spring samples (R<sup>2</sup> = 0.953), R<sup>2</sup> values for all other models were > 0.99. This indicates a good fit of the model to the net cumulative CH<sub>4</sub> production (R<sup>2</sup> > 0.95) [23]. First-order kinetics (Microsoft Excel (2016)) was then used to illustrate differences in the decay constant (*k*), or hydrolysis rate, of the substrates using the values obtained from the modelling.

$$M(t) = M_0 \times \exp\left\{-\exp\left[\frac{R_{\max} \times e}{M_0}(\Delta - t) + 1\right]\right\} \quad (1)$$

$$Y(t) = Y_m \times (1 - \exp^{-kt}) \quad (2)$$

where *M(t)* and *Y(t)* is the net cumulative CH<sub>4</sub> yield (mL CH<sub>4</sub> g<sup>-1</sup> VS) at time *t* (day), *Y<sub>m</sub>* and *M<sub>0</sub>* is the maximum CH<sub>4</sub> potential (mL CH<sub>4</sub> g<sup>-1</sup> VS), *k* is the decay constant (day<sup>-1</sup>) which represents the degradation rate of the substrates, *R<sub>max</sub>* is the maximum CH<sub>4</sub> production rate (mL CH<sub>4</sub> g<sup>-1</sup> VS day<sup>-1</sup>), *e* is 2.71828,  $\Delta$  is the lag phase (days) which indicates the number of days before significant CH<sub>4</sub> production starts [24].

### 2.7.3. Statistical analysis

Excel (2016) was used for student's t-test, and IBM SPSS version 25 was used for one-way, two-way and three-way ANOVA analysis. Statistical significance was determined by *p* < 0.05. Dependent variable: cumulative CH<sub>4</sub> yield. Independent variables: treatment (washed, FD samples), season (spring, summer), day (time after incubation).

## 3. Results and discussion

### 3.1. Effect of washing on the composition of *S. muticum*

An increase in the relative carbon content by 11.2% and 7.1%, with a concurrent reduction in the relative nitrogen and sulphur content, is evident in the extensively washed spring and summer seaweeds compared to FD seaweeds, respectively (Table 1). In contrast, a reduction in the relative carbon content and an increase in the relative nitrogen and sulphur content was revealed when wet, whole *S. muticum* biomass was washed lightly for 30 s [8].

Washing of *S. muticum* significantly reduced the relative ash content (*p* < 0.05) (Table 2). Summer- and spring- washed *S. muticum* showed a 48.7% and 53.9% ash reduction relative to their unwashed counterparts, respectively. This resulted in a higher VS content, commensurate with an increase in the content of the organic fraction of washed *S. muticum*. The ash-to-VS ratio (A: V ratio), which at high ratios can have inhibitory effects on AD [8], was 55.5% and 62.2% lower in washed summer and spring samples relative to the FD counterparts, respectively.

Other potential inhibitors of AD highlighted in literature are high protein and polyphenolic contents. Proteins were more easily removed by washing from spring samples compared to summer *S. muticum* (Table 2). Protein content in washed spring samples was reduced by 1.4% DW relative to FD spring samples, whereas only 0.5% DW appeared to be removed from FD summer seaweed after washing. Polyphenolic content of FD samples measured in this study was in the range of polyphenolic content reported for *S. muticum* (0.66–4.28% DW) [26]. FD samples of spring *S. muticum* have significantly lower polyphenolic content (2.18% DW lower) relative to FD summer samples (*p* < 0.05), and their polyphenolic content was reduced by 45% after washing. Polyphenolic content in washed summer samples was 80.5% lower compared to FD summer samples. Water has been shown to be capable of removing up to 2.7% DW polyphenolic content from *S. siliquastrum* [27].

### 3.2. Effect of season and extensive washing on CH<sub>4</sub> yield

The highest CH<sub>4</sub> yields recorded after 36 days (BMP test) were 128.2 and 139.7 mL CH<sub>4</sub> g<sup>-1</sup> VS for FD summer- and spring-harvested *S. muticum*, respectively (Table 3). These values are in the range similar to those reported in literature for *S. muticum* (100–177 mL CH<sub>4</sub> g<sup>-1</sup> VS) [1,9,28]. Other studies have measured CH<sub>4</sub> yields of *Sargassum* as high as 380 mL CH<sub>4</sub> g<sup>-1</sup> VS [29].

Net CH<sub>4</sub> yields produced from extensively washed spring and summer samples were not statistically different to FD spring and FD summer *S. muticum* (one-way ANOVA, *p* > 0.05). Notably, FD *S. muticum* had a significantly higher variance relative to the washed summer *S. muticum*. These results suggest that the net yield of CH<sub>4</sub> accumulated by day 36 of the BMP test was not significantly impacted by the harvesting season or by extensively washing the seaweed. This is in contrast to variations in CH<sub>4</sub> yields between spring- and summer-collected *Laminaria digitata* and *Ascophyllum nodosum* [4,25,30]. However, the existence of this variation also appears to be dependent on the location of harvest [31].

The biodegradability index is used to express the degradability or the efficiency of the bioconversion of the biomass to CH<sub>4</sub> [8]. The biodegradability indices of FD *S. muticum* samples (Table 3) measured in this study were in the range of those measured during the BMP tests for *A. nodosum* (16–46%) [4] and *Sargassum* spp. (17–37%) [32], but lower than those measured in other brown seaweeds such as *L. digitata* (44–72%) [25].

Although not statistically significant, FD samples of summer *S. muticum* showed a lower degradability of 7.6% and 10.9% compared to FD spring *S. muticum* and washed summer samples, respectively (*p* > 0.05) (Table 3). Similarly, the biodegradability index was not significantly impacted by washing for spring samples (difference of 0.5%) (*p* > 0.05), despite the higher relative carbon content (Table 1).

**Table 1**  
Elemental composition expressed as a percentage of DW, and the carbon-to-nitrogen ratio in FD and extensively washed spring and summer *S. muticum*

Residue type (Empirical formula)	% Composition DW					
	C	H	N	O	S	C: N ratio
FD Summer (C <sub>12.9</sub> H <sub>25.0</sub> O <sub>8.8</sub> NS <sub>0.1</sub> )	33.3	5.4	3.0	30.2	0.6	11.1
Summer washed (C <sub>16.3</sub> H <sub>27.2</sub> O <sub>11.4</sub> N)*	40.4	5.6	2.9	37.8	0.2	13.9
FD Spring (C <sub>8.4</sub> H <sub>5.1</sub> O <sub>6.7</sub> NS <sub>0.1</sub> )	30.4	5.1	4.2	32.3	0.5	7.2
Spring washed (C <sub>12.5</sub> H <sub>22.3</sub> O <sub>8.1</sub> N)*	41.6	6.2	3.9	35.9	0.1	10.7

\* Sulphur content in the empirical formula is negligible for the washed summer (S<sub>0.02</sub>) and washed spring (S<sub>0.008</sub>) *S. muticum*.

**Table 2**  
Proximate composition (dry weight, VS and ash content), A: V ratio, protein and polyphenolic content of FD and extensively washed spring and summer *S. muticum*

	% DW (n = 3)	% VS of DW (n = 3)	% Ash of DW (n = 3)	A: V ratio	Protein content (% of DW)	Polyphenolic content (% of DW) (n = 3)
FD Summer	89.1 ± 0.0	73.5 ± 0.7	26.5 ± 0.7	0.36	13.7	2.98 ± 0.13
Summer Washed	12.2 ± 0.1	86.4 ± 0.4	13.6 ± 0.4	0.16	13.2	0.58 ± 0.01
FD Spring	92.6 ± 0.1	73.1 ± 0.0	26.9 ± 0.0	0.37	19.2	0.80 ± 0.00
Spring Washed	11.2 ± 0.4	87.6 ± 0.3	12.4 ± 0.3	0.14	17.8	0.44 ± 0.02

**Table 3**  
Highest net cumulative CH<sub>4</sub> yield after 36 days, theoretical yield, biodegradability index (BI), and specific CH<sub>4</sub> yield of FD and extensively washed spring and summer *S. muticum*

	Net CH <sub>4</sub> Yield (mL CH <sub>4</sub> g <sup>-1</sup> VS) (n = 3)	Theoretical yield (mL CH <sub>4</sub> g <sup>-1</sup> VS)	BI (%)	Specific CH <sub>4</sub> yield (L CH <sub>4</sub> kg <sup>-1</sup> WW)
FD Summer	128.2 ± 43.3	463.8	27.6	13.0
Summer Washed	170.7 ± 10.9	443.4	38.5	14.5
FD Spring	139.7 ± 39.0	397.0	35.2	19.7
Spring Washed	163.2 ± 25.6	470.2	34.7	16.1

Statistical similarities in the biodegradability and net CH<sub>4</sub> yield after 36 days for the samples do not reflect the differences in the elemental composition between summer and spring *S. muticum* samples ( $p > 0.05$ ) (Table 1). The C: N ratio of FD and washed summer samples (Table 1), which had a C: N ratio closer to those deemed optimal in the literature (20–30) or 14 for kelp [33,34], would otherwise suggest a higher biodegradability index and CH<sub>4</sub> yield compared to FD and washed spring samples. Additionally, A: V ratios were more than halved by extensively washing samples for both seasons (Table 2), yet CH<sub>4</sub> yields were statistically similar to the FD samples ( $p > 0.05$ ).

Although high sulphur content was suggested to negatively impact CH<sub>4</sub> yields, a difference of 0.1% DW in the sulphur content between the two seasons (Table 1), and the negligible sulphur contents in the washed samples suggest that sulphur content is unlikely to play a significant role on the biodegradability in this experiment. Additionally, these results suggest that differences in protein content of 5.5% DW between the FD summer and spring samples (Table 2) have little influence on the final CH<sub>4</sub> yield of the BMP test for *S. muticum*.

### 3.3. Effect of extensive washing on specific CH<sub>4</sub> yield

The specific CH<sub>4</sub> yield could aid in the identification of the suitable harvesting season and the evaluation of the effectiveness of washing seaweed biomass for CH<sub>4</sub> production, as it also takes into account the moisture content and the influence of washing on VS content. Fig. 2 shows the mass of the VS and ash content of the washed and FD spring and summer *S. muticum* that would be added to an AD reactor if 1 kg wet-weight of *S. muticum* was processed in the manner described in Fig. 1.

Despite similar net yields of CH<sub>4</sub> accumulated by day 36, the specific CH<sub>4</sub> yields suggest that washing is unsuitable for spring samples as washed spring-harvested samples showed a lower specific CH<sub>4</sub> yield

of 3.6 L CH<sub>4</sub> kg<sup>-1</sup> WW relative to the FD spring samples (Table 3). This could be related to the lower VS content of 42.4 g in washed residues relative to FD spring samples (Fig. 2). Nevertheless, both FD and washed spring samples have higher specific CH<sub>4</sub> yields compared to FD and washed summer samples (Table 3), suggesting that spring-collected samples could be more suitable for CH<sub>4</sub> production than the summer-collected samples.

Washed summer samples produced a specific CH<sub>4</sub> yield of 1.5 L CH<sub>4</sub> kg<sup>-1</sup> WW higher than FD summer samples despite the removal of 16.8 g VS from FD summer samples (Table 3, Fig. 2). This suggests the suitability of the summer samples for CH<sub>4</sub> production could be enhanced by washing.

### 3.4. Effect of season on rate of CH<sub>4</sub> production

The profiles for the rate of CH<sub>4</sub> production for each season were significantly different ( $p < 0.05$  for a two-way ANOVA between seasonality and days after incubation) even though the net yields of CH<sub>4</sub> accumulated by day 36 were similar for FD spring- and summer-harvested samples, and similar for extensively washed spring- and summer-harvested samples (see Table 3). FD spring-harvested *S. muticum* showed a rapid increase in CH<sub>4</sub> production, producing up to 80.6 mL CH<sub>4</sub> g<sup>-1</sup> VS in the first 3 days. By comparison, FD summer-harvested samples showed a net reduction in CH<sub>4</sub> production from days 2 to 6; net positive CH<sub>4</sub> production started only after day 6. A significant lag in CH<sub>4</sub> production of ca. 6 days was observed for washed summer-harvested *S. muticum* samples, whereas no such lag was observed for washed spring-harvested samples (Fig. 3).

The rapid increase in CH<sub>4</sub> production from FD spring samples could be partially related to higher availability of readily degradable substrates that are easily converted to CH<sub>4</sub>, such as mannitol [35]. Younger

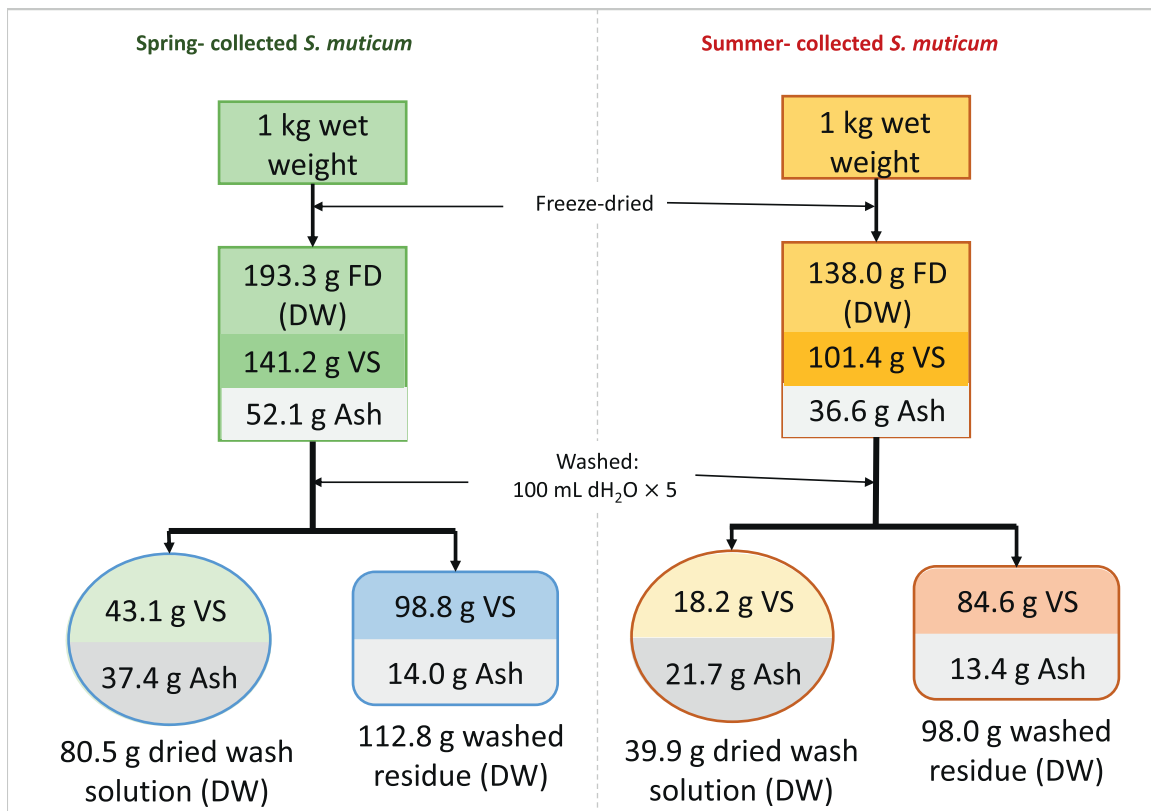


**Fig. 2.** Mass balance of VS and ash content in the FD samples, dried wash solutions, and washed residues following the washing process (Fig. 1) of spring- and summer-collected seaweed.

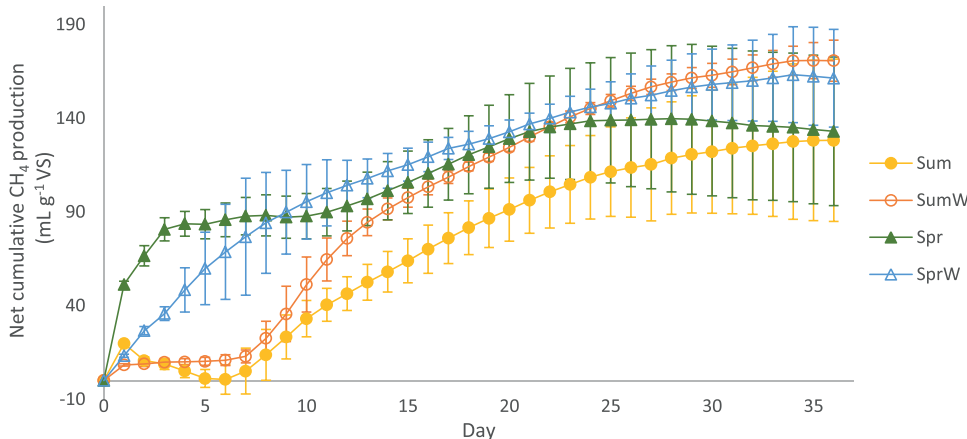


**Fig. 3.** Net cumulative CH<sub>4</sub> production of spring and summer FD and washed *S. muticum* over the BMP test (36 days). Error bars are standard deviations ( $n = 3$ ). Sum: Summer FD *S. muticum*; Spr: Spring FD *S. muticum*; SumW: Summer washed *S. muticum*; SprW: Spring washed *S. muticum*.

parts of *S. wightii* contain higher mannitol content compared to older parts of the thallus, which have higher contents of cellulose and hemicellulose that need to be hydrolysed before anaerobic metabolism to CH<sub>4</sub> [37]. However, it may also depend on the relative contents of polyphenolics: these were 3.8 fold higher in more mature summer FD samples compared to spring FD samples (Table 2). Tabassum *et al.* (2016) suggested high polyphenolic content as a significant factor in contributing to low CH<sub>4</sub> yields regardless of high carbohydrate content, low ash content and suitable C: N ratios [4]. Polyphenolic content was also indicated to inhibit methanogenesis and the hydrolysis of more complex substrates such as alginate, with a longer lag phase associated with high polyphenolic content [36].

Additionally, microorganisms within the inoculum need adaptation time to develop the mechanisms to hydrolyse the components of the seaweed. During AD of *L. saccharina*, alginate lyase activity was developed

to hydrolyse alginates after 3 days when the dissolved mannitol and laminaran content was depleted [37]. Hence, the initial spike in CH<sub>4</sub> production by FD summer samples on day 1 is likely to be due to the utilisation of readily degradable substrates. The requirement for adaptation of the microorganisms in the inoculum (more commonly exposed to cellulose from paper) to utilise the remaining substrates of seaweed may be the contributory factor in causing the delay in CH<sub>4</sub> production. Different sources of inoculum and the inoculum-to-substrate ratio was also indicated to impact the lag phases during AD [23,38].

### 3.5. Effect of extensive washing on CH<sub>4</sub> production

A three-way ANOVA showed that washing has a significant effect on CH<sub>4</sub> production ( $p < 0.05$ ). Additionally, the effects of washing on CH<sub>4</sub> production is significantly influenced by seasonality shown by the sig-

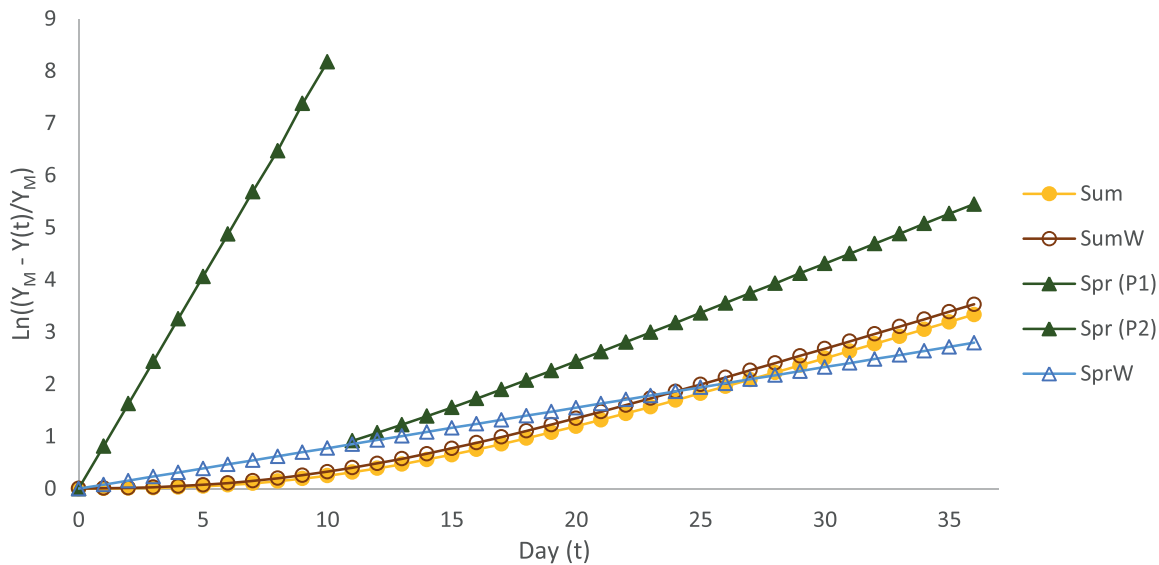


Fig. 4. First-order kinetics utilised to obtain the decay constant,  $k$ , determined from the slope of the curves. Sum: Summer FD *S. muticum*; Spr (P1, P2): Spring FD *S. muticum* (Phase 1 and 2); SumW: Summer washed *S. muticum*; SprW: Spring washed *S. muticum*.

nificant interaction between washing and season ( $p < 0.05$ ). In contrast to the net cumulative  $\text{CH}_4$  production from summer samples which were statistically influenced by washing ( $p < 0.05$ ), spring samples were not ( $p > 0.05$ ).

Washing of spring *S. muticum* did not show a statistically significant interaction between day, treatment and season on  $\text{CH}_4$  yields ( $p > 0.05$ ). Washed and FD spring *S. muticum* only showed statistical differences between days 1 and 4, with washed *S. muticum* having a mean yield of up to  $44.9 \text{ mL CH}_4 \text{ g}^{-1}$  VS lower than FD spring *S. muticum* within these days ( $p < 0.05$ ). This result coincides with those revealed by AD of freshwater washed *S. muticum*: lower initial rates of  $\text{CH}_4$  production in the initial stages of AD and no statistical difference in the final  $\text{CH}_4$  yield, relative to the unwashed seaweed, were found [9]. Hence, washing may remove soluble carbohydrates that are more readily converted to  $\text{CH}_4$  [9]. Significantly lower  $\text{CH}_4$  production of  $11.3 \text{ mL CH}_4 \text{ g}^{-1}$  VS by washed summer *S. muticum* on the first day relative to the FD summer samples ( $p < 0.05$ ) (Fig. 3) also supports this.

Washing of summer *S. muticum* showed a statistically significant interaction between day, treatment and season on  $\text{CH}_4$  yields in the three-way ANOVA ( $p < 0.05$ ). This statistical difference started from day 13 to the end of the BMP test (36 days), highlighting the importance of time required for substrate hydrolysis and their conversion to  $\text{CH}_4$ . Unlike FD summer samples, washed summer samples did not show a net reduction in  $\text{CH}_4$  production on days 2–6 relative to the inoculum control (Fig. 3). Differences in  $\text{CH}_4$  production per day between FD and washed summer *S. muticum* was statistically significant on days 2, 5, and 10–12, with washed summer *S. muticum* producing up to  $9.6 \text{ mL CH}_4 \text{ g}^{-1}$  VS higher than FD summer *S. muticum* ( $p < 0.05$ ) (data not shown). Hence, extensive washing may increase the bioconversion of summer *S. muticum* to  $\text{CH}_4$ .

Extensive washing may remove inhibitory compounds that limit the hydrolysis of substrates in summer *S. muticum*, where polyphenolic content was 80.5% lower in washed summer samples relative to FD summer samples (Table 2). Alternatively, scanning electron microscopy revealed that washing seaweed with water can erode seaweed surfaces [39]. Deionised water was also used for cell disruption of seaweed samples via osmotic shock [40,41]. Extensive washing may, therefore, modify the cell architecture of seaweed, increasing the surface area for hydrolysis, allowing for higher  $\text{CH}_4$  production rates. Hence, the removal of inhibitory compounds, the increase in surface area for hydrolysis, or the combination of these factors may be contributing to the lack of net re-

duction in  $\text{CH}_4$  production from days 2 to 6 and the higher  $\text{CH}_4$  production rates from washed summer *S. muticum* relative to the FD summer samples (Fig. 3).

### 3.6. Effect of extensive washing on process dynamics

Lag phases of FD and extensively washed summer samples, calculated by the modified Gompertz model, are 5.9 and 4.8 days, respectively. The non-linear decay constant of summer samples (Fig. 4) indicates a change in the degradation rate with time. Both of these substrates have the same maximum decay constant of  $0.14 \text{ day}^{-1}$ . The shape of the slopes, however, indicate that extensively washed summer samples have higher decay constants during the BMP test, with the highest difference of  $0.01 \text{ day}^{-1}$  between the two substrates, suggesting a higher overall degradation rate of extensively washed summer samples. This small difference could be related to the loss of readily utilisable substrates. The positive impacts of washing summer *S. muticum* are indicated by the shorter lag phase and higher degradation rate. These characteristics may make washed summer samples more suitable substrates for AD compared to FD summer samples [24].

The decay constant of FD and extensively washed summer samples are higher than extensively washed spring samples after days 12 and 11, respectively. Extensively washed spring samples have a decay constant of  $0.08 \text{ day}^{-1}$ . Comparatively, the biodegradation of FD spring samples appears to be biphasic; with a fast initial decay of substrates at a constant of  $0.81 \text{ day}^{-1}$  in the first 10 days, followed by a decay constant of  $0.18 \text{ day}^{-1}$  for the remainder of the BMP test. The higher degradation rate and the lack of lag phase indicate that its components are more easily digestible by microorganisms in the inoculum compared to the summer samples. The biphasic  $\text{CH}_4$  production has been attributed to potential inhibitors of AD and the presence of components with different degradation rates [42]. Overall, these results indicate the negative impact of extensively washing spring samples on its hydrolysis rate, and subsequently, on  $\text{CH}_4$  production.

Further biochemical analyses of the carbohydrate, fibre and lipid content of the biomass are required to fully understand the differences in  $\text{CH}_4$  production. This may also help to elucidate other methods that can be undertaken to further enhance  $\text{CH}_4$  yields and ultimately use *S. muticum* for biofuel production. As freshwater is a valuable resource, further optimisation steps to reduce the use of freshwater and techno-economic studies to evaluate whether the benefits from additional  $\text{CH}_4$

production outweighs the use of freshwater are needed. Additionally, analysis and identification of water-soluble compounds which may serve as potential valuable products from the wash solutions of summer seaweed may make this process more environmentally and economically viable.

#### 4. Conclusion

Washing of summer *S. muticum* increased its biodegradation rate during AD compared to the unwashed biomass. Differences in the response to washing were evident between spring- and summer-harvested *S. muticum*, both in terms of the initial rate of production and the degradation rates, indicating that seasonal variation in the biochemical composition of the seaweed has a significant impact on the bacterial digestion processes. The reasons for the differences in the rate of CH<sub>4</sub> production are not clear, but may reflect the relative availability of easily digested sugars and more complex substrates coupled to the requirement for a shift in bacterial population dynamics and/or induction of suitable enzyme systems. The potential removal of readily utilisable substrates may hinder other effects achieved by washing that may have beneficial impacts on CH<sub>4</sub> yields. The relative carbon content in *S. muticum* that are increased by washing, revealed through ultimate analysis, do not always translate to higher CH<sub>4</sub> yields. Further biochemical analyses are, therefore, required to comprehend differences in CH<sub>4</sub> production yields over the BMP test from summer and spring *S. muticum*. Additional CH<sub>4</sub> enhancements, process optimisations, and analysis of wash solutions from *S. muticum* are needed for a more environmentally and economically viable process to produce biogas from *S. muticum*.

#### Declaration of Competing Interest

The authors declare no conflict of interest.

#### CRedit authorship contribution statement

**Supattra Maneein:** Investigation, Methodology, Formal analysis, Writing - original draft. **John J. Milledge:** Resources, Supervision, Writing - review & editing. **Patricia J. Harvey:** Resources, Supervision, Writing - review & editing. **Birthe V. Nielsen:** Resources, Supervision, Writing - review & editing.

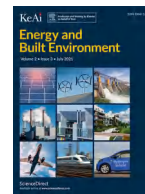
#### Acknowledgements

The author would like to acknowledge the financial support of the University of Greenwich and the Doctoral Training Alliance.

#### References

- J.J. Milledge, P.J. Harvey, Ensilage and anaerobic digestion of *Sargassum muticum*, *J. Appl. Phycol.* 28 (2016) 3021–3030, doi:10.1007/s10811-016-0804-9.
- C. Austin, D. Stewart, J.W. Allwood, G.J. McDougall, Extracts from the edible seaweed, *Ascophyllum nodosum*, inhibit lipase activity in vitro: contributions of phenolic and polysaccharide components, *Food Funct.* 9 (2018) 502–510, doi:10.1039/C7FO01690E.
- N. Wei, J. Quarterman, Y.-S.S. Jin, Marine macroalgae: an untapped resource for producing fuels and chemicals, *Trends Biotechnol.* 31 (2013) 70–77, doi:10.1016/j.tibtech.2012.10.009.
- M.R. Tabassum, A. Xia, J.D. Murphy, Seasonal variation of chemical composition and biomethane production from the brown seaweed *Ascophyllum nodosum*, *Bioresour. Technol.* 216 (2016) 219–226, doi:10.1016/j.biortech.2016.05.071.
- A. Mhatre, S. Gore, A. Mhatre, N. Trivedi, M. Sharma, R. Pandit, A. Anil, A. Lali, Effect of multiple product extractions on bio-methane potential of marine macrophytic green alga *Ulva lactuca*, *Renew. Energy.* 132 (2018) 742–751, doi:10.1016/j.renene.2018.08.012.
- S. Maneein, J.J. Milledge, B.V. Nielsen, P.J. Harvey, A review of seaweed pretreatment methods for enhanced biofuel production by anaerobic digestion or fermentation, *Fermentation* 4 (2018) 100, doi:10.3390/fermentation4040100.
- J.V. Oliveira, M.M. Alves, J.C. Costa, Design of experiments to assess pretreatment and co-digestion strategies that optimize biogas production from macroalgae *Gracilaria vermiculophylla*, *Bioresour. Technol.* 162 (2014) 323–330, doi:10.1016/j.biortech.2014.03.155.
- M.R. Tabassum, A. Xia, J.D. Murphy, Comparison of pre-treatments to reduce salinity and enhance biomethane yields of *Laminaria digitata* harvested in different seasons, *Energy* 140 (2017) 546–551, doi:10.1016/j.ENERGY.2017.08.070.
- J.J. Milledge, B.V. Nielsen, M.S. Sadek, P.J. Harvey, Effect of freshwater washing pretreatment on *Sargassum muticum* as a feedstock for biogas production, *Energies* 11 (2018) 1771, doi:10.3390/en11071771.
- A. Bruhn, J. Dahl, H.B. Nielsen, L. Nikolaisen, M.B. Rasmussen, S. Markager, B. Olesen, C. Arias, P.D. Jensen, Bioenergy potential of *Ulva lactuca*: biomass yield, methane production and combustion, *Bioresour. Technol.* 102 (2011) 2595–2604, doi:10.1016/J.BIORTECH.2010.10.010.
- R. Koivikko, J. Loponen, T. Honkanen, V. Jormalainen, Contents of soluble, cell-wall-bound and exuded phlorotannins in the Brown Alga *Fucus vesiculosus*, with implications on their ecological functions, *J. Chem. Ecol.* 31 (2005), doi:10.1007/s10886-005-0984-2.
- M.I. Errea, M.C. Matulewicz, Unusual structures in the polysaccharides from the red seaweed *Pterocladia capillacea* (Gelidiales, Gelidiales), *Carbohydr. Res.* 338 (2003) 943–953, doi:10.1016/S0008-6215(03)00037-5.
- R. Agregán, P.E.S. Munekata, D. Franco, R. Dominguez, J. Carballo, J.M. Lorenzo, Phenolic compounds from three brown seaweed species using LC-DAD-ESI-MS/MS, *Food Res. Int.* 99 (2017) 979–985, doi:10.1016/j.foodres.2017.03.043.
- Z. Rastani, M. Mehranian, F. Vahabzadeh, K. Sartavi, Antioxidant activity of brown algae *Sargassum vulgare* and *Sargassum angustifolium*, *J. Aquat. Food Prod. Technol.* 16 (2007) 17–26, doi:10.1300/J030v16n02\_03.
- I. Angelidaki, W. Sanders, Assessment of the anaerobic biodegradability of macropollutants, *Rev. Environ. Sci. Bio/Technol.* 3 (2004) 117–129, doi:10.1007/s11157-004-2502-3.
- BSI, Solid biofuels - Determination of moisture content - Oven dry method. Part 2: Total moisture - Simplified method, in: BS EN 14774-2:2009, BS EN 1477, BSI, UK, 2009.
- BSI, Solid biofuels - Determination of ash content, in: BS EN 14775:2009, BS EN 1477, UK, 2009.
- A.M. Buswell, H.F. Mueller, Mechanism of methane fermentation, *Ind. Eng. Chem.* 44 (1952) 550–552, doi:10.1021/ie50507a033.
- M.R. Tabassum, A. Xia, J.D. Murphy, Potential of seaweed as a feedstock for renewable gaseous fuel production in Ireland, *Renew. Sustain. Energy Rev.* 68 (2017) 136–146, doi:10.1016/J.RSER.2016.09.111.
- Y. Li, X. Fu, D. Duan, X. Liu, J. Xu, X. Gao, Y. Li, X. Fu, D. Duan, X. Liu, J. Xu, X. Gao, Extraction and identification of phlorotannins from the brown alga, *Sargassum fusiforme* (Harvey) Setchell, *Mar. Drugs* 15 (2017) 49, doi:10.3390/md15020049.
- P. Matanjun, S. Mohamed, N.M. Mustapha, K. Muhammad, C.H. Ming, Antioxidant activities and phenolics content of eight species of seaweeds from north Borneo, *J. Appl. Phycol.* 20 (2008) 367–373, doi:10.1007/s10811-007-9264-6.
- A.R. Angell, L. Mata, R. de Nys, N.A. Paul, The protein content of seaweeds: a universal nitrogen-to-protein conversion factor of five, *J. Appl. Phycol.* 28 (2016) 511–524, doi:10.1007/s10811-015-0650-1.
- E. Allen, D.M. Wall, C. Herrmann, A. Xia, J.D. Murphy, What is the gross energy yield of third generation gaseous biofuel sourced from seaweed? *Energy* 81 (2015) 352–360, doi:10.1016/J.ENERGY.2014.12.048.
- E. Allen, J. Browne, S. Hynes, J.D. Murphy, The potential of algae blooms to produce renewable gaseous fuel, *Waste Manag.* 33 (2013) 2425–2433, doi:10.1016/J.WASMAN.2013.06.017.
- M.R. Tabassum, A. Xia, J.D. Murphy, The effect of seasonal variation on biomethane production from seaweed and on application as a gaseous transport biofuel, *Bioresour. Technol.* 209 (2016) 213–219, doi:10.1016/j.biortech.2016.02.120.
- A. Tanniou, L. Vandanjon, M. Incera, E. Serrano Leon, V. Husa, J. Le Grand, J.-L. Nicolas, N. Poupard, N. Kervarec, A. Engelen, R. Walsh, F. Guerard, N. Bourgoignon, V. Stiger-Pouvreau, Assessment of the spatial variability of phenolic contents and associated bioactivities in the invasive alga *Sargassum muticum* sampled along its European range from Norway to Portugal, *J. Appl. Phycol.* 26 (2013) 1215–1230, doi:10.1007/s10811-013-0198-x.
- S. Cho, S. Kang, J. Cho, A. Kim, S. Park, Y.-K. Hong, D.-H. Ahn, The antioxidant properties of brown seaweed (*Sargassum siliquastrum*) extracts, *J. Med. Food* 10 (2007) 479–485, doi:10.1089/jmf.2006.099.
- G. Jard, H. Marfaing, H. Carrère, J.P. Delgenes, J.P. Steyer, C. Dumas, French Brittany macroalgae screening: Composition and methane potential for potential alternative sources of energy and products, *Bioresour. Technol.* 144 (2013) 492–498, doi:10.1016/j.biortech.2013.06.114.
- D.P. Chynoweth, J.M. Owens, R. Legrand, Renewable methane from anaerobic digestion of biomass, *Renew. Energy* 22 (2001) 1–8, doi:10.1016/S0960-1481(00)00019-7.
- J.M.M. Adams, T.A. Toop, I.S. Donnison, J.A. Gallagher, Seasonal variation in *Laminaria digitata* and its impact on biochemical conversion routes to biofuels, *Bioresour. Technol.* 102 (2011) 9976–9984, doi:10.1016/j.biortech.2011.08.032.
- M. D'Este, M. Alvarado-Morales, A. Ciofalo, I. Angelidaki, Macroalgae *Laminaria digitata* and *Saccharina latissima* as potential biomasses for biogas and total phenolics production: focusing on seasonal and spatial variations of the algae, *Energy Fuels* 31 (2017) 7166–7175, doi:10.1021/acs.energyfuels.7b00853.
- J.J. Milledge, S. Maneein, E. Arribas Lopez, D. Bartlett, *Sargassum* inundations in turks and caicos: methane potential and proximate, ultimate, lipid, amino acid, metal and metalloid analyses, *Energies* 13 (2020) 1–27, doi:10.3390/en13061523.
- D.P. Chynoweth, V.J. Srivastava, Methane production from marine biomass, in: *Int. Symp. Biogas, Microalgae, Livest. Wastes*, Institute of Gas Technology, Chicago, IL (USA), 1980, pp. 15–17. <https://www.osti.gov/scitech/servlets/purl/6710029>.
- J. McKennedy, O. Sherlock, Anaerobic digestion of marine macroalgae: a review, *Renew. Sustain. Energy Rev.* 52 (2015) 1781–1790, doi:10.1016/j.rser.2015.07.101.

- [35] J.M.M. Adams, A. Schmidt, J.A. Gallagher, The impact of sample preparation of the macroalgae *Laminaria digitata* on the production of the biofuels bioethanol and biomethane, *J. Appl. Phycol.* 27 (2015) 985–991, doi:10.1007/s10811-014-0368-5.
- [36] E. Moen, S. Horn, K. Østgaard, Alginate degradation during anaerobic digestion of *Laminaria hyperborea* stipes, *J. Appl. Phycol.* 9 (1997) 157–166, doi:10.1023/A:1007966126570.
- [37] K. Østgaard, M. Indergaard, S. Markussen, S.H. Knutsen, A. Jensen, Carbohydrate degradation and methane production during fermentation of *Laminaria saccharina* (Laminariales, Phaeophyceae), *J. Appl. Phycol.* 5 (1993) 333–342, doi:10.1007/BF02186236.
- [38] G.P.B. Marquez, W.T. Reichardt, R.V. Azanza, M. Klocke, M.N.E. Montaña, Thalassic biogas production from sea wrack biomass using different microbial seeds: Cow manure, marine sediment and sea wrack-associated microflora, *Bioresour. Technol.* 133 (2013) 612–617, doi:10.1016/j.biortech.2013.01.082.
- [39] Y. Hu, S. Wang, Q. Wang, Z. He, X. Lin, S. Xu, H. Ji, Y. Li, Effect of different pre-treatments on the thermal degradation of seaweed biomass, *Proc. Combust. Inst.* 36 (2017) 2271–2281, doi:10.1016/j.proci.2016.08.086.
- [40] P.A. Harnedy, R.J. FitzGerald, Extraction of protein from the macroalga *Palmaria palmata*, *LWT – Food Sci. Technol.* 51 (2013) 375–382, doi:10.1016/j.lwt.2012.09.023.
- [41] K. Wong, P. Chikeung Cheung, Influence of drying treatment on three *Sargassum* species 2. Protein extractability, in vitro protein digestibility and amino acid profile of protein concentrates, *J. Appl. Phycol.* 13 (2001) 51–58 <https://doi.org/10.1023/A:1008188830177>. (Accessed 12 February 2019).
- [42] D.P. Chynoweth, C.E. Turick, J.M. Owens, D.E. Jerger, M.W. Peck, Biochemical methane potential of biomass and waste feedstocks, *Biomass Bioenergy* 5 (1993) 95–111, doi:10.1016/0961-9534(93)90010-2.



## Optimal generation mix for frequency response adequacy in future power system

Vivek Prakash<sup>a,\*</sup>, Kailash Chand Sharma<sup>b</sup>, Rohit Bhakar<sup>c</sup>

<sup>a</sup> School of Automation, Banasthali Vidyapith, Rajasthan, India

<sup>b</sup> Department of Electrical Engineering, NIT Jalandhar, India

<sup>c</sup> Department of Electrical Engineering, Malaviya National Institute of Technology, Jaipur, India

### ARTICLE INFO

#### Keywords:

Frequency response  
Generation mix  
Inertial response  
Net load  
Primary frequency response  
System security  
Unit commitment

### ABSTRACT

Strict enforcement of government policies to integrate high generation share from renewable energy sources (RES) like wind and PV would create inevitable operational challenges for the utilities to deliver Frequency Response (FR) services. Uncertain RES generation characteristics would worsen the situation for SO, to detain initial frequency deviation following the largest generation outage. This necessitates investigation of optimal generator combination for securing PFR adequacy with simultaneous characterization of uncertainty. In this regard, this paper proposes a novel Modified Interval (MI) based optimal generation mix formulation for operation cost minimization and FR adequacy. RES uncertainty is characterised by forecasted upper and lower bound, while hourly ramp needs are based on the net load scenarios. Proposed model is assessed on one area IEEE reliability test system. Rate of change of frequency (ROCOF) and frequency deviation are considered as network security limits to obtain optimal generation mix. Results obtained provide, overall cost performance, PFR and optimal generation mix, without violating system security criteria. This model would certainly assist SO, to enhance system's inertia and PFR adequacy at short-term system operations and could be extended for long-term planning framework.

### 1. Introduction

OVER the last decade, quantum of electricity generation from fossil fuel-based generation sources has reduced, while generation share of renewable energy sources (RES) has increased rapidly over the same period [1]. The Europe's energy targets for 2020-2030 are to accommodate at least 45% generation from RES [2]. Recent study by the National Renewable Energy Laboratory shows that the United States can generate 80% of its electricity from RES by 2050 [3]. As the generation mix of a power system evolves away from traditional generation units, behavior of the power system in response to a power imbalance also changes. Increasing RES share in overall generation mix would pose additional formidable challenges from the technical and economical perspectives [4,5]. Uncertain RES generation characteristics would create several new challenges for System Operator (SO) in terms of Frequency Response (FR) adequacy. Recent studies on FR assessment in global interconnections like European interconnections, Western interconnection and Eastern interconnections, USA, indicate FR reduction over the last years [6,7]. One of the main causes for this reduction is displacement of synchronous generators with non-synchronous RES generation. Hence,

FR assessment with large RES is an issue of concern for the SO aiming to enhance the power system security.

Displacement of conventional generation reduce system's inherent FR ability like inertia and PFR, to control dynamic changes in system frequency in contingent conditions. System FR reduction would result in frequent generation-demand imbalance. Hence, there would be large frequency deviations, following inevitable contingencies. FR service is automatic corrective measures deployed by the system, in response to frequency deviations [8,9].

RES integration could lead to both diversifications of generation sources and increase in overall cost due to the additional resource requirement for flexibility and hence secure system operation [10,11]. National Grid, United Kingdom reports observed that there would be significant increase in PFR requirements over the next decade. Over the next 5 years this amounts to an increase of 30-40% [12]. This requires efficient generation mix by balancing the profits of generation source variation and system security cost with the PFR provision.

PFR requirement analysis is done for the quantification of variability and uncertainty of the RES [13–15]. It is observed that the PFR requirements could be partly compensated by the interaction of different type of loads and wind power [13]. Another scenario-based study is performed for different combinations of wind, solar and ocean wave power

\* Corresponding author.

E-mail address: [vivekprakash@banasthali.in](mailto:vivekprakash@banasthali.in) (V. Prakash).

**Nomenclature**

*Indexes and sets*

$t, T$	Index and set of time period.
$i, I$	Index and set of generator units.
$b, B$	Index and set of linear segments of generator cost curve.
$j, J$	Index and set of generator start-up costs.
$G_{ng}$	Generator set with disabled governor.
$w, W$	Index and set of wind farms.
$pv, PV$	Index and set of PV plants.

*Variables*

$G_{i,t}$	Unit $i$ output power in time interval $t$ (MW).
$G_{b,i,t}^s$	Cost curve segment $b$ power output for unit $i$ in time period $t$ (MW).
$S_{i,t}$	Combined start-up and shut down cost of generator $i$ in time interval $t$ (\$).
$Su_{i,t,j}$	Decision variable, start-up cost matrix for generator $i$ during time $t$ for cost segment $j$ .
$\chi_{i,t}$	Decision variable, generator up/down status for generator $i$ during hour $t$ .
$\chi_{i,t}^{up}, \chi_{i,t}^{dn}$	Decision variable, generator start-up/down status for generator $i$ starts up in time period $t$ .
$\gamma_{i,t}$	Decision variable, headroom availability status for generator $i$ in time $t$ .
$P_{i,t}^{nad} / P_{i,t}^{ss}$	PFR available from generator $i$ at nadir / steady-state time $t$ (MW).
$P_{i,t}$	Total PFR from generator $i$ at time period $t$ (MW).
$\Delta f_{i,t}^{nad} / \Delta f_{i,t}^{ss}$	Frequency deviation at nadir/steady state (Hz).
$\delta_{i,t}$	Generator $i$ governor status at time $t$ .

*System parameters and constants*

$LF_t$	Forecasted load in time period $t$ (MW).
$LN_t$	Net Load at time period $t$ (MW).
$AP_i$	Rated apparent power of generator $i$ (VA).
$W_{t,w}^{av} / P_{t,pv}^{av}$	Available wind & PV power from wind farm $w$ & PV plant $pv$ at time period $t$ (MW).
$W^p / PV^p$	Wind & PV penetration (%).
$W^{cap} / PV^{cap}$	Installed wind & PV capacity (MW).
$G_i^{max} / G_i^{min}$	Generator $i$ maximum/ minimum output (MW).
$R_i^{up} / R_i^{dn}$	Generator $i$ ramp up/down limit (MW/h).
$Suc_{i,j}$	Generator $i$ start-up cost of segment $j$ (\$).
$f_0$	Nominal frequency (Hz).
$\Delta P$	Infeed loss (MW).
$LD$	Load damping rate (1/Hz).
$t^{de}$	PFR delivery time (s).
$\Delta f^{max}$	Maximum frequency deviation (Hz).
$f^{ss}$	Steady state frequency (Hz).
$H_i / H_i^L$	Inertia constant of generator/ Lost generator $i$ (s).
$H^{eqload}$	Equivalent load inertia (s).
$t^{ss} / t^{nad}$	Time to reach steady-state/ nadir frequency (s).
$f^{nad}$	Nadir frequency (Hz).
$P^C / P^C_{nad} / P^C_{ss}$	PFR requirement, overall / at nadir/ at steady-state (MW).
$H_{sys} / H_{req}$	System Inertia available/requirement (MWs).
$G_i^{db} / G_i^{dbmax}$	Generator governor dead band/ maximum permissible dead band $i$ (Hz).
$D_i^e / D_i$	Equivalent droop/ governor droop of generator $i$ (Hz/MW).

generation for computation of PFR requirements caused due to uncertainty. It is concluded that PFR requirements and uncertainty is reduced with RES mix [14,15]. Diversified RES mix provides smooth generation portfolio. Hence, generation predictability would increase and probabil-

ity of extremes values would decrease. This would result in reduction in overall system FR requirements.

A generation mix model is proposed in a security-constrained generation expansion model, considering the uncertainties of wind and load [16]. However, primary reserve constraints to handle uncertain wind generation is not considered. A robust optimization-based generation mix is proposed [17]. The proposed methodology handles the load demand uncertainty. However, in robust formulations, the uncertainty range at each optimization interval is defined as upper and lower bound on net load. Therefore, ignores the probability of a specific uncertainty realization within the given range [18].

Conventional and RES technology have an idiosyncratic effect on system frequency and there is limited understanding of FR adequacy with various generation mix characteristics. FR capability of the system is highly dependent on optimal generator commitment decisions. Thus, a detailed study of optimal generation mix under uncertain wind and PV generation is necessary for understanding SO's FR adequacy problem in the right perspective. A prior understanding of optimal generation mix with secured PFR in future low carbon power system would corroborate SO to maintain a secure and stable power system.

In the above context, this paper puts forward the following contributions:

- (i) Propose a novel exposition of optimal generation mix with the objective of reduced operation cost while maintaining systems' FR ability.
- (ii) Assess PFR adequacy with diversified generation mix.
- (iii) Model RES uncertainty with pragmatic characterization in the generation mix optimization problem.
- (iv) Analyse overall cost for different generation mix cases.

Prior information of system FR with optimal combination of conventional and RES generation could support SO, to efficiently handle inevitable contingencies, like largest infeed loss.

In rest of the paper: Section III discusses problem formulation. In Section IV, proposed methodology is described. In Section V, mathematical formulation is provided. Results are discussed in Section VI, while Section VII discusses the relevant conclusions.

**2. Problem formulation**

In the proposed model ROCOF and frequency nadir, initial generation mix, system data and net load profile are the inputs. It considers thermal, hydro, nuclear, uncertain renewable wind and PV units as candidate generators, and provides generator combination mapped with frequency security criteria and total cost under this mix as outputs. In this work generation from wind and PV is given priority as candidate generators, considering environmental concerns. The formulation considers the candidate generator addition to the initial generation mix, stage by stage following network security parameters. Candidate generator selection at any stage is based on the frequency security criteria like ROCOF and maximum frequency deviation limit. Wind and PV generation uncertainty is characterized and represented in the proposed model for the pragmatic problem formulation.

**2.1. RES uncertainty characterization**

Power system operations like generation scheduling and dispatch are decision-making problem. Decisions obtained through these operations impact the system security and reliability. Wind and PV power uncertainty makes this problem more critical [19]. Accurate modeling of involved uncertainties is necessary to solve these decision-making problems. Wind and PV generation variability is characterized by an Autoregressive Integrated Moving Average (ARIMA) model. ARIMA is one of the benchmark time series-based model used for generation and load forecasting [20]. A stationary time series data is required as input to autoregressive (AR) and moving average (MA) model. Load, wind and

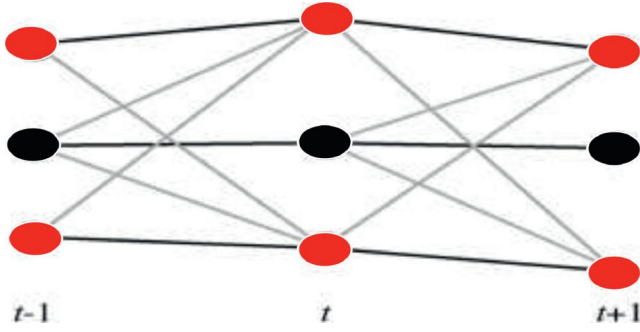


Fig. 1. Interval scenarios (red) with changeover constraints (grey).

PV time series data is non-stationary and requires differentiation technique to obtain stationary time series data before applying in ARIMA for modelling. Eq. (1) is formulated to obtain the first order differentiation.

$$\Delta\alpha_t = \alpha_t - \alpha_{t-1} = (1 - \beta)\alpha_t \quad (1)$$

Where,  $\Delta$  is the backward difference operator,  $\alpha_t$  and  $\alpha_{t-1}$  are the  $t^{th}$  &  $t - 1^{th}$  time series data respectively,  $\beta$  is the backward shift operator. After differentiation, ARIMA( $p, d, q$ ) value is obtained using Eq. (2).

$$\theta_p(\beta)\Delta^d \gamma_t = \varphi_q(\beta)\epsilon_t \quad (2)$$

Where,  $\theta_p(\beta)$  is the AR operator,  $\Delta^d$  is the  $d^{th}$  order difference,  $\varphi_q(\beta)$  is the MA operator,  $p$  is AR order,  $q$  is MA order,  $\epsilon_t$  represents normal distribution of arbitrary number series with zero mean and  $\sigma_\epsilon^2$  variance. Suitable model order is obtained through observation of Autocorrelation Function (ACF) and Partial Autocorrelation Function (PACF). ACF and PACF plot provides the MA and AR order through observation of the zero cut off at  $t^{th}$  time period.

### 2.2. Modified interval based optimal generation mix

MI based generation mix model is incorporated to minimize the overall operation cost under uncertain wind and PV generation with the aim to determine optimal generator combination [21,22]. In this formulation features of computationally fast interval optimization and economical stochastic optimization models is included to improve day-ahead unit scheduling. In MI based approach, PV and wind variability is characterized by ramp up and down scenarios, formulated within the forecasted upper and lower limit as shown in Fig. 1. Hourly ramp needs of formulated scenarios depend on net load. Thus, it precisely represents the expected RES output. In MI based approach, problem is formulated with Mix Integer Linear Programming (MILP) constraints with the aim to minimize the operating cost of central forecasted scenario of wind and PV generation,  $n_w$  and  $n_{pv}$ .

Objective function shown by Eq. (3) includes start-up cost, no-load cost and running cost of each generating unit. Non-linear cost function is converted to linear segments using piece wise linearization.

$$\min C^o = \sum_{i \in T} \sum_{i \in I} \left( su_{i,t,j} + Ln_i * \chi_{i,t} + \sum_{b \in B} C s_{i,b} * g_{b,i,t,n_{w,pv}}^s \right) \quad (3)$$

Optimization problem is subject to power balance constraints as (4).

$$\sum_{i \in I} G_{i,t} = LN_t \quad \forall t \in T \quad (4)$$

$$LN_t = LF_t - \sum_{i,w} (W^p * W^{av} * W^{cap}) - \sum_{i,pv} (PV^p * PV^{av} * PV^{cap}) \quad (5)$$

Eq. (5) calculates the net load as the difference of forecasted load and generation by RES. Other constraints like generator start-up cost, minimum up/down time and ramping constraints are formulated as proposed in [21].

### 2.3. Frequency security limits based generation mix optimization

In this section, generation mix optimization sub-problem is formulated with FR constraints. This formulation would work as a performance evaluator for the main problem. System data and demand profile is used to evaluate the total generation costs and PFR cost for the required time period. Generation mix is restructured with the expansion and contraction of some generation technologies. Hence, investment cost,  $C^{invest}$  of generators is considered in the total cost,  $C^{total}$ . In this work, wind and PV generation expansion is considered. Large integration of wind and PV would create reliability and system security issues. Hence, this would give rise to loss of load probability or under frequency load shedding issues and in turn incur societal cost. This cost is considered through increase in PFR requirements. Parameter  $PR$  is the price per MW, primary response capacity from the conventional generation plants. For simplicity, PFR price is assumed equal for different responsive conventional generation. The optimization problem could now be represented as (6)

$$\min C^{total} = C^o + C^{invest} + PR * \sum_{i \in T} \sum_{i \in I} (P_{i,t}) \quad (6)$$

Subject to following frequency security constraints:

$ROCOF_{max}$  should respect minimum  $H_{sys}$  in case of maximum infeed loss, as shown in Eq. (7).

$$H_{sys} = \frac{\sum_{i \in I} H_i * A p_i * \chi_{i,t} - \Delta P * H_i^L}{f_0} \geq \left| \frac{\Delta P}{2 * ROCOF_{max}} \right| \quad (7)$$

Constraint (8) takes care of available system inertial response, such that  $ROCOF_{max}$  does not violate protection setting and cause instability.

$$\sum_{i \in I} \{ \chi_{i,t} * H_i * G_i^{max} \} + H^{eqload} * FL_t \geq H_{req} \quad \forall t \in T \quad (8)$$

Constraint (9) ensures PFR adequacy after system inertial response is exhausted.

$$\sum_{i \in I} P_{i,t} \geq P^C - LD * t^{de} * \frac{\Delta f^{max}}{f_0}, \quad \forall t \in T \quad (9)$$

Eqs. (10)–(16) provides governor droop setting and governor setting for providing PFR [23]. In (10) equivalent droop curve is estimated and given in Hz/MW. Eq. (11) ensures PFR adequacy following large frequency variations. Eqs. (12) and (13) maintain headroom availability and governor droop. Eq. (14) ensures generator commitment for enabled governor. Eqs. (15) and (16) assign  $\delta$  value zero for blocked governor mode and generators with high governor deadband.

$$D_i^e = \frac{D_i * f_0}{G_i^{max}}, \quad \forall i \in I \quad (10)$$

$$P_{i,t} \leq \frac{\delta_{i,t}}{D_i^e} (\Delta f^{max} - G_i^{db}), \quad \forall i \in I, \forall t \in T \quad (11)$$

$$G_{i,t} + \frac{1}{D_i^e} (\Delta f^{max} - G_i^{db}) \geq G_i^{max} * \delta_{i,t} - G_i^{max} * \gamma_{i,t}, \quad \forall t \in T, \forall i \in I \quad (12)$$

$$P_{i,t} \geq \frac{\gamma_{i,t}}{D_i^e} (\Delta f^{max} - G_i^{db}) - G_i^{max} (1 - \delta_{i,t}), \quad \forall i \in I, \forall t \in T \quad (13)$$

$$\delta_{i,t} \leq \chi_{i,t} \quad \forall i \in I, \quad \forall t \in T \quad (14)$$

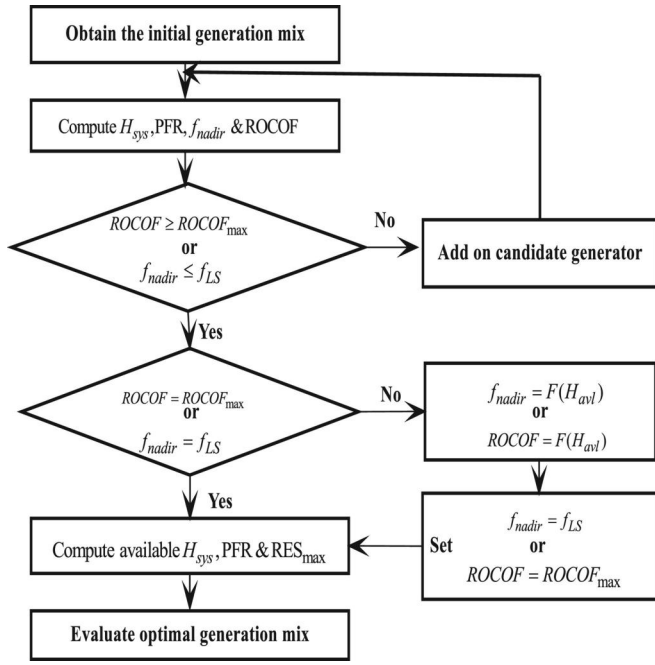


Fig. 2. Flow diagram of the FR constrained generation mix.

$$\delta_{i,t} = 0 \quad \forall i \in G_{ng}, \quad \forall t \in T \quad (15)$$

$$G_i^{db} \leq G_i^{db\max} + f_0(1 - \delta_{i,t}), \forall i \in I, \forall t \in T \quad (16)$$

Eq. (17) determines the quasi-steady-state frequency value. It depends upon generator PFR capacity, infeed loss value, load damping rate and forecasted demand. Its value should be less than  $\Delta f^{nadir}$ .

$$\Delta f^{ss} = \frac{\Delta P - P_{i,t}}{LD * LF_i} \leq \Delta f^{nadir} \quad (17)$$

### 3. Methodology

In this paper novel exposition of FR constrained generation mix optimization is proposed to uphold the system security criteria considering RES uncertainty and largest infeed loss of the system. Proposed method is complex to solve directly by single optimization. In this paper an innovative technique is proposed to handle the problem using two-stage optimization. Proposed work flow is shown in Fig. 2.

First objective would take care of sub-operational problem with RES uncertainty characterization, while addition of candidate generators from available generation technology and resulting generation mix based on frequency security criteria is evaluated by second objective. At first, initial generation mix is evaluated using MILP based MIUC, and examined whether the frequency security criteria are violated. If it is violated, that shows the generation mix is already at optimal state, otherwise optimization would follow next step.

Based on initial generation mix, assuming  $U$  units are added to form the final generation mix without violating system security parameters. The optimization is divided into  $U$  cycles. In each cycle, one unit would be added as candidate generator and system security parameter is evaluated. Program is terminated, if security limit reaches. If ROCOF and frequency deviation limit is not violated, another unit would be added into the generation mix for the  $u$ th cycle. The  $(u + 1)$ th cycle decisions would be determined by the optimal generation mix obtained for  $u$ th cycle, by repeating the above steps. The program would iterate  $U$  times to obtain optimal mix.

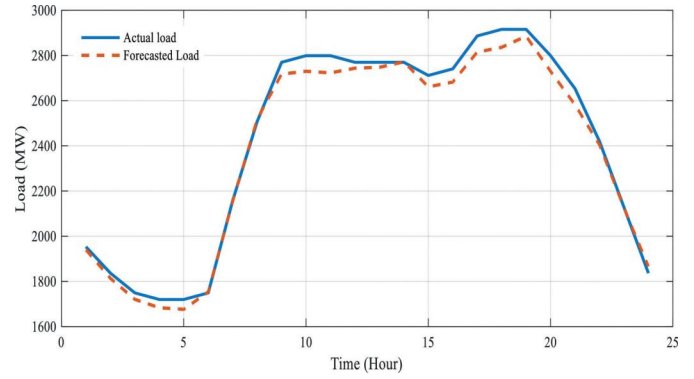


Fig. 3. Actual and forecasted load curve for peak load day [16].

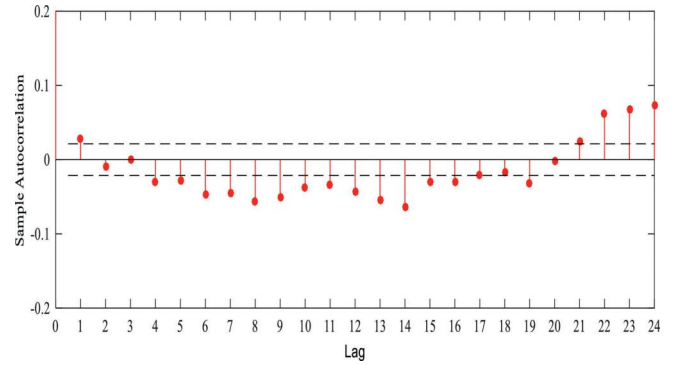


Fig. 4. ACF plot for wind power data.

### 4. Case study

This section demonstrates the application of the proposed optimal generation mix model on standard one area IEEE RTS [24]. Peak demand and installed capacity of the system is 2850 MW and 3405 MW respectively. Wind and PV plant of 50 MW capacity is considered in this work, mapped with the system buses. Nominal frequency, governor settings, load damping rate and PFR time are considered as per National Grid standards [25]. Fuel cost is obtained from [26]. PFR cost is considered as 6\$/MW, similar to the [27]. ROCOF of 1.2 Hz/s is considered for the studied test system [28]. There are two nuclear generators of largest capacity of 400 MW, outage of one is considered in this work. PFR requirement is considered 30% of system's total responsive capacity. Maximum generator governor dead band is considered as 100 mHz. Simulation work is carried out in GAMS 24.2.3 using CPLEX 12.6.0, MIP solver with 0.1% duality gap and MATLAB on Intel Core i7 with a 2.2-GHz processor and 8 GB RAM.

Table 1 shows each generator parameters. This model considers FR parameters of different generation types. Hence, separate model for each generation type is avoided. Since, wind and PV generation expansion are considered in this work, generator data is modified to include the parameters for these RES. Actual and forecasted demand for peak load day is shown in Fig. 3.

#### 4.1. Wind and PV generation uncertainty modeling

In case of wind uncertainty modelling, first differentiation of time series data provides stationary data series. Therefore, suitable value of  $dis$  one. It could be inferred from ACF and PACF plot of Figs. 4 and 5, that both plots cut off after first lag. Hence, ARIMA (1, 1, 1) model is found suitable for wind power interval forecasting as shown in Fig. 5. Value of AR and MA coefficients are 0.619 and 0.614 with white noise variance as 0.983.

**Table 1**  
Generator parameters [16].

Unit Type	$G_i^{up}$ (MW)	Number of units installed	$H_i$ (s)	$D_i$ (p.u.)	$G^{db}$ (mHz)	$C^{invest}$ (\$/kW)
Oil/Steam	12	5	2.6	0.05	15	962
Oil/CT	20	4	2.8	0.05	15	714
Hydro	50	6	3.5	0.05	15	2500
Coal/Steam	76	3	3.0	0.05	15	1610
Oil/Steam	100	3	2.8	0.05	15	962
Coal/Steam	155	3	3.0	0.05	15	962
Oil/Steam	197	3	2.8	0.05	15	962
Coal steam	350	3	3.0	0.05	15	1610
Nuclear	400	2	5.0	0.05	15	1610
Wind	50	1	-	-	-	1240
PV	50	1	-	-	-	1260

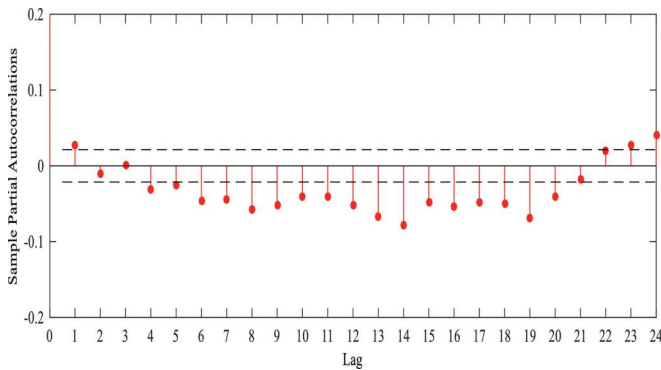


Fig. 5. PACF plot for wind power data.

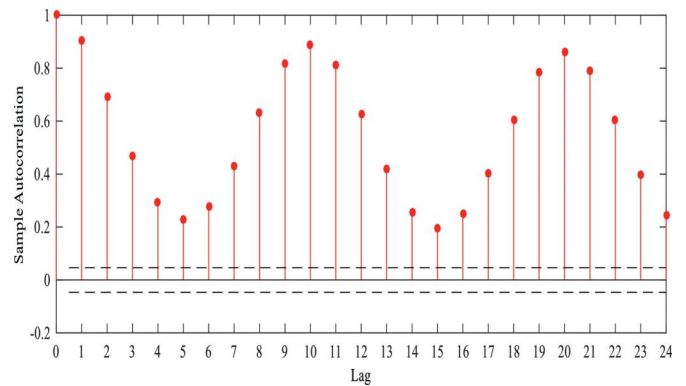


Fig. 7. ACF plot for PV power data.

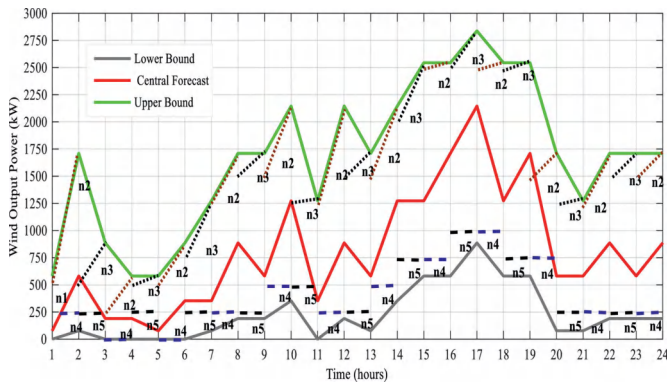


Fig. 6. Wind power intervals: Up (dotted line) and down (dashed lines) ramp requirement.

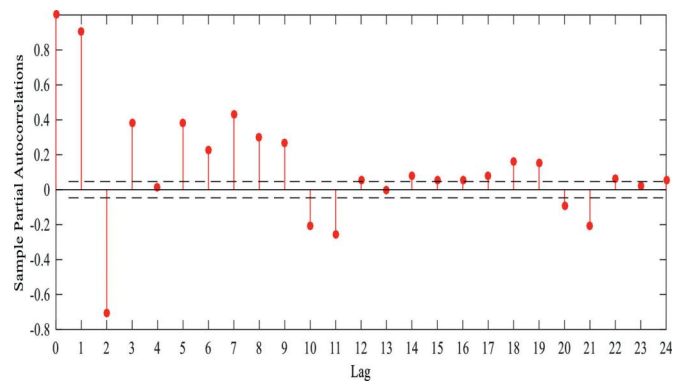


Fig. 8. PACF plot for PV power data.

In case of PV uncertainty modelling, ACF and PACF plots of Figs. 7 and 8 depicts that ARIMA (3, 0, 0) model is appropriate for forecasting PV power interval. AR1, AR2 and AR3 values are 1.820, -1.031 and 0.383 and values of variance is 0.236. Wind speed data and PV radiation data for the duration 01.01.2018 to 31.12.2018 is considered, online available from Chicago, USA [29]. Fig. 9 show, forecasted PV power interval for 24 hours with up and low bounds. Wind and PV power forecasted intervals are considered in MIUC formulation for modeling uncertainty considering five ramping scenarios. These ramping scenarios are depicted as n1, central forecast scenario and n2, n3, n4&n5 shows odd and even hour ramp up/down needs based on net load, as shown in Figs. 6 and 9. Hence, this consideration accurately captures wind and PV power outputs.

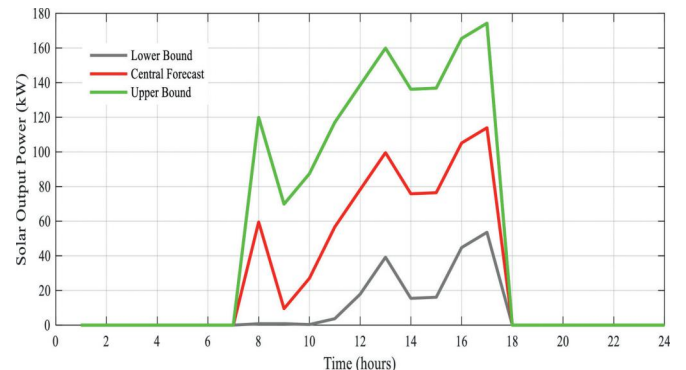


Fig. 9. Hourly PV power intervals.

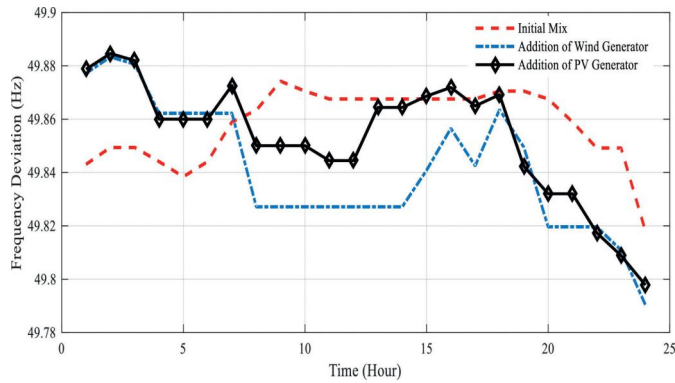


Fig. 10. Frequency deviation in all the three cases.

4.2. Generation mix following frequency security limits

This section analyses the optimal generation mix following frequency security criteria. Effect of largest generation outage on ROCOF and frequency deviation is analysed and contribution from different generators is obtained. Three cases are considered: (i) Base Case (without wind and PV) (ii) Wind as candidate generator (iii) PV as candidate generator.

(i) Base Case (without wind and PV):

This case considers initial generation mix available with the test system. It is observed from Figs. 10 and 11, ROCOF and frequency deviation values are within the limit, i.e., maximum ROCOF is 1.088 Hz/s and maximum frequency deviation is 49.818 Hz. This reflects sufficient inertia and PFR availability with the system. Generation contribution from different generators is shown in Fig. 11. As system frequency limit is not violated; candidate generators like wind and PV could be added to the initial generation mix.

(i) Wind as candidate generator:

In this case wind as candidate generator is added to the initial generation mix and system frequency security criteria are assessed. Wind power contribution to feed the demand over the day is shown in Fig. 12. Effect of uncertain wind generation on frequency deviation and ROCOF over a day could be seen from Figs. 10 and 12. It could be observed that maximum value of ROCOF is 1.183 Hz/s and maximum frequency deviation is 49.79 Hz. This is due to the fact that a smaller number of conventional generators is committed to provide inertial response and PFR. However, these limits are within the prescribed security criteria.

Most of the new wind power plants are run as variable speed wind turbines and connected with the grids through converters, thus completely decoupling the wind inertia from the grid. Wind power plant control mechanism aim is to imitate the inertial response of conventional

synchronous generators and in particular the ability of autonomous response to frequency changes. This imitates kinetic energy release or absorption like that of synchronous generators, thus wind power plant acts as a dispatchable source [30]. Hence, additional RES generation unit could be added to further assess the system FR adequacy.

(i) PV as candidate generator:

This case considers PV as candidate generator. Addition of PV along with wind generating unit made ROCOF to reach the maximum limit of 1.195 Hz/s while maximum frequency deviation reaches to 49.79 Hz/s as shown in Fig. 13. Non dispatchable wind and PV generating units jointly feeds MWs of demand, hence commitment of conventional units is lesser. This would result in high ROCOF and frequency deviation. Now, further addition of RES generating unit would lead to violation of considered frequency security criteria. Hence, obtained generation mix is considered as the optimal generation mix for the considered test system.

PFR contributions from generating units like Oil/CT, Coal/Steam, Oil/Steam and Hydro in all the three cases are shown in Figs.14, 15, 16 and 17 respectively. It could be observed from Fig. 14 that Oil/CT plant's PFR contribution is for few hours in case of initial mix, however, in case of addition of wind generation, its magnitude and duration are higher compared to both the cases. In case of addition of PV generation, PFR magnitude is constant for most of the time period. From Figs. 15 and 16, it could be observed that Coal/Steam and Oil/Steam plant's PFR contribution is almost similar for the addition of wind and PV cases. In both, the cases magnitude of PFR is higher, because of their higher capacity and number in the overall generation mix. In case of Hydro generator as shown in Fig. 17, PFR contribution is almost negligible for most of the time. However, its maximum contribution is for the hour t18. Further, it is observed that in all three cases, nuclear-generating units are weak in providing PFR and it is zero for the entire time interval. Therefore, its contribution is not shown here.

Fig. 18 presents the overall PFR availability for all three cases. It is observed that PFR contribution is higher for initial generation mix. This is due to the fact that number of generators committed per hour is higher. In case of addition of wind and PV unit, net load is reduced. This would lead to displacement of conventional units, hence PFR availability is reduced in both the cases. This PFR reduction would cause higher frequency deviation and further lead to under frequency load shedding if sufficient response is not provided.

4.3. Overall cost performance

This section discusses the cost performance for all the three cases. It could be observed from Table 2 that operation cost reduces with the addition of wind generation and reduces more with the addition of PV unit along with wind. This reduction is because of displacement of conventional units. Wind and PV unit's operation cost is negligible, as they are free from fuel cost.

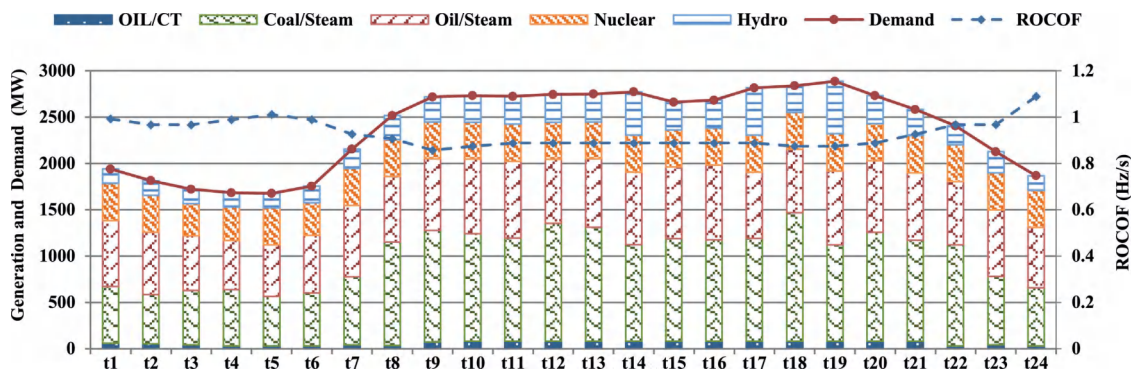


Fig. 11. Initial generation mix.

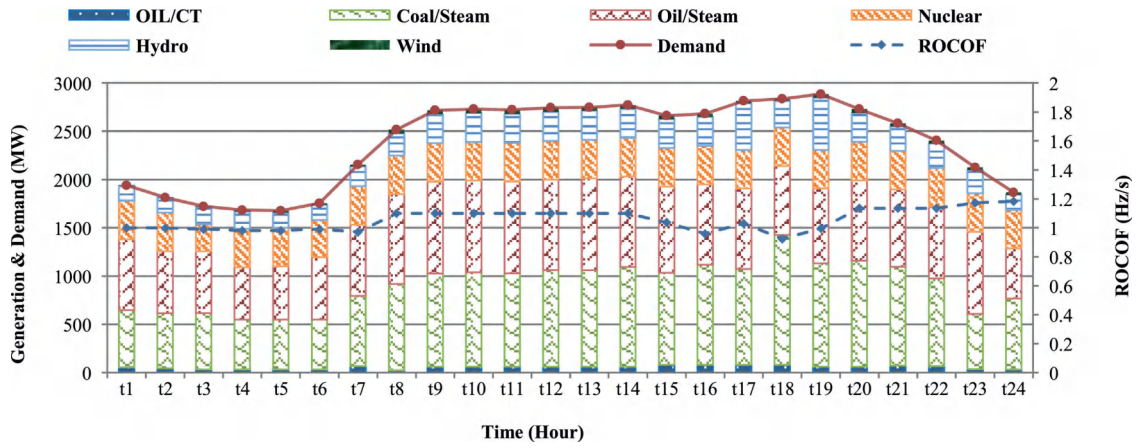


Fig. 12. Initial generation mix with wind as candidate generator.

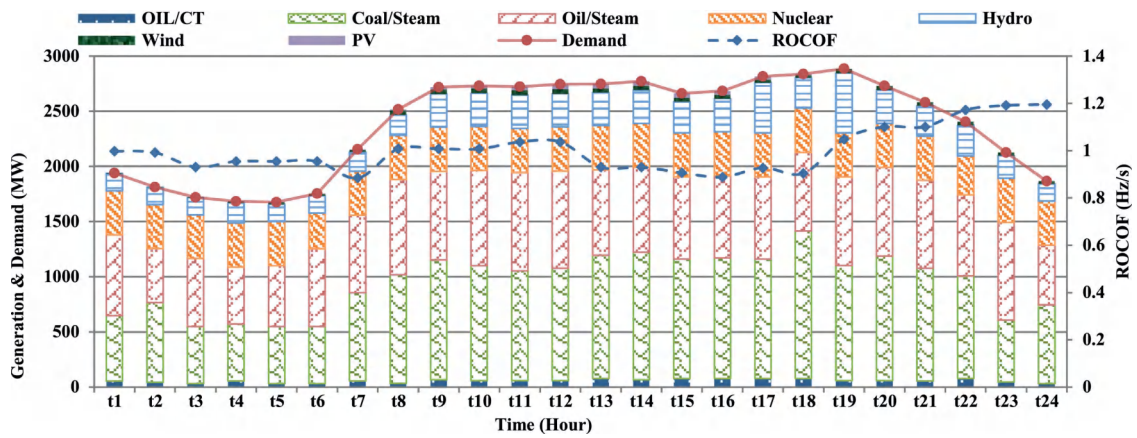


Fig. 13. Initial generation mix with PV as candidate generator.

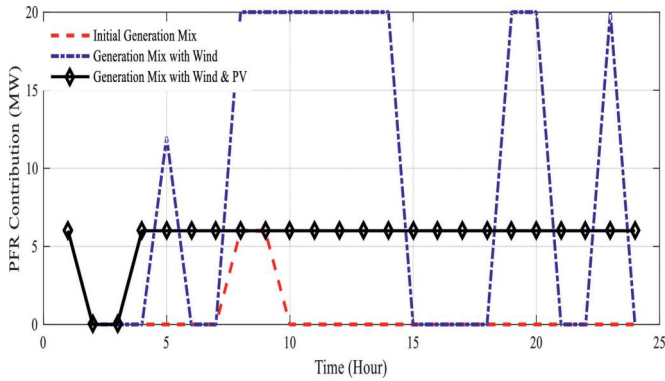


Fig. 14. PFR contribution from Oil/CT generating units.

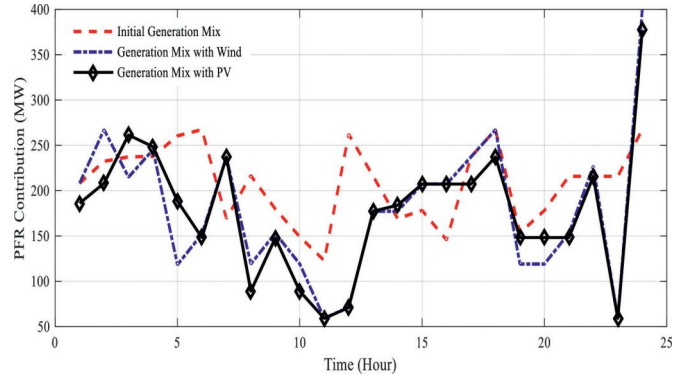


Fig. 16. PFR contribution from Oil/Steam generating units.

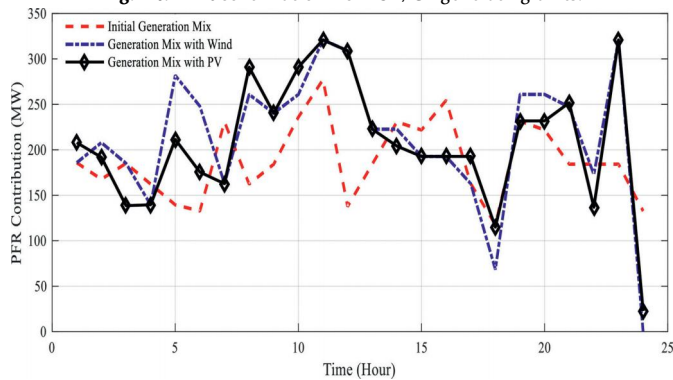


Fig. 15. PFR contribution from Coal/Steam generating units.

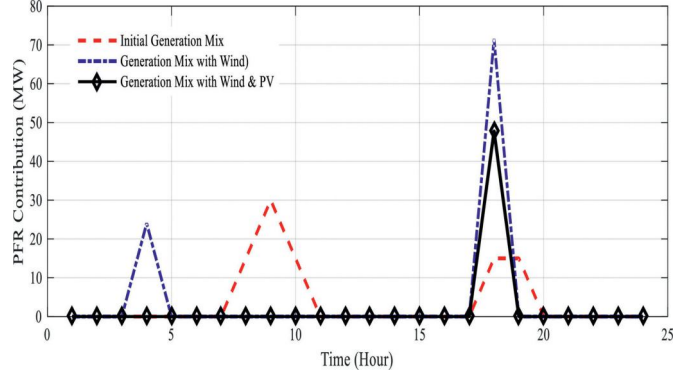


Fig. 17. PFR contribution from Hydro generating units.

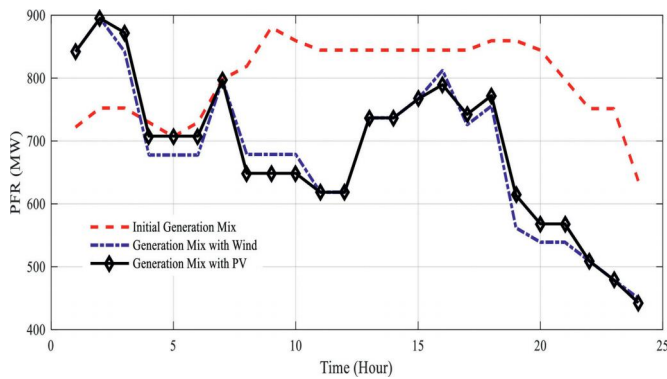


Fig. 18. Available PFR in all the three cases.

Table 2

Cost performance.

Cases	Operation Cost (\$)	Overall Cost (\$)
Initial Generation Mix	499368.5783	44703368.58
Addition of wind	486216.2251	45930216.23
Addition of PV	480444.8847	47184444.88

Hence, these units are not adding any amount in overall operating cost. Overall cost includes operation cost and investment cost. It could be observed from Table 2 that this cost is increasing from initial generation mix case to addition of wind and PV units. As the investment cost of wind and PV unit is higher. This would increase the overall cost.

## 5. Conclusion

This paper presents a novel exposition of MI based optimal generation mix formulation for inertial response and PFR adequacy with RES generation expansion. Wind and PV uncertainty is characterized using forecasted upper and lower interval with inter hour ramp requirements consideration based on net load scenarios. Hence, wind and PV output is accurately captured. ROCOF setting and frequency deviation is considered as frequency security limit to obtain optimal generation mix. Results obtained provide system specific optimal generation output, PFR contribution and overall cost performance from different generating units. Optimal generation mix is obtained through step by step evaluation of system frequency security criteria. It is observed that PFR requirement would increase with the RES expansion. Hence, additional response is required to meet the same. Technologies like energy storage, demand-response and electric vehicle could be envisaged to enhance the PFR and maintain the system security in low carbon power system.

Proposed framework has potential to assist SO, to enhance system's inertia and PFR adequacy at short-term operations and could be enhanced for achieving economical generation mix considering network security limits in a long-term planning framework. Proposed work could be extended for long term planning by consideration of the emission cost in operational level and assess its impact on the long-term emission target-oriented generation planning with the co-optimization of energy and ancillary service market for renewable generation expansion together into one long-term generation planning model.

## Declaration of Competing Interest

MNIT Jaipur, Banasthali Vidyapith, NIT Jalandhar

## CRedit authorship contribution statement

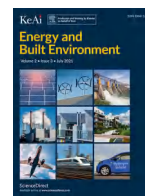
**Vivek Prakash:** Conceptualization, Methodology, Software.  
**Kailash Chand Sharma:** Methodology. **Rohit Bhakar:** Supervision.

## Acknowledgement

This work is supported by the DST grant for UKICERI project, DST/RCUK/JVCCE/2015/02.

## References

- [1] M. Kejunen, What drives Great Britain's electricity generation mix?, 2016, [Online]. Available: <https://www.ofgem.gov.uk/news-blog/our-blog/what-drives-great-britain-s-electricity-generation-mix>.
- [2] Viability of the energy mix, 2017, [Online]. Available: <http://tyndp.entsoe.eu/insight-reports/energy-mix/>.
- [3] NREL report on renewable energy can provide 80 Percent of U.S. electricity by 2050, [Online]. Available: [http://www.ucsusa.org/clean\\_energy/smart-energy-solutions/increase-renewables/renewable-energy-80-percent-us-electricity.html](http://www.ucsusa.org/clean_energy/smart-energy-solutions/increase-renewables/renewable-energy-80-percent-us-electricity.html).
- [4] P. Zou, Electricity markets evolution with the changing generation mix: an empirical analysis based on China 2050 High Renewable Energy Penetration Roadmap, *Appl. Ener.* vol.185 (2017) 56–67.
- [5] M. Paturet, U. Markovic, S. Delikaraoglou, E. Vrettos, P. Aristidou, G. Hug, Stochastic unit commitment in low-inertia grids, *IEEE Trans. Power Syst.* (2020), doi:10.1109/TPWRS.2020.2987076.
- [6] N.W. Miller, et al., Frequency Response of California and WECC Under High Wind and Solar Conditions, *IEEE PES GM, San Diego*, 2012.
- [7] National Energy Technology Laboratory (NETL), final report, DOE/NETL-2011/1473, "Frequency Instability Problems in North American Interconnections", 2011, [online]. Available: <https://www.netl.doe.gov>.
- [8] P. Du, R. Baldick, A. Tuohy, Integration of Large-Scale Renewable Energy into Bulk Power Systems from Planning to Operation, Springer, 2017.
- [9] H. Bevrani, *Robust Power System Frequency Control*, Springer, New York, NY, USA, 2009.
- [10] P. Daly, H.W. Qazi, D. Flynn, RoCoF-constrained scheduling incorporating non-synchronous residential demand response, *Proceedings of the IEEE Transaction on Power System*, 34, 2019, pp. 3372–3383.
- [11] A. Inzunza, CVaR constrained planning of renewable generation with consideration of system inertial response, reserve services and demand participation, *Energy Econ.* (2016) 104–117.
- [12] System operability framework, 2016, [Online]. Available: <http://www2.nationalgrid.com/UK/Industry-information/Future-of-Energy/System-Operability-Framework/>.
- [13] H. Holttinen, Currents of change: European experience and perspectives with high wind penetration levels, *IEEE Power Energy Mag.* 9 (6) (Nov./Dec. 2011) 47–59.
- [14] D.A. Halamay, T.K.A. Brekken, A. Simmons, S. McArthur, Reserve requirements impacts of large-scale integration of wind, solar and ocean wave power generation, *IEEE Trans. Sustain. Energy* 2 (2011) 321–328.
- [15] H. Holttinen, Impacts of large amounts of wind power on design and operation of power systems, results of IEA collaboration, *Wind Energy* 14 (2011) 179–192.
- [16] C. De Jonghe, et al., Optimal generation mix with short-term demand response and wind penetration, *IEEE Trans. Power Syst.* 27 (2012) 830–839.
- [17] S. Dehghan, N. Amjadi, A. Kazemi, Two-Stage Robust Generation Expansion Planning: A Mixed Integer Linear Programming Model, *Proceedings of the IEEE Transaction on Power System*, 29, 2014, pp. 584–597.
- [18] H. Pandzic, Y. Dvorkin, T. Qiu, Y. Wang, D.S. Kirschen, Toward cost-efficient and reliable unit commitment under uncertainty, *IEEE Trans. Power Syst.* 31 (2) (2016) 970–982.
- [19] A.J. Conejo, M. Carrión, J.M. Morales, *Decision Making under Uncertainty in Electricity Markets*, Springer, 2010.
- [20] K.C. Sharma, P. Jain, R. Bhakar, Wind power scenario generation and reduction in stochastic programming framework, *Elect. Power Compo. Syst.* 41 (3) (2013) 271–285.
- [21] V. Prakash, K.C. Sharma, R. Bhakar, H.P. Tiwari, F. Li, Frequency response constrained modified interval scheduling under wind uncertainty, *IEEE Trans. Sustain. Energy* vol.9 (2018) 302–309.
- [22] V. Prakash, K.C. Sharma, R. Bhakar, H. Tiwari, Modified interval-based generator scheduling for PFR adequacy under uncertain PV generation, *IET Gener. Transmiss. Distrib.* 13 (16) (2019) 3725–3733.
- [23] E. Ela, V. Gevorgian, A. Tuohy, B. Kirby, M. Milligan, M.O' Malley, Market designs for the primary frequency response ancillary service—Part I: Motivation and design, *IEEE Trans. Power Syst.* 29 (1) (2014) 421–431.
- [24] Reliability Test System Task Force, The IEEE reliability test system—1996, *IEEE Trans. Power Syst.* 14 (3) (1999) 1010–1020.
- [25] National Grid, Security and Quality of Supply Standards [Online]. Available: <http://www2.nationalgrid.com/UK/Industry-information/Electricity-codes/System-Security-and-Quality-of-Supply-Standards/>.
- [26] "U.S. Energy Information Administration. 'Short-Term Energy Outlook,'" [Online]. Available: <http://www.eia.gov/forecasts/steo>.
- [27] C. Yuan, C. Gu, F. Li, B. Kuri, R.W. Dunn, New problem formulation of emission constrained generation mix, *IEEE Trans. Power Syst.* 28 (4) (2013) 4064–4071.
- [28] "International review of frequency control adaptation," 2016, [Online]. Available: <https://www.aemo.com.au/-/media/Files/Electricity>
- [29] /NEM/Security and Reliability/Reports/FPSS-International-Review-of-Frequency-Control.pdf. [Online]. Available: <https://www.renewables.ninja/>.
- [30] F. Teng, G. Strbac, Assessment of the role and value of frequency response support from wind plants, *IEEE Trans. Sustain. Energy* 7 (2) (2016) 586–595.



## Effect of the spectrally selective features of the cover and emitter combination on radiative cooling performance

Mingke Hu<sup>a</sup>, Suhendri<sup>a</sup>, Bin Zhao<sup>b</sup>, Xianze Ao<sup>b</sup>, Jingyu Cao<sup>b</sup>, Qiliang Wang<sup>c</sup>, Saffa Riffat<sup>a</sup>, Yuehong Su<sup>a,\*</sup>, Gang Pei<sup>b,\*</sup>

<sup>a</sup> Department of Architecture and Built Environment, University of Nottingham, University Park, Nottingham NG7 2RD, UK

<sup>b</sup> Department of Thermal Science and Energy Engineering, University of Science and Technology of China, Hefei 230027, China

<sup>c</sup> Department of Building Services Engineering, The Hong Kong Polytechnic University, Kowloon, Hong Kong, China

### ARTICLE INFO

#### Keywords:

Radiative cooling  
Sky cooling  
Spectral selectivity  
Sensitive analysis  
Cover  
Solar energy

### ABSTRACT

Radiative cooling (RC) shows good potential for building energy saving by throwing waste heat to the cosmos in a passive and sustainable manner. However, most available radiative coolers suffer from low cooling flux. The situation becomes even deteriorated in the daytime when radiative coolers are exposed to direct sunlight. To tackle this challenge, an idea of employing both a spectrally selective cover and a spectrally selective emitter is proposed in this study as an alternative approach. A comparative study is conducted among four RC modules with different spectral characteristics for the demonstration of how the spectral profiles of the cover and the emitter affects the RC performance. The results under given conditions show that the RC module with a spectrally selective cover and a spectrally selective emitter (SC/SE) reaches a net RC power of 62.4 W/m<sup>2</sup> when the solar radiation is 800 W/m<sup>2</sup>, which is about 1.8 times that of the typical RC module with a spectrally non-selective cover and a spectrally selective emitter (n-SC/SE). When the ambient temperature is 30 °C, the SC/SE based RC module realizes a daytime sub-ambient temperature reduction of 20.0 °C, standing for a further temperature decrement of 9.2 °C compared to the n-SC/SE based RC module.

### 1. Introduction

Radiative cooling (RC) is a completely passive cooling technology that attracts increasing attention in the research community [1]. An RC module mainly reaches a sub-ambient state by dissipating heat to the deep outer space via the well-known “atmospheric window (8–13 μm)” [2]. RC is a phenomenon widely existing in nature. For example, RC process is attributed to the surface frosting of grasses and leaves in later autumn and the surface water freezing in a still lake in winter even though the local ambient air is above the freezing temperature. Any real-world object can radiate heat to the surroundings and meanwhile receives heat from the outside environment according to the fundamental of heat transfer [3]. Therefore, if the outward radiative heat flux is greater than the inward absorbed heat flux, a net RC effect is produced.

RC technology has great potential to be applied in the building sector due to its structural simplicity and environmental friendliness [4,5]. By combining RC collectors that consume no or negligible energy with building envelopes, a portion of building energy demand can be covered by the building-integrated RC system in a renewable and green manner. According to the architectural configuration, the RC module can generally be installed either on the facade [6,7], or the flat roof [8,9], or

the pitched roof [10], especially on the non-sunward facing roof where solar radiation usually remains at low levels and thus making possible the daytime RC even with materials showing not extremely high solar reflectance [11]. Generally, the building-integrated RC system can either be designed as a passive or an active system. A passive RC system such as a cool roof usually delivers coldness to the indoor space through buoyancy-driven or reduces heat gain to the building mass by strongly rejecting solar radiation and radiating waste heat simultaneously, but suffer from lower cooling performance and undesired cooling gain in cold seasons [9]. By contrast, an active RC system supplies cooling energy to the indoor environment in a more effective way through a driving unit such as a water pump or a draft fan which consumes a small amount of external energy [12]. The active RC system shows a higher cooling capacity compared to the passive system and matches with the seasonal energy demand better in buildings, but also bring unfortunate side effect of adding complexity and operating cost to the system.

RC performance is highly influenced by local environmental conditions. In general, a radiative cooler will reach a lower stagnation temperature or offer a greater RC flux in an environment with lower relative humidity [13], less cloud coverage [14], higher altitude [15], and lower solar intensity (for daytime RC application scenarios) [16]. Exper-

\* Corresponding authors.

E-mail addresses: yuehong.su@nottingham.ac.uk (Y. Su), peigang@ustc.edu.cn (G. Pei).

### Nomenclature

$d$	distance/thickness, m;
$\rho$	reflectance, -;
$E$	radiation power, W/m <sup>2</sup> ;
$\sigma$	Stefan–Boltzmann constant, -;
$G$	solar radiation, W/m <sup>2</sup> ;
$\lambda$	wavelength, $\mu\text{m}$ ;
$h$	heat transfer coefficient, W/(m <sup>2</sup> ·K);
$\beta$	inclination angle, rad;
$k$	thermal conductivity, W/(m·K);
$\theta$	zenith angle, rad;
$l$	length, m;
$\tau$	transmittance, -;
$Nu$	Nusselt number, -

### Abbreviation and subscripts

$Q$	thermal power, W/m <sup>2</sup> ;
$a$	ambient air;
$Ra$	Rayleigh number, -;
$c$	cover;
$U$	Overall heat-transfer coefficient, W/(m <sup>2</sup> ·K);
conv	convection;
$u$	wind velocity, m/s;
$e$	emitter

### Greek Symbols

rad	radiation;
$(\tau\alpha)$	Transmittance-absorptance product, -;
rad_net	net radiation;
$\varepsilon$	emissivity, -;
$s$	sky

imental studies have demonstrated that an RC module with a daytime cooling capacity in a quite arid region failed to realize the same effect under a circumstance where the air is extremely humid [17]. The RC performance will be deteriorated if the sky is cloudy, as a cloud is essentially a cluster of water droplets and/or ice crystals which will severely block the radiative heat transfer between the radiative cooler and the extremely cold outer space; under such situation RC mainly happens between the radiative cooler and the upper atmosphere where the temperature is a couple of degrees lower than the earthbound bodies but much higher than the deep universe. It is easy to understand that the RC performance of an RC module will benefit from higher altitude, as the higher the ground is, the thinner air becomes and thus the less the atmosphere radiates heat to the RC module and obstructs the upward thermal emission from the RC module. The solar radiation is the most sensitive factor which influences the RC performance. Basically, the RC power is one order lower than the intensity of solar radiation, hence a tiny addition of solar energy will cause a large increment of stagnation temperature or a great decrement of net RC power or even vanish the RC effect.

Considering that the above uncontrollable environmental parameters affect the RC performance to a large extent, one can sustain RC in an active way by regulating the spectral profiles of the RC module itself. Although RC technology had been restricted to nighttime application for many years, daytime radiative cooling (d-RC) has been realized in recent years due to the realize of radiative emitter with near-ideal spectral selectivity. In 2014, Fan's group [18] designed and prepared a spectrally selective photonic radiative cooler which shows extremely high solar reflectance and high emissivity in the “atmospheric window”. The radiative cooler can be cooled to 4.9 °C below ambient temperature when exposed to direct sunlight exceeding 850 W/m<sup>2</sup>. Fan et al.'s work [18] is widely seen as a milestone in the development of RC technology. Thereafter, RC saw rapid development towards scalization, high-efficiency,

affordability, and reliability, etc. With the increasing advancement in regulating the spectral profile of the radiative emitter in micro- and nano-scales, RC has been involved in outdoor personal cooling [19,20], passive cooling of solar cells [21,22], and nighttime power generation [23,24], etc. Particularly, many researchers have attempted to enhance the RC capacity by optimizing the spectral selectivity of the radiative emitter in a easier, cheaper, and more scalable way [25–29]. For the realization of RC to the greatest extent, the emitter of an RC module should at least possess the highest possible emissivity in the “atmospheric window” to strongly dump long-wave radiative heat to the sky [30]. Meanwhile, the emitter shall exhibit the highest possible reflectance in other bands, allowing the emitter to reject radiative heat from the local environment and to reach the lowest possible stagnation temperature [31]. For radiative coolers that aim to effectively work during the daytime under a high-level incident solar radiation, in particular, the emitter is restricted to show a reflectance of around 95% or even more in the solar spectrum (0.2–3  $\mu\text{m}$ ) in order to reject the vast majority of solar radiation [18,32]. For spectrally selective nighttime radiative coolers, on the other hand, the emitter only has to show spectral selectivity in the middle- and far-infrared wavelengths, regardless of its spectral profile in the solar radiation band. d-RC is supposed to be more suitable for building energy saving of office and commercial buildings in which energy consumption mainly takes place during the daytime [33]. The spectral characteristic of the ideal d-RC emitter is shown in Fig. 1 (red line). The AM 1.5 (AM = air mass) solar spectrum is a widely adopted physical quantity in solar energy technologies and is defined as the spectral distribution of solar intensity projected onto the earth's surface with an incident angle of about 48.2 °C [34].

The relatively low power density of d-RC modules, compared to that of the vapor compression refrigerator, is the main barrier for its promotion to real-world applications [35]. Though scholars have successfully developed near-ideal d-RC emitters with solar reflectance greater than 95%, the d-RC module still suffers from low-level RC flux during the daytime and there is little space for further development of the emitter regarding sunlight rejection. Besides, even a 1% improvement of solar reflectance under such a big base figure may involve massive efforts. While the effect of spectral modification of the emitter is widely appreciated by researchers, the great impacts that can result from controlling the spectral property of the convection cover are frequently not considered to be too profitable. The cover in an RC module is mainly used to limit the convection cooling loss as the emitter approaches its stagnation temperature. The most common cover material employed in existing RC modules is the low-density polyethylene (LDPE) film which shows high transmittance throughout the concerned bands from solar spectrum to far-infrared region, that is, the LDPE film presents no spectral selectivity in these bands [36]. Therefore, an extra opportunity brings out by developing spectrally selective covers that match better with the spectral requirement of d-RC cover [37,38]. Equipping with a cover that shows high solar reflectance while high mid-infrared transmittance can boost the net RC cooling power of a typical d-RC device to nearly 100 W/m<sup>2</sup> [37]. Provided the cover works as a mid-infrared transparent solar absorber, the underneath radiative cooler can also be free from the exposure of sunlight and reach a deep sub-ambient temperature [38]. However, the cooling potential of a radiative cooler can be further enhanced by employing a cover with better spectral selectivity. As is shown in Fig. 1 (blue line), the ideal d-RC cover should show high transmittance within the “atmospheric window” to allow thermal radiation from the emitter to go through freely. Besides, the cover should show low transmittance (high reflectance) excluding the transparent window, especially in the solar spectrum for d-RC applications, indicating that the cover can act as a guardian rejector to rebound most of the solar radiation and only allow a small fraction of sunlight projecting onto the emitter which also shows strong solar reflectance. Preparing a spectrally selective cover that can simultaneously achieve high solar reflectance and long-wave transmittance is challenging but engineering accessible [39–41], especially with the booming development in micro- and

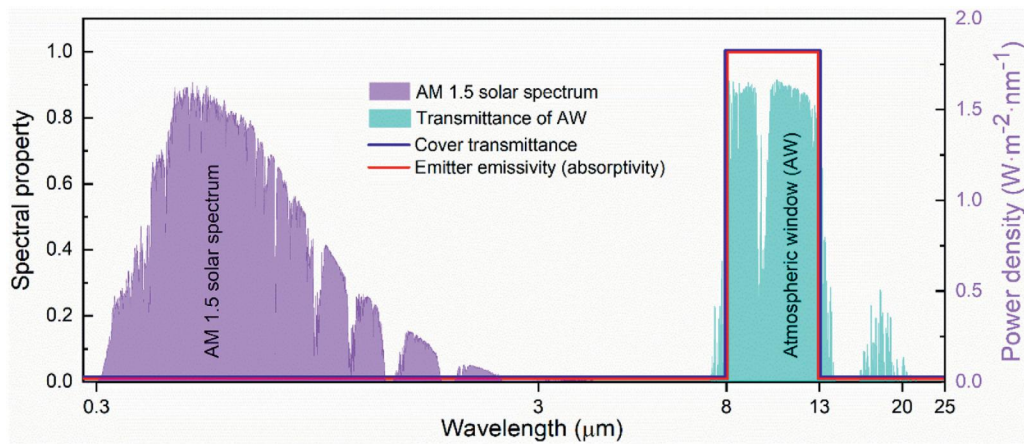


Fig. 1. Spectral characteristics of the ideal cover and emitter for daytime radiative cooling.

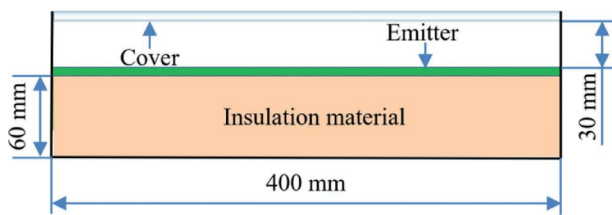


Fig. 2. Section structure of the radiative cooling module.

nano-material technologies. The cold mirror that has been widely applied in infrared instruments is a good candidate that meets the spectral selectivity of d-RC cover [42,43].

Though the effect of the spectral selectivity of the cover on the cooling performance of the radiative cooler has been experimentally demonstrated [37,38], a systematic parametric study can be further conducted to elucidate the underlying mechanisms of the spectral profile of the cover. In the present study, therefore, we quantitatively characterized the performance enhancement of the RC module equipped with a spectrally selective cover via heat transfer analysis. A mathematic model is developed for calculating the cooling performance of the RC module under different working conditions. Four RC modules, with different spectral profiles of the cover and emitter, is selected and compared with each other to demonstrate the effect of spectral selectivity on the key performance indicators, i.e., stagnation temperature and net RC power, of the modules.

## 2. Description of the RC module

The RC module present in this study is shown in Fig. 2, which mainly includes a convection cover and an emitter, associated with some insulation materials below the emitter. The basic functions of the cover and insulations are suppressing convective and conductive cooling losses. The emitter of the RC module, with a dimension of  $0.4 \times 0.4$  m, is placed horizontally to get the maximum view factor relative to the sky and thus get the best RC performance [44]. The vertical distance between the cover and the emitter is 0.03 m. A 60 mm-thick layer of phenolic foam, with a thermal conductivity of 0.028 W/(m·K) served as the insulation material.

According to the spectral profiles of the cover and emitter, four different RC modules is proposed as follows:

- The RC module with a spectrally non-Selective Cover and a non-Selective Emitter (n-SC/n-SE)
- The RC module with a spectrally non-Selective Cover and a Selective Emitter (n-SC/SE, the most common RC device in previous studies)

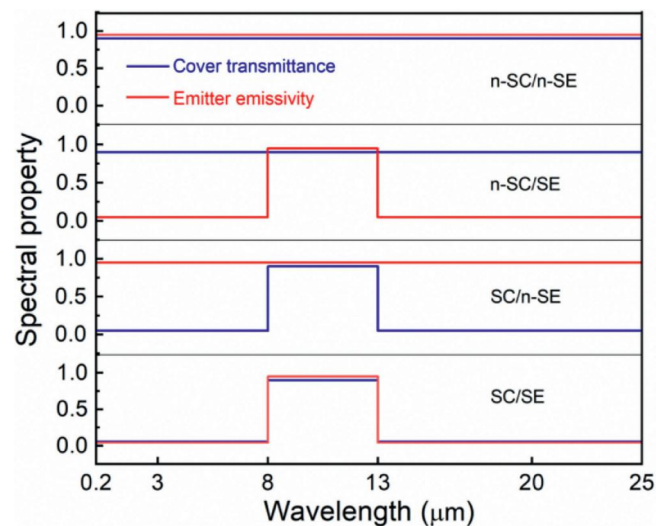


Fig. 3. The spectral profile of the cover and emitter of the four RC modules.

- The RC module with a spectrally Selective Cover and a non-Selective Emitter (SC/n-SE)
- The RC module with a spectrally Selective Cover and a Selective Emitter (SC/SE)

The spectral profile of the cover and emitter of the four RC modules are detailed in Table 1 and Fig. 3. It is clear that the cover transmittance and emitter emissivity in the “atmospheric window” is 0.9 and 0.95 respectively for all the four RC modules as a base for the RC feature. The spectral difference among the four modules lies in other bands aside from the “atmospheric window” (hereafter referred to as the “other bands”). For those modules with a spectrally non-selective cover, the cover transmittance in the other bands is 0.9 but switch to 0.05 for those modules with a spectrally selective cover. For those modules with a spectrally non-selective emitter, the emitter emissivity in the other bands is 0.95 but switch to 0.05 for those modules with a spectrally selective emitter. The schematic diagram of the SC/SE based module is further shown in Fig. 4.

## 3. Mathematic model

A steady-state mathematic model is developed for the characterization of the RC performance of the four modules. The following assumptions are adopted to simplify modeling and analysis [45]:

**Table 1**  
The spectral profile of the cover and emitter of the four RC modules.

Spectral profile	n-SC/n-SE	n-SC/SE	SC/n-SE	SC/SE
Cover transmittance in the “atmospheric window” ( $\alpha = 0.05$ )	0.9	0.9	0.9	0.9
Cover transmittance in the other bands ( $\alpha = 0.05$ )	0.9	0.9	0.05	0.05
Emitter emissivity (absorptivity) in the “atmospheric window”	0.95	0.95	0.95	0.95
Emitter emissivity (absorptivity) in the other bands	0.95	0.05	0.95	0.05

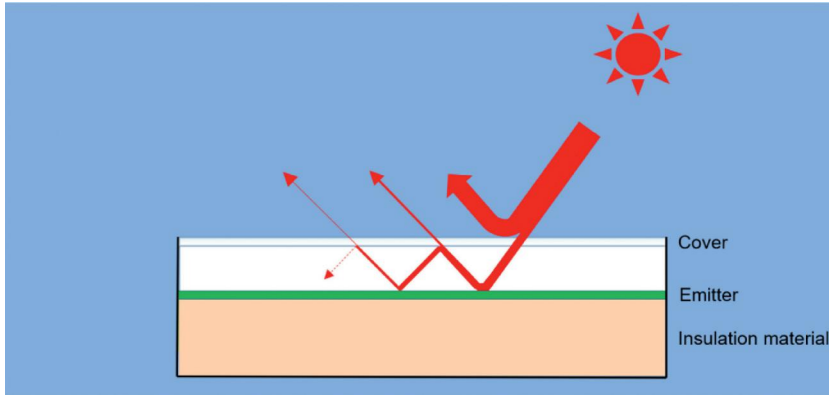


**Fig. 4.** Schematic diagram of the radiative cooling module equipped with a spectrally selective cover and emitter.

- The spectral properties of the cover and emitter are independent of temperature.
- The temperatures of the cover and emitter are independent of direction.
- The cover and emitter are considered as diffusers; thus, their spectral properties are independent of angle.
- The heat or cooling loss takes place along the four side edges of the RC module is negligible.

As the RC module mainly consists of two components, namely, the cover and the emitter, the mathematic model primarily comprises two main equation sets, namely, (i) energy-balance equation of the cover and (ii) energy-balance equation of the emitter.

### 3.1. Energy-balance equation of the cover

Take the cover as the control volume, it exchanges heat with the ambient air, the sky, the emitter, and absorbs solar energy from the sun. Therefore, the heat balance equation of the transparent cover is expressed as follows:

$$h_{ac}(T_a - T_c) + h_{sc}(T_s - T_c) + h_{ec}(T_e - T_c) + \alpha_c G = 0 \tag{1}$$

where  $h_{ac}$  and  $h_{sc}$  are respectively the convective and radiative heat transfer coefficients between the cover and the local environment,  $W/(m^2 \cdot K)$ ;  $h_{ec}$  is the heat transfer coefficient between the cover and the emitter,  $W/(m^2 \cdot K)$ ;  $T_a$ ,  $T_c$ ,  $T_s$ , and  $T_e$  are the temperatures of the ambient air, cover, sky, and emitter, respectively, K;  $\alpha_c$  is the absorptivity of the cover in the solar spectrum; and  $G$  is the solar radiation,  $W/m^2$ .

The sky temperature is derived as follows [46]:

$$T_s = 0.0552T_a^{1.5} \tag{2}$$

The convective and radiative heat transfer coefficients between the cover and the environment are calculated as Eqs. (3) and (4), respectively [47]:

$$h_{ac} = 2.8 + 3.0u_a \tag{3}$$

and

$$h_{sc} = \epsilon_c \sigma (T_s^2 + T_c^2) (T_s + T_c) \tag{4}$$

where  $u_a$  is the wind velocity, m/s;  $\epsilon_c$  is the cover emissivity; and  $\sigma$  is the Stefan-Boltzmann constant.

The heat exchange between the cover and the emitter consists of two parts, i.e., heat convection and heat radiation. The heat transfer coefficient can be calculated as follows:

$$h_{ec} = h_{ec,conv} + h_{ec,rad} \tag{5}$$

The convective heat transfer coefficient between the cover and the emitter is written as follows [3]:

$$h_{ec,conv} = \frac{Nu \cdot k_a}{d_{ec}} \tag{6}$$

where  $Nu$  is the Nusselt number;  $k_a$  is the thermal conductivity of air between the cover and the emitter,  $W/(m \cdot K)$ ; and  $d_{ec}$  is the vertical distance of the air gap, m.

For a rectangular enclosure with inclination angles ranging from  $0^\circ$  to  $75^\circ$ , if  $T_e > T_c$ , then the Nusselt number can be calculated as follows [3]:

$$Nu = 1 + 1.44 \left( 1 - \frac{1708 \cdot (\sin 1.8\beta)^{1.6}}{Ra \cdot \cos \beta} \right) \left[ 1 - \frac{1708}{Ra \cdot \cos \beta} \right]^+ + \left[ \left( \frac{Ra \cdot \cos \beta}{5830} \right)^{1/3} - 1 \right]^+ \tag{7}$$

where the + exponent indicates that only positive values are used for terms within the square brackets; in case of negative values, zero is used;  $\beta$  is the inclination angle of the collector, rad; and  $Ra$  is the Rayleigh number.

If  $T_e < T_c$ , then the Nusselt number is expressed as follows [48]:

$$Nu = 1 + \left[ 0.364 \frac{l_e}{d_{ec}} Ra^{1/4} - 1 \right] \sin \beta \tag{8}$$

where  $l_e$  is the length of the emitter, m.

If  $T_e = T_c$ , then no heat convection occurred between the cover and the emitter. Therefore, the Nusselt number is equal to zero.

The radiative heat transfer coefficient between the cover and the emitter, considering the transmittance of the cover and the multiple-reflections between the two components, is derived as follows [45]:

$$h_{ec,rad} = \frac{\alpha_c \epsilon_e \sigma T_e^4 - \alpha_e \epsilon_c \sigma T_c^4}{(1 - \rho_c \rho_e) \cdot (T_e - T_c)} \tag{9}$$

where  $\epsilon_e$  is the emitter emissivity;  $\alpha_c$  and  $\alpha_e$  are respectively the absorptivity of the cover and the emitter;  $\rho_c$  and  $\rho_e$  are the reflectance of the cover and the emitter, respectively.

### 3.2. Energy-balance equation of the emitter

Take the emitter as the control volume, it exchanges heat with the cover, the sky, the hypothetical backside working medium, and with the ambient air through the backside thermal insulation, as well as absorbs solar energy from the sun. Therefore, the heat balance equation of the collecting surface is expressed as follows:

$$U_{ae}(T_a - T_e) + h_{ec}(T_c - T_e) + (\tau\alpha)_e G - Q_{rad,net} \pm Q_{output} = 0 \quad (10)$$

where  $U_{ae}$  is the overall heat transfer coefficient between the emitter and the local environment,  $W/(m^2\cdot K)$ ;  $(\tau\alpha)_e$  is the effective transmittance-absorptance product of the RC module;  $Q_{rad,net}$  is the net radiative power of the emitter,  $W/m^2$ ;  $Q_{output}$  is the heat (“-” sign) or cooling energy (“+” sign) extracted from the emitter in order to maintain the emitter at a set temperature,  $W/m^2$ . Obviously,  $Q_{output}$  will turn to zero if the emitter reaches its stagnation temperature.

The backside thermal insulation and the backboard are two thermal barriers between the emitter and ambient air. The heat convective coefficient between the backboard and ambient air is equal to that between the cover and ambient air since the backboard and cover are both in flat-plate structures. Therefore, the overall heat transfer coefficient between the emitter and the local environment is calculated as follows [49]:

$$U_{ae} = \frac{1}{\frac{1}{h_{ac}} + \frac{d_b}{k_b}} \quad (11)$$

where  $d_b$  is the thickness of the back insulator, m; and  $k_b$  is the thermal conductivity of the back insulator,  $W/(m\cdot K)$ .

The effective transmittance-absorptance product of the module is derived as follows [46]:

$$(\tau\alpha)_e = \frac{\tau_c \alpha_e}{1 - (1 - \alpha_e) \rho_c} \quad (12)$$

where  $\alpha_e$  is the absorptivity of the emitter; and  $\tau_c$  and  $\rho_c$  are respectively the transmittance and reflectance of the cover.

The net radiative power of the emitter is written as follows:

$$Q_{rad,net} = Q_{rad,e} - Q_{rad,se} \quad (13)$$

The outward radiation of the emitter ( $Q_{rad,e}$ ) is computed as follows [50]:

$$Q_{rad,e} = \int_0^\infty \left[ \frac{E_{b,\lambda}(T_e) \cdot (1 - \rho_{c,\lambda}) - \epsilon_{c,\lambda} \cdot E_{b,\lambda}(T_c)}{1/\epsilon_{e,\lambda} - ((1 - \epsilon_{e,\lambda})/\epsilon_{e,\lambda}) \cdot \rho_{c,\lambda}} \right] d\lambda \quad (14)$$

where  $E_{b,\lambda}$  is the spectral radiation power of the blackbody,  $W/(m^2 \cdot \mu m)$ ;  $\rho_{c,\lambda}$  and  $\epsilon_{c,\lambda}$  are respectively the spectral reflectance and emissivity of the cover; and  $\epsilon_{e,\lambda}$  is the spectral emissivity of the emitter.

The radiation from the sky to the emitter  $Q_{rad,se}$  is expressed as follows [50]:

$$Q_{rad,se} = 2 \int_0^\infty \int_0^{\pi/2} \epsilon_{s,\lambda}(\lambda, \theta) \cdot E_{b,\lambda}(\lambda, T_a) \cdot \alpha_{e,\lambda}(\lambda, \theta) \times \tau_{c,\lambda}(\lambda, \theta) \sin \theta \cos \theta d\theta d\lambda \quad (15)$$

where  $\epsilon_{s,\lambda}$  and  $\tau_{c,\lambda}$  are respectively the spectral emissivity of the sky and transmittance of the cover; and  $\theta$  is the zenith angle, rad.

The mathematic model was experimentally validated in a previous work focused on the thermal analysis of a combined photovoltaic-photothermic-nocturnal radiative cooling (PV-PT-RC) module [50]. A favorable consistency was observed between the experimental and simulated stagnation temperatures of the PV-PT-RC module. The geometric structure of the PV-PT-RC module is similar to that of the present RC module and hence the simulation results of this study are convincing.

## 4. Results and discussion

Based on the mathematic model developed in Section 3, we conduct an extensive investigation on the performance of the four RC modules under different working conditions. Standard operating conditions are set before the simulation study, as listed in Table 2.

**Table 2**  
Standard operating conditions for the RC module.

Parameter	Value
Wind velocity (m/s)	2
Ambient temperature (°C)	30
Relative humidity (%)	50
Solar radiation ( $W/m^2$ )	800 (daytime) or 0 (nighttime)

### 4.1. RC performance in daytime

Fig. 5 illustrates the performance of the four typical RC modules during the daytime exposed to the sunlight directly with solar radiation of  $800 W/m^2$ . Different from the other three modules, the n-SC/n-SE based module cannot achieve a d-RC effect in such a case. In fact, it shows quite good solar heating performance during the daytime. Specifically, its net solar heating power reaches around  $605.1 W/m^2$  at zero-reduced temperature (when the emitter temperature equals the ambient temperature) and its stagnation temperature records about  $92.6^\circ C$ . As the emitter shows a high absorptivity of 0.95 in the solar spectrum and the cover allows 90% of solar radiation to get through, most of the incident solar energy is absorbed and then is dissipated into thermal energy which, in turn, heats up the emitter of the n-SC/n-SE based module. On the other hand, due to the high emissivity (0.95) in those bands outside the solar spectrum, the n-SC/n-SE based module loses a part of long-wave thermal emission and thus is expected to be inferior in thermal efficiency than the typical solar thermal collector which is usually equipped with solar selective absorbing coatings.

The other three modules, by contrast, show d-RC capacities and the same changing trend as the emitter temperature increases. The cooling performance of the n-SC/SE based and SC/n-SE based modules are rather close. Their net RC power is respectively  $35.7$  and  $33.8 W/m^2$  and their stagnation temperature is  $19.2$  and  $19.8^\circ C$ , respectively. It is indicated that, therefore, the approach that adopts a spectrally non-selective emitter but a spectrally selective cover can be treated as an alternative to the typical solution of employing a spectrally selective emitter but a spectrally non-selective cover. This makes sense indeed for those situations the emitter has to show high emissivity outside the “atmospheric window” for other purposes but also has a demand for d-RC. It is also clear from Fig. 5 that, by fully taking advantage of the benefit from spectral selective cover and spectrally emitter together, the SC/SE based module presents much better cooling performance than the n-SC/SE and SC/n-SE based modules in such a daytime working condition with strong solar intensity. In specific, the SC/SE based module can realize a stagnation temperature of approximately  $10.0^\circ C$ , achieving a further temperature reduction of  $9.2^\circ C$  compared to the typical n-SC/SE based module. Besides, the net RC power of the SC/SE based module reaches about  $62.4 W/m^2$ , indicating that a performance improvement of 74.8% is observed in this case. Therefore, applying the SC/SE based structure offers a potential strategy for mitigating the challenge of improving RC density. It is admitted that achieving a near-perfect spectrally selective cover is challenging. However, referring to the development route of high-performing radiative emitter over the past few years, it is conceivable to realize the desired spectrally selective cover in the near future.

### 4.2. RC performance in nighttime

Along with the investigation of the four typical modules working in daytime conditions, we also evaluated their performance in the nighttime case. As shown in Fig. 6, the cooling power of all the four modules decline almost linearly as the emitter temperature decreases. Unlike the situation in the daytime, the net RC flux of the n-SC/n-SE based module is even slightly greater than the rest of RC modules in the nighttime, with the value approaches  $83.9 W/m^2$ . This is because the high emissivity in the other bands also promotes the cooling performance

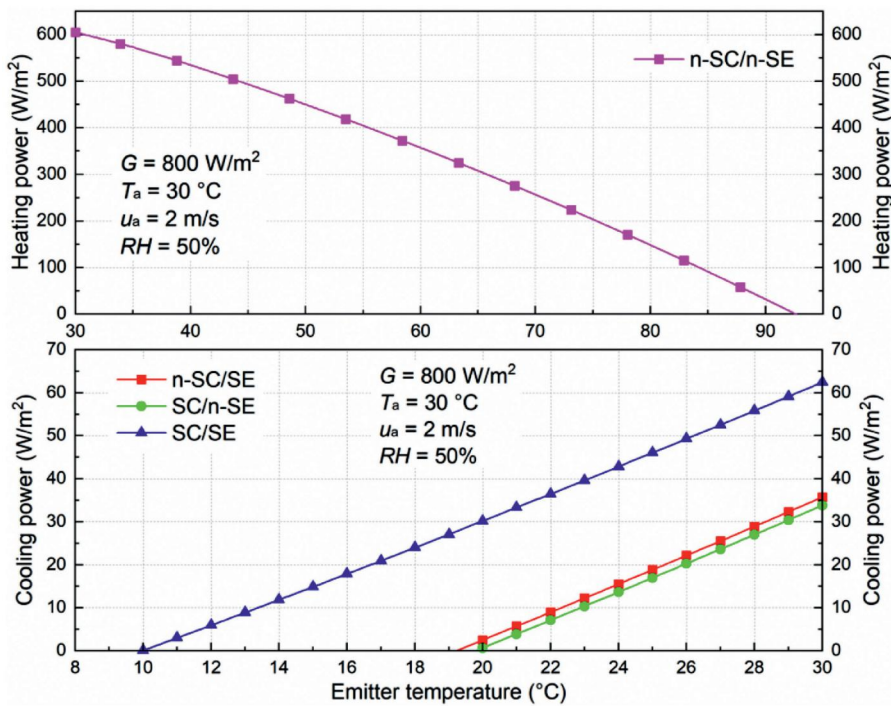


Fig. 5. Performance of the four RC modules in a day-time condition.

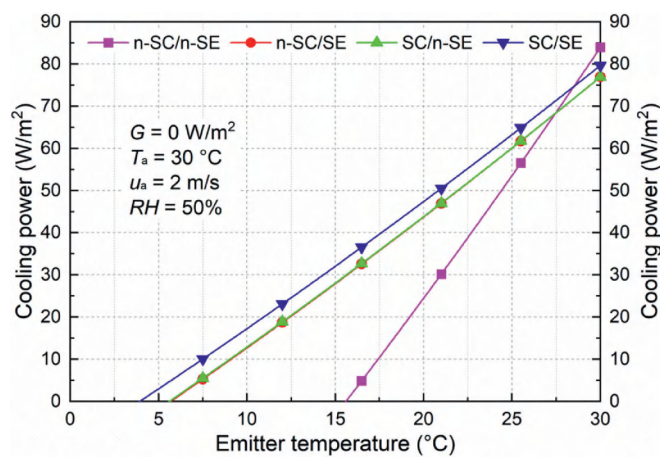


Fig. 6. Performance of the four RC modules in a nighttime condition.

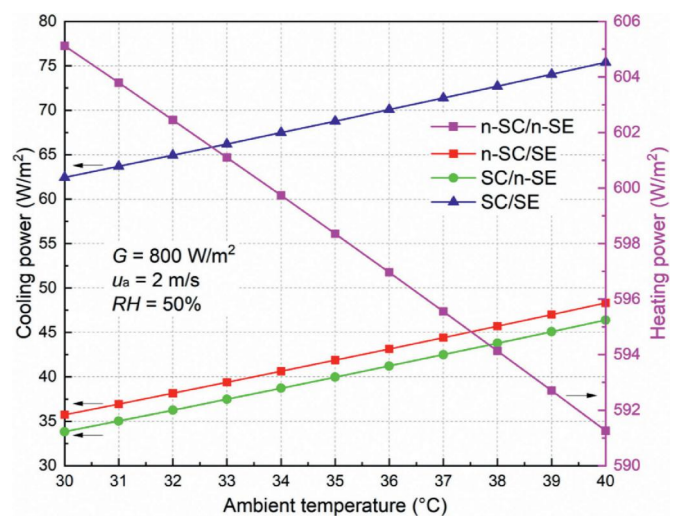


Fig. 7. Performance of the four RC modules at different ambient temperatures.

by realizing a net inward cooling flux when the emitter temperature is higher than a certain level which depends on certain conditions. In the present study, for example, the cooling density of the n-SC/n-SE based module is greater than the n-SC/SE based and SC/n-SE based modules when the emitter temperature is higher than 27.4 °C and is superior to the SC/SE based module when the emitter temperature is higher than 28.5 °C. However, the cooling power of the n-SC/n-SE based module declines much faster than that of the rest three modules as the emitter temperature decreases, resulting in a much higher stagnation temperature. In this study, the nighttime stagnation temperature of the n-SC/n-SE based module is 15.6 °C, which is over 10 °C higher than that of the n-SC/SE based, SC/n-SE based, and SC/SE based modules. Considering that the n-SC/n-SE based module also shows a good daytime solar heating capacity, as demonstrated in Section 4.1, it has the potential to be a dual-functional collector and provide both heat and cooling energy for buildings [35].

The changing curve of the cooling power for the n-SC/SE based and SC/n-SE based modules is nearly overlapped in nighttime working conditions, indicating that their nocturnal cooling performance is more or less the same. Their net RC power and stagnation temperature are about 77.0 W/m<sup>2</sup> and 5.6 °C, respectively. Distinct from the case in the daytime, the cooling performance improvement by employing the SC/SE based structure is not that much in the nighttime condition. Compared to the typical n-SC/SE based module, the net RC flux of the SC/SE based module only increases relatively by 3.5%, and a further stagnation temperature reduction of only 1.8 °C is observed. Therefore, for the nighttime RC application, it may not make much sense to equip the module with both spectrally selective cover and emitter. It is more feasible to employ only a spectrally selective cover or a spectrally selective emitter considering the preparation cost.

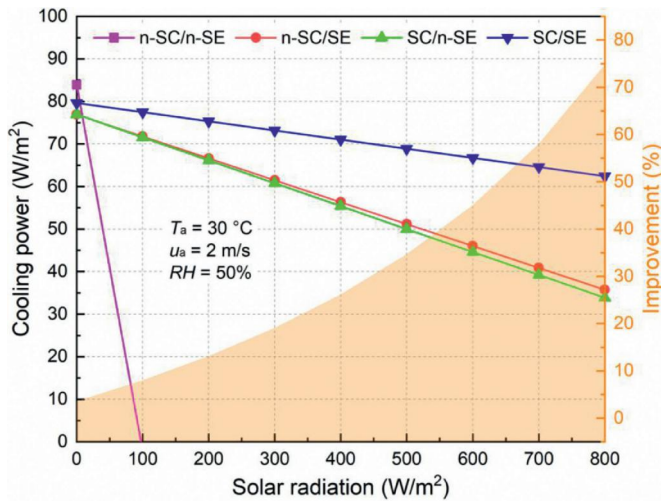


Fig. 8. Performance of the four RC modules under different solar radiation.

4.3. RC performance under different ambient temperatures

Cooling energy is more required in high-temperature weather. Therefore, we also assessed the RC performance of the four modules in an

tended range of high ambient temperatures, and the results are shown in Fig. 7. Higher ambient temperature leads to higher emitter temperature and thus greater outward thermal emission of the emitter. As the solar radiation is set at 800 W/m<sup>2</sup>, the n-SC/n-SE based module cannot achieve the cooling effect and its net solar heating power decreases gradually from 605.1 to 591.3 W/m<sup>2</sup> as the ambient temperature increases from 30 to 40 °C. In contrast, the other three modules exhibit enhanced cooling performance as the ambient temperature increases. The SC/SE based module still shows the best cooling behavior among the four modules, with the net RC power increases from 62.4 to 75.4 W/m<sup>2</sup> as the ambient temperature elevates from 30 to 40 °C. The n-SC/SE and SC/n-SE based modules exhibit close net RC power, with the values being about 35 and 47 W/m<sup>2</sup> when the ambient temperature is respectively 30 and 40 °C.

4.4. RC performance under different solar radiation

As the solar intensity is a key factor that affects the cooling performance of the RC module in the daytime. We further studied the cooling performance of the four modules under different solar radiation, and the results are shown in Fig. 8. The cooling performance of the n-SC/n-SE based module is very sensitive to the solar intensity, with the cooling power descends sharply from 83.9 to 0 W/m<sup>2</sup> as the solar radiation increases from 0 to around 100 W/m<sup>2</sup>, indicating that the n-SC/n-SE based module is unable to realized RC effect in most daytime situations. The

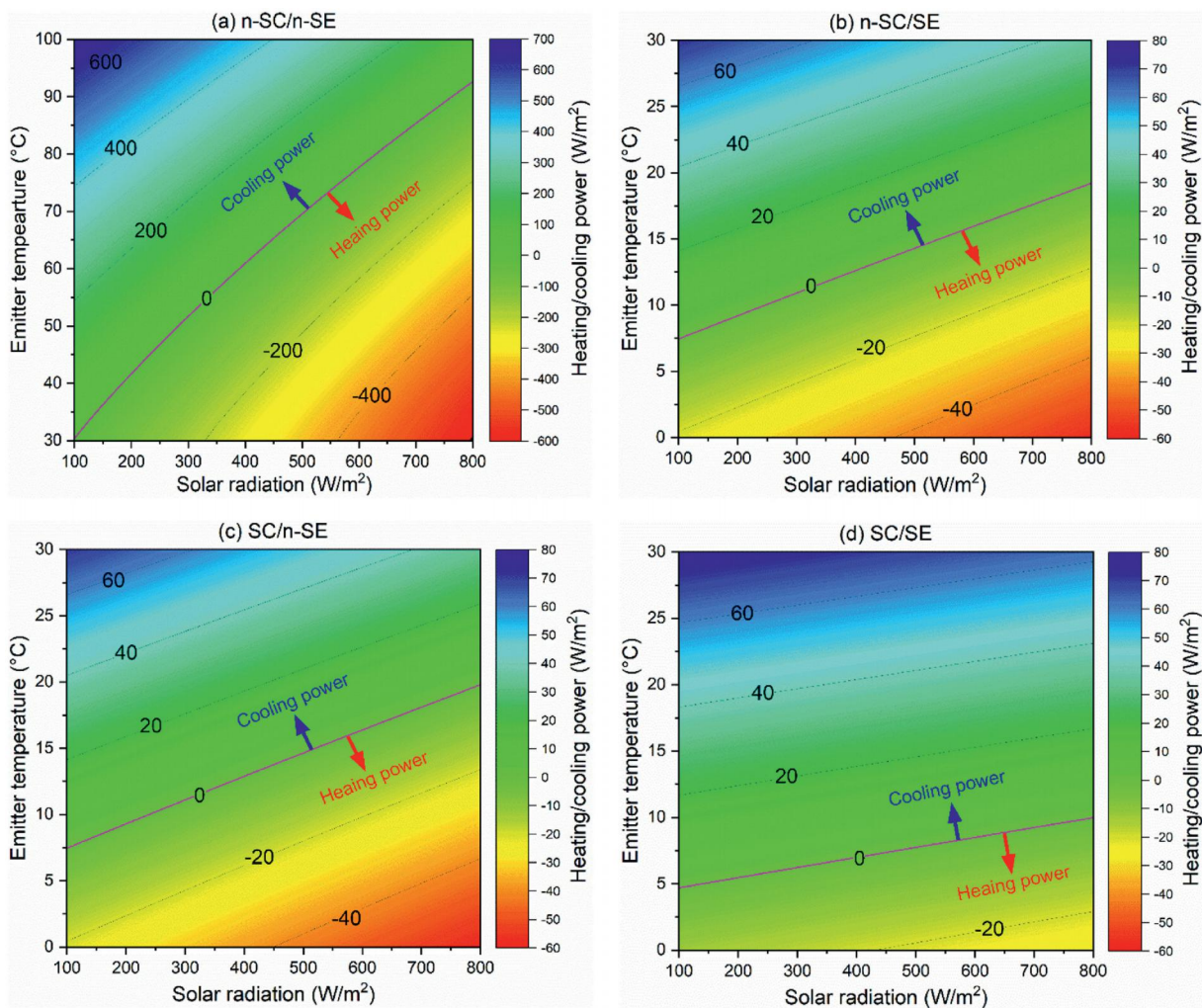
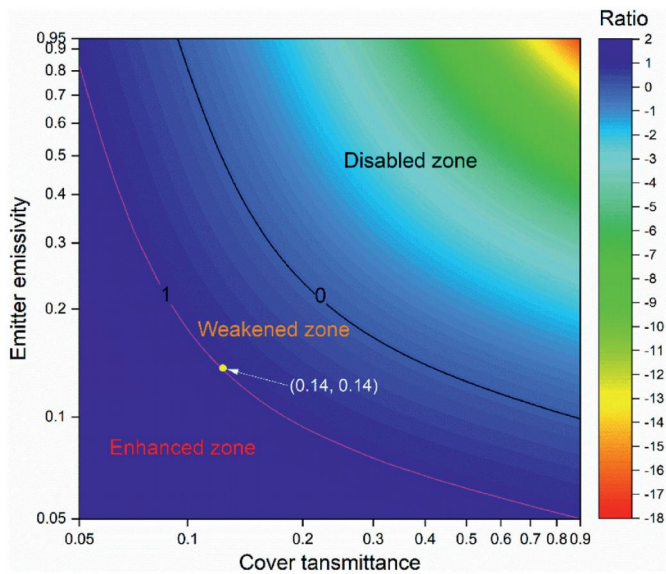


Fig. 9. Coupling effect of emitter temperature and solar radiation on the performance of the four modules at the ambient temperature of 30 °C.



**Fig. 10.** The cooling capacity of the SC/SE based module with different spectral profiles (relative to the cooling performance of the n-SC/SE based module).

cooling power of the n-SC/SE based module is getting greater than that of the SC/n-SE based module as the solar radiation increases, but the gap is tiny even at a very high solar intensity of  $800 \text{ W/m}^2$ . The SC/SE based module is the least sensitive to the solar radiation regarding cooling performance, with the cooling power decreases gradually from  $79.7$  to  $62.4 \text{ W/m}^2$  as the solar radiation goes up from  $0$  to  $800 \text{ W/m}^2$ . Besides, as the solar radiation increases, the superiority of the SC/SE based module in terms of cooling performance comparing the typical n-SC/SE based module magnifies. As is shown in Fig. 8, the cooling power improvement rises from  $3.5\%$  to  $74.7\%$  as the solar radiation increases from  $0$  to  $800 \text{ W/m}^2$ .

#### 4.5. Coupling effects of emitter temperature and solar radiation

Emitter temperature is another key parameter, in addition to solar radiation, that affects the cooling performance. In this section, therefore, we examined the coupling effect of emitter temperature and solar radiation on the performance of the four modules, as the results presented in Fig. 9. It is clear from the contour plots that greater cooling power will be gained at higher emitter temperature and lower solar radiation for all the four modules. As illustrated in Fig. 9(a), the n-SC/n-SE based module cannot achieve a sub-ambient d-RC effect as the solar radiation is greater than  $100 \text{ W/m}^2$ . The contour plots of the n-SC/SE based and SC/n-SE based modules are quite similar, with the sub-ambient d-RC effect can be realized in nearly half of the situations. By contrast, the SC/SE based module can reach a sub-ambient d-RC effect in most situations, except in those the emitter temperature is extremely low or the solar radiation is rather higher, further demonstrating that the SC/SE based module is more suitable for d-RC application scenarios.

#### 4.6. Compromised strategy to daytime radiative cooling for the SC/SE based module

As demonstrated in the above Sections, the SC/SE based module shows much better cooling performance than the n-SC/SE based structure that is widely adopted in reported studies, but it may be the case in real-world applications that achieving near-perfect spectral properties for the cover and the emitter simultaneously is laboursome and costly. But from another point of view, the SC/SE idea provides a compromised strategy to realize effective d-RC by using not very elaborated cover and

emitter. Fig. 10 illustrates the cooling capacity of the SC/SE based module with different spectral profiles under solar radiation of  $800 \text{ W/m}^2$  by comparing it to the cooling power of the n-SC/SE based module. The contour plot is divided into three zones, namely, disabled zone, weakened zone, and enhanced zone. The words “disabled zone” signifies that in this area the SC/SE based module is unable to achieve d-RC in such an environmental condition due to the poor spectral selectivity of both the cover and the emitter. In the weakened zone, the SC/SE based module can realize d-RC but its performance is inferior to the n-SC/SE based module with a near-perfect emitter regarding spectral selectivity. The emphasis lies in the enhanced zone as the SC/SE based module shows better d-RC performance than the n-SC/SE based module in this section. The larger the enhanced zone is, the more leeway leaves for compromises regarding the spectral selective of the cover and the emitter. While the n-SC/SE based module requires an emitter that reflects around  $95\%$  of solar radiation, the SC/SE based module can reach a same cooling performance by, for example, employing an easily engineered emitter that reflects only  $86\%$  of solar radiation ( $\alpha = 0.14$ ), associated with a cover that shows solar transmittance of  $0.14$ .

## 5. Conclusions

In the present work, four different types of RC modules with individual spectral profiles are proposed to demonstrate the effect of spectral selectivity on the RC performance under different environmental conditions. A mathematic model is developed to conduct the simulation analysis and help to draw the following main findings:

- (1) The n-SC/n-SE based module cannot achieve d-RC in most of the daytime situations but has the potential to be a dual-functional collector for daytime heating and nighttime cooling.
- (2) The SC/SE based module shows a net RC power which is 1.8 times that of the typical n-SC/SE based module in a daytime working case, but the nocturnal performance enhancement by applying the SC/SE based structure is not distinct.
- (3) The SC/SE based module can reach the sub-ambient d-RC effect in most situations, except in those the emitter temperature is extremely low or the solar radiation is rather higher.
- (4) The SC/SE based structure offers an opportunity to achieve d-RC by employing devices equipped with moderate spectrally selective cover and emitter.

Overall, the idea of using spectrally selective cover and emitter together contributes an alternative strategy to alleviate the challenge of effectively running d-RC devices in real-world applications. Further researches should attach primary importance to potential cover materials with fitted spectral selectivity, as well as mechanical strength weather fastness.

## Declaration of Competing Interest

We declare that we have no financial and personal relationships with other people or organizations that can inappropriately influence our work, there is no professional or other personal interest of any nature or kind in any product, service and/or company that could be construed as influencing the position presented in, or the review of, the manuscript entitled, “Effect of the spectrally selective features of the cover and emitter combination on radiative cooling performance”.

Authors

## CRedit authorship contribution statement

**Mingke Hu:** Methodology, Software, Formal analysis, Investigation, Funding acquisition, Writing - original draft, Writing - review & editing. **Suhendri:** Software, Formal analysis, Writing - review & editing. **Bin Zhao:** Methodology, Formal analysis, Writing - review & editing.

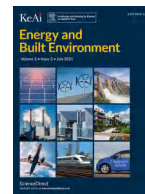
**Xianze Ao:** Formal analysis, Writing - review & editing. **Jingyu Cao:** Formal analysis, Funding acquisition. **Qiliang Wang:** Formal analysis. **Saffa Riffat:** Resources, Project administration, Supervision. **Yuehong Su:** Supervision, Project administration, Funding acquisition, Writing - review & editing. **Gang Pei:** Conceptualization, Resources, Supervision, Project administration, Funding acquisition.

## Acknowledgments

This study was sponsored by the National Key R and D Program of China (2018YFD0700200), H2020 Marie Skłodowska-Curie Actions - Individual Fellowships (842096), National Natural Science Foundation of China (NSFC 51906241, 51761145109 and 51776193), Anhui Provincial Natural Science Foundation (1908085ME138), and China Postdoctoral Science Foundation (2019M652209).

## References

- J. Liu, Z. Zhou, J. Zhang, W. Feng, J. Zuo, Advances and challenges in commercializing radiative cooling, *Mater. Today Phys.* (2019).
- J. Feng, K. Gao, M. Santamouris, K.W. Shah, G. Ranzi, Dynamic impact of climate on the performance of daytime radiative cooling materials, *Solar Energy Mater. Solar Cells* 208 (2020) 110426.
- T.L. Bergman, F.P. Incropera, D.P. DeWitt, A.S. Lavine, *Fundamentals of Heat and Mass Transfer*, John Wiley & Sons, 2011.
- X. Lu, P. Xu, H. Wang, T. Yang, J. Hou, Cooling potential and applications prospects of passive radiative cooling in buildings: the current state-of-the-art, *Renew. Sustain. Energy Rev.* 65 (2016) 1079–1097.
- M. Zeyghami, D.Y. Goswami, E. Stefanakos, A review of clear sky radiative cooling developments and applications in renewable power systems and passive building cooling, *Solar Energy Mater. Solar Cells* 178 (2018) 115–128.
- M. Sameti, A. Kasaeian, Numerical simulation of combined solar passive heating and radiative cooling for a building, *Building Simulation* 8 (2015) 239–253.
- C. Yong, W. Yiping, Z. Li, Performance analysis on a building-integrated solar heating and cooling panel, *Renew Energy* 74 (2015) 627–632.
- D. Goodfield, G.B. Smith, A.R. Gentle, M.D. Arnold, M.A. Gali, M.B. Cortie, The importance of surface finish to energy performance, *Renew. Energy Environ. Sustain.* (2017) 2.
- H. Fang, D. Zhao, J. Yuan, A. Aili, X. Yin, R. Yang, et al., Performance evaluation of a metamaterial-based new cool roof using improved Roof Thermal Transfer Value model, *Appl. Energy* 248 (2019) 589–599.
- D. Zhao, A. Aili, X. Yin, G. Tan, R. Yang, Roof-integrated radiative air-cooling system to achieve cooler attic for building energy saving, *Energy Build.* (2019) 203.
- B. Zhao, X. Ao, N. Chen, Q. Xuan, M. Hu, G. Pei, General strategy of passive sub-ambient daytime radiative cooling, *Solar Energy Mater. Solar Cells* 199 (2019) 108–113.
- K. Zhang, D. Zhao, X. Yin, R. Yang, G. Tan, Energy saving and economic analysis of a new hybrid radiative cooling system for single-family houses in the USA, *Appl. Energy* 224 (2018) 371–381.
- B. Zhao, M. Hu, X. Ao, G. Pei, Performance evaluation of daytime radiative cooling under different clear sky conditions, *Appl. Therm. Eng.* 155 (2019) 660–666.
- U. Eicker, A. Dalibard, Photovoltaic-thermal collectors for night radiative cooling of buildings, *Solar Energy* 85 (2011) 1322–1335.
- S.N. Bathgate, S.G. Bosi, A robust convection cover material for selective radiative cooling applications, *Solar Energy Mater. Solar Cells* 95 (2011) 2778–2785.
- X. Ao, M. Hu, B. Zhao, N. Chen, G. Pei, C. Zou, Preliminary experimental study of a specular and a diffuse surface for daytime radiative cooling, *Solar Energy Mater. Solar Cells* 191 (2019) 290–296.
- C.Y. Tso, K.C. Chan, C.Y.H. Chao, A field investigation of passive radiative cooling under Hong Kong's climate, *Renew. Energy* 106 (2017) 52–61.
- A.P. Raman, M.A. Anoma, L. Zhu, E. Rephaeli, S. Fan, Passive radiative cooling below ambient air temperature under direct sunlight, *Nature* 515 (2014) 540–544.
- L. Cai, A.Y. Song, W. Li, P.C. Hsu, D. Lin, P.B. Catrysse, et al., Spectrally Selective Nanocomposite Textile for Outdoor Personal Cooling, *Adv. Mater.* 30 (2018) e1802152.
- Y.-N. Song, Y. Li, D.-X. Yan, J. Lei, Z.-M. Li, Novel passive cooling composite textile for both outdoor and indoor personal thermal management, *Compos. Part A: Appl. Sci. Manuf.* (2020) 130.
- B. Zhao, M. Hu, X. Ao, Q. Xuan, G. Pei, Comprehensive photonic approach for diurnal photovoltaic and nocturnal radiative cooling, *Solar Energy Mater. Solar Cells* 178 (2018) 266–272.
- W. Li, Y. Shi, K. Chen, L. Zhu, S. Fan, A comprehensive photonic approach for solar cell cooling, *ACS Photon.* 4 (2017) 774–782.
- A.P. Raman, W. Li, S. Fan, Generating Light from Darkness, *Joule* 3 (2019) 2679–2686.
- T. Deppe, J.N. Munday, Nighttime photovoltaic cells: electrical power generation by optically coupling with deep space, *ACS Photon.* 7 (2019) 1–9.
- D. Wu, C. Liu, Z. Xu, Y. Liu, Z. Yu, L. Yu, et al., The design of ultra-broadband selective near-perfect absorber based on photonic structures to achieve near-ideal daytime radiative cooling, *Mater. Des.* 139 (2018) 104–111.
- J. Mandal, Y. Fu, A.C. Overvig, M. Jia, K. Sun, N.N. Shi, et al., Hierarchically porous polymer coatings for highly efficient passive daytime radiative cooling, *Science* 362 (2018) 315–319.
- X. Wang, X. Liu, Z. Li, H. Zhang, Z. Yang, H. Zhou, et al., Scalable flexible hybrid membranes with photonic structures for daytime radiative cooling, *Adv. Funct. Mater.* (2019) 30.
- P. Yang, C. Chen, Z.M. Zhang, A dual-layer structure with record-high solar reflectance for daytime radiative cooling, *Solar Energy* 169 (2018) 316–324.
- S. Atigyanun, J.B. Plumley, S.J. Han, K. Hsu, J. Cytrynbaum, T.L. Peng, et al., Effective radiative cooling by paint-format microsphere-based photonic random media, *ACS Photon.* 5 (2018) 1181–1187.
- A.R. Gentle, G.B. Smith, Radiative heat pumping from the Earth using surface phonon resonant nanoparticles, *Nano Lett.* 10 (2010) 373–379.
- Z. Huang, X. Ruan, Nanoparticle embedded double-layer coating for daytime radiative cooling, *Int. J. Heat Mass Transf.* 104 (2017) 890–896.
- Y. Zhai, Y. Ma, S.N. David, D. Zhao, R. Lou, G. Tan, et al., Scalable-manufactured randomized glass-polymer hybrid metamaterial for daytime radiative cooling, *Science* 355 (2017) 1062–1066.
- D. Zhao, A. Aili, Y. Zhai, S. Xu, G. Tan, X. Yin, et al., Radiative sky cooling: fundamental principles, materials, and applications, *Appl. Phys. Rev.* (2019) 6.
- C. Riordan, R. Hulstron, What is an air mass 1.5 spectrum? (Solar cell performance calculations), *Proceedings of the IEEE Conference on Photovoltaic Specialists: IEEE*, 1990, pp. 1085–1088.
- M. Hu, B. Zhao, X. Ao, J. Feng, J. Cao, Y. Su, et al., Experimental study on a hybrid photo-thermal and radiative cooling collector using black acrylic paint as the panel coating, *Renew. Energy* 139 (2019) 1217–1226.
- B. Zhao, M. Hu, X. Ao, N. Chen, G. Pei, Radiative cooling: a review of fundamentals, materials, applications, and prospects, *Appl. Energy* 236 (2019) 489–513.
- A. Leroy, B. Bhatia, C.C. Kelsall, A. Castillejo-Cuberos, H.M. Di Capua, L. Zhao, et al., High-performance subambient radiative cooling enabled by optically selective and thermally insulating polyethylene aerogel, *Sci. Adv.* 5 (2019) eaat9480.
- Z. Chen, L. Zhu, W. Li, S. Fan, Simultaneously and synergistically harvest energy from the sun and outer space, *Joule* 3 (2019) 101–110.
- Y. Mastai, Y. Diamant, S. Aruna, A. Zaban, TiO<sub>2</sub> nanocrystalline pigmented polyethylene foils for radiative cooling applications: synthesis and characterization, *Langmuir* 17 (2001) 7118–7123.
- T.M. Nilsson, G.A. Niklasson, Radiative cooling during the day: simulations and experiments on pigmented polyethylene cover foils, *Solar Energy Mater. Solar Cells* 37 (1995) 93–118.
- T.M. Nilsson, G.A. Niklasson, C.G. Granqvist, A solar reflecting material for radiative cooling applications: ZnS pigmented polyethylene, *Solar Energy Mater. Solar Cells* 28 (1992) 175–193.
- Y.A.O. C-I, W.A.N.G. Y-h, H. ZHANG, Coating technique for near UV cold-mirror reflector, *Vacuum* (2007) 3.
- T.G. Parham, L. Auyang, Durable Cold-Mirror Coatings for Display Lighting, *J. Illuminat. Eng. Soc.* 23 (1994) 31–39.
- E. Erell, Y. Etzion, Heating experiments with a radiative cooling system, *Build. Environ.* 31 (1996) 509–517.
- M. Hu, B. Zhao, X. Ao, Y. Su, Y. Wang, G. Pei, Comparative analysis of different surfaces for integrated solar heating and radiative cooling: a numerical study, *Energy* 155 (2018) 360–369.
- J.A. Duffie, W.A. Beckman, *Solar Engineering of Thermal Processes*, John Wiley & Sons, 2013.
- G. Guo, J. Ji, W. Sun, J. Ma, W. He, Y. Wang, Numerical simulation and experimental validation of tri-functional photovoltaic/thermal solar collector, *Energy* 87 (2015) 470–480.
- A. Bejan, *Convection Heat Transfer*, John Wiley & Sons, 2013.
- A. Allouhi, M. Benzakour Amine, M.S. Buker, T. Kousksou, A. Jamil, Forced-circulation solar water heating system using heat pipe-flat plate collectors: energy and exergy analysis, *Energy* 180 (2019) 429–443.
- M. Hu, B. Zhao, J. Li, Y. Wang, G. Pei, Preliminary thermal analysis of a combined photovoltaic-photothermic-nocturnal radiative cooling system, *Energy* 137 (2017) 419–430.



## A review of intensified conditioning of personal micro-environments: Moving closer to the human body

Bin Yang<sup>a</sup>, Xin Ding<sup>b</sup>, Faming Wang<sup>c,\*</sup>, Angui Li<sup>a</sup>

<sup>a</sup> School of Building Services Science and Engineering, Xi'an University of Architecture and Technology, Xi'an, China

<sup>b</sup> Department of Civil Engineering, Purdue University, West Lafayette, USA

<sup>c</sup> School of Architecture and Art, Central South University, Changsha, China

### ARTICLE INFO

#### Keywords:

Task ambient conditioning  
Personal environmental control system  
Personal thermal management system

### ABSTRACT

Various systems and technologies have been developed in recent years to fulfil the growing needs of high-performance HVAC systems with better performance of energy efficiency, thermal comfort, and occupancy health. Intensified conditioning of human occupied areas and less intensified conditioning of surrounding areas are able to effectively improve the overall satisfaction by individual control of personalized micro-environments and also, achieve maximum energy efficiency. Four main concepts have been identified chronologically through the development of personal environmental conditioning, changing the intensified conditioning area closer to the human body and enhancing conditioning efforts, namely the task ambient conditioning (TAC) system, personal environmental control system (PECS), personal comfort system (PCS), and the personal thermal management (PTM) system. This review follows a clue of the concept progress and system evaluation, summarizes important findings and feasible applications, current gaps as well as future research needs.

### 1. Introduction

Building related energy consumption increases strikingly with the ever-higher demand on building conditioning due to frequent heatwaves and cold spells in recent years [1]. People spend 80-90% of their daily time in indoor environments [2]. Sick building syndrome (SBS), one of the most commonly seen phenomena caused by poor indoor air quality, has become a serious concern for modern offices. SBS could cause headaches, dizziness, sore eyes and throat, or reduction of productivity [3]. A high concentration of pollutants may further induce chronic respiratory diseases and even a reduction of the life expectancy [4]. Under spatially uniform conditioning, the occupants cannot be effectively prevented from indoor air pollutants. Meanwhile, energy waste is unavoidable because of the intensified conditioning for non-occupied spaces.

Buildings consume around 20% to 40% of the total energy consumption. If it keeps the status quo, the rate of building energy consumption growth would have an annual increase of around 2%. The colossal amount of energy consumption also led to serious environmental problems. Energy efficiency becomes an urgent call for governments and societies in most countries. Reduction in energy consumption could not only result in economic savings but also environmental improvements [1].

The Predicted Mean Vote/Predicted Percentage Dissatisfied (PMV/PPD) model and adaptive model were commonly used for evaluating occupants' thermal comfort. A uniformed indoor environment, which is considered acceptable for over 80% percent of occupants, is provided for all occupants, leaving around 20% percent of people unsatisfied. To achieve a higher satisfaction ratio among groups of people with large individual differences, the heating, ventilation, and air conditioning (HVAC) system is required to be operated at a higher

*Abbreviations:* AC, Air cooling; AH, Air heating; ASHRAE, American Society of Heating Refrigerating and Air-Conditioning Engineers; CH, Chemical heating; CHC, Chemical heating clothing; COP, Coefficient of performance; EC, Evaporative cooling; EH, Electric heating; EHC, Electrical heating clothing; FH, Fluid heating; HVAC, Heating, ventilation, and air conditioning; HYC, Hybrid cooling; ITVOF, Infrared transparent and visible opaque fabrics; LC, Liquid cooling; PCC, Personal cooling clothing; PCD, Personal comfort device; PCMC, Phase change material cooling; PCMH, Phase change material heating; PCMs, Phase change materials; PCS, Personal comfort system; PE, Polyethylene; PECS, Personalized environmental control system; PEM, Personal environment module; PES, Personalized exhaust system; PI, Passive insulation; PMV, Predicted mean vote; PP, Polypropylene; PPD, Predicted percentage dissatisfied; PTMS, Personal thermal management systems; PV, Personalized ventilation; RH, Relative humidity (%); SBS, Sick building syndrome; TAC, Task ambient conditioning; TCV, Thermal comfort vote; TEC, Thermoelectric cooling; TECU, Thermoelectric energy conversion unit; TSV, Thermal sensation vote.

\* Corresponding author.

E-mail address: [dr.famingwang@gmail.com](mailto:dr.famingwang@gmail.com) (F. Wang).

<https://doi.org/10.1016/j.enbenv.2020.06.007>

Available online 6 July 2020

2666-1233/Copyright © 2020 Southwest Jiatong University. Publishing services by Elsevier B.V. on behalf of KeAi Communication Co. Ltd. This is an open access article under the CC BY-NC-ND license (<http://creativecommons.org/licenses/by-nc-nd/4.0/>)

performance level, which ends up with a larger amount of energy consumption but a relatively slight satisfaction ratio increment. New systems, considering individual difference, were developed as a solution for solving the dilemma. As a non-uniformed conditioning system, the new system provides a thermally comfortable micro-environment to each user, which allows personalized control of the micro-environment. Combining with the conventional HVAC system as a background system, the new system has been proved having the capability of ensuring over 90% percent of occupant's thermal satisfaction, elevating inhaled air quality (convective manner by fresh air) while reducing a significant amount of energy consumption [5–7].

This paper describes the concept development of personal environmental conditioning systems in a chronological order. Beginning from early 1990s, the concept of “Task Ambient Conditioning (TAC) System” was proposed by combing several relatively conventional strategies such as zoning and occupant-defined comfort to provide individual occupants better thermal comfort. The controlled area included the occupant and a part of his/her working area [8]. In the 2000s, the “Personalized Environmental Control System (PECS)” emerged as a further development of TAC. A PECS focuses not only on occupant thermal comfort improvement but also takes the air quality in the occupied area into consideration. The controlled area shrank to the torso or head of the human body [9]. Two sub-concepts, “Personal Comfort System (PCS)” and “Personalized Ventilation (PV) System”, aiming at enhancing thermal comfort and air quality respectively, were proposed. The two sub-concepts were applied to different conditions. After PECS, the concept was developed again with “Personal Thermal Management System (PTMS)” added in. PTMS are primarily focused on the enhancement of occupant thermal comfort. The controlled area is the microclimate close to the user's skin. The usage of PTMS enabled the conditioned area moving closer to users rather than being limited in a fix position [10].

Presently, a very limited number of reviews have been published on the conditioning of personal micro-climate [11–13]. The review paper by Veselý and Zeiler [11] did not distinguish the TAC system and PECS, rather than discussing the thermal comfort and energy performance of the concept as a whole. Godithi et al. [12] overviewed technologies of personal environmental control systems (PECS) including task/ambient control (TAC) and personal ventilation (PV) systems. The most recent development on the personal thermal management systems (PTMS) has not reviewed. More recently, Rawal et al. [13] comprehensively summarized various personal comfort system, but very limited information was made on the personal thermal management systems. Another review work comprehensively described numerous forms of ventilation and air distribution systems, which included the PV system as a part of the non-uniformed ventilation systems [14]. Studies of PTMS, as a continuation of the TAC and PECS, have not been systematically reviewed and comprehensively evaluated yet. It should be mentioned that, in this review, it is the authors' intention to give brief introductions to TAC and PECS, and an extensive overview was focused on PTMS.

During the development of aforementioned systems, the conditioned area was gradually reduced and closed to the human body (Fig. 1). A comprehensive review of the TAC, PECS and PTMS is given, in terms of their energy performance, thermal comfort management, improvement of air quality, and relative applications.

## 2. Methodology

To conduct the searching process, “task ambient conditioning”, “personalized ventilation/cooling/heating”, “personal comfort management”, “personal comfort system”, “personal comfort device”, “personal environment control”, “wearable thermal devices”, “personal cooling system”, “personal heating clothing” and related items were used as keywords to search for influenced publications through the database of ScienceDirect, Web of Science, Wiley Online Library, China National Knowledge Infrastructure.

Academic publications that developed the concepts of aforementioned systems, implemented new methods and technologies to test the system performance, improved forms and components of the system for better overall performance, designed and tested new applications, tested system performance in varying conditions, are considered strongly related with the focuses of this paper.

Experimental data that is commonly reported and consistent with theoretical are extracted. Distinguishing values and extreme values that are considered representative of the performance of the systems, and the conditions they were found are extracted and discussed.

The reviewed publications are sorted by their publication dates, listing with an order as TAC system, PECS, and PTMS in the references, which gives a clear clue of how this paper develops and how each section is formulated.

## 3. TAC (Task Ambient conditioning)

### 3.1. Working principle and available devices

TAC is a strategy that distributes thermally conditioned air to specified thermal zones surrounding the occupants. TAC allows occupants regulate supply air (e.g. air velocity, supply air volume, supply air temperature, supply air direction) to achieve a better effect of personal thermal satisfaction [5,6,8,15–19]. TAC contributes to less intensifying requirements of ambient environments, and thereby, to reduce energy consumption as well as provide comfortable and healthy work environments [7]. Attentions were mainly paid to provide local thermal comfort without supplying 100% fresh air. TAC systems were typically designed for commercial office buildings. Forms of air terminal units of a TAC system are commonly located closely to occupants. Different forms of TAC systems may include raised-floor distribution unit, desk-mounted unit, desk-edge-mounted type, ceiling-mounted grill, desk fan, desk-top unit, partition unit, personal environment module (PEM), and combinations of some of those systems, etc. In Fig. 2, commercially available TAC systems, including PEM and ClimaDesk, are demonstrated.

Multiple experiments have been performed in controlled environment chambers by using thermal manikins and human subjects. Field studies were also performed to analyze practical applications under non-uniform thermal environments created by TAC systems. Most cases were based on temperate and tropical climates. Few modules have the heating function. Questionnaire surveys were frequently used to measure the impact of TAC system. Sitting and standing positions were all tested while walking activity was seldom tested.

### 3.2. Cons and pros

TAC systems significantly improve thermal comfort. Supply air temperature varies from 19°C to 25°C [20]. A temperature difference up to 2.5°C between the ambient environment and controlled area was observed [6,15]. Higher air velocity was found preferred by occupants without cool air supply. It is found that the occupants will generally increase the supply air velocity when they gained control. The maximum air velocity was reported being raised to around 3 m/s in some rare cases [15]. The supply air volume has a strong impact on stratification [6]. With increasing supply air velocity, the risk of draft becomes a serious concern. However, the initiative of control allowed a higher tolerance of supply air velocity [6,18,21]. Although cool and fresh air are preferred, occupants could show acceptability for surrounding air temperature from up to 30.5°C with the usage of recirculating air [22]. Air velocity higher than the ASHRAE standard limitation was found acceptable and even preferred by occupants. Occupants commonly report a higher level of satisfaction due to better temperature and ventilation conditions compared with the conventional systems [15,23,24]. Under increased activity levels, the desk-top conditioning system could maintain temperature in workstation 1–2°C lower than ambient.

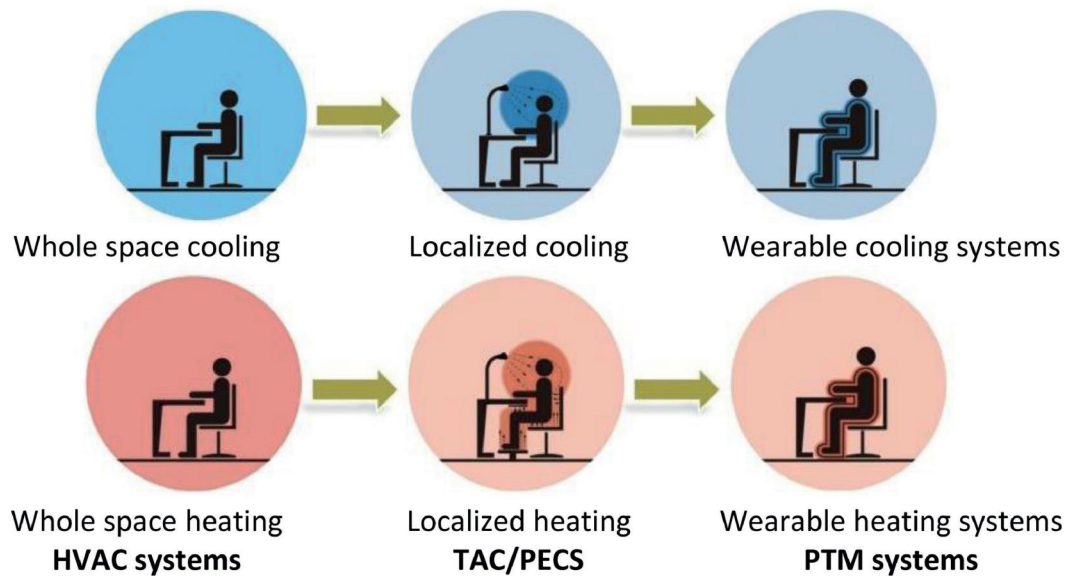


Fig. 1. The intensified conditioning area moving closer to the human body.

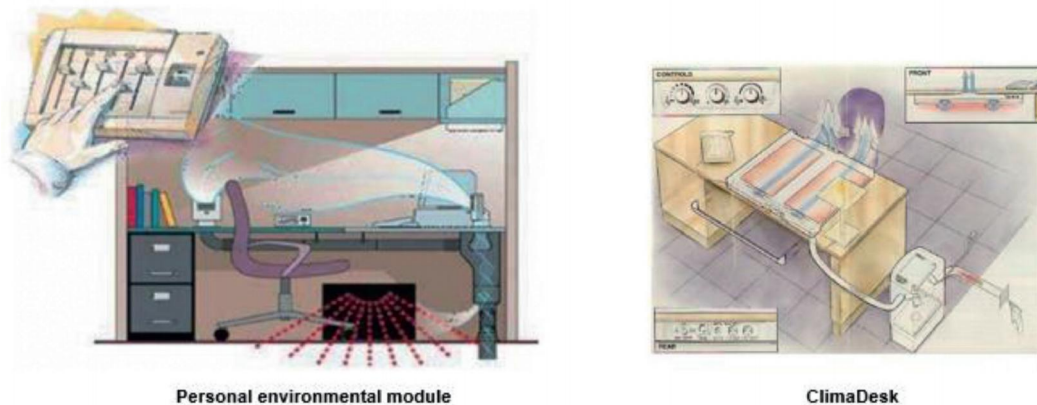


Fig. 2. Different prototypes of TAC systems [5–8].

Air quality, even not be intended, is believed to be another most affected category by the TAC system, especially being found promoted in the breathing level. The air change efficiency of the TAC system was reported (1.4 to 2.7) higher than that of conventional displacement ventilation [20,25]. To test the best performance of the floor-based task ventilation system on improving indoor air quality, a task supply using 100% fresh air was conducted, and the age of air in occupancy breathing level was found 20%~40% lower than that of the mixing ventilation when supplying straight towards occupants. Concentration of smoke particles when using the floor-based task ventilation system could be 50% lower than the average workspace concentration. Studies found that the workspace controlled by TAC system could not be completely protected from a pollution source located in adjacent working spaces under the operation of a task ventilation system. However, the height where transmit pattern occurred is higher than the breathing zone, which could leave seated occupants unaffected. A novel parameter, calculated by the Archimedes number of the supply jets and the ratio of total supply flow rate divided by the magnitude of internal heat loads, was proposed and found to have a linear relationship with the change in the age of air with height, which could serve as a new strategy of evaluation [26]. Up to 25% decrease of the probability of allergy and up to 50% decrease that of sick building syndrome (SBS) could also be expected by TAC based on currently existing technologies and procedures [27,28].

Applications of TAC system could contribute to economic benefits by energy saving and cost reduction. By maintaining suitable thermal comfort around the occupied area, ambient space conditions could be controlled and maintained under a lower standard, which may result in lower energy consumption of the background HVAC system. Up to 15% of electricity usage could be saved by a TAC system comparing with using the conventional HVAC system (mixing ventilation) [7]. However, under some circumstances, energy consumed by the air distribution system could rise due to the increased amount of personalized air and increased amount of fan in every air terminal device [24]. The increment of occupant's productivity, which will lead to a considerable amount of economic interests increment, was believed to have a significant positive relation with high overall-satisfaction of the working environment [7,9,17,19,27,29]. A reduction of illnesses, allergy, asthma symptoms, and other building related diseases, by using TAC, was also announced that could lead to an increase in productivity [27,28]. However, reported annual productivity improvement only varied 0.08% to 2.8% due to increased thermal comfort and air quality by the application of TAC system alone [7].

There are still some research gaps remaining in this period of study of TAC system. Although being claimed capable of operating the TAC system to achieve thermal comfort in varying conditions, occupants typically operate the supply air velocity, direction, volume and other parameters infrequently (from daily to monthly) and insufficiently [30].

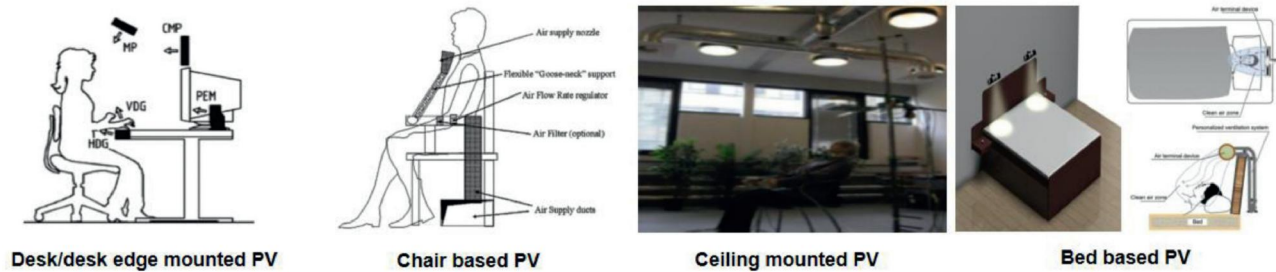


Fig. 3. Different prototypes of PECS (PV) [31,34,37–39].

Usually, the optimal energy saving potential and thermal comfort improvement cannot be fully achieved.

#### 4. PECS (Personalized Environmental Control System)

##### 4.1. Working principle and available devices

The concept of PECS, emerging in early 2000s, is based on the TAC system. Aiming to not only thermal comfort but also air quality, clean, cool and dry air are supplied to occupants. The controlled area of some PECS is narrowed down to occupants' breathing zone [9,28].

Forms of PECS include desk mounted systems [31,32], desk-edge mounted systems [20,25], ceiling mounted systems [33–36], chair-based systems ([37]), bed-based systems [38,39], and varying types of combinations (Fig. 3).

During the development of PECS, a dichotomous branch of the studies was documented. What should PECS mainly focus on, thermal comfort or air quality? In this section, personalized ventilation (PV) system is considered as one branch of PECS followed by the personal comfort system (PCS) as another branch.

The PV system, mainly focuses on the capability of improving inhaled air quality to avoid cross infection, sick building syndrome (SBS) and other building related illness [9,28]. By supplying 100% fresh air, PV system can significantly improve inhaled air quality in breathing zone to achieve a triumph of strongly protecting users from cross infection and contaminant inhalation in high polluted area such as hospitals and industrial circumstances, and places with a high occupant density [40–44].

Supply momentum and temperature of personalized air are considered having a high impact on the performance of the PV system [40,45]. The supply airflow rate that has been put into test varies from 4 L/s up to 23 L/s. In some cases, supply air velocity was reported could be elevated up to 0.9 m/s [23,31,34]. Supply air velocity over 0.2 m/s could break the thermal plume around the human body to reduce the mixture of personalized air and ambient air. As a result, better inhaled air quality can be achieved [41]. The distance between air terminal devices and occupants' facial area also plays a critical rule in the inhaled air quality. Therefore, the importance of proper air terminal devices design which would determine characteristics of supplying airflow was extensively studied by researchers. Several nozzles were designed and tested to compare ventilation effects and energy saving potentials [34,46–48]. Several methods and indices were developed to evaluate the efficiency of PV system. Compared with mixing ventilation, ventilation effectiveness of the PV system is up to 50% higher.

Background ventilation system, working together with PV system, has an impact on the pollutant removal efficiency [49–51]. Different types of background ventilation system would cause different mixture between personalized supply air and surrounding polluted air. The less the mixture process, the better the inhaled air quality. With different combinations of background ventilation systems, PV systems might have different performances, not only for air quality but also on thermal comfort.



The performance of PV system for occupants with lying positions was tested within ward and bedroom environments [38]. PV system can provide a thermally neutral environment to users [39]. Sleeping quality is also reported higher than conditions without the PV system [52]. Cross infection between patients can be avoided in hospital wards [53]. To provide more personalized air towards occupants' breathing area, a "Personalized Exhaust System" (PES) placing small exhaust ducts around occupants has been introduced. PV system combined with the PE system could extract exhaled air in a very short period of time and increase the proportion of fresh air in inhaled air than the PV system alone [54].

For personal comfort system (PCS), more attention is paid to the aspects of personal thermal comfort. In winter condition, radiant heating devices (e.g. footwarmer, legwarmer, kneehole radiant panels, hand/palm warmer, heated chair, etc.) are mainly used to stimulate local body segments (Fig. 4) [55–60]. Ambient room temperature can be reduced to some extent. In summer condition, elevated air movement created by different types of electric fans (e.g. ceiling fan, stand fan, table fan, small USB fan, box fan, fan aided ventilated chair, etc.) or local isothermal jets (e.g. nozzle, slot diffuser in desk or partition, etc.) can improve thermal comfort by enhanced isothermal convective cooling [56,61–67]. Ambient room temperature can be elevated to some extent. Compared with negative draft for neutral-slightly cool thermal environments, elevated air movement can be regarded as a positive factor for neutral-slightly warm thermal environments. By using aforementioned PCS, the dead band can be expanded to achieve energy efficiency by less intensified ambient heating/cooling during winters/summers [68].

##### 4.2. Cons and pros

Without supplying fresh air into personal environments, PCS can only improve personal thermal comfort but not inhaled air quality. That's why PV system, as one competitive alternative, is necessary especially for heavily polluted and infectious premises, although the limit of extended air duct exists. As further development of PCS, PTMS improve personal thermal comfort by moving closer to the human body and further narrowing down personal environment by mainly considering attirement.

#### 5. PTMS (Personal Thermal Management System)

In indoor environments, there are four adaptive ways to help occupants achieve individual thermal comfort. In non-air-conditioned buildings, the most often used method to adjust indoor thermal environments is the opening of windows and/or doors [69]. Opening windows is considered as the most favored measures to improve air quality as well as the indoor thermal comfort. In air-conditioned buildings, HVAC is the most popular measure to provide occupants thermal comfort conditions. It has been well known that the use of HVAC systems results in enormous energy consumption [70–73]. Besides, HVAC conditioned thermal environments could only ensure up to 80% of occupant satisfaction [74]. Third, small personal comfort devices (PCDs) such as electric fans and



Fig. 4. Different prototypes of PECS (PCS) [55–68].

radiators could also be used to improve individual thermal comfort [75–80]. Compared to HVAC systems, PCDs consume much less heating or cooling energy and the power consumption of personal comfort devices is often less than 1500 Wh (watt-hour). The fourth method to maintain indoor thermal comfort is the adjustment of clothing [81]. Traditional clothing has a very limited capability to help occupants maintain thermal comfort because traditional clothing serves as an unchangeable thermal insulator between the human body and its surrounding environment [82].

In recent years, the concept of personal thermal management emerges as a promising approach to further enhance individual thermal comfort as well as to help pushing building energy consumption to the minimum limit [83,84]. The main goal of personal thermal management is to help enhance heat exchange between an individual body and wearable systems such as clothing incorporated with wearable cooling and heating devices. In hot indoor environments, PTMS enhance body heat dissipation so that the body temperature could be maintained in thermally neutral range. Conversely, in cool or cold indoor environments, PTMS help occupants preserve body heat or even receive heat energy from either the PTMS or the surrounding environment. Hence, PTMS have a much high energy efficiency compared to other means such as the usages of HVAC systems and PCDs. In addition, PTMS are portable, flexible, light-weight and have almost no restrictions on body movement. Besides, PTMS are environmentally and ergonomic friendly and consume minimal energy.

Generally, personal thermal management systems may be categorized into two main groups: PTMS incorporated with cooling and/or heating modules and PTMS made of specially designed materials or with unique structures. Presently, heating and cooling modules/units may be incorporated with clothing include air ventilation fans, vortex cooling unit, thermoelectric module, phase change materials (PCMs), warmers, resistance wires, Janus fibrous membrane, conductive fabric pads, solar heating systems, thermoelectric heater and coolers, portable refrigerator, pre-cooled air or liquid circulating tubes, dry ice and frozen gels [82,85–94]. PTMS made of specially designed materials or with unique structures may include fabrics made with yarns encapsulated with PCMs, infrared transparent and visible opaque fabrics (ITVOF), metallic nanowire-coated textiles, ultrathin graphene paper, graphene and carbon-based materials, and moisture management textiles [10,83,84,95–100].

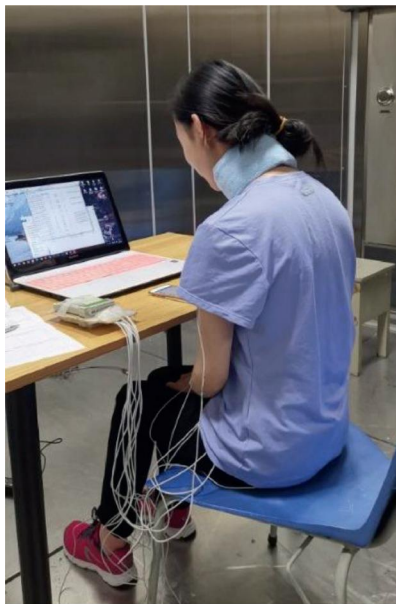
The concept of PTMS incorporated with heating and cooling devices such as ventilation fans, fluid circulation tubing, PCMs, and resistance wire is not new [101,102]. The energy draw of PTMS incorporated with

wearable heating/cooling devices is normally less than 30 W. Various types of personal cooling clothing (PCC) have been developed during past eight decades. In general, personal cooling mechanisms may be divided into six categories: phase change material cooling (PCMC), evaporative cooling (EC), liquid cooling (LC), air cooling (AC), thermoelectric cooling (TEC) and hybrid cooling (HYC) combining more than one cooling technique [89].

PCM cooling relies on PCMs such as frozen gels, ice, and paraffins to provide body cooling during melting. PCMs should be placed closely to the human body to draw body heat. Cooling effect of PCMs is determined mainly by PCM's melting temperature, specific heat, latent heat of fusion, total mass of PCMs, body coverage area, location of PCMs inside clothing, ambient temperature, and insulation between PCMs and the ambient environment [103–106]. For example, the larger the amount of PCMs being incorporated into clothing, the better the cooling performance. Unfortunately, the entire PCM cooling system will be heavy. Existing PCM cooling vests weighs about 1.5–2.5 kg per piece. The effect of a cooling vest incorporated with PCM packs (total weight of 2.2 kg) on occupant thermal comfort at 34°C with RH=60% was examined [87]. Results showed that the torso skin temperature of occupants was decreased by 2–3°C and overall torso temperature remained at 33.3°C during the 90 min experimental duration. Besides, overall thermal sensation, torso thermal sensation and skin wittedness sensation have been greatly improved by the PCM cooling vest.

EC may be achieved by wearing clothing incorporated with dry ice or clothing with the capability to store moisture. Dry ice incorporated clothing was found to be effective in mitigating heat strain in hot and humid conditions, but they may cause local body cold discomfort due to the huge amount of heat absorbed during sublimation [107,108]. Cooling performance of EC clothing with stored moisture is mainly determined by ambient humidity and such EC clothing normally performs good in dry environments because water evaporation is dependent on the water vapour pressure gradient between the wetted surface and the ambient condition. EC clothing is light, cheap, environmentally friendly and convenient to be used as compared to other wearable cooling systems.

LC utilizes pre-cooled liquid, usually water, circulating in tubes over the skin surface, to conduct the body heat away [102]. Performance of LC clothing is affected by the inlet liquid temperature, tubing length, the diameter of the tube, flow rate, body coverage area, location, tubing density, clothing fit and cooling control modes [107]. LC is powerful because water has a very high specific heat. Nevertheless, LC clothing is normally heavy, bulky and cold water may cause condensation on the



(a)



(b)

**Fig. 5.** A cooling collar incorporated with (a) PCMs and (b) the portable liquid cooling vest.

tubing so that the wear comfort could be greatly affected (Fig. 5). LC technique could also be used for fabricating cooling scarfs so that vital body parts such as the neck (where the carotid arteries are located) can be cooled down in warm indoor environments. A LC collar was developed and the effect of LC collar was explored on occupant thermal comfort at 33°C environment [86]. The liquid temperature was maintained at 16°C. Results demonstrated that the occupant thermal comfort has been greatly improved by using the LC collar in the studied warm environment.

AC utilizes circulated natural air or pre-cooled air to enhance convective heat loss at the body surface. Existing AC systems can be engineered by incorporating arrayed fine hoses with pores into high elastic fabrics to direct air flow to the skin surface. The air flow is powered by an air compressor and sometimes a Ranque–Hilsch vortex tube could be applied to pre-cool the supply air. An AC system could also be fabricated by mounting small air ventilation fans to clothing at discrete clothing locations such as the lateral back [109,110]. Such AC clothing circulates natural air to the clothing microclimate so that excessive body heat could be dissipated to the ambient environments via convection and/or evaporation. AC clothing powered by small fan units could greatly improve indoor occupant thermal comfort in warm indoor environments at 32°C [90]. Air ventilation clothing consumed only about 5 Wh energy whereas PCDs such as a traditional desk fan has a power consumption of 40 Wh. Hence, the use of air ventilation cooling clothing could provide 7–8% more energy saving as compared to desk fans. The AC shirt could also significantly reduce the occupant local temperatures at the scapula and the chest in a hot environment (38°C, 45%RH) [111]. Occupants reported cooler TSVs during the initial 10 min after the AC shirt was worn. However, the cooling effectiveness of the AC shirt was not high on occupants while performing light office work under the studied high temperature.

Over the past decade, the use of thermoelectric cooling (TEC) to fabricate PTMS has garnered considerable research attention. Thermoelectric devices are developed based on the so-called Peltier–Seebeck effect. Thermoelectric cooler serves as a micro heat pump that creates a heat flux at the junction of two types of materials, which can be used to generate either cooling or heating energy. Solid-state thermoelectric modules are compact, light-weight, reliable, environmentally friendly for refrigeration and more important, the cooling power is readily ad-

justable. A portable thermoelectric energy conversion unit (TECU) was developed and incorporated into clothing [93]. A micro blower continuously supplies TECU cooled ambient air to the clothing microclimate through a tree-like rubber tube network, which was knitted into the TEC clothing. An axial fan was located at the air rejection side. Thermal manikin tests showed that the TEC clothing could provide a cooling power of 24.6 W and expand the building temperature setpoints by around 2.2°C. Thereby, the use of TEC clothing could result in 15% building energy saving. Further, thermoelectric modules could also be designed as wearable devices such as a bracelet or a head cooler (Fig. 6). The Embr Labs Inc. (Boston, MA) developed a commercial wearable bracelet called Embr Wave wrist band which was worn on the inside of the wrist and delivered cooling rhythms tuned to human temperature perceptions. This wearable device has a cooling area of 6.25 cm<sup>2</sup> and the amplitude of wave rhythms can be adjusted. The effect of wearing an Embr wave bracelet on occupant thermal comfort was evaluated [94]. Results demonstrated that the Embr bracelet could improve overall thermal comfort, thermal sensation by 0.5–1.0 scale unit, which is roughly equivalent to 2–3°C temperature difference during the 3 to 45 min time period of use. A high coefficient of performance (COP=1.5) wearable TEC device was fabricated [112]. This TEC device was worn on the arm and infrared thermo-images showed that the local temperature of skin covered by the TEC device was 2.5°C lower than the rest of the skin. The TEC device could expand the indoor ambient temperature zone to 36°C and thereby save 20% of the energy for a typical building. Similarly, a wearable TEC cooler was developed and applied to the wrist area for personal cooling [113]. This newly developed TEC device was composed of several p- and n-type TEC thermocouples that were connected electrically in series and thermally in parallel. This TEC cooler could cool down the human skin up to 8.2°C below the ambient temperature. Besides, cost-benefit analysis revealed that the cooling over material value of the new TEC cooler was 5 times greater than commercial modules. Despite the evident cooling effect on occupant thermal comfort shown by TEC devices, the limitations of TEC are obvious. TEC devices consume a considerable amount of electricity to generate cooling energy and thereby they have a high requirement on battery capacity. If a battery with a reasonable weight is desired, the TEC has to be designed in small size (e.g. a bracelet). Small sized TEC devices have a very limited cooling capacity and hence, cooling effect on the human body is



Fig. 6. The Embr TEC bracelet (Embr Labs, Boston, MA, USA) and a commercial TEC forehead cooler.

relatively limited. On the other hand, TEC devices should cover a much greater body surface area to provide significant body cooling. High performance TEC devices require large capacity batteries for extended usage duration, which makes the overall weight of the TEC cooling system relatively heavy. In addition, presently the thermoelectric conversion efficiency is still much lower compared to a refrigeration system [114].

The majority of existing personal cooling systems (PCS) use one cooling technique to provide cooling energy to occupants. One of the known limitations of such PCS is that they function well in a certain range of environmental conditions but their cooling performance under the rest of thermal conditions tends to be pretty low. For instance, PCS incorporated with PCMs showed good cooling performance in warm and humid environments under which both the dry heat and latent heat transfer are restricted. In order to further extend the application of PCS to a wider range of ambient environments, hybrid cooling (HYC) combines multiple cooling techniques in a clothing system has been proposed [115]. A portable HYC clothing was developed and its impact on the improvement of occupant thermal comfort in a hot indoor environment (34°C, 65%RH) was investigated [89]. It was found that the HYC clothing could remarkably improve overall thermal sensation votes (TSVs), skin wetness sensation votes and thermal comfort votes (TCVs). Besides, thermophysiological parameters such as the mean skin temperature and total sweat production were also greatly reduced while using HYC clothing as compared to no cooling (i.e. control).

Despite the extensive application of PTMS incorporated with cooling devices/systems to improve occupant thermal comfort in indoor environments, aforementioned PTMS still require external energy input (i.e., supplied power). Presently the development of state-of-art PTMS with zero or near-zero energy input becomes a hot topic. PTMS with zero or near-zero energy input are developed by using novel materials or materials with specially designed structures [83,84,98]. The main principle of such novel PTMS is that the material or the special structure enables the heat exchange between the human body and its surrounding environment and thereby increases wearer thermal comfort. One the prominent examples is the infrared transparent visible opaque fabrics (ITVOF) [83]. Presently potential materials for ITVOF include polyethylene (PE) and polypropylene (PP). ITVOF are transparent in the infrared spectrum, which allow passive radiative cooling. It has been well established that the human body emits most the infrared radiation in the wavelength between 9.3 and 9.7  $\mu\text{m}$ . Hence, ITVOF enable radiative heat dissipation on the human body. Traditional textiles made of natural and synthetic fibers do not allow body heat dissipation via infrared radiation [83]. Thus, wearing ITVOF increases an occupant's cooling rate. Obviously, the increment in a person's cooling rate allows a higher ambient temperature to achieve the same level of thermal comfort. For example, a 23W increase in the body cooling rate allows a thermal comfort ambient temperature increase from 23.9°C to 26.1°C (i.e., increase of 2.2°C) and thereby, significant built energy savings could be expected [83]. Nanoporous polyethylene (nanoPE) textiles were fabricated and results from hotplate tests showed that the simulated skin temperature

was reduced by 2.7°C when being covered with nanoPE cloth as compared to cotton textiles [84]. The actual performance of clothing made with ITVOF on the improvement of thermal comfort in various indoor conditions were examined [97]. The ITVOF clothing enables thermal comfort at an ambient temperature of up to 27°C, which is 1.5°C higher than the indoor thermal comfort upper limit recommended ASHRAE. Therefore, the use of ITVOF clothing could save around 9-15% cooling energy in a typical built environment. In addition to the aforementioned example on improvement of radiative heat transfer on the human body, other approaches to enhance conductive, convective and evaporative heat transfer on the human body could also be proposed. Detailed methods to enhance other means of heat transfer mechanisms by using near-zero energy input materials can be found in recently published literature reviews [99,116]. It should be noted that translating findings from such material-level studies into actual indoor applications should be made with caution because the majority of evaluation tests reported in material-level studies were performed on 2-dimensional equipment. The test condition, test protocol, design specifications of PTMS and individual difference could largely affect the actual performance of PTMS in indoor settings.

Over the past few decades, personal heating systems have also been developed to improve occupant thermal comfort in various cool or cold indoor environments. The concept of incorporated auxiliary heating into clothing could be dated back to the early 1940s [117]. Properly designed personal heating clothing is capable of providing the human body with sufficient heating energy in cool and cold indoor environments with no access to central HVAC heating systems. Existing personal heating technology may be divided into four types: electrical heating (EH); chemical heating (CH), phase change material heating (PCMH), air/fluid flow heating (AH/FH) and passive insulation from special structured materials (PI).

EH is the most practical and widely used heating technology for personal heating. Electrical heating clothing (EHC) is slim, lightweight, washable, flexible and does not restrict body movement. An EHC system is normally comprised of heating elements, a power source, and a user interface [118]. The most often used heating elements may include electrical resistance wires, electrically conductive rubbers, metalized textile fabrics, intrinsic conductive polymers, carbon polymer heating elements, carbon fabrics, graphene heaters, Janus fibrous membranes and TEC heaters (Fig. 7). EHC can greatly improve occupant thermal comfort while working in unheated indoor environments during cold weather. The effect of EH clothing on thermal comfort of university students while studying in a cold classroom condition was investigated, where the air temperature was 8.0°C and RH=80% [88]. Results showed that EHC could remarkably increase skin temperatures. Overall and local TSVs and TCVs were improved in EHC compared to non-heating. The heating performance of EHC and two PCD combinations including a radiant heating panel & a heated table pad (i.e., HB1) and a heated chair & a heated mattress (denoted as HB2) at two cool indoor temperatures (15 and 18°C) was examined [91]. It was found that EHC received

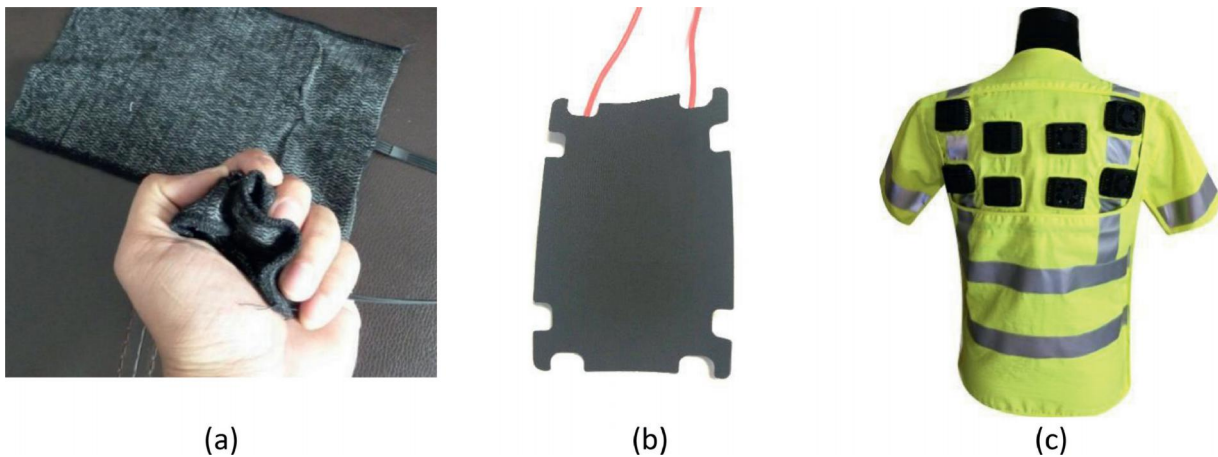


Fig. 7. An electrical heating fabric made from (a) the carbon fiber, (b) the graphene fabric heater, and (c) a heated jacket incorporated with thermoelectric heating modules.

better thermal acceptability over HB1 and HB2 at both two cool conditions. EHC significantly improved overall TSVs as compared to HB1. EHC consumed less than 15 W power and this only accounted for 4.4% and 14.8% of the total power draw of HB1 and HB2. Therefore, EHC is much more effective than PCDs in enhancing occupant thermal comfort in unheated cool indoor environments. More important, EHC is super energy saving as compared to traditional PCDs. EH technique can be conveniently incorporated into various clothing, sleepingbags and accessories including, but not limited to, hats, hoods, scarfs, jackets, trousers, gloves/mittens, socks and insoles [92,118]. EHC accessories are found effective for maintaining local skin temperature as well as improving local body thermal comfort, which have a similar function with PCDs such as foot warmers, palm warmers, heated keyboards, desk radiators, heated chairs, heated tables and warm-barrels [57,59,119]. Nevertheless, EHC accessories consume even less heating energy and their power consumption is always less than 5 Wh.

Compared to the EH technique, other heating technologies received less attention during the past few decades. Chemical heating clothing (CHC) was designed and its effect on occupant thermal comfort in a cold indoor environment at 8.0°C was examined [88]. Fourteen chemical body warmers (chemical ingredients: iron powder, activated carbon, water, vermiculite and salt) were incorporated in an insulative vest and kneecaps and the CHC had an effective heating power of 6.9 W. Results showed that CHC could greatly improve skin surface temperature, local skin temperature at the fingers as well as the finger blood flow. TSVs at the hands and feet were also improved in CHC compared to non-heating. Thermoelectric heating clothing (warm air was pre-heated by the thermoelectric unit and then being supplied to clothing microclimate using a blower) was designed and its performance was assessed using a thermal manikin [93]. The thermoelectric heating clothing could provide a heating power of 18.5 W.

Similar to the development of personal cooling systems with near zero energy input, a recent hot research direction on personal heating is to develop personal heating systems with near zero energy input. By properly controlling the conductive, convective and radiative heat transfer avenues, novel PTMS with zero energy input could be achieved. Nanophotonic structure textiles were fabricated using nanoporous metallized PE [96]. An infrared reflective layer was constructed on an infrared transparent layer with embedded nanopores. The nanoporous metallized PE textile exhibited a high infrared reflectivity of 98.5% on the outer surface of the textile, which could effectively suppress radiative heat loss. Hotplate tests showed that the newly fabricated PE textile could maintain a simulated skin surface temperature of 33°C at 15°C ambient temperature, which is 7.1°C lower than that with cotton fabrics. The 7.1°C set-point reduction could save >35% building heating energy.

Similarly, a multifunctional fabric coated with a nanoporous cellulose acetate layer followed by depositing a thin silver film was developed [98]. The silver film acted as both an infrared reflector and a highly conductive heater. This multifunctional fabric could decrease the fabric surface temperature by 1.3–1.6°C at room temperature (i.e., 25°C) compared to normal textiles. The silver sheet has an electrical resistance of 2.8–4 Ohm per square meter, which enabled Joule heating at a low voltage. Results showed that applied low voltages of 0.5, 1.2 and 1.5 V could induce fabric surface temperatures of 34.1, 44.8 and 56.7°C, respectively, at the 25°C ambient temperature. Again, it should be emphasized that the above results obtained from simplified hotplate measurements are expected to present a big discrepancy with results from human trials with full-scale PTMS.

Table 1 summarizes some common advantages of PTMS over central HVAC systems and PECS (PCDs). First, the usage of PTMS could significantly save building cooling and heating energy. The controlled target cooling and heating area is very close to the occupants. Hence, it is effective and efficient to provide heating and cooling to the near-skin microclimate of an individual occupant. Also, PTMS do not require an air distribution system, which is a considerable aspect of energy consumption for conventional PV systems. Up to hundreds of watts per person can be saved using wearable PTMS compared to conventional heaters. Furthermore, PTMS with near zero energy input could further reduce built environment energy consumption to the minimum. Next, PTMS could prevent draft risks caused by the elevated supply air velocity, which is commonly found problem in TAC system and PV system. Nevertheless, PTMS also have limitations. PTMS are usually worn either directly on the skin surface or pretty close to the human body, its effect on suppression of sweat/moisture transport may be a serious concern. Most PTMS or some parts of the PTMS are impermeable, which could restrict the moisture transfer between the human skin and the surrounding environment, and thereby leading to worsened wear comfort. Thus, the breathability of PTMS components should be considered while developing PTMS. Presently, most PTMS are expensive and some PTMS use expensive modules or materials, which hinders the large-scale production of PTMS to various workplaces. Alternative manufacture techniques should be sought to reduce the cost of PTMS components. Lastly, some components used in PTMS are pretty rigid and heavy compared to traditional textile fibers. Future PTMS should be more flexible, lightweight, cheap, durable, reliable and environmentally friendly.

## 6. Conclusions

Based on the concept of spatially non-uniform conditioning, intensified conditioning of human occupied areas and less intensified condi-

**Table 1**  
Features of PTMS as compared to HVAC and PECS (including PV, PCS or PCDs).

System	Targeted conditioning area	Main functions	Energy consumption	Advantages	Limitations
HVAC	Entire building spaces	Provide fresh air and temperature control (heating and cooling)	Often >>1000 Wh [120]	Improves both indoor air quality and ambient conditions	Huge energy consumption, maximally 80% occupants could achieve thermal comfort
PECS	Localized space	Heating and cooling local body parts, some systems could provide fresh air	2-1000 Wh, often > 20 Wh [14,16-20,34-41,51-64]	Some devices are relatively portable, Individual control, Improves local body thermal comfort and inhaled air quality, energy efficient, low dissatisfaction	Most PECS (personal comfort systems) could not provide fresh air
PTMS	Clothing micro-climate	Heating and cooling	0-100 Wh, often <20 Wh [83-97,104-108,121, 122]	Portable, further improved body thermal comfort, even lower energy consumption, efficient to provide heating and cooling (high COP)	Could not provide fresh air, some systems are heavy and bulky, ergonomic issues, limited battery capacity [117]

tioning of surrounding areas in terms of thermal comfort and air quality were developed from TAC systems in 1990s, through PECS after 2000, to PTMS recently. All aforementioned systems give personal control to overcome individual difference in terms of thermal comfort. PV systems also give personal control to improve inhaled air quality individually. Several trials have been performed to avoid extended PV air duct, which confine the practical application of the PV system. As the necessity of PV for heavily polluted/infectious premises, the goal is to minimize its practical limitations and achieve flexibility, functionality and adjustability. As another one of the dichotomous branches, PCS can achieve personal thermal comfort by consuming less energy and integrating functional design into personal furniture. By moving closer to the human body, PTMS was introduced and explored extensively. The findings should be cautiously translated and applied into actual indoor applications because the majority of tests reported in material-level studies were performed on 2-dimensional equipment. Results obtained from simplified hotplate measurements are expected to present a big discrepancy with results from human trials with full-scale PTMS. Permeability and wearability of the studied materials should also be considered before practical application for clothing. With regard to documented research work on PTMS, most existing research studies were focused on the cooling effect of PTMS in various warm and hot indoor environments, whereas left the heating effect less emphasized. Further investigations on the heating effect of PTMS in unheated built environments in cold climate zones are needed. Moreover, the effect of PTMS responding to varying occupant characteristics including age, weight, body shape, race, gender and fitness is still missing. In addition, the wearability (e.g. ergonomic comfort, visual comfort, movement comfort) of PTMS requires further investigations because almost no published work has addressed this issue. Lastly, physiological studies on which body parts require extensive heating or cooling supply to further improve occupant overall and local thermal comfort in non-ideal indoor environments are also required.

#### Declaration of Competing Interest

None.

#### Acknowledgments

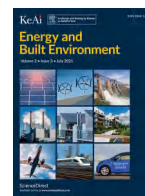
The authors would like thank Professor Emeritus William Nazaroff from the Department of Civil and Environmental Engineering at University of California Berkeley for his suggestions

#### References

- [1] L. Pérez-Lombard, J. Ortiz, C. Pout, A review on buildings energy consumption information, *Energy Build.* 40 (2008) 394–398.
- [2] N.E. Klepeis, W.C. Nelson, W.R. Ott, et al., The national human activity pattern survey (NHAPS): a resource for assessing exposure to environmental pollutants, *J. Expos. Sci. Environ. Epidemiol.* 11 (2001) 231–252.
- [3] A.P. Jones, Indoor air quality and health, *Atmos. Environ.* 33 (1999) 4535–4564.
- [4] P. Wargocki, D.P. Wyon, J. Sundell, et al., The effects of outdoor air supply rate in an office on perceived air quality, sick building syndrome (SBS) symptoms and productivity, *Indoor Air* 10 (2000) 222–236.
- [5] W.J. Fisk, D. Faulkner, D. Pih, et al., Indoor air flow and pollutant removal in a room with task ventilation, *Indoor Air* 1 (3) (1991) 247–262.
- [6] F.S. Bauman, L. Johnston, H. Zhang, et al., Performance testing of a floor-based, occupant-controlled office ventilation system, *ASHRAE Trans.* 97 (1) (1991) 553–565.
- [7] J.E. Seem, J.E. Braun, The impact of personal environmental control on building energy use, *ASHRAE Trans.* 98 (1) (1992) 903–909.
- [8] K.E. Heinemeier, G.E. Schiller, C.C. Benton, Task conditioning for the workplace: Issues and challenges, *ASHRAE Trans.* 96 (2) (1990) 678–689.
- [9] P.O. Fanger, Indoor air quality in the 21st century: Search for excellence, *Indoor Air* 10 (2) (2000) 68–73.
- [10] P.C. Hsu, X. Liu, C. Liu, et al., Personal thermal management by metallic nanowire-coated textile, *Nano Lett.* 15 (1) (2015) 365–371.
- [11] M. Vesely, W. Zeiler, Personalized conditioning and its impact on thermal comfort and energy performance—A review, *Renew. Sustain. Energy Rev.* 34 (2014) 401–408.
- [12] S.B. Godithi, E. Sachdeva, V. Garg, et al., A review of advances for thermal and visual comfort controls in personal environmental control (PEC) systems, *Intell. Build. Int.* 11 (2) (2019) 75–104.
- [13] R. Rawal, M. Schweiker, O.B. Kazanci, et al., Personal comfort systems: a review on comfort, energy and economics, *Energy Build.* 214 (2020) 109858.
- [14] B. Yang, A.K. Melikov, A. Kabanshi, et al., A review of advanced air distribution methods—theory, practice, limitations and solutions, *Energy Build.* 202 (2019) 109359.
- [15] E.A. Arens, F. Bauman, L. Johnston, et al., Testing of localized ventilation systems in a new controlled environment chamber, *Indoor Air* 1 (3) (1991) 263–281.
- [16] F.S. Bauman, H. Zhang, E. Arens, et al., Localized comfort control with a desktop task conditioning system: laboratory and field measurements, *ASHRAE Trans.* 99 (2) (1993) 733–749.
- [17] A. Hedge, A. Michael, S. Parmelee, Reactions of facilities managers and office workers to underfloor task air ventilation, *J. Arch. Plan. Res.* 10 (1993) 203–218.
- [18] M. Fountain, E. Arens, R. de Dear, et al., Locally controlled air movement preferred in warm isothermal environments, *ASHRAE Trans.* 100 (2) (1994) 937–952.
- [19] W.M. Kroner, Environmentally responsive workstations and office-worker productivity, *ASHRAE Trans.* 100 (2) (1994) 750–755.
- [20] D. Faulkner, W.J. Fisk, D.P. Sullivan, et al., Ventilation efficiencies of desk-mounted task/ambient conditioning systems, *Indoor Air* 9 (4) (1999) 273–281.
- [21] A.K. Melikov, R.S. Arakelian, L. Halkjaer, et al., Spot Cooling. Part 2: Recommendations for Design of Spot-Cooling Systems (No. CONF-9406105-), American Society of Heating, Refrigerating and Air-Conditioning Engineers, Inc., Atlanta, GA United States, 1994.
- [22] Y. Zhang, R. Zhao, Effect of local exposure on human responses, *Build. Environ.* 42 (7) (2007) 2737–2745.
- [23] N. Gong, K.W. Tham, A.K. Melikov, et al., The acceptable air velocity range for local air movement in the tropics, *HVAC&R Res.* 12 (4) (2006) 1065–1076.
- [24] S. Schiavon, A.K. Melikov, Energy saving and improved comfort by increased air movement, *Energy Build.* 40 (10) (2008) 1954–1960.
- [25] D. Faulkner, W.J. Fisk, D.P. Sullivan, et al., Ventilation efficiencies and thermal comfort results of a desk-edge-mounted task ventilation system, *Indoor Air* 14 (Suppl 8) (2004) 92–97.
- [26] D. Faulkner, W.J. Fisk, D.P. Sullivan, Indoor airflow and pollutant removal in a room with floor-based task ventilation: results of additional experiments, *Build. Environ.* 30 (3) (1995) 323–332.
- [27] W.J. Fisk, Health and Productivity Gains from Better Indoor Environments and Their Implications for the US Department of Energy (No. LBNL-47458), Lawrence Berkeley National Lab., CA (US), 2000.
- [28] P.O. Fanger, Human requirements in future air-conditioned environments, *Advances in Building Technology*, Elsevier, 2002, pp. 29–38.

- [29] F. Bauman, A. Baughman, G. Carter, et al., A Field Study of PEM (Personal Environmental Module) Performance in Bank of America's San Francisco Office Buildings, Center for Environmental Design Research, University of California, Berkeley, 1997.
- [30] T. Akimoto, F.S. Bauman, C.C. Benton, et al., Field study of a desktop-based task conditioning system, *J. Arch. Plan. Environ. Eng.* 61 (490) (1996) 35–46.
- [31] A.K. Melikov, R. Cermak, M. Majer, Personalized ventilation: evaluation of different air terminal devices, *Energy Build.* 34 (8) (2002) 829–836.
- [32] M. Dalewski, A.K. Melikov, M. Vesely, Performance of ductless personalized ventilation in conjunction with displacement ventilation: Physical environment and human response, *Build. Environ.* 81 (2014) 354–364.
- [33] B. Yang, C. Sekhar, The influence of evenly distributed ceiling mounted personalized ventilation devices on the indoor environment, *Int. J. Vent.* 7 (2) (2008) 99–112.
- [34] B. Yang, A. Melikov, C. Sekhar, Performance evaluation of ceiling mounted personalized ventilation system, *ASHRAE Trans.* 115 (2) (2009) 395–406.
- [35] B. Yang, C. Sekhar, A.K. Melikov, Ceiling mounted personalized ventilation system integrated with a secondary air distribution system—A human response study in hot and humid climate, *Indoor Air* 20 (4) (2010) 309–319 a.
- [36] B. Yang, C. Sekhar, A.K. Melikov, Ceiling mounted personalized ventilation system in hot and humid climate—An energy analysis, *Energy Build.* 42 (12) (2010) 2304–2308 b.
- [37] J. Niu, N. Gao, M. Phoebe, et al., Experimental study on a chair-based personalized ventilation system, *Build. Environ.* 42 (2) (2007) 913–925.
- [38] D. Pan, M. Chan, L. Xia, et al., Performance evaluation of a novel bed-based task/ambient conditioning (TAC) system, *Energy Build.* 44 (2012) 54–62.
- [39] L. Lan, Z. Lian, X. Zhou, et al., Pilot study on the application of bedside personalized ventilation to sleeping people, *Build. Environ.* 67 (2013) 160–166.
- [40] N. Gao, J. Niu, J. CFD study on micro-environment around human body and personalized ventilation, *Build. Environ.* 39 (7) (2004) 795–805.
- [41] N. Gao, J. Niu, Modeling the performance of personalized ventilation under different conditions of room air and personalized air, *HVAC&R Res.* 11 (4) (2005) 587–602.
- [42] A.K. Melikov, Personalized ventilation, *Indoor Air* 14 (Suppl. 7) (2004) 157–167.
- [43] R. Cermak, A.K. Melikov, L. Forejt, et al., Performance of personalized ventilation in conjunction with mixing and displacement ventilation, *HVAC&R Res.* 12 (2) (2006) 295–311.
- [44] S. Kato, J.H. Yang, Study on inhaled air quality in a personal air-conditioning environment using new scales of ventilation efficiency, *Build. Environ.* 43 (4) (2008) 494–507.
- [45] A. Melikov, T. Ivanova, Seat headrest-incorporated personalized ventilation: Thermal comfort and inhaled air quality, *Build. Environ.* 47 (2012) 100–108.
- [46] J.S. Russo, T.Q. Dang, H.E. Khalifa, Computational analysis of reduced-mixing personal ventilation jets, *Build. Environ.* 44 (8) (2009) 1559–1567.
- [47] H.E. Khalifa, M.I. Janos, J.F. Dannenhoffer III, Experimental investigation of reduced-mixing personal ventilation jets, *Build. Environ.* 44 (8) (2009) 1551–1558.
- [48] A. Makhoul, K. Ghali, N. Ghaddar, Thermal comfort and energy performance of a low-mixing ceiling-mounted personalized ventilator system, *Build. Environ.* 60 (2013) 126–136.
- [49] C. Shen, N. Gao, T. Wang, CFD study on the transmission of indoor pollutants under personalized ventilation, *Build. Environ.* 63 (2013) 69–78.
- [50] B. Yang, S. Schiavon, C. Sekhar, et al., Cooling efficiency of a brushless direct current stand fan, *Build. Environ.* 85 (2015) 196–204.
- [51] J. Yang, C. Sekhar, D. Cheong, et al., Performance evaluation of an integrated Personalized Ventilation–Personalized Exhaust system in conjunction with two background ventilation systems, *Build. Environ.* 78 (2014) 103–110.
- [52] X. Zhou, Z. Lian, L. Lan, Experimental study on a bedside personalized ventilation system for improving sleep comfort and quality, *Indoor Built Environ.* 23 (2) (2014) 313–323.
- [53] Z.A. Adamu, M.J. Cook, A.D. Price, Natural personalised ventilation—a novel approach, *Int. J. Vent.* 10 (3) (2011) 263–275.
- [54] M.P. Bivolarova, A.K. Melikov, C. Mizutani, et al., Bed-integrated local exhaust ventilation system combined with local air cleaning for improved IAQ in hospital patient rooms, *Build. Environ.* 100 (2016) 10–18.
- [55] Y. Zhang, D. Wyon, L. Fang, et al., The influence of heated or cooled seats on the acceptable ambient temperature range, *Ergonomics* 50 (4) (2007) 586–600.
- [56] H. Zhang, E. Arens, D. Kim, et al., Comfort, perceived air quality, and work performance in a low-power task-ambient conditioning system, *Build. Environ.* 45 (1) (2010) 29–39.
- [57] W. Pasut, H. Zhang, E. Arens, et al., Effect of a heated and cooled office chair on thermal comfort, *HVAC&R Res.* 19 (5) (2013) 574–583.
- [58] W. Pasut, H. Zhang, E. Arens, et al., Energy efficient comfort with a heated/cooled chair: results from human subject tests, *Build. Environ.* 84 (2015) 10–21.
- [59] H. Zhang, E. Arens, M. Taub, et al., Using footwarmers in office for thermal comfort and energy savings, *Energy Build.* 104 (2015) 233–243.
- [60] B. Yang, Z. Li, B. Zhou, et al., Enhanced effects of footwarmer by wearing sandals in winter office: A Swedish case study, *Indoor Built Environ.* (2020), doi:10.1177/1420326X20913975.
- [61] S. Aththajariyakul, C. Lertsattitanakorn, Small fan assisted air conditioner for thermal comfort and energy saving in Thailand, *Energy Convers. Manag.* 49 (10) (2008) 2499–2504.
- [62] S. Watanabe, A.K. Melikov, G.L. Knudsen, Design of an individually controlled system for an optimal thermal microenvironment, *Build. Environ.* 45 (3) (2010) 549–558.
- [63] Y. Zhai, H. Zhang, Y. Zhang, et al., Comfort under personally controlled air movement in warm and humid environments, *Build. Environ.* 65 (2013) 109–117.
- [64] L. Huang, Q. Ouyang, Y. Zhu, et al., A study about the demand for air movement in warm environment, *Build. Environ.* 61 (2013) 27–33.
- [65] Y. Zhai, Y. Zhang, H. Zhang, et al., Human comfort and perceived air quality in warm and humid environments with ceiling fans, *Build. Environ.* 90 (2015) 178–185.
- [66] J. Yang, S.C. Sekhar, K.W.D. Cheong, et al., Performance evaluation of a novel personalized ventilation–personalized exhaust system for airborne infection control, *Indoor Air* 25 (2) (2015) 176–187.
- [67] S. Schiavon, B. Yang, Y. Donner, Thermal comfort, perceived air quality and cognitive performance when personally controlled air movement is used by tropically acclimatized persons, *Indoor Air* 27 (3) (2017) 690–702.
- [68] H. Zhang, E. Arens, Y. Zhai, A review of the corrective power of personal comfort systems in non-neutral ambient environments, *Build. Environ.* 91 (2015) 15–41.
- [69] X. Du, R. Bokel, A. van den Dobbelen, Building microclimate and summer thermal comfort in free-running buildings with diverse spaces: a Chinese vernacular house case, *Build. Environ.* 82 (2014) 215–227.
- [70] G.N. Spyropoulos, C.A. Balaras, Energy consumption and the potential of energy saving in Hellenic office buildings used a bank branches—a case study, *Energy Build.* 43 (4) (2011) 770–778.
- [71] I.P. Knight, Assessing electric energy use in HVAC systems, *REHVA J.* 49 (1) (2012).
- [72] H. Ma, N. Du, S. Yu, et al., Analysis of typical public building energy consumption in northern China, *Energy Build.* 136 (2017) 139–150.
- [73] R. Jing, M. Wang, R. Zhang, et al., A study on energy performance of 30 commercial office building in Hong Kong, *Energy Build.* 144 (2017) 117–128.
- [74] ASHRAEASHRAE 55 Thermal Environmental Conditions for Human Occupancy, American Society of Heating, Refrigerating and Air Conditioning Engineers, Technology Park, GA, 2017.
- [75] S. Schiavon, A.K. Melikov, Introduction of a cooling-fan efficiency index, *HVAC&R Res.* 15 (6) (2009) 1121–1144.
- [76] J.A. Myhren, S. Holmberg, Design considerations with ventilation-radiators: comparisons to traditional two-panel radiators, *Energy Build.* 41 (1) (2009) 92–100.
- [77] G. Selvilgen, M. Kilib, Numerical analysis of air flow, heat transfer, moisture transport and thermal comfort in a room heated by two-panel radiators, *Energy Build.* 43 (1) (2011) 137–146.
- [78] S. Oxizidis, A.M. Papadopoulos, Performance of radiant cooling surfaces with respect to energy consumption and thermal comfort, *Energy Build.* 57 (2013) 199–209.
- [79] S.W. Hsiao, H.H. Lin, C.H. Lo, A study of thermal comfort enhancement by the optimization of airflow induced by a ceiling fan, *J. Interdiscipl. Math.* 19 (4) (2016) 859–891.
- [80] A. Lipczynska, S. Schiavon, L.T. Graham, Thermal comfort and self-reported productivity in an office with ceiling fans in the tropics, *Build. Environ.* 135 (2018) 202–212.
- [81] K.C. Parsons, The effects of gender, acclimation state, the opportunity to adjust clothing and physical disability on requirements for thermal comfort, *Energy Build.* 34 (6) (2002) 593–599.
- [82] X. Yue, T. Zhang, D. Yang, et al., Multifunctional Janus fibrous hybrid membranes with sandwich structure for on-demand personal thermal management, *Nano Energy* 63 (2019) 103808.
- [83] J.K. Tong, X. Huang, S.V. Boriskina, et al., Infrared-transparent visible-opaque fabrics for wearable personal thermal management, *ACS Photonics* 2 (6) (2015) 769–778.
- [84] P.C. Hsu, A.Y. Song, P.B. Catrysee, et al., Radiative human body cooling by nanoporous polyethylene textile, *Science* 353 (6303) (2016) 1019–1023.
- [85] J.F. Ham, Use of a Vortex tube in safety clothing, *Arch. Environ. Health* 10 (4) (1965) 619–623.
- [86] B.A. Williams, A.B. Chambers, Effect of neck warming and cooling on thermal comfort, *Proceedings of the 2<sup>nd</sup> Conference on Portable Life Support Systems*, 1972, pp. 289–294. Report No. NASA SP-302.
- [87] C. Gao, K. Kuklane, F. Wang, et al., Personal cooling with phase change materials to improve thermal comfort from a heat wave perspective, *Indoor Air* 22 (6) (2012) 523–530.
- [88] W. Song, F. Wang, C. Zhang, et al., On the improvement of thermal comfort of university students by using electrically and chemically heated clothing in a cold classroom environment, *Build. Environ.* 94 (2015) 704–713.
- [89] W. Song, F. Wang, F. Wei, Hybrid cooling clothing to improve thermal comfort of office workers in a hot indoor environment, *Build. Environ.* 100 (2016) 92–101.
- [90] Z. Li Udayraj, Y. Ke, et al., Personal cooling strategies to improve thermal comfort in warm indoor environments: comparison of a conventional desk fan and air ventilation clothing, *Energy Build.* 174 (2018) 439–451.
- [91] Z. Li Udayraj, Y. Ke, et al., A study of thermal comfort enhancement using three energy-efficient personalized heating strategies at two low indoor temperatures, *Build. Environ.* 143 (2018) 1–14.
- [92] C. Zhang, C. Ren, Y. Li, et al., Designing a smart electrically heated sleeping bag to improve wearers' feet thermal comfort while sleeping in a cold ambient environment, *Text. Res. J.* 87 (10) (2016) 1251–1260.
- [93] D. Zhao, X. Lu, T. Fan, et al., Personal thermal management using portable thermoelectric for potential building energy saving, *Appl. Energy* 218 (2018) 282–291.
- [94] Z. Wang, K. Warren, M. Luo, et al., Evaluating the comfort of thermally dynamic wearable devices, *Build. Environ.* 167 (2020) 106443.
- [95] Y. Guo, C. Dun, J. Xu, et al., Ultrathin, washable, and large-area graphene papers for personal thermal management, *Small* 13 (44) (2017) 1702645.
- [96] L. Cai, A.Y. Song, P. Wu, et al., Warming up human body by nanoporous metalized polyethylene textile, *Nat. Commun.* 8 (2017) 496.
- [97] Y. Ke, F. Wang, P. Xu, et al., On the use of a novel nanoporous polyethylene

- (nanoPE) passive cooling materials for personal thermal comfort management under uniform indoor environments, *Build. Environ.* 145 (2018) 85–95.
- [98] Q. Liu, J. Huang, J. Zhang, et al., Thermal, waterproof, breathable, and antibacterial cloth with a nanoporous structure, *ACS Appl. Mater. Interfaces* 10 (2) (2018) 2026–2032.
- [99] L. Peng, B. Su, A. Yu, et al., Review of clothing for thermal management with advanced materials, *Cellulose* 26 (10) (2019) 6415–6448.
- [100] Z. Zhu, J. Zhang, Y.L. Tong, et al., Reduced graphene oxide membrane induced robust structural colors toward personal thermal management, *ACS Photonics* 6 (1) (2019) 116–122.
- [101] S.A. Nunneley, Water cooled garments: a review, *Space Life Sci.* 2 (3) (1970) 335–360.
- [102] K.L. Speckman, A. Allan, M.N. Sawka, et al., Perspectives in microclimate cooling involving protective clothing in hot environments, *Int. J. Ind. Ergonom.* 3 (2) (1988) 121–147.
- [103] C. Gao, K. Kuklane, I. Holmér, Cooling vest with phase change material packs: the effects of temperature gradient, mass and covering area, *Ergonomics* 53 (5) (2010) 716–723.
- [104] X. Wan, F. Wang, Udayraj, Numerical analysis of cooling effect of hybrid cooling clothing incorporated with phase change material (PCM) packs and air ventilation fans, *Int. J. Heat Mass Transf.* 126 (2018) 636–648.
- [105] Z. Kang, X. Wan Udayraj, et al., A new hybrid personal cooling system (HPCS) incorporating insulation pads for thermal comfort management: experimental validation and parametric study, *Build. Environ.* 145 (2018) 276–289.
- [106] F. Wang Udayraj, W. Song, et al., Performance enhancement of hybrid personal cooling clothing in a hot environment: PCM cooling energy management with additional insulation, *Ergonomics* 62 (7) (2019) 928–939.
- [107] Y. Heled, Y. Epstein, D.S. Moran, Heat strain attenuation while wearing NBC clothing: dry-ice vest compared to water spray, *Aviat. Space Environ. Med.* 75 (5) (2004) 391–396.
- [108] F. Wang, C.S.W. Chow, Q. Zheng, et al., On the use of personal cooling suits to mitigate heat strain of mascot actors in a hot and humid environment, *Energy Build.* 205 (2019) 109561.
- [109] J. Yang, F. Wang, G. Song, et al., Effects of clothing size and air ventilation rate on cooling performance of air ventilation clothing in a warm condition, *Int. J. Occup. Saf. Ergon.* (2020), doi:10.1080/10803548.2020.1762316.
- [110] M. Zhao, C. Gao, F. Wang, et al., A study on local cooling of garments with ventilation fans and openings placed at difference torso sites, *Int. J. Ind. Ergonom.* 43 (3) (2013) 232–237.
- [111] M. Zhao, K. Kuklane, K. Lundgren, et al., A ventilation cooling shirt worn during office work in a hot climate: cool or not? *Int. J. Occup. Saf. Ergon.* 21 (4) (2015) 457–463.
- [112] S. Hong, Y. Gu, J.K. Seo, et al., Wearable thermoelectrics for personalized thermoregulation, *Sci. Adv.* 5 (5) (2019) eaaw0536.
- [113] R.A. Kishore, A. Nozariasbmarz, B. Poudel, et al., Ultra-high performance wearable thermoelectric coolers with less materials, *Nat. Commun.* 10 (2019) 1765.
- [114] L.E. Bell, Cooling, heating, generating power, and recovering waste heat with thermoelectric systems, *Science* 321 (5895) (2008) 1457–1461.
- [115] F. Wang, W. Song, An investigation of thermophysiological responses of human while using four personal cooling strategies during heatwave, *J. Therm. Biol.* 70 (2017) 37–44.
- [116] R. Hu, Y. Liu, S. Shin, et al., Emerging materials and strategies for personal thermal management, *Adv. Energ. Mater.* (2020), doi:10.1002/aenm.201903921.
- [117] F. Wang, C. Gao, K. Kuklane, et al., A review of technology of personal heating garments, *Int. J. Occup. Saf. Ergon.* 16 (3) (2010) 387–404.
- [118] P. Xu, F. Wang, M. Zhao, Electrically heated clothing (EHC) for protection against cold stress, in: F. Wang, C. Gao (Eds.), *Protective clothing: managing thermal stress*, Woodhead Publishing, Cambridge, UK, 2014, pp. 281–295.
- [119] Y. He, N. Li, L. Zhou, et al., Thermal comfort and energy consumption in cold environment with retrofitted Huotong (warm-barrel), *Build. Environ.* 112 (2017) 285–295.
- [120] A. Kusiak, G. Xu, Z. Zhang, Minimization of energy consumption in HVAC systems with data-driven models and an interior-point method, *Energy Convers. Manag.* 85 (2014) 146–153.
- [121] Y. Peng Y, Y. Cui, Advanced textiles for personal thermal management and energy, *Joule* 4 (4) (2020) 724–742.
- [122] F. Wang, Z. Kang, J. Zhou, Model validation and parametric study on a personal heating clothing system (PHCS) to help occupant attain thermal comfort in unheated buildings, *Build. Environ.* 162 (2019) 106308.



## Preparation, characterization and thermophysical properties investigation of A70/polyaniline nanocomposite phase change material for medium temperature solar applications

A.K. Pandey<sup>a,\*</sup>, Mathew George<sup>b</sup>, Nasrudin Abd Rahim<sup>b,c,\*\*</sup>, V.V. Tyagi<sup>d</sup>, Syed Shahabuddin<sup>e</sup>, R. Saidur<sup>a</sup>

<sup>a</sup> Research Centre for Nano-Materials and Energy Technology (RCNMET), School of Science and Technology, Sunway University, No. 5, Jalan Universiti, Bandar Sunway, Petaling Jaya, 47500 Selangor Darul Ehsan, Malaysia

<sup>b</sup> Higher Institution Centre of Excellence (HiCoE), UM Power Energy Dedicated Advanced Centre (UMPEDAC), Level 4, Wisma R&D, University of Malaya, Jalan Pantai Baharu, 59990 Kuala Lumpur, Malaysia

<sup>c</sup> Renewable Energy Research Group, King Abdulaziz University, Jeddah 21589, Saudi Arabia

<sup>d</sup> School of Energy Management, Shri Mata Vaishno Devi University, Katra 182320, (J&K), India

<sup>e</sup> Department of Science, School of Technology, Pandit Deendayal Petroleum University, Knowledge Corridor, Raisan Village, Gandhinagar 382007, Gujrat, India

### ARTICLE INFO

#### Keywords:

Phase change materials  
Solar energy  
Thermal conductivity  
Latent heat  
Polyaniline

### ABSTRACT

The ever-present demand for energy from various application in industrial and domestic processes has led to the consumption of fossil fuel at a rapid rate with adverse effect due to global warming. This study focuses on the thermal energy storage aspect intended for medium temperature applications. A novel composite A70 and PANI was prepared and characterized. The study investigates the composites thermophysical and optical properties. Differential Scanning Calorimetry and Transient Hot Bridge measured thermal storage capacity and thermal conductivity of the composite, respectively. The heat storage capacity of the composite remained stable within 4% whereas a highest rise of 11.96% in thermal conductivity was measured. The composites thermal, chemical, and physical stability were analysed from Thermogravimetric Analyser, Fourier Infrared Transform, and Scanning Electron Microscope, respectively. The composites were thermally stable up to a temperature of 250 °C. No chemical reaction occurred between the nanomaterial and base PCM matrix. The microscopic visuals did not show any considerable change in the microscopic structure of the material. In the case of optical properties, the composites showed significant reduction in transmittance of solar spectrum with respect to pure A70. The maximum decrement in transmission was around ~89% compared to A70. As the composite prepared were thermally stable till 250 °C, hence may be utilized for solar thermal and low concentrated photovoltaic application but not limited to these.

### 1. Introduction

Energy demand is increasing as the global population is growing and becoming more affluent [1]. Building energy consumes 40% of the energy supplied [2], while medium temperature source is required for domestic purposes [3]. Heating burns fossil fuels which in turn increases the greenhouse gasses [4] and oil shortage [5]. Various sources like solar, waste heat from industrial processes, geothermal spots etc., provides thermal energy. The challenge is to store the thermal energy effectively

and utilize it for various application like saline water to portable water, hot water for domestic use, preheating in thermal power plants, battery temperature management, lowering energy consumption in buildings and so on [6,7,3]. Latent heat storage, sensible heat storage and chemical heat storage are three forms of storing thermal energy. Phase change material (PCM), especially organic PCM, can store and release thermal energy at a transition temperature, is a form of latent heat storage system. Organic PCM are attractive than other forms of thermal energy due to their high storage capacity and small change in temperature dur-

\* Corresponding author at: Research Centre for Nano-Materials and Energy Technology (RCNMET), School of Science and Technology, Sunway University, No. 5, Jalan Universiti, Bandar Sunway, Petaling Jaya, 47500 Selangor Darul Ehsan, Malaysia.

\*\* Corresponding author at: Higher Institution Centre of Excellence (HiCoE), UM Power Energy Dedicated Advanced Centre (UMPEDAC), Level 4, Wisma R&D, University of Malaya, Jalan Pantai Baharu, 59990 Kuala Lumpur, Malaysia.

E-mail addresses: [adarsh.889@gmail.com](mailto:adarsh.889@gmail.com), [adarshp@sunway.edu.my](mailto:adarshp@sunway.edu.my) (A.K. Pandey), [nasrudin@um.edu.my](mailto:nasrudin@um.edu.my) (N.A. Rahim).

ing phase change process. Three broad categories of PCMs are organics, inorganics, and eutectics. Paraffin wax and fatty acids fall into the category of organics, while salt hydrates and metallic PCM falls into inorganics whereas a homogenous mixture of two or more PCM is defined by eutectic PCM. Inorganics are cost effective, have larger storage capacities, and larger energy density but lack chemical stability compared to organics [8,9]. Whereas in organic PCM, paraffin wax is widely utilized for its flexibility in its transition temperature, chemical and physical stability, cost effectiveness, large scale production industrially and application as thermal energy storage medium in solar and industrial waste heat management [10,11]. Hence, in the present study, A70 a paraffin product from PULSICE is selected due to the feasible option for immediate implementation.

Recent studies investigated in paraffin wax is related to improvement in light absorption or decrement in light transmission, enhancement in thermal conductivity for indirect thermal transport, effect on heat storage capacity, weight degradation over temperature for thermal stability and so on [12–16]. Addition of CuO nanoparticles to prepare paraffin wax composite resulted in improved light absorption. Improved light absorption increases the steady state temperature attained as investigated by Chen et al. [17]. Recent literature showed the thermal conductivity enhancement of paraffin wax with the addition of expanded perlite [18], ceramic foam [10], expanded graphite [11] and vanadium dioxide [5] by 80 to 450%. The improved thermal conductivity also resulted in the reduction of latent heat value from 15% to 63%. The proportion of reduction in latent heat was equivalent to the addition of non-phase change material [4,18]. Graphite and CuO was added to water to improve the solar direct absorption capability in solar stills [19]. Conducting polymer, Polyaniline(PANI), has been applied in the field of photocatalysis, batteries, thermoelectric devices and so on. This is attributed to its facile production, porosity, insolubility in water and nontoxic nature [20,21]. PANI has been utilized in fabricating composites with PCMs *n*-octadecane [21], 1-Tetrandeconal [22], Stearic Acid [23], and myristic acid [20] till date. PANI was utilized for shape stability of PCM due to its porous nature. The percentage weight addition varied from 20% to 50%. Therefore, there was considerable reduction in the heat storage capability. PANI possesses the capability to reduce infrared emissivity of the composite, increase electrical conductivity, and improve shape-stability.

From the literature review mentioned above, it is evident, adding nanoparticles can improve properties of PCM like enhancing the thermal conductivity, optical capability, and shape-stability. In this study, PANI was selected for the purpose of direct solar absorption system as the nanoparticle is known for its photocatalysis process and reduced emissivity in infrared region. To improve the efficiency of a solar thermal system, the coating provided should have high absorptance and lower emissivity [24]. The objective is to improve the light absorption or reduce the light transmission of the base PCM matrix. In previous studies involving PANI and PCM, the weight percentage was varied from 20% to 50% which in turn reduced the latent heat storage capacity significantly. This study investigates the thermal conductivity, latent heat, light transmission and thermal stability of the composite A70 with PANI. In authors knowledge, the novelty of the study is the preparation of the composite of A70 from PLUSICE and PANI for coating purpose in solar thermal system. The composite material may be applied to any surface as a coating for absorption of light in the ultraviolet and visible region wavelength. For example, the composite may be applied on the solar thermal absorber with prospects of reducing the storage tank capacity. The study also investigates microscopic and chemical compositional structure of the composite. This investigation intends the composite may be utilized for applications like heating in solar stills, solar domestic hot water and solar air heater (40 °C to 80 °C) [25], solar collector(60 °C to 67 °C) [26], cooling of pavements (42 °C to 78 °C) [27], low concentrated photovoltaic thermal system (37 °C to 65 °C) [6], and cooling of electric devices(40 °C to 80 °C) [28].

## 2. Materials and methods

### 2.1. Materials

A70 PLUSICE phase change material was purchased from PCM Products Ltd. Polyaniline (PANI) nanoparticles were synthesized from a previous study [29].

### 2.2. Nanocomposite fabrication

A70 is a phase change material (PCM) with phase transition temperature of 70 °C. A water bath at a temperature greater than 70 °C was maintained to melt A70. Analytical microbalance (Model: EX224, OHAUS) measured the required weight percentage (0.5%, 1% and 5%) of PANI. PANI was added to the liquid A70. The mixture was probe sonicated (Model: FS-1200 N) for a period of 30 mins under the influence of a water bath greater than 70 °C. The resultant mixture was cooled to ambient condition by natural method under static atmospheric conditions. The preparation of the composite is schematically shown in Fig. 1. A70 PCM with 0%, 0.5%, 1% and 5% PANI concentration are termed as A70, AP-0.5, AP-1 and AP-5 respectively.

### 2.3. Characterization

Fourier Transform Infrared (FTIR) Spectrum Two instrument from Perkin Elmer measured the transmission spectrum from 450 cm<sup>-1</sup> to 4000 cm<sup>-1</sup> with spectral-grade KBr pellets. LAMBDA 750 (Perkin Elmer) spectrometer measured light transmission from 200 nm to 800 nm. THB-500 (Linseis) Hot Point Kapton sensor measured the thermal conductivity of the samples. The accuracy of thermal conductivity is ± 5% and can measure thermal conductivities between 0.01 Wm<sup>-1</sup>K<sup>-1</sup> to 30.0 Wm<sup>-1</sup>K<sup>-1</sup>. Differential Scanning Calorimeter Analyzer (Model: DSC-100/C) measured and evaluated the latent heat and melting point values of the samples. Cold compression was utilized for sealing the samples in aluminum crucible of volume 40 µl. Measurements were carried out from 30 °C to 100 °C at a heating rate of 10 °C/min under N<sub>2</sub> atmosphere. The instrument can evaluate temperature range of –50 °C to 600 °C with heating rates varying from 0.001 to 1000 °C/min. The accuracy of the latent heat was 2% and temperature within ± 0.2 K. Thermogravimetric Analyzer (Model: TGA 4000, Perkin Elmer) evaluated the percentage weight loss for the samples with a maximum temperature range of 30 °C to 1000 °C. The samples were placed in a 180 µl crucible and subjected to a 10 °C/min from 30 °C to 1000 °C under N<sub>2</sub> atmosphere

## 3. Results and discussion

### 3.1. Morphology

In Fig. 2, surface structure of PANI nanoparticles, base A70 and AP composite are shown. Magnification lower than 1 µm of A70 and AP were not possible as the high electron beam melted the material. Tube-like structure of PANI is visible from the higher magnification of PANI nanoparticles. The outer diameter of the tube varied from 50 to 80 nm and termed as nanoparticle as the size remained lower than 100 nm [30]. Upon addition of PANI to A70 to fabricate the composite AP, the smooth surface integrated with PANI is visible from the microscopic image shown in Fig. 2(b) and Fig. 2(c), respectively. To understand the dispersion of PANI in A70, the elemental mapping of AP is shown in Fig. 2(d) and Fig. 2(e). From the elemental mapping it is evident the dispersion of the PANI is uniform with no agglomeration noticeable.

### 3.2. Latent heat capacity

The DSC curve of the base A70 and its prepared composites are plotted in Fig. 3 and tabulated in Table 1. The latent heat value for A70, AP-0.5, AP-1 and AP-5 are 171.19 J/g, 173.57 J/g, 164.88 J/g and 166.61 J/g, respectively. It is noted that AP-0.5 has an increment in its latent heat whereas all other composites show a decrement in its latent heat capacity compared to A70. The melting temperature are 71.9 °C,

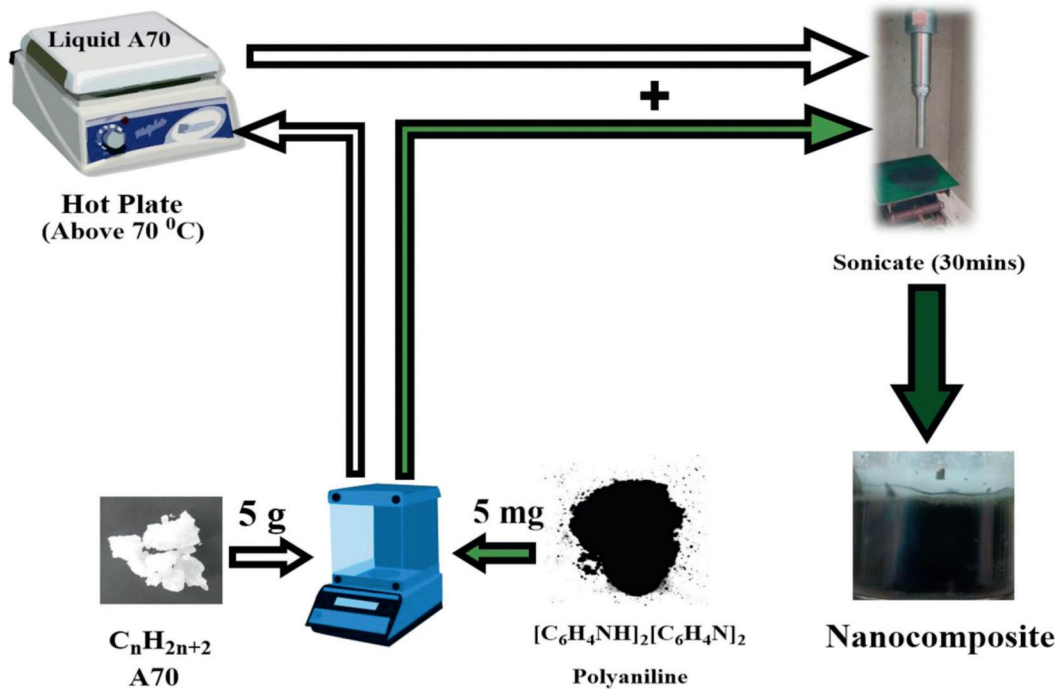


Fig. 1. Preparation of A70 nanocomposite.

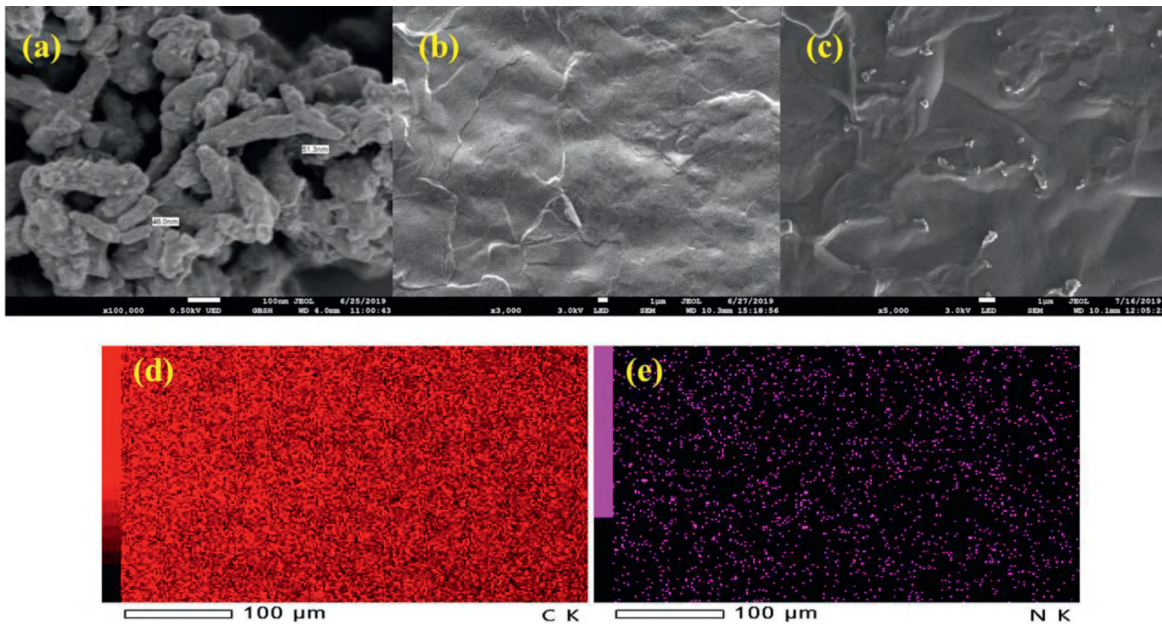


Fig. 2. Microscopic (FESEM) images of (a) Polyaniline, (b) A70, (c) AP and the elemental mapping of AP with (d) C and (e) N.

**Table 1**  
The DSC data for A and its composites.

Composites	Latent Heat(J/g)	Melting Temp.(°C)	Change in Latent Heat(%)	Change in Melting Temp.(%)
A70	171.19	71.9	-	-
AP-0.5	173.57	70.0	1.39	-2.64
AP-1	164.88	70.7	-3.67	-1.66
AP-5	166.61	74.7	-2.67	3.89

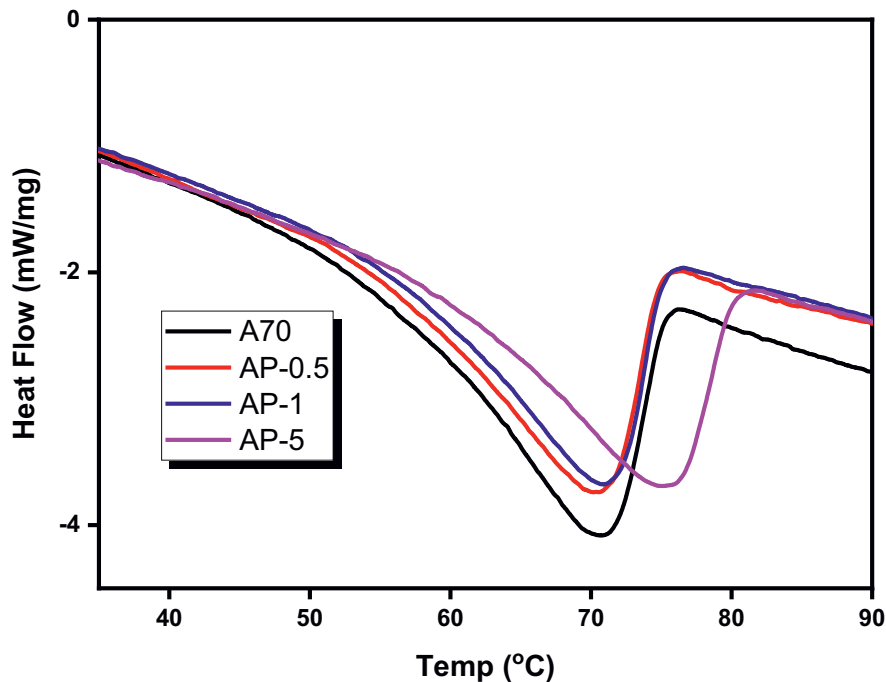


Fig. 3. DSC curve of A, AP-0.5, AP-1 and AP-5.

70.0 °C, 70.7 °C, and 74.7 °C for A, AP-0.5, AP-1 and AP-5, respectively. In terms of melting temperature, it is observed that all the composites except for AP-5 has no significant change in melting temperature. But in the case of AP-5, melting temperature increased relative to A70 by 2.8 °C.

Three cases need to be understood in the present study regarding the DSC data (1) increase in latent heat and (2) decrease in latent heat and (3) change in melting temperature. For the first case, the increase in latent heat may due to improved intermolecular attraction between the PANI nanoparticles and base A70 [31]. The large surface of PANI nanoparticles enhances the intermolecular forces between the PANI and A70 which may be greater than the energy needed to break the intermolecular forces between A70. This leads to greater energy expenditure for phase transition from solid state to liquid state. For the second case of decrement in latent heat capacity, this may be attributed to the addition of non-phase change material which replaces existing PCM and hence reduces the overall storage capacity [15]. The changes in latent heat capacity is not linear with respect to the concentration of the nanoparticles in A70. Finally, the third case of the shift in melting temperature may be attributed to the size, mass fraction and structure of the nanoparticles [32]. Another aspect for the increase may due to the immobilization of macromolecules on the surface of the filler which increases the melting temperature [33].

### 3.3. Thermal stability

Thermogravimetric Analyzer (TGA-4000, Perkin Elmer) is utilized for determining the thermal degradation of the composite. In Fig. 4 the weight degradation of the samples is illustrated. A one-step degradation of A70 and its composite can be observed between 200 °C to 450 °C. The onset of the degradation was evaluated based on 3% weight loss for all the samples. The onset temperature for A70, AP-0.5, AP-1 and AP-5 are 273 °C, 269.98 °C, 255.66 °C and 251.5 °C respectively. From the data, as PANI concentration rises, degradation onset temperature decreases. The reduction in onset temperature may be attributed to the aggregation of the nanoparticles to form micro-composite rather than nanocomposites [34]. But the composite is thermally stable to be utilized up to a temperature of 200 °C without thermal degradation.

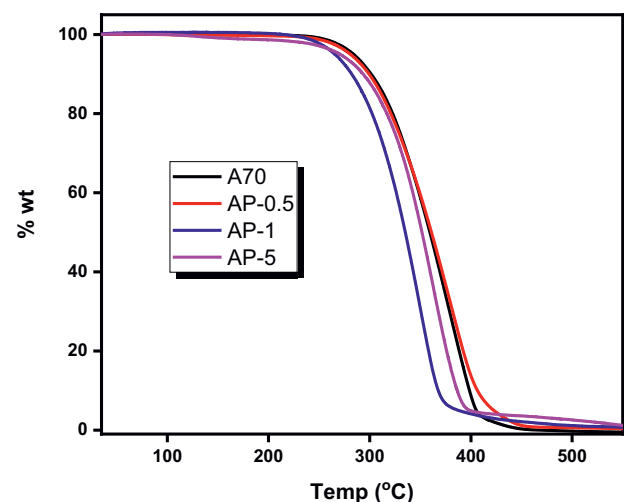


Fig. 4. TGA curve for A70, AP-0.5, AP-1 and AP-5.

### 3.4. Composition

The FTIR analysis is conducted to understand the composition of the prepared composite. The FTIR curves of PANI, A70 and AP-5 is plotted in Fig. 5. The manufacturer claims A70 is paraffin based and this can be identified by  $-\text{CH}_2$  group rocking motion ( $719$  to  $725\text{ cm}^{-1}$ ),  $-\text{CH}_3$  and  $-\text{CH}_2$  deformation ( $1350$ – $1470\text{ cm}^{-1}$ ), and  $-\text{CH}_3$  and  $-\text{CH}_2$  group symmetric vibration ( $2800$  –  $3000\text{ cm}^{-1}$ ) [35,18]. From the literature, the peaks of interest for PANI are C–C stretching of quinoid rings ( $1561\text{ cm}^{-1}$ ), C–C stretching of benzenoid rings ( $1481\text{ cm}^{-1}$ ), and C–N and C=N stretching ( $1301\text{ cm}^{-1}$ ) [29]. In Fig. 5, the FTIR curve of base A70 clearly exhibits peaks at  $719\text{ cm}^{-1}$ ,  $1463\text{ cm}^{-1}$ ,  $2848\text{ cm}^{-1}$ , and  $2917\text{ cm}^{-1}$  which corresponds identification peaks of paraffin wax. The peaks after the fabrication of AP composite, exhibits no new peak formation apart from A70 and PANI, hence the prepared material is a composite.

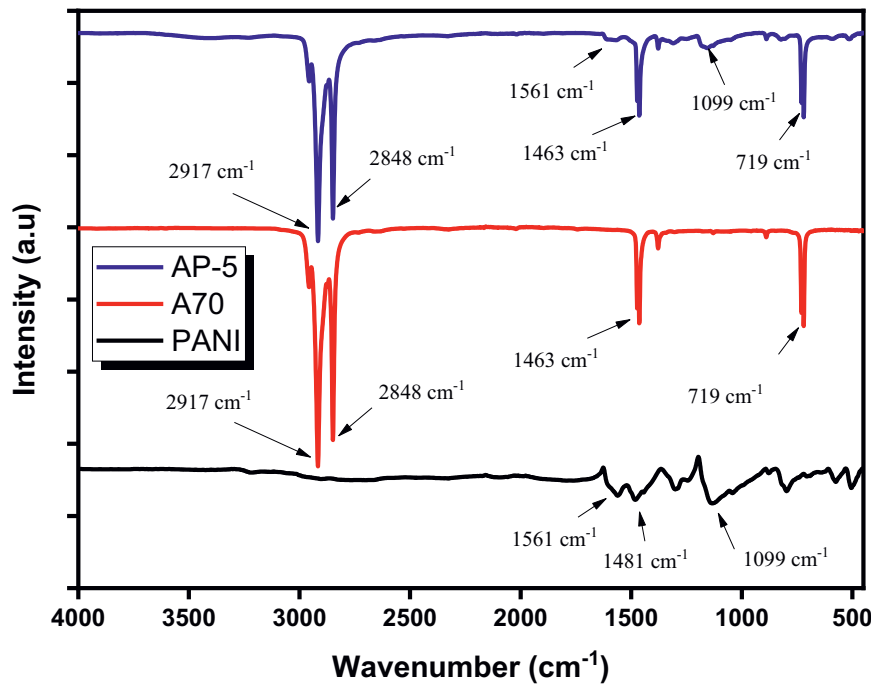


Fig. 5. The FTIR curve of PANI, A70 and AP-5 composite.

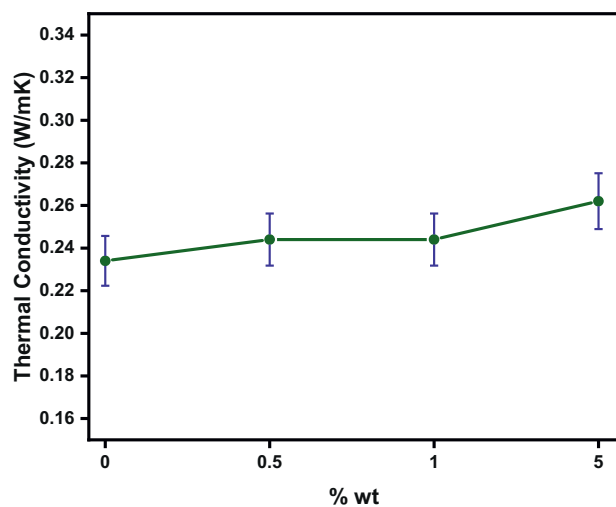


Fig. 6. Thermal conductivity of the samples prepared.

### 3.5. Thermal conductivity

Thermal conductivity provides an important thermal property of the material for indirect heat transportation purpose. Higher the thermal conductivity, better the material at transferring heat from one medium to another. The measured values of the samples with the corresponding error bars is represented in Fig. 6. The thermal conductivity values are  $0.234 \pm 0.0117 \text{ Wm}^{-1}\text{K}^{-1}$ ,  $0.244 \pm 0.0122 \text{ Wm}^{-1}\text{K}^{-1}$ ,  $0.244 \pm 0.0122 \text{ Wm}^{-1}\text{K}^{-1}$  and  $0.262 \pm 0.0131 \text{ Wm}^{-1}\text{K}^{-1}$  for A70, AP-0.5, AP-1 and AP-5 respectively. Maximum increment in thermal conductivity is around 11.96% for AP-5 composite. Hence the optimum composite for indirect thermal transfer is AP-5. Metals and conducting polymers use electron transfer for thermal transport whereas insulators use phonon transfer for thermal transfer [36,37]. In the present case, PANI is a conducting polymer and A70 is an insulator and hence thermal transport in the com-

posite is carried out via both phonon and electron transfer. For better electron transfer, a stable thermal network is required, while for effective phonon transfer mean free path of the phonon must be as large as possible [38]. Phonon thermal transfer is improved when phonons have larger mean free path. But mean free path is affected by three types of phonon scattering namely, phonon-phonon scattering, phonon-impurity scattering, and phonon-boundary scattering [38]. One of the above interactions will have the most significant effect on the mean free path of phonons. In this study, the nanoparticles (impurities) weight percentage is varied. The addition of nanoparticles increases the phonon scattering from nanoparticles which in turn reduces the thermal transport from phonon, if the limiting factor was phonon-impurity scattering. But simultaneously, an increment in thermal conductivity due to electron transport may occur from the thermal network formation of the nanoparticles added. Hence, two factors contribute an essential part in thermal conductivity of the composite, enhancement from thermal network formation from PANI nanoparticles added and decrement from phonon-impurity scattering with increase in PANI (impurity) concentration.

### 3.6. Light transmission

The UV-VIS of A70 and its composites are represented in Fig. 7. Increasing the concentration of nanoparticles reduced the light transmission of the composite. The reduction in light transmission may be attributed to the light conversion of PANI. The reduced light can also be stated as improved light absorption of the material. Therefore, the composites prepared shows excellent attribute for direct absorption of solar energy application. This is further validated by using solar spectrum data provided by NREL [39], to calculate the solar transmission percentage if solar spectrum was incident on the composite. It is observed A70, AP-0.5, AP-1, and AP-5 transmits 23.94%, 22.13%, 8.53% and 2.67% with respect to incident solar spectrum, respectively. Hence, with increase in concentration the absorption of the solar energy increases, thereby increasing its applicability in direct solar thermal application.

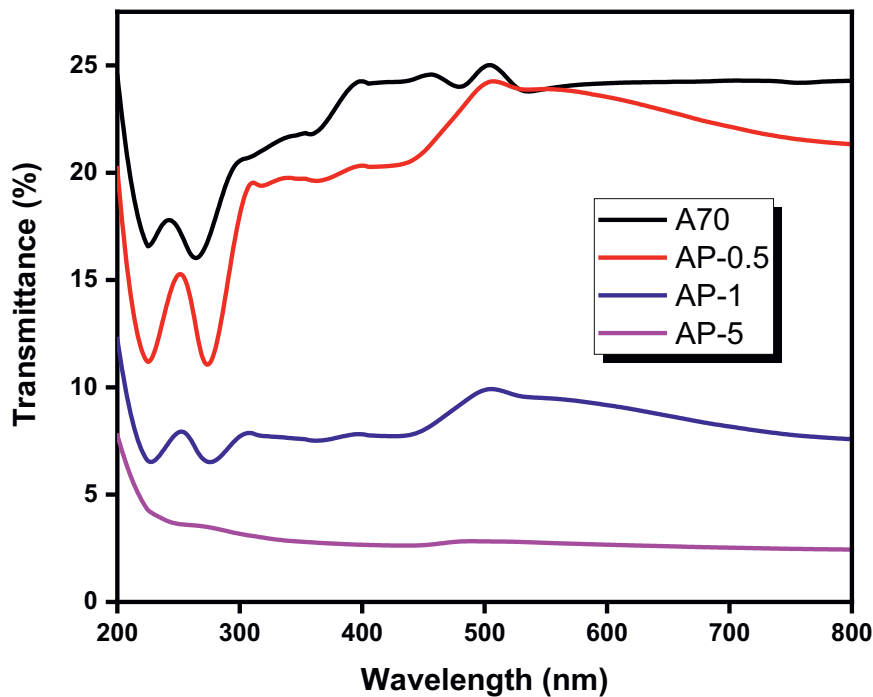


Fig. 7. The UV–VIS of A70 and its composites.

#### 4. Conclusions

In the present work, a composite between A70 and PANI was prepared and thermophysical properties investigated. FTIR analysis proved the compositional stability of the composite prepared. TGA confirmed the composite can be utilized till 200 °C without weight degradation. The addition of nanoparticles did not significantly alter the latent heat of composite with respect to A70. Thermal conductivity was enhanced by 11.96% for AP-5 composite. A significant reduction in solar spectrum transmission occurs with increase in concentration of PANI nanoparticles. The light transmission of the composite with respect to solar spectrum reduced from 23.94% to 2.67% from A70 to AP-5, respectively. The composite shows significant promise in the application involving direct solar spectrum. From the significance of the values measured and evaluated, AP-5 composite is the optimized composite with only 2.67% reduction in latent heat followed by an increment of 11.96% in thermal conductivity and 88.84% decline in solar spectrum transmission with respect to pure A70. Future work will be to investigate the composite in real world application and reliability analysis through thermal cycling.

#### Declaration of Competing Interest

The authors declare that they have no known competing financial interests or personal relationships that could have appeared to influence the work reported in this paper.

#### CRedit authorship contribution statement

**A.K. Pandey:** Conceptualization, Data curation, Methodology, Validation, Visualization, Supervision, Project administration, Funding acquisition, Writing - original draft. **Mathew George:** Formal analysis, Methodology, Investigation, Data curation, Writing - original draft. **Nasrudin Abd Rahim:** Supervision, Project administration, Funding acquisition. **V.V. Tyagi:** Writing - review & editing, Validation. **Syed Shahabuddin:** Resources. **R. Saidur:** Resources, Project administration, Funding acquisition.

#### Acknowledgements

One of the author (A K Pandey) duly acknowledges the financial assistance through Sunway University collaborative research fund: MRU 2019 (STR-RMF-MRU-004-2019) for carrying out this research. The authors thank the technical and financial assistance of UM Power Energy Dedicated Advanced center (UMPEDAC) and the Higher Institution center of Excellence (HiCoE) Program Research Grant, UMPEDAC - 2018 (MOHE HiCoE - UMPEDAC), Ministry of Education Malaysia, TOP100UMPEDAC and RU012–2019, University of Malaya.

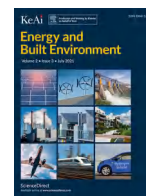
#### Supplementary materials

Supplementary material associated with this article can be found, in the online version, at doi:10.1016/j.enbenv.2020.09.001.

#### References

- [1] X. Zhang, C. Zhu, G. Fang, Preparation and thermal properties of n-eicosane/nano-SiO<sub>2</sub>/expanded graphite composite phase-change material for thermal energy storage, *Mater. Chem. Phys.* 240 (2020) 122178, doi:10.1016/j.matchemphys.2019.122178.
- [2] S. Wi, S. Yang, J.H. Park, S.J. Chang, S. Kim, Climatic cycling assessment of red clay/perlite and vermiculite composite PCM for improving thermal inertia in buildings, *Build Environ.* 167 (2020) 106464, doi:10.1016/j.buildenv.2019.106464.
- [3] W. Lu, G. Liu, Z. Xiong, Z. Wu, G. Zhang, An experimental investigation of composite phase change materials of ternary nitrate and expanded graphite for medium-temperature thermal energy storage, *Sol. Energy* 195 (2020) 573–580, doi:10.1016/j.solener.2019.11.102.
- [4] A. Reyes, L. Henríquez-Vargas, J. Vásquez, N. Pailahueque, G. Aguilar, Analysis of a laboratory scale thermal energy accumulator using two-phases heterogeneous paraffin wax-water mixtures, *Renew. Energy* 145 (2020) 41–51, doi:10.1016/j.renene.2019.06.007.
- [5] T. Cheng, N. Wang, H. Wang, R. Sun, C.P. Wong, A newly designed paraffin@VO<sub>2</sub> phase change material with the combination of high latent heat and large thermal conductivity, *J. Colloid Interface Sci.* 559 (2020) 226–235, doi:10.1016/j.jcis.2019.10.033.
- [6] M. George, A.K. Pandey, N. Abd Rahim, V.V. Tyagi, S. Shahabuddin, R. Saidur, Concentrated photovoltaic thermal systems: a component-by-component view on the developments in the design, heat transfer medium and applications, *Energy Convers. Manag.* (2019) 186, doi:10.1016/j.enconman.2019.02.052.
- [7] A. Verma, S. Shashidhara, D. Rakshit, A comparative study on battery thermal management using phase change material (PCM), *Therm. Sci. Eng. Prog.* 11 (2019) 74–83, doi:10.1016/j.tsep.2019.03.003.

- [8] K.Y. Leong, M. Rosdzimin, A. Rahman, B.A. Gurunathan, Nano-enhanced phase change materials : a review of thermo-physical properties, applications and challenges, *J. Energy Storage* 21 (2019) 18–31, doi:10.1016/j.est.2018.11.008.
- [9] J. Zhang, Z. Wang, X. Li, X. Wu, Novel composite phase change materials with enhancement of light-thermal conversion, thermal conductivity and thermal storage capacity, *Sol. Energy* 196 (2020) 419–426, doi:10.1016/j.solener.2019.12.041.
- [10] R. Li, Y. Zhou, X. Duan, A novel composite phase change material with paraffin wax in tailings porous ceramics, *Appl. Therm. Eng.* 151 (2019) 115–123, doi:10.1016/j.applthermaleng.2019.01.104.
- [11] M. Kenisarin, K. Mahkamov, F. Kahwash, I. Makhkamova, Enhancing thermal conductivity of paraffin wax 53–57 °C using expanded graphite, *Sol. Energy Mater. Sol. Cells* 200 (2019) 110026, doi:10.1016/j.solmat.2019.110026.
- [12] N. Sahan, H.O. Paksoy, Thermal enhancement of paraffin as a phase change material with nanomagnetite, *Sol. Energy Mater. Sol. Cells* 126 (2014) 56–61, doi:10.1016/j.solmat.2014.03.018.
- [13] Yu Z.T., Fang X., Fan L.W., Wang X., Xiao Y.Q., Zeng Y., et al. Increased thermal conductivity of liquid paraffin-based suspensions in the presence of carbon nano-additives of various sizes and shapes. *Carbon NY* 2013;53:277–85. doi:10.1016/j.carbon.2012.10.059.
- [14] M. Li, A nano-graphite/paraffin phase change material with high thermal conductivity, *Appl. Energy* 106 (2013) 25–30, doi:10.1016/j.apenergy.2013.01.031.
- [15] L.W. Fan, X. Fang, X. Wang, Y. Zeng, Y.Q. Xiao, Z.T. Yu, et al., Effects of various carbon nanofillers on the thermal conductivity and energy storage properties of paraffin-based nanocomposite phase change materials, *Appl. Energy* 110 (2013) 163–172, doi:10.1016/j.apenergy.2013.04.043.
- [16] Z. Zhengguo, Z. Ni, P. Jing, F. Xiaoming, G. Xuenong, F. Yutang, Preparation and thermal energy storage properties of paraffin/expanded graphite composite phase change material, *Appl. Energy* 91 (2012) 426–431, doi:10.1016/j.apenergy.2011.10.014.
- [17] M. Chen, Y. He, Q. Ye, Z. Zhang, Y. Hu, Solar thermal conversion and thermal energy storage of CuO/Paraffin phase change composites, *Int. J. Heat Mass Transf.* 130 (2019) 1133–1140, doi:10.1016/j.ijheatmasstransfer.2018.11.026.
- [18] N. Mekaddem, Ali S Ben, M. Fois, A Hannachi, Paraffin/ expanded perlite/plaster as thermal energy storage composite, *Energy Procedia* 157 (2019) 1118–1129, doi:10.1016/j.egypro.2018.11.279.
- [19] S.W. Sharshir, G. Peng, A.H. Elsheikh, E.M.A. Edreis, M.A. Eltawil, T. Abdelhamid, et al., Energy and exergy analysis of solar stills with micro/nano particles: a comparative study, *Energy Convers. Manag.* 177 (2018) 363–375, doi:10.1016/j.enconman.2018.09.074.
- [20] S. Shahabuddin, R. Khanam, M. Khalid, R Saidur, Synthesis of 2D boron nitride doped polyaniline hybrid nanocomposites for photocatalytic degradation of carcinogenic dyes from aqueous solution, *Arab. J. Chem.* 11 (2018) 1000–1016, doi:10.1016/j.arabj.2018.05.004.
- [21] C. Ju, Y. Wang, D. He, Q. Gao, L. Gao, M. Fu, Synthesis and infrared property of polyaniline/phase-change nanocapsule composite, *J. Nanosci. Nanotechnol.* 11 (2012) 9665–9670, doi:10.1166/jnn.2011.5218.
- [22] J.L. Zeng, Y.Y. Liu, Z.X. Cao, J. Zhang, Z.H. Zhang, L.X. Sun, et al., Thermal conductivity enhancement of MWNTs on the PANI/tetradecanol form-stable PCM, *J. Therm. Anal. Calorim.* 91 (2008) 443–446, doi:10.1007/s10973-007-8545-2.
- [23] Y. Wang, H. Ji, H. Shi, T. Zhang, T.D Xia, Fabrication and characterization of stearic acid/polyaniline composite with electrical conductivity as phase change materials for thermal energy storage, *Energy Convers. Manag.* 98 (2015) 322–330, doi:10.1016/j.enconman.2015.03.115.
- [24] R.B. Pettit, R.R. Sowell, Solar absorptance and emittance properties of several solar coatings, *J. Vac. Sci. Technol.* 13 (1976) 596–602, doi:10.1116/1.569041.
- [25] K. B. A.K. Pandey, S. Shahabuddin, M. Samykano, T. M, R Saidur, Phase change materials integrated solar thermal energy systems: global trends and current practices in experimental approaches, *J. Energy Storage* 27 (2020) 101118, doi:10.1016/j.est.2019.101118.
- [26] K. Chopra, A.K. Pathak, V. Tyagi V, AK Pandey, S Anand, A Sari, Thermal performance of phase change material integrated heat pipe evacuated tube solar collector system: an experimental assessment, *Energy Convers Manag.* 203 (2020) 112205, doi:10.1016/j.enconman.2019.112205.
- [27] B.R. Anupam, U. Chandra, P. Rath, Phase change materials for pavement applications : a review, *Constr. Build. Mater.* 247 (2020) 118553, doi:10.1016/j.conbuildmat.2020.118553.
- [28] K. Du, J. Calautit, Z. Wang, Y. Wu, H. Liu, A review of the applications of phase change materials in cooling, heating and power generation in different temperature ranges, *Appl. Energy* 220 (2018) 242–273, doi:10.1016/j.apenergy.2018.03.005.
- [29] S. Shahabuddin, N.M. Sari, S. Mohamad, J.J. Ching, SrTiO<sub>3</sub> nanocube-doped polyaniline nanocomposites with enhanced photocatalytic degradation of methylene blue under visible light, *Polymers (Basel)* (2016) 8, doi:10.3390/polym8020027.
- [30] W.G. Kreyling, M. Semmler-Behnke, Q. Chaudhry, A complementary definition of nanomaterial, *Nano Today* 5 (2010) 165–168, doi:10.1016/j.nantod.2010.03.004.
- [31] L. Colla, L. Fedele, S. Mancin, L. Danza, O. Manca, Nano-PCMs for enhanced energy storage and passive cooling applications, *Appl. Therm. Eng.* 110 (2017) 584–589, doi:10.1016/j.applthermaleng.2016.03.161.
- [32] S. Harikrishnan, S. Imran Hussain, A. Devaraju, P. Sivasamy, S. Kalaiselvam, Improved performance of a newly prepared nano-enhanced phase change material for solar energy storage, *J. Mech. Sci. Technol.* 31 (2017) 4903–4910, doi:10.1007/s12206-017-0938-y.
- [33] O.A. Serenko, V.I. Roldughin, A.D. Askadskii, E.S. Serkova, V. Strashnov P, Shifrina ZB. The effect of size and concentration of nanoparticles on the glass transition temperature of polymer nanocomposites, *RSC Adv.* 7 (2017) 50113–50120, doi:10.1039/c7ra08152a.
- [34] D. Bikiaris, Can nanoparticles really enhance thermal stability of polymers? Part II: an overview on thermal decomposition of polycondensation polymers, *Thermochim. Acta* 523 (2011) 25–45, doi:10.1016/j.tca.2011.06.012.
- [35] N. Şahan, H. Paksoy, Investigating thermal properties of using nano-tubular ZnO powder in paraffin as phase change material composite for thermal energy storage, *Compos. Part B Eng.* 126 (2017) 88–93, doi:10.1016/j.compositesb.2017.06.006.
- [36] S. Wu, T. Yan, Z. Kuai, W Pan, Thermal conductivity enhancement on phase change materials for thermal energy storage: a review, *Energy Storage Mater.* 25 (2020) 251–295, doi:10.1016/j.ensm.2019.10.010.
- [37] L. Zhu, M. Gao, C.K.N. Peh, G.W Ho, Recent progress in solar-driven interfacial water evaporation: advanced designs and applications, *Nano Energy* 57 (2019) 507–518, doi:10.1016/j.nanoen.2018.12.046.
- [38] J.E. Juliá, D. Wen, M.E. Navarro, N. Navarrete, Y. Ding, R. Mondragón, Thermal energy storage of molten salt -based nanofluid containing nano-encapsulated metal alloy phase change materials, *Energy* 167 (2018) 912–920, doi:10.1016/j.energy.2018.11.037.
- [39] C.A. Gueymard, The sun's total and spectral irradiance for solar energy applications and solar radiation models, *Sol. Energy* 76 (2004) 423–453, doi:10.1016/j.solener.2003.08.039.



# Parametric analysis of a solar-driven trigeneration system with an organic Rankine cycle and a vapor compression cycle

Evangelos Bellos\*, Christos Tzivanidis

Thermal Department, School of Mechanical Engineering, National Technical University of Athens, Zografou, Heroon Polytechniou 9, 15780 Athens, Greece

## ARTICLE INFO

### Keywords:

Solar concentrating power  
Trigeneration  
ORC  
Exergy  
Parabolic trough collector

## ABSTRACT

The objective of this paper is the parametric analysis of a solar-fed trigeneration system ideal for the building sector that produces useful heat, electricity and cooling. The examined unit is driven by 100 m<sup>2</sup> of parabolic trough collectors which are combined with a sensible storage tank with thermal oil. An organic Rankine cycle is fed by solar useful heat production and it produces electricity while a part of its power drives a vapor compression cycle with R290. Heating is also produced by separate heat exchangers in the solar loop. The parametric analysis is conducted in steady-state conditions with a developed model in Engineering Equation Solver. The examined parameters are the following: superheating degree in the turbine inlet, cooling production, heating production, solar beam irradiation intense, sun angle, pressure level in the turbine inlet and heat source temperature level. For the nominal scenario of 10 kW cooling production at 5°C and 10 kW heating production at 60°C, the system produces 6.14 kW electricity, while the exergy and energy efficiencies are found 12.14% and 37.34% respectively. Assuming that the system operates 2500 h yearly, the simple payback period of the investment is calculated at 8.5 years. The maximum examined values for both heating and cooling production are at 20 kW.

## Abbreviations

DHW	Domestic Hot Water
EES	Engineering Equation Solver
HRS	Heat Recovery System
ORC	Organic Rankine Cycle
O&M	Operation and Maintenance
PTC	Parabolic Trough Collector
VCC	Vapor Compression Cycle

## 1. Introduction

Solar irradiation is a vital energy source for facing important energy issues such as global warming, the depletion of the ozone layer and high electricity prices [1]. The exploitation of solar energy in highly efficient energy systems, such as trigeneration/polygeneration systems is an interesting idea in order to produce clean energy with high effectiveness [2]. The trigeneration units are attractive choices in the building sector and they usually produce electricity, heating and cooling [3]. Their overall high performance is justified by the exploitation of internal energy flows and so the entropy generation is reduced [4]. Trigeneration systems are ideal units for the building sector because they provide the main energy needs of the buildings which are space-heating, cooling and electricity. Moreover, the building sector is a huge-energy consumer and

the adoption of renewable energies on it leads to future energy sustainability [5].

In the existing literature, there is plenty of works about solar-driven trigeneration configurations in terms of energy, exergy and financial analysis. Usually, parabolic trough collectors (PTC) are usually applied in these systems because they are one of the most developed solar technologies for high-temperature levels [6]. Usually, the researchers combine an organic Rankine cycle (ORC) with an absorption chiller in the studied trigeneration systems.

Al-Sulaiman et al. [7] studied a trigeneration configuration with PTCs and an organic Rankine cycle coupled to a cooling absorption heat pump which presents a 20% system exergy efficiency. A similar system has been optimized exergetically by Bellos and Tzivanidis [8] who found 29.4% maximum exergy efficiency and 152% energy efficiency. Ahmadi et al. [9] examined a multigeneration system with a double-stage ORC, two absorption machines, a drying device and an electrolyzer that produces cooling, electricity, heating, dry biomass and hydrogen. They found that the exergy and the energy efficiencies were 13.7% and 20.7% respectively. Mathkor et al. [10] examined a system that produces electricity, cooling and fresh-water. This unit uses an organic Rankine cycle, an absorption machine and a desalination unit, while its exergetic performance is close to 42%.

Except for solar energy, other energy sources have been also used in the literature. Khalid et al. [11] investigated a topology with an absorp-

\* Corresponding author.

E-mail address: [bellose@central.ntua.gr](mailto:bellose@central.ntua.gr) (E. Bellos).

**Nomenclature**

$A_{col}$	solar collecting area, $m^2$
$c_p$	specific heat capacity under constant pressure, $kJ\ kg^{-1}\ K^{-1}$
$C_0$	investment initial cost, €
CF	hourly cash flow, $€\ h^{-1}$
$G_b$	solar direct beam irradiation level, $W\ m^{-2}$
$h$	specific fluid enthalpy, $kJ\ kg^{-1}$
$K$	incident angle modifier, -
$K_{cool}$	cooling price, $€\ kWh_{cool}^{-1}$
$K_{el}$	electricity price, $€\ kWh_{el}^{-1}$
$K_{heat}$	heating price, $€\ kWh_{heat}^{-1}$
$K_{hex}$	heating heat exchanger cost, €
$K_{orc}$	specific cost of the organic Rankine cycle, $€\ kW_{el}^{-1}$
$K_{O\&M}$	operating and maintenance cost on a yearly basis, €
$K_{tank}$	specific cost of the sensible storage tank, $€\ m^{-3}$
$K_{vcc}$	specific cost of the vapor compression cycle, $€\ kW_{cool}^{-1}$
$m$	mass flow rate, $kg\ s^{-1}$
$P_{crit}$	critical pressure level, bar
$P_{el}$	net electricity production of the system, kW
$P_{el,orc}$	power production of the organic Rankine cycle, kW
$P_{high}$	high-pressure level in the organic Rankine cycle, bar
PP	pinch point (minimum temperature difference), °C
Q	heat/energy rate, kW
$s$	specific entropy, $kJ\ kg^{-1}\ K^{-1}$
SPP	simple Payback Period of the investment, years
$U_T$	overall tank thermal loss coefficient, $W\ m^{-2}\ K^{-1}$
T	temperature level, °C
$T_{sun}$	sun temperature level, K
$T_0$	reference temperature for exergy calculations, K
Time	yearly operating time, hours
$V_{tank}$	volume of the storage tank, $m^3$
$W_p$	organic fluid pump consumption, kW
$W_T$	turbine work product, kW

**Greek symbols**

$\alpha$	pressure ratio parameter, -
$\Delta T_s$	heat source temperature difference, °C
$\Delta T_{sh}$	turbine inlet superheating, °C
$\Delta T_{rc}$	minimum temperature difference in the recuperator, °C
$\eta_{en}$	system energy efficiency, -
$\eta_{ex}$	system exergy efficiency, -
$\eta_{is,com}$	compressor isentropic efficiency, -
$\eta_{is,T}$	turbine isentropic efficiency, -
$\eta_g$	electrical generator efficiency, -
$\eta_{hex}$	heating heat exchanger effectiveness, -
$\eta_m$	mechanical efficiency in the shaft, -
$\eta_{th,col}$	collector solar thermal efficiency, -
$\theta$	sun incident angle, °

**Subscripts and superscripts**

am	ambient
col	collector
com	compressor
con	condenser
cool	cooling
is	isentropic
in	inlet
heat	heating
hex	heat exchanger
high	high
hrs	heat recovery system
loss	tank thermal loss

orc	working fluid in the organic Rankine cycle
out	outlet
ref	working fluid in the vapor compression cycle
s	heat source
sat	saturation in the heat recovery system
sol	solar
st	storage tank
T	turbine
u	useful

tion chiller and ORC fed by solar collectors. The ORC assists with heat a vapor compression cycle for heating production at a proper temperature, while geothermic energy and wind energy are included in the system. The final results proved that the energetic and exergetic system performances were 76% and 7.3% respectively. Wu et al. [12] compared different trigeneration systems with ORC and they concluded exploiting the solar beam irradiation is a more effective technique financially compared to biomass and geothermal energy. Calise et al. [13] examined a trigeneration system that is fed by solar energy and geothermal energy which includes ORC and absorption chiller. The system exergetic performance was found close to 50%. In another work, Kasaeian et al. [3] investigated the combination of solar energy and biomass for electricity, heating, and refrigeration. The system includes gasifier, absorption chiller, heating heat exchangers and internal combustion engine. They found 51.4 system energy efficiency and they stated that the utilization of solar irradiation enhances the system performance by about 6%.

The next part of the literature includes studies that incorporate a vapor compression cycle (VCC) with other energy devices in trigeneration systems. The use of the VCC is an interesting idea because this is a relatively cheap device with high efficiency and so it can be easily utilized in the trigeneration system. Usually, this idea tries to avoid using a sorption machine (absorption or adsorption chiller) due to its high cost and its high complexity. Bellos et al. [14] analyzed a multigeneration system that produces electricity, cooling and two heating outputs. This system is driven by solar PTC and biomass while it includes ORC, vapor compression cycle (VCC) and boiler. According to their findings, the payback period is found at 5 years, the energy performance 51.3% and the exergy performance 21.8%. In another study, Karellas and Braimakis [15] studied a trigeneration unit with biomass and PTC as the heat sources for heating, cooling and electricity production. The PTC is used only for superheating the organic fluid in the ORC, while the biomass is the main heat source. The ORC is coupled to a VCC through the condenser device. The results showed exergy efficiency at 7% and the payback period at 7 years.

Moreover, there are other studies in the literature about complex trigeneration and polygeneration systems. Haghghi et al. [16] investigated a polygeneration system with molten carbonate fuel cells for fresh water, electricity, cooling and heating production. They found 80% energy efficiency and 52% exergy efficiency. In another work, Haghghi et al. [17] studied a system with PTC, ORC, two heat processes and two absorption chillers and they found energy efficiency up to 98% and exergy efficiency up to 17%. In another work [18], a polygeneration system based on a solid oxide fuel cell for hydrogen, electricity, fresh water and cooling production presented 78% energy efficiency and 47% exergy efficiency.

The aforementioned literature studies show that there is a lot of interest in the trigeneration systems driven by renewable energy sources and especially by solar irradiation. In this direction, this investigation comes to examine a solar-driven trigeneration system that is fed by PTC and produces heating, cooling and electricity. This system is studied parametrically and it is analyzed energetically, exergetically and financially. More specifically, the investigated unit includes PTC, storage tank, ORC and a VCC. The ORC operates with toluene and VCC with R290 as the

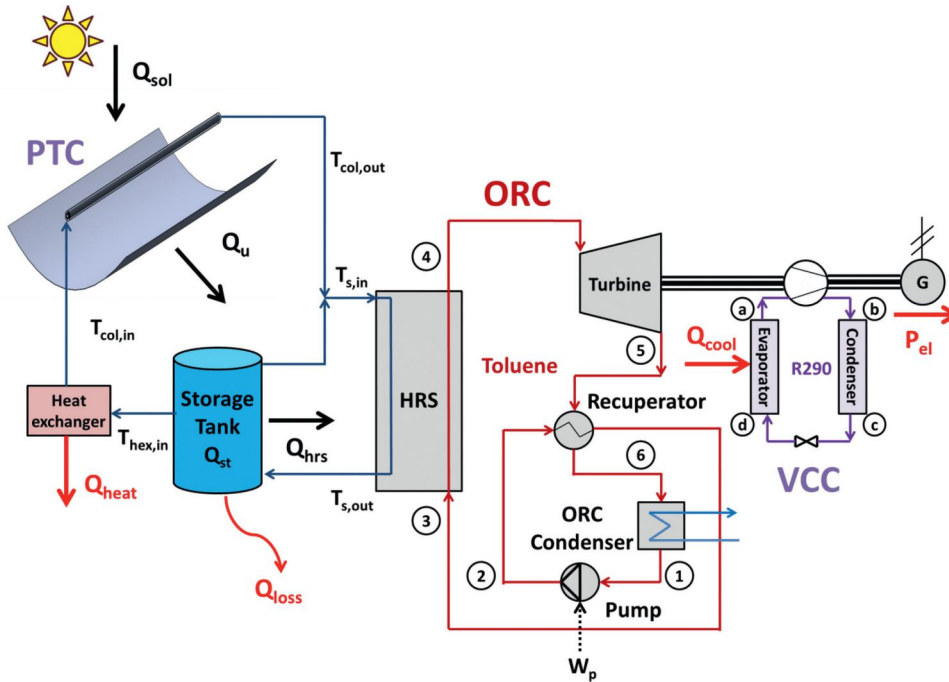


Fig. 1. The investigated configuration of the present work which includes PTC, PRC, VCC and a storage tank.

working fluids. This system is a simple configuration that can be easily applied in the buildings sector for covering the energy needs. The PTC feeds the ORC and also heat exchanging surfaces for heating production. The VCC is fed with work by the ORC turbine output and the net electricity of the shaft is assumed the net production of the system. Generally, in the literature, the studies with ORC and VCC are not usual, and especially the studies with solar-only systems. Also, as it has highlighted in the aforementioned literature review, the incorporation of a VCC in a trigeneration system can reduce the investment cost. Thus, the suggested unit is a promising choice for designing high efficient solar-driven trigeneration systems with a reasonable investment cost in order to create viable units. To our knowledge, the present solar-driven system has not been examined in the existing literature. In the end, it has to be said that the present work is done with a created thermodynamic model in Engineering Equation Solver (EES) environment [19].

## 2. Material and methods

### 2.1. Trigeneration topology

The investigated polygeneration system is exhibited in Fig. 1 in detail. This configuration produces heating at 60°C through a heat exchanger, electricity through an ORC and cooling with the VCC. The heating temperature level is an appropriate one for domestic hot water production (DHW) and/or space-heating in buildings. It has to be said that in this work, the examined system is studied for the simultaneous production of the three useful outputs. There are applications that need all these useful outputs during the year. For example, data centers need cooling during the year period and also domestic hot water demand exists during the year. So, a trigeneration system as the present one can be used in cases of building commodities and general in cases that many consumers (e.g. building clusters).

Parabolic trough collectors are used for feeding the studied unit and more specifically the Eurotrough PTC [20–21] is used with Therminol VP-1 [22] as the working fluid in the solar loop and in the tank. The ORC is a regenerative cycle and it operates with toluene. This working fluid is a promising one according to other studies [23]. The VCC operates with R290 which is a natural refrigerant and thus it is environmentally friendly. The cooling is produced at 5°C in order to be used for building

applications. The pinch point or minimum temperature difference in the heat recovery system (HRS) is 5°C [24]. The solar mass flow rate is chosen at 2 kg s<sup>-1</sup> which corresponds to a specific mass flow rate at 0.02 kg s<sup>-1</sup> m<sup>-2</sup> [25]. The heat rejection temperature is selected at 40°C both for ORC and VCC.

### 2.2. Mathematical modeling part

Section 2.2 includes the basic equations of the used mathematical model for the system simulation. The presented equations have been used in the simulation tool (EES). The modeling equations of the collector, of the organic Rankine cycle and of the VCC are included in this section.

#### 2.2.1. Solar collector and tank mathematical modeling

The solar field modeling consists of the PTC, the storage tank and the heat exchanger. The PTC thermal efficiency ( $\eta_{th,col}$ ) is described by the next literature formula which has been created through experimental investigation [20,21]:

$$\eta_{th,col} = 0.7408 \cdot K(\theta) - 0.0432 \cdot \frac{T_{col,in} - T_{am}}{G_b} - 0.000503 \cdot \frac{(T_{col,in} - T_{am})^2}{G_b} \quad (1)$$

The collector inlet temperature ( $T_{col,in}$ ), the ambient temperature ( $T_{am}$ ) and the solar beam irradiation ( $G_b$ ) are used in Eq. (1) for the thermal efficiency calculation. The incident angle modifier ( $K$ ) of the PTC is depended on the value of the sun incident angle on the collector aperture ( $\theta$ ). The next expression gives the way that the incident angle modifier is calculated in this work [26]:

$$K(\theta) = \cos(\theta) - 5.25091 \cdot 10^{-4} \cdot \theta - 2.859621 \cdot 10^{-5} \cdot \theta^2 \quad (2)$$

The PTC useful heating product ( $Q_u$ ) is found by using the next expression:

$$Q_u = m_{col} \cdot c_p \cdot (T_{col,out} - T_{col,in}) \quad (3)$$

The collector mass flow rate ( $m_{col}$ ), the specific heat capacity of the fluid ( $c_p$ ) and the temperature levels of the solar collector, inlet ( $T_{col,in}$ ) and outlet ( $T_{col,out}$ ), are used in Eq. (3) for the useful heat production calculation.

The PTC thermal efficiency ( $\eta_{th,col}$ ) is calculated according to the next formula:

$$\eta_{th,col} = \frac{Q_u}{Q_{sol}} \quad (4)$$

The available solar beam irradiation on the collector ( $Q_{sol}$ ) is calculated as below:

$$Q_{sol} = G_b \cdot A_{col} \quad (5)$$

Where ( $A_{col}$ ) is the total aperture of the PTC. The heating product in the heat exchanger surfaces ( $Q_{heat}$ ) is calculated according to the next formula:

$$Q_{heat} = m_{col} \cdot c_p \cdot (T_{hex,in} - T_{col,in}) \quad (6)$$

The inlet temperature in the heat exchanger ( $T_{hex,in}$ ) is used in the previous formula. It has to be said that the ( $T_{col,in}$ ) is greater than the heating production temperature level in all the cases and a minimum pinch point always exists.

The energy-balance in the solar field and the tank devices is described by the following formula. The thermal zones strategy is followed for having the proper temperature stratification in the tank [25, 27]:

$$Q_{st} = Q_u - Q_{hrs} - Q_{heat} - Q_{loss} \quad (7)$$

The stored heat ( $Q_{st}$ ) is found as the difference between the input heat in the system and the output heat. It has to be said that the input heat in the heat recovery system ( $Q_{hrs}$ ), the heating production ( $Q_{heat}$ ) and the tank thermal losses ( $Q_{loss}$ ) are the outputs heat rates, while the useful heat production by the PTC ( $Q_u$ ) is the input. The overall storage tank thermal losses ( $Q_{loss}$ ) are modeled by using the thermal loss coefficient ( $U_T$ ) which comprises conduction, convection and irradiation losses, and it is  $0.5 \text{ W m}^{-2} \text{ K}^{-1}$  for this work [28]. The tanks' volume is selected at  $4 \text{ m}^3$  which is a reasonable selection according to the collecting area [27].

### 2.2.2. Organic Rankine cycle mathematical modeling

Firstly, the energy balance in the HRS is given as:

$$Q_{hrs} = m_{orc} \cdot (h_4 - h_3) \quad (8)$$

Where the mass flow rate of the organic fluid ( $m_{orc}$ ) and the enthalpy levels ( $h$ ) are used in the energy balance formulas.

The turbine work production ( $W_T$ ) in the shaft is given below:

$$W_T = m_{orc} \cdot (h_4 - h_5) \quad (9)$$

The pumping work demand on the ORC pump ( $W_p$ ) is calculated as:

$$W_p = \frac{m_{orc} \cdot \Delta P}{\rho_1 \cdot \eta_{motor}} \quad (10)$$

The pressure increase in the pump ( $\Delta P$ ), the fluid density ( $\rho$ ) and the motor efficiency ( $\eta_{motor}$ ) are used in the previous formula. The definition of the turbine isentropic efficiency ( $\eta_{is,T}$ ) is given below. In this study, the isentropic efficiency is selected at 85% [29].

$$\eta_{is,T} = \frac{h_4 - h_5}{h_4 - h_{5,is}} \quad (11)$$

### 2.2.3. Vapor compression cycle modeling

The energy balance in the evaporator for cooling production ( $Q_{cool}$ ) is given below:

$$Q_{cool} = m_{ref} \cdot (h_a - h_d) \quad (12)$$

The compressor work demand ( $W_{com}$ ) is given below:

$$W_{com} = m_{ref} \cdot (h_b - h_a) \quad (13)$$

The definition of the compressor isentropic efficiency ( $\eta_{is,com}$ ) is given below. In this work, this parameter has been selected to be 85% [30]. The isentropic efficiency value is a relatively high value and thus

**Table 1**

Inputs of the financial investigation [33–35].

Parameter	Value
Electricity price ( $K_{el}$ )	0.2 € kWh <sub>el</sub> <sup>-1</sup>
Cooling price ( $K_{cool}$ )	0.067 € kWh <sub>cool</sub> <sup>-1</sup>
Heating price ( $K_{heat}$ )	0.1 € kWh <sub>heat</sub> <sup>-1</sup>
ORC specific cost ( $K_{orc}$ )	3000 € kW <sub>el</sub> <sup>-1</sup>
VCC specific ( $K_{vcc}$ )	300 € kW <sub>cool</sub> <sup>-1</sup>
Heat exchangers cost ( $K_{hex}$ )	1000 €
Tank specific cost ( $K_{tank}$ )	1000 € m <sup>-3</sup>
PTC specific cost ( $K_{col}$ )	250 € m <sup>-2</sup>
O&M cost ( $K_{O\&M}$ )	1% of the investment cost

a careful and accurate design of this device is needed in order to achieve high performance.

$$\eta_{is,com} = \frac{h_{b,is} - h_a}{h_b - h_a} \quad (14)$$

The subscript “is” corresponds to the respective isentropic point. The process in the throttling valve is assumed to be adiabatic and thus the following formula is used:

$$h_c = h_d \quad (15)$$

### 2.2.4. System evaluation criteria

In order to evaluate properly the examined unit, the net electricity production ( $P_{el}$ ) has to be calculated. Practically, from the net shaft power, the pumping work demand of the ORC is reduced.

$$P_{el} = \eta_g \cdot \left( \eta_m \cdot W_T - \frac{W_{com}}{\eta_m} \right) - W_p \quad (16)$$

In this work, the mechanical efficiency in the shaft ( $\eta_m$ ) is chosen at 99% and the generator electrical efficiency ( $\eta_g$ ) at 98% which are usual values and correspond to an electromechanical efficiency of 97% [31].

The energy efficiency of the examined configuration ( $\eta_{en}$ ) is calculated by using the next formula:

$$\eta_{en} = \frac{P_{el} + Q_{cool} + Q_{heat}}{Q_{sol}} \quad (17)$$

The exergy efficiency of the examined configuration ( $\eta_{ex}$ ) is calculated by using the next formula:

$$\eta_{ex} = \frac{P_{el} + Q_{cool} \cdot \left( \frac{T_0}{T_e} - 1 \right) + Q_{heat} \cdot \left( 1 - \frac{T_0}{T_{heat}} \right)}{Q_{sol} \cdot \left( 1 - \frac{4}{3} \cdot \frac{T_0}{T_{sun}} + \frac{1}{3} \cdot \left( \frac{T_0}{T_{sun}} \right)^4 \right)} \quad (18)$$

The solar beam irradiation exergy flow is calculated according to the Petela model [32]. Kelvin units have to be used in Eq. (18); the sun temperature ( $T_{sun}$ ) is 5770 K; the reference temperature level ( $T_0$ ) is 298.15 K. The refrigeration production temperature ( $T_e$ ) and the heating production temperature ( $T_{heat}$ ) are also included in the previous formula.

The last step in the system evaluation is the financial investigation. During this process, the simple payback period ( $SPP$ ) is the used parameter for a basic financial evaluation:

$$SPP = \frac{C_0}{Time \cdot CF} \quad (19)$$

The investment cost ( $C_0$ ) is defined according to the next formula:

$$C_0 = K_{col} \cdot A_{col} + K_{tank} \cdot V_{tank} + K_{orc} \cdot P_{el,orc} + K_{vcc} \cdot Q_{cool} + K_{hex} \quad (20)$$

The specific costs and the costs of the previous formula are given in table 1. The cost of the ORC is found by using its electricity production and not the overall system's electricity production. More specifically:

$$P_{el,orc} = \eta_g \cdot \eta_m \cdot W_T - W_p \quad (21)$$

**Table 2**  
Values of the constant variables in this work.

Parameter	Value
PTC area ( $A_{col}$ )	100 m <sup>2</sup>
Solar mass flow rate ( $m_{col}$ )	2 kg s <sup>-1</sup>
Volume of the tank ( $V_{tank}$ )	4 m <sup>3</sup>
Pinch point in the HRS ( $PP$ )	5°C
Overall tank thermal loss coefficient ( $U_T$ )	0.5 W m <sup>-2</sup> K <sup>-1</sup>
Compressor isentropic efficiency ( $\eta_{is,com}$ )	85%
Turbine isentropic efficiency ( $\eta_{is,T}$ )	85%
Motor efficiency ( $\eta_{motor}$ )	80%
Shaft mechanical efficiency ( $\eta_m$ )	99%
Electrical generator efficiency ( $\eta_g$ )	98%
Cooling production temperature ( $T_{cool}$ )	5°C
Heating production temperature ( $T_{heat}$ )	60°C
Recuperator pinch point ( $\Delta T_{rec}$ )	10°C
Condensing temperature level ( $T_{con}$ )	40°C
Mean ambient temperature level ( $T_{am}$ )	25°C
Operating time during the year ( $Time$ )	2500 h

In this work, the yearly operating time ( $Time$ ) is chosen at 2500 h which is a typical value for the location of Athens in Greece [28]. The hourly cash flow of the system ( $CF$ ) is calculated as below:

$$CF = P_{el} \cdot K_{el} + Q_{heat} \cdot K_{heat} + Q_{cool} \cdot K_{cool} - \frac{K_{O\&M}}{Time} \quad (22)$$

The cost for operation and maintenance is selected to be 1% of the initial investment cost ( $K_{O\&M} = 0.01 \cdot C_0$ ). Moreover, it has to be said that the selected heat exchanger cost has a reasonable cost for the needed heat exchanging area.

### 2.3. Followed methodology

The present investigation regards a polygeneration system which operates in steady-state conditions. The analysis is performed by using the mathematical modeling of Section 2.2. The analysis is done with a homemade model in Engineering Equation Solver [19]. The values of the constant parameters of this work can be found in Table 2.

During the parametric study, only one parameter changes in every scenario and the other parameters have their nominal values. Table 3 includes the parameters of the parametric study, their nominal values and the range of their values through the parametric investigation.

It is important to be said that high pressure of the ORC ( $p_{high}$ ), or the turbine inlet pressure is studied by applying the dimensionless pressure parameter ( $\alpha$ ). For this work, the working fluid is toluene and its critical pressure ( $p_{crit}$ ) is 41.3 bar.

$$\alpha = \frac{p_{high}}{p_{crit}} \quad (23)$$

The heat source temperature level ( $T_{s,in}$ ) is studied through the parameter ( $\Delta T_s$ ) which is the temperature difference between the ( $T_{s,in}$ ) and the minimum possible ( $T_{s,in-min}$ ). This minimum value is the minimum possible in order to have a suitable heat transfer in the HRS. This value is calculated by assuming that there is a pinch point ( $PP$ ) both at the HRS inlet and at the start of the evaporator. So, the parameter ( $\Delta T_s$ ) can be written as:

$$\Delta T_s = T_{s,in} - (T_{sat} + \Delta T_{sh} + PP) \quad (24)$$

The saturation temperature in every case ( $T_{sat}$ ) is determined by the used value of the parameter ( $\alpha$ ).

At this point, it is interesting to give some comments about the selection of the nominal values. About solar irradiation, the selection of the 700 W m<sup>-2</sup> gives overall a reasonable solar potential for the examined location (Athens) if it is multiplied with the 2500 h (operating time of the system) [28, 36]. The solar angle of 30°, this value gives a relatively reasonable value which is close to the mean yearly incident angle modifier for Athens [37]. The heating and the cooling loads have selected arbitrarily at these values in order to produce useful outputs of similar

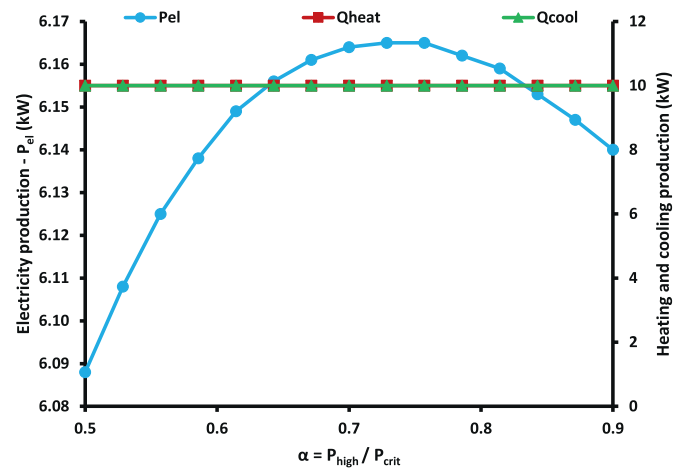


**Fig. 2.** The impact of the pressure ratio parameter on electricity, heating and cooling.

quantities. More analysis of them is done in this work. The superheating is selected not to be so high because it is usually low in the ORC. The zero value of the heat source temperature difference and the value of 90% for the pressure ratio parameter are the optimum results of another previous work [8], so they can be used as nominal values in this paper. It is also remarkable to be said that the maximum examined value of the pressure level is equal to 90% of the respective critical pressure, as it is usually done in other literature studies [8, 31].

In the end, it has to be said that in dynamic operation, the storage tank temperature and consequently the heat source temperature are variable. When the temperature level in the tank is over the designed value, the tank provides heat to the ORC and in a real operation, there is a proper control strategy based on the heat source mass flow rate in order to adjust the heat rates.

## 3. Results and discussion

Section 3 is devoted to presenting the results of the present work. The systems' useful outputs are energy efficiency, the exergy efficiency, the cash flow and the simple payback period are given in all the cases. The parameters are separated into three categories; design parameters, solar potential parameters and loads. At this point, it has to be said that in the nominal operating scenario (see Table 3), the net electricity output is 6.14 kW, the heating load 10 kW, the cooling load 10 kW, the energy performance 37.34%, the exergy performance 12.13%, the hourly cash flow 2.90 €/h and the simple payback period 8.50 years. Moreover, the VCC has a coefficient of performance at 5.46 which is a relatively high value.

### 3.1. The influence of the design parameters on the examined system

Firstly, the influence of the design parameters on the system performance is presented. Figs. 2–5 show the impact of the pressure ratio parameter on the system performance. More specifically, Fig. 2 shows that electricity production is maximized for the pressure ratio parameter of 0.73 at 6.17 kW, while the other outputs are not influenced by this parameter. For this optimum pressure ratio, also the energy and exergy efficiencies are maximized as Fig. 3 shows. The maximum energy efficiency is 37.4% and the respective maximum exergy efficiency 12.2%. At this point, it has to be said that the optimum value of the pressure ratio parameter is associated with a respective optimum high pressure (turbine inlet) and an optimum evaporation temperature in the heat recovery system. The general rule is that higher temperature leads to higher ORC efficiency but it also leads to reduces solar collector efficiency because of the mean system temperature increases. These two

**Table 3**  
The examined values of the parametric variables.

Parameter	Symbol	Values		
		Nominal	Minimum	Maximum
Superheating degree	$\Delta T_{sh}$ (°C)	20	0	40
Pressure ratio	$\alpha$ (-)	90%	50%	90%
Source temperature difference	$\Delta T_s$ (°C)	0	0	40
Cooling load	$Q_{cool}$ (kW)	10	0	20
Heating load	$Q_{heat}$ (kW)	10	0	20
Solar irradiation	$G_b$ ( $W m^{-2}$ )	700	400	1000
Solar angle	$\theta$ (°)	30	0	50

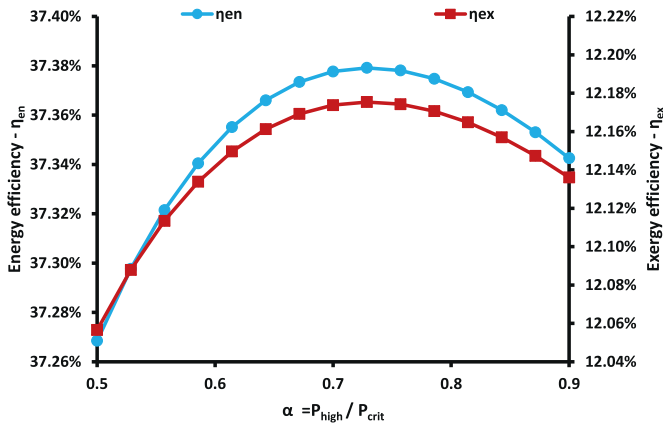


Fig. 3. The impact of the pressure ratio parameter on the energy and exergy efficiencies.

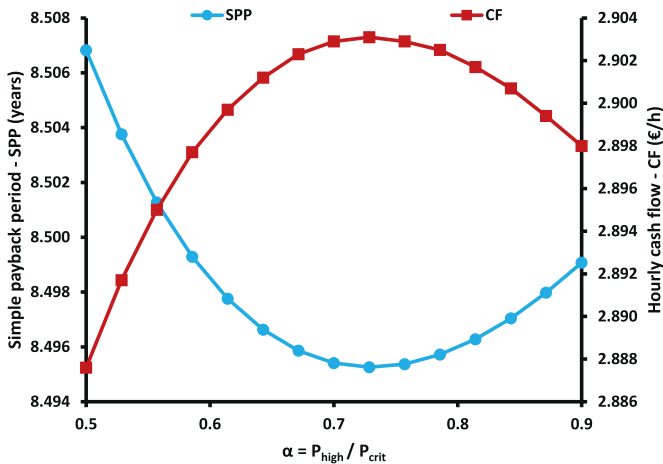


Fig. 4. The impact of the pressure ratio parameter on the simple payback period and on the hourly cash flow.

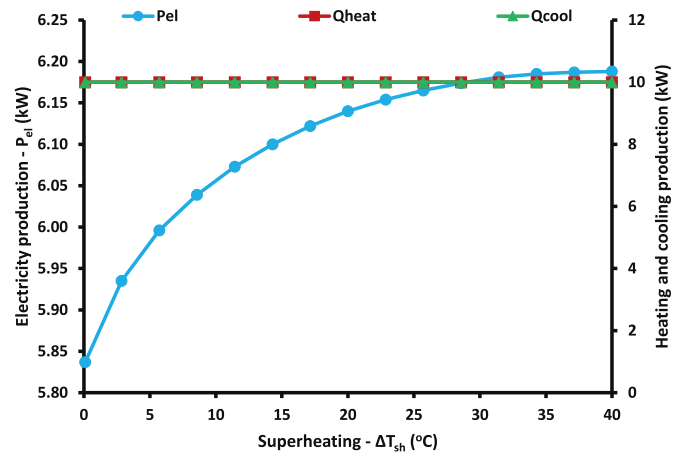


Fig. 5. The impact of the superheating on electricity, heating and cooling.

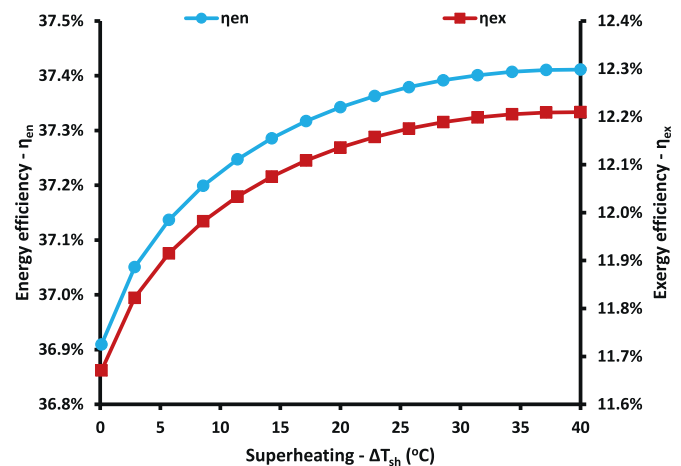


Fig. 6. The impact of the superheating on the energy and exergy efficiencies.

conflicting factors make the existence of an optimum pressure level. Moreover, the saturation curve of the organic fluid and the selected superheating degree have also an influence on the results.

Fig. 4 indicates that the simple payback period is minimized at 8.5 years and the hourly cash flow is maximized at 2.9 €/h for the same global optimum pressure ratio. In any case, it is important to state that small deviations from the optimum pressure ratio do not lead to the great variation of the aforementioned indexes.

The next investigated design parameter is the superheating degree in the turbine inlet. More specifically, Fig. 5 proves that the greater superheating leads to higher electricity production while the other outputs are not influenced. This is an interesting result because, in other literature studies, generally small superheating values are selected. In any case,

the saturation curve shape plays a significant role in this result and thus there is a need for parametric study in every case. Fig. 6 proves that both energy and exergy efficiencies increase with higher superheating. Fig. 7 makes clear that higher superheating leads to lower simple payback period and to higher hourly cash flow. So, there is a need for designing systems with high superheating in order to have optimum performance.

The last examined design parameter is the temperature increase of the heat source, over the minimum possible value. Fig. 8 indicates that higher heat source temperature reduces electricity production because the solar thermal efficiency is getting lower. The collector operating in higher temperature is not beneficial for the overall system performance and so there is a need for designing a system with relatively low-temperature levels in the solar field, something that can be done by using high flow rates on the solar field. Fig. 9 comes in accordance with

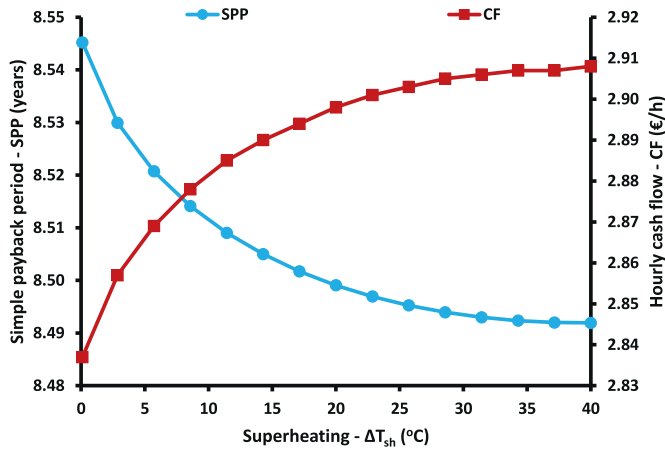


Fig. 7. The impact of the superheating on the simple payback period and on the hourly cash flow.

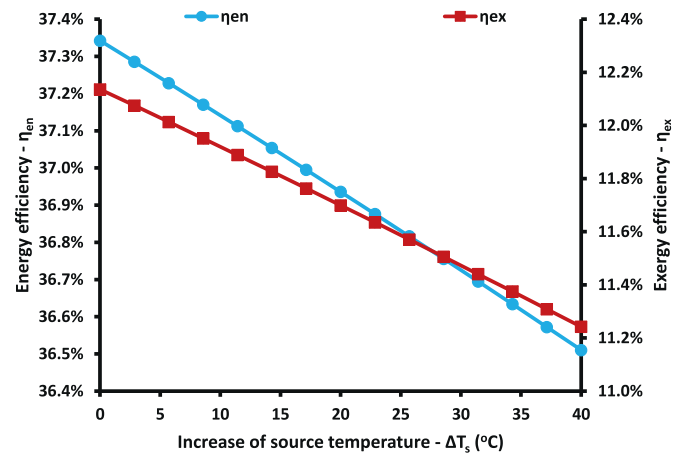


Fig. 9. The impact of the heating source temperature difference on the energy and exergy efficiencies.

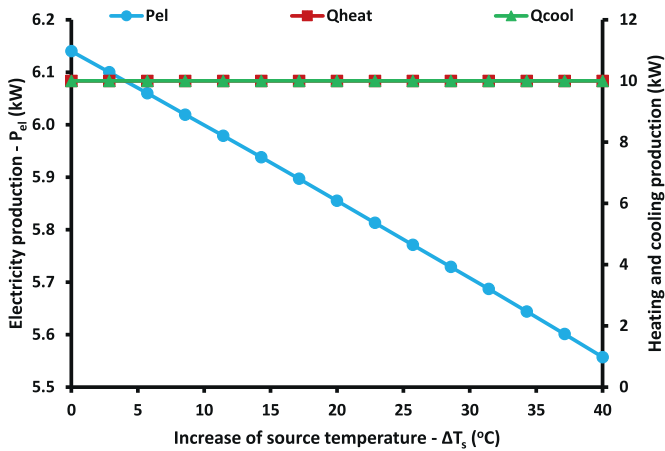


Fig. 8. The impact of the heating source temperature difference on electricity, heating and cooling.

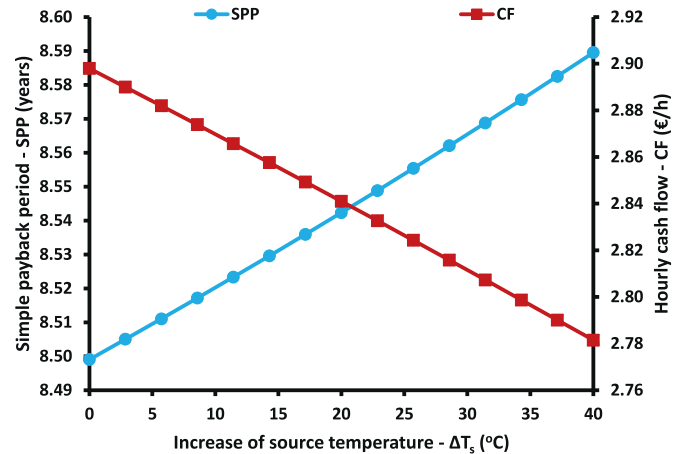


Fig. 10. The impact of the heating source temperature difference on the simple payback period and on the hourly cash flow.

the previous statements and shows that the heat source temperature leads to lower energy and exergy efficiency. Also, the simple payback period increases and the hourly cash flow reduce with the higher heat source temperature level, as Fig. 10 illustrates.

### 3.2. The influence of the solar potential parameters on the examined system

Section 3.2 includes results about the system performance for different solar irradiation values. Figs. 11 to 13 show the system performance for different values of the solar beam irradiation from  $400 \text{ W m}^{-2}$  up to  $1000 \text{ W m}^{-2}$ . Fig. 11 indicates that higher solar irradiation increases linearly the electricity production which is ranged from 0.18 kW up to 12.1 kW. For solar beam irradiation levels lower than  $400 \text{ W m}^{-2}$ , the system is practically unable to operate properly and to produce the demanded useful outputs. At this point, it has to be said that the linear character of the electricity production curve is associated with the small deviation of the collector efficiency with the solar irradiation variation, especially in high irradiation values.

Moreover, higher solar irradiation leads to higher exergy efficiency but to lower energy efficiency, as Fig. 12 indicates. Practically, higher amounts of solar irradiation lead to higher solar heat input, while the heating and cooling loads are constant. This situation makes unable the proper utilization of extra solar energy for heating and cooling products. On the other hand, higher solar irradiation increases significantly the electricity production which is the critical quantity for the exergy

efficiency and thus the exergy efficiency increases. Fig. 13 shows that higher nominal solar potential leads to lower simple payback period and to higher hourly cash flow. However, the deviation of the simple payback period is not high; from 10.03 years to 7.87 years, something that indicates the investment is viability in all the cases. Different values of the nominal solar irradiation practically correspond to different locations with different solar potential.

Figs. 14–16 depict the influence of the sun incident angle on the unit performance. This parameter influences the PTC incident angle modifier and so it plays an important role in the collector thermal efficiency. Fig. 14 indicates that the higher values of this parameter lead to lower electricity production and practically for solar angles after the  $50^\circ$ , the system stops to operate. The electricity production curve trend has a similar shape with the incident angle modifier shape which is a reasonable result. Fig. 15 shows that both energy and exergy efficiencies are getting lower with the increase of the sun incident angle. The exergy efficiency is more influenced by the increase of the solar angle compared to the energy efficiency. Fig. 15 indicates the use of a higher nominal solar angle leads to a less efficient investment and so the simple payback period increases and the hourly cash flow decreases. However, the investment is always viable and this fact indicates that the selection of a different location, through the use of a different solar angle, does not has a so great impact on the financial viability of the investment but it

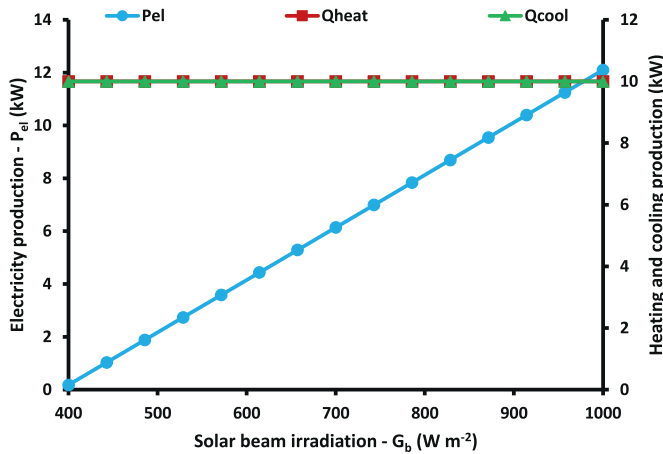


Fig. 11. The impact of the solar irradiation level on electricity, heating and cooling.

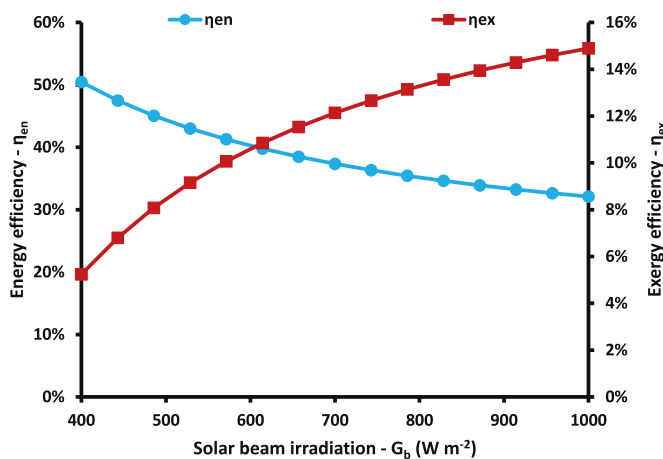


Fig. 12. The impact of the solar irradiation level on the energy and exergy efficiencies.

has a greater impact on the thermodynamic indexes and especially in the exergy efficiency.

### 3.3. Simple parametric study for different cooling and heating loads

The next step in this analysis is the investigation of different heating and cooling load values on the system performance. Figs. 17–19 show the impact of the cooling load on the results and Figs. 20–22 the impact of the heating load on the results.

Fig. 17 exhibits that a higher cooling load reduces electricity production because higher amounts of produced work are taken from the shaft and so lower net electricity is available. Fig. 18 indicates that the increase of the cooling load has a positive impact on the system energetic performance but a negative impact on the system’s exergetic performance. This fact is explained by the decrease of the electricity with a cooling load increase which is an important parameter for the exergy efficiency. Fig. 19 illustrates the impact of the cooling load on the financial viability of the system. Higher cooling load leads to lower simple payback period and to higher hourly cash flow.

Fig. 20 exhibits that a higher heating load reduces electricity production because the increase of the heating product leads to lower heat amounts entering into the heat recovery system. Fig. 21 indicates that the increase in the heating load has a positive influence on energy efficiency but a negative influence on the system’s exergy efficiency. This fact is explained by the decrease of the electricity when heating load

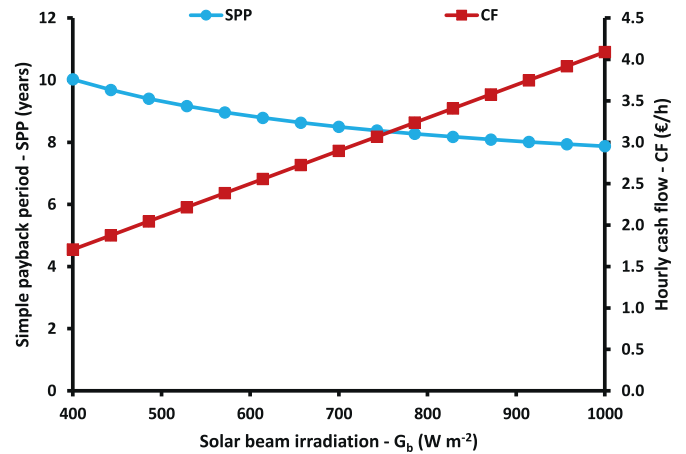


Fig. 13. The impact of the solar irradiation level on the simple payback period and on the hourly cash flow.

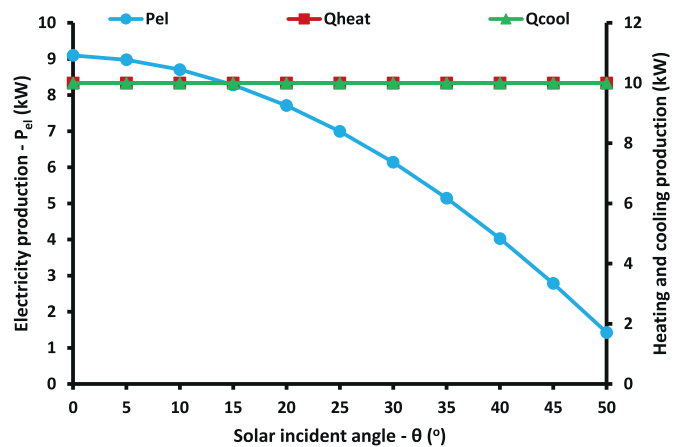


Fig. 14. The impact of the solar incident angle on the electricity, heating and cooling.

increases and the high dependence of electricity with the exergy efficiency. Fig. 22 illustrates the impact of the heating load on the financial viability of the system. Higher heating load leads to smaller simple payback period and to higher hourly cash flow.

### 3.4. System performance for different combinations of heating-cooling loads

The last part of the results section regards the investigation of different design scenarios by studying different combinations of heating and cooling loads. Figs. 23–27 show the system performance indexes for different heating loads (horizontal axis) and cooling loads (different curves). Generally, it can be said that the curves have a linear character and this is an interesting result for the design procedure of the system.

Fig. 23 indicates that electricity production is reduced with the increase in heating and cooling loads. Fig. 24 shows that energy efficiency is enhanced by the higher design values of heating and cooling loads. On the other hand, Fig. 25 validates that the exergy efficiency is decreased with the increase in heating and cooling loads. Fig. 26 shows that the hourly cash flow is enhanced with the higher heating and cooling production, while Fig. 27 indicates that the increase of the cash flow leads to a lower simple payback period for the cases with higher heating and cooling loads. Generally, the curves in the Figs. 23–26 are approximately linear, while the curves of Fig. 27 are not linear. Practically, the higher heating load leads to a small increase in the hourly cash flow (see the small slope of curves in Fig. 26) because of the simultaneous

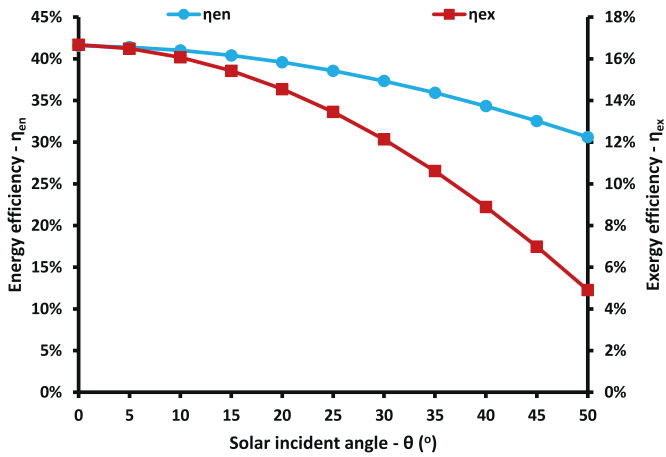


Fig. 15. The impact of the solar incident angle on the energy and exergy efficiencies.

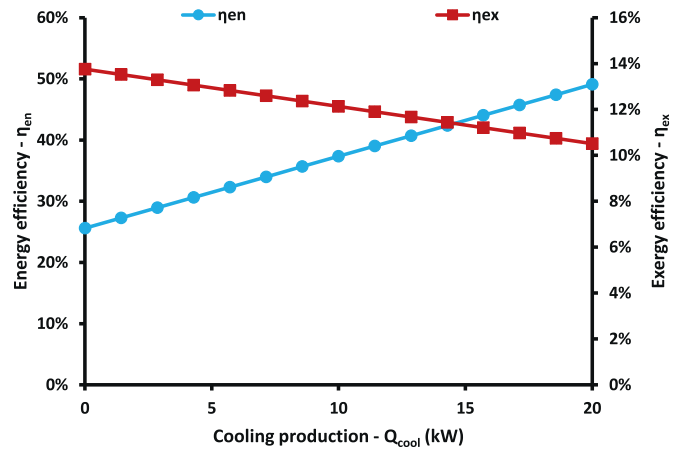


Fig. 18. The impact of the cooling load on the energy and exergy efficiencies.

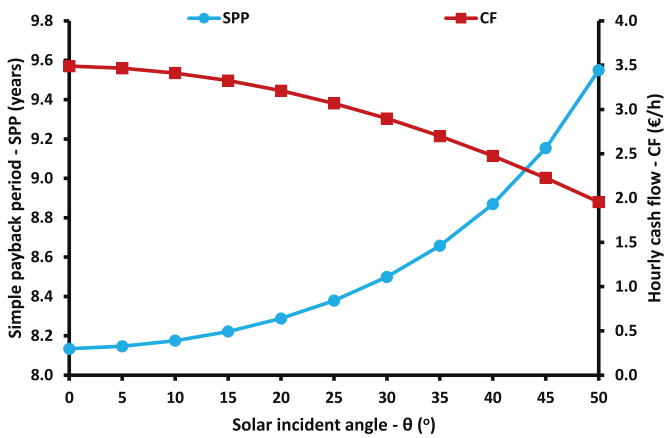


Fig. 16. The impact of the solar incident angle on the simple payback period and on the hourly cash flow.

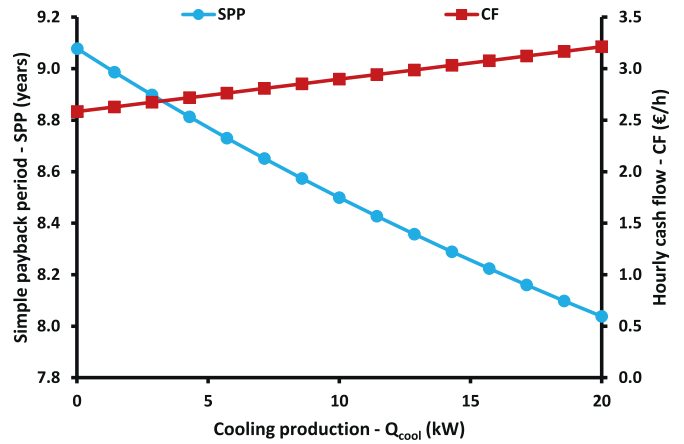


Fig. 19. The impact of the cooling load on the simple payback period and on the hourly cash flow.

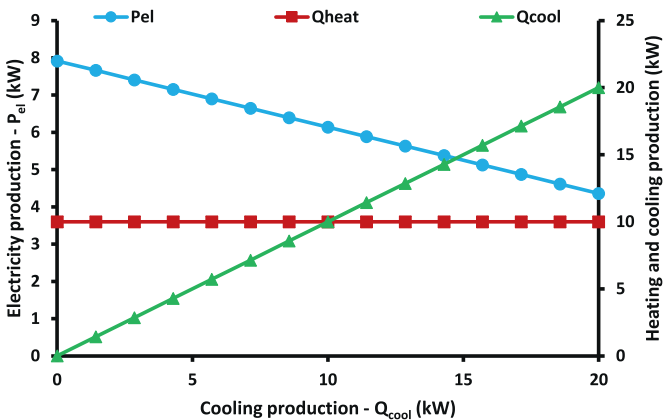


Fig. 17. The impact of the cooling load on the useful outputs.

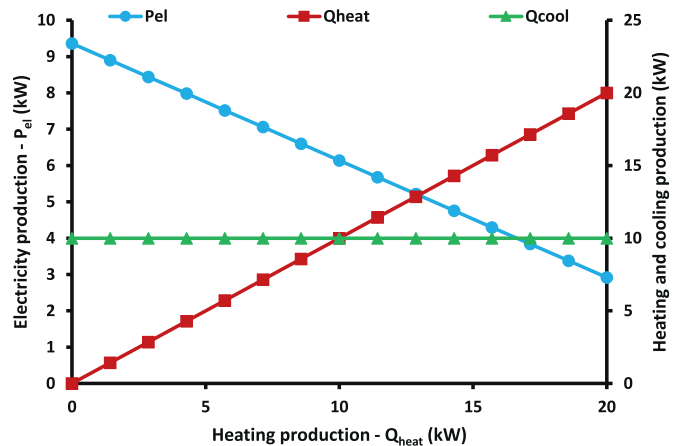


Fig. 20. The impact of the heating load on the useful outputs.

electricity production decrease. So, for heating production over 5 kW, the financial gain is not so high in order to give an important decrease in the simple payback period.

### 3.5. Discussion and future research

In this analysis, a promising trigeneration system is investigated parametrically in detail. This system is ideal for the building sector and it

can produce all the useful outputs that are needed in the buildings. One important advantage of this system is its simplicity and the ability to adjust the heating and cooling production. The system can be designed for different combinations of heating and cooling loads, something which is very important due to the variation of these loads among the buildings. Also, an extra advantage of this system is that it can produce heating at

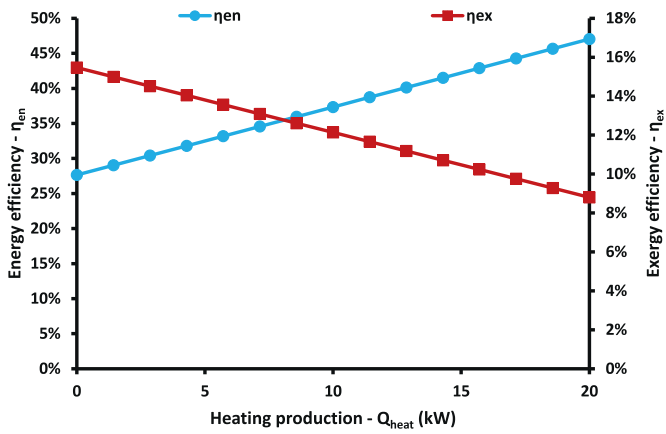


Fig. 21. The impact of the heating load on the energy and exergy efficiencies.

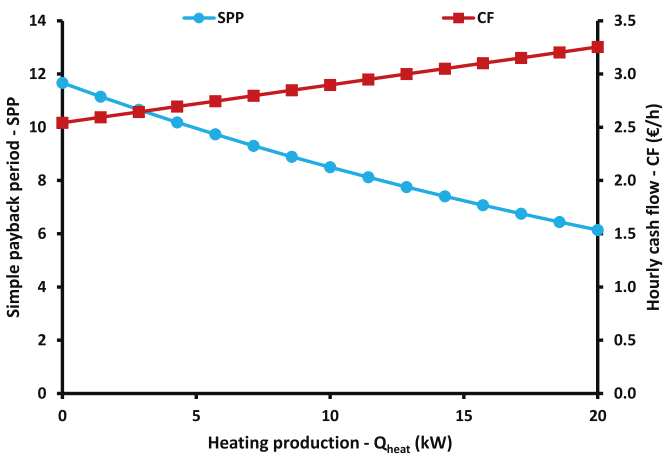


Fig. 22. The impact of the heating load on the simple payback period and on the hourly cash flow.

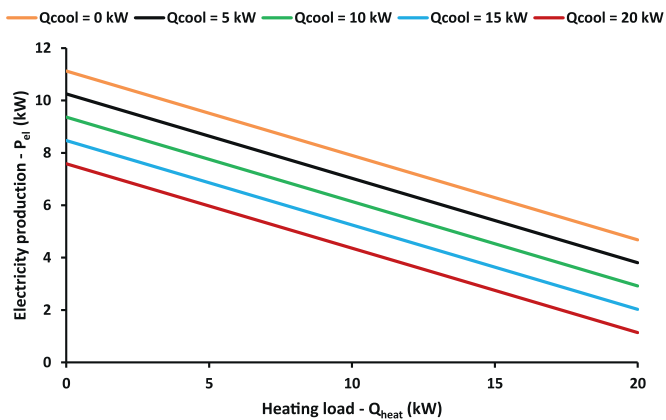


Fig. 23. Electricity production for different combinations of heating-cooling loads.

higher temperature levels than 60°C if it is needed, for example at 90°C if there are radiators in the examined building.

Table 4 summarizes the main findings of the unit performance in the nominal operating scenario. It is remarkable to highlight that the nominal electricity rate is 6.14 kW, the heating rate 10 kW, the cooling rate 10 kW, while the respective yearly productions 15.4 MWh, 25 MWh and 25 MWh respectively. The energy efficiency is 37.34% which is not

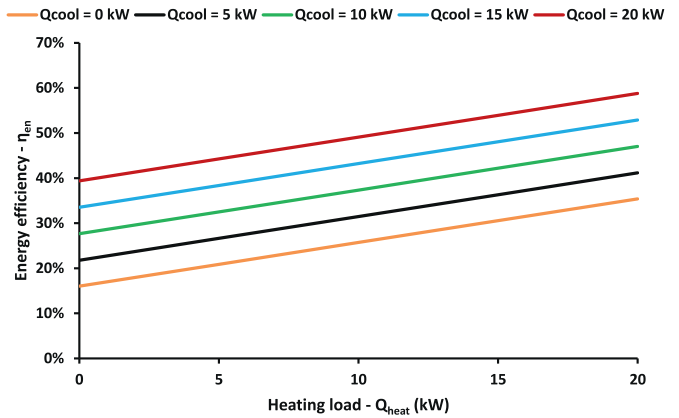


Fig. 24. Energy efficiency for different combinations of heating-cooling loads.

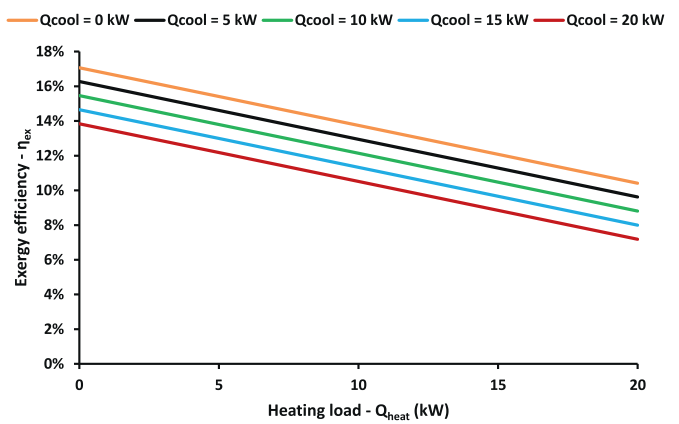


Fig. 25. Exergy efficiency for different combinations of heating-cooling loads.

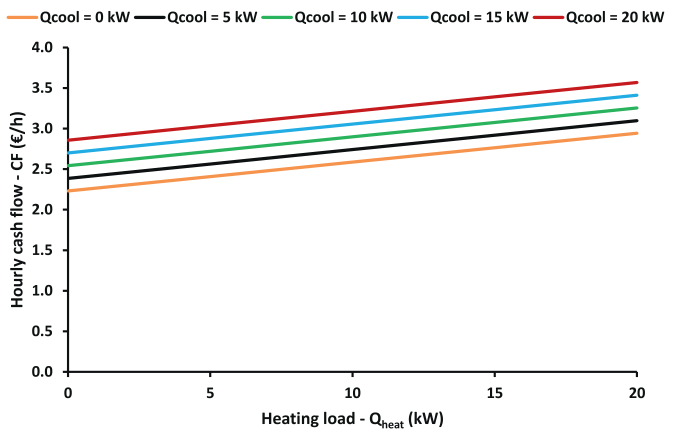


Fig. 26. Hourly cash flow for different combinations of heating-cooling loads.

as so high value but it has to be said that the input solar data were representative for the whole year period and they are not the maximum possible values as in other studies. More specifically, this work uses solar irradiation of 700 W m<sup>-2</sup> and 30° solar angle, while the majority of other studies use 1000 W m<sup>-2</sup> and zero incident angle. Moreover, the present system sacrifices electricity in order to feed the VCC, something that has a negative influence on the exergetic performance. In any case, the financial analysis shows a relatively low investment cost and an acceptable payback period of 8.5 years for a system that is driven only by solar irradiation. For a better understanding of the system performance,

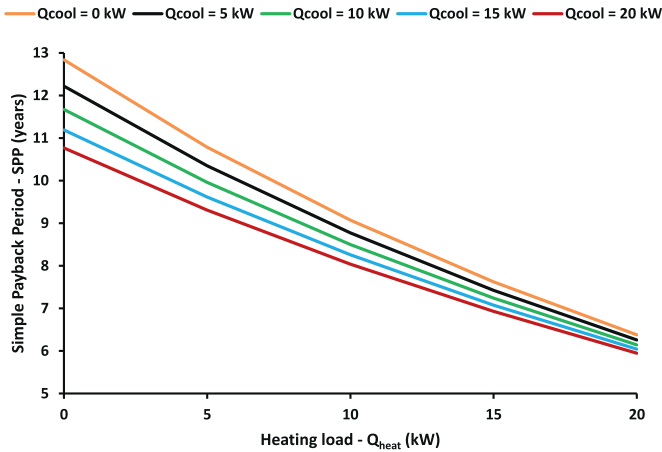


Fig. 27. Simple payback period for different combinations of heating-cooling loads.

**Table 4**  
Final results for the nominal operating scenario.

Parameters	Values
Electricity rate	6.14 kW
Heating rate	10 kW
Cooling rate	10 kW
Energy efficiency	37.34%
Exergy efficiency	12.13%
Yearly electricity production	15.4 MWh
Yearly heating production	25 MWh
Yearly cooling production	25 MWh
Simple payback period	8.50 years
Hourly cash flow	2.90 €/h
Investment cost	61.6 k€

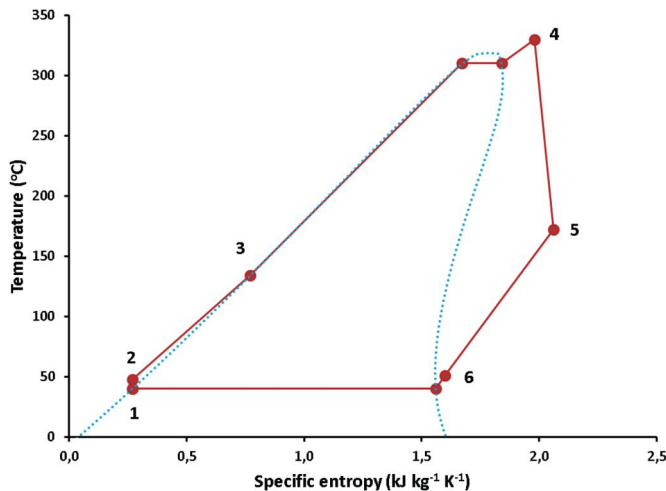


Fig. 28. Temperature-specific entropy diagram (T-s) for the ORC with toluene at default conditions.

Fig. 28 shows the temperature-specific entropy diagram of the ORC and Fig. 29 shows the respective depiction for the vapor compression cycle.

In the future, the examined configuration can be examined and optimized in dynamic conditions by using a different time-dependent model. The emphasis can be given in the adjustment of the building loads with the system productions, as well as in the use of extra stor-

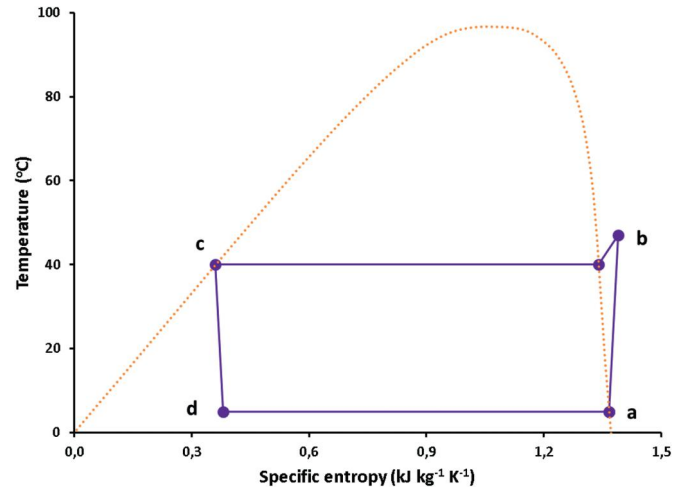


Fig. 29. Temperature-specific entropy diagram (T-s) for the VCC with R290 at default conditions.

age devices such as batteries, heating production and cooling production tanks. Different heating production temperatures can be examined and also the production of heating in two temperature levels for different applications. Moreover, the investigation of different collector types such as solar dishes and linear Fresnel reflectors can be also performed.

#### 4. Conclusions

The goal of this study is the investigation of a solar-driven trigeneration unit that produces cooling, heating and electricity. The examined configuration includes PTC, ORC and VCC, while there are also heating heat exchangers and a storage tank. A developed model in EES is used in order to extract the results of the system performance. The most valuable conclusions are described by the following bullets:

- In the nominal operating scenario for heating and cooling at 10 kW, the electricity product is 6.14 kW. It is found that the energy and exergy efficiencies are 37.34% and 12.13% respectively. Moreover, the hourly cash flow is 2.90 €/h and the simple payback period is 8.5 years.
- The design parameters have an impact on electricity production. More specifically, the optimum pressure ratio which maximizes electricity production is close to 0.73. Higher superheating and lower heat source temperature are also beneficial to electricity production.
- The use of higher nominal solar irradiation and lower nominal solar angle in the system design leads to a more efficient system and a more viable investment. However, the solar potential indicators have a higher impact on the exergy efficiency than energy efficiency, while they have a relatively small influence on the economic analysis of the investment.
- Higher heating and cooling loads lead to lower electricity, higher energy performance, lower exergy performance and lower simple payback period.
- In the future, the studied configuration can be optimized for a separate study case by using a dynamic model for taking into consideration the fluctuations of the solar irradiation during the day and real building loads. Moreover, different thermal storage systems can be evaluated (e.g. phase change materials or chemical storage) in order to achieve more sustainable configurations.

## Acknowledgments



**Operational Programme**  
**Human Resources Development,**  
**Education and Lifelong Learning**

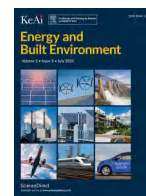
Co-financed by Greece and the European Union



This research is co-financed by Greece and the European Union (European Social Fund - ESF) through the Operational Programme «Human Resources Development, Education and Lifelong Learning» in the context of the project “Reinforcement of Postdoctoral Researchers - 2nd Cycle” (MIS-5033021), implemented by the State Scholarships Foundation (IKY).

## References

- [1] M. Yao-Ping Peng, C. Chen, X. Peng, M. Marefati, Energy and exergy analysis of a new combined concentrating solar collector, solid oxide fuel cell, and steam turbine CCHP system, *Sustain. Energy Technol. Assess.* 39 (2020) 100713.
- [2] A. Kasaeian, G. Nouri, P. Ranjbaran, D. Wen, Solar collectors and photovoltaics as combined heat and power systems: a critical review, *Energy Convers. Manag.* 156 (2018) 688–705.
- [3] A. Kasaeian, E. Bellos, A. Shamaeizadeh, C. Tzivanidis, Solar-driven polygeneration systems: Recent progress and outlook, *Appl. Energy* 264 (2020) 114764.
- [4] G.J. Nathan, M. Jafarian, B.B. Dally, W.L. Saw, P.J. Ashman, E. Hu, A. Steinfeld, Solar thermal hybrids for combustion power plant: a growing opportunity, *Prog. Energy Combust. Sci.* 64 (2018) 4–28.
- [5] J. Zhou, X. Zhao, Y. Yuan, J. Li, M. Yu, Y. Fan, Operational performance of a novel heat pump coupled with mini-channel PV/T and thermal panel in low solar radiation, *Energy Built Environ.* 1 (1) (2020) 50–59.
- [6] E. Bellos, C. Tzivanidis, Alternative designs of parabolic trough solar collectors, *Prog. Energy Combust. Sci.* 71 (2019) 81–117.
- [7] F.A. Al-Sulaiman, I. Dincer, F. Hamdullahpur, Exergy modeling of a new solar driven trigeneration system, *Sol. Energy* 85 (9) (2011) 2228–2243.
- [8] E. Bellos, C. Tzivanidis, Parametric analysis and optimization of a solar driven trigeneration system based on ORC and absorption heat pump, *J. Clean. Prod.* 161 (2017) 493–509.
- [9] M. Almahdi, I. Dincer, M.A. Rosen, A new solar based multigeneration system with hot and cold thermal storages and hydrogen production, *Renew. Energy* 91 (2016) 302–314.
- [10] R.Z. Mathkor, B. Agnew, M.A. Al-Weshahi, F. Latrsh, Exergetic analysis of an integrated tri-generation organic rankine cycle, *Energies* 8 (2015) 8835–8856.
- [11] F. Khalid, I. Dincer, M.A. Rosen, Techno-economic assessment of a renewable energy based integrated multigeneration system for green buildings, *Appl. Therm. Eng.* 99 (2016) 1286–1294.
- [12] Q. Wu, H. Ren, W. Gao, P. Weng, J. Ren, Design and operation optimization of organic Rankine cycle coupled trigeneration systems, *Energy* 142 (2018) 666–677.
- [13] F. Calise, M. Dentice d’Accadia, A. Macaluso, A. Piacentino, L. Vanoli, Exergetic and exergoeconomic analysis of a novel hybrid solar–geothermal polygeneration system producing energy and water, *Energy Convers. Manag.* 115 (2016) 200–220.
- [14] E. Bellos, L. Vellios, I.-C. Theodosiou, C. Tzivanidis, Investigation of a solar-biomass polygeneration system, *Energy Convers. Manag.* 173 (2018) 283–295.
- [15] S. Karellas, K. Braimakis, Energy–exergy analysis and economic investigation of a cogeneration and trigeneration ORC–VCC hybrid system utilizing biomass fuel and solar power, *Energy Convers. Manag.* 107 (2016) 103–113.
- [16] M.A. Haghghi, M. Shamsaiee, S.G. Holagh, A. Chitsaz, M.A. Rosen, Thermodynamic, exergoeconomic, and environmental evaluation of a new multi-generation system driven by a molten carbonate fuel cell for production of cooling, heating, electricity, and freshwater, *Energy Convers. Manag.* 199 (2019) 112040.
- [17] M.A. Haghghi, S.M. Pestei, A. Chitsaz, J. Hosseinpour, Thermodynamic investigation of a new combined cooling, heating, and power (CCHP) system driven by parabolic trough solar collectors (PTSCs): A case study, *Appl. Therm. Eng.* 163 (2019) 114329.
- [18] M.A. Haghghi, S.G. Holagh, A. Chitsaz, K. Parham, Thermodynamic assessment of a novel multi-generation solid oxide fuel cell-based system for production of electrical power, cooling, fresh water, and hydrogen, *Energy Convers. Manag.* 197 (2019) 111895.
- [19] F-Chart Software, Engineering Equation Solver (EES), 2015. Available at: (<http://www.fchart.com/ees>).
- [20] EuroTrough: Development of a Low Cost European Parabolic Trough Collector - EuroTrough. Final Report, Research funded in part by The European Commission in the framework of the Non-Nuclear Energy Programme JOULE III. Contract JOR3-CT98-0231; 2001.
- [21] M. Geyer, E. Lüpfert, R. Osuna, A. Esteban, W. Schiel, A. Schweitzer, E. Zarza, P. Nava, J. Langenkamp, E. Mandelberg, EUROTROUGH - Parabolic trough collector developed for cost efficient solar power generation, in: Proceedings of the 11th SolarPACES International Symposium on Concentrated Solar Power and Chemical Energy Technologies, Zurich, Switzerland, 2002 Sept 4-6.
- [22] <http://twf.mpei.ac.ru/tthb/hedh/htf-vp1.pdf>.
- [23] E. Bellos, C. Tzivanidis, Optimization of a solar-driven trigeneration system with nanofluid-based parabolic trough collectors, *Energies* 10 (2017) 848.
- [24] R. Loni, E.A. Asli-Ardeh, B. Ghoobadian, G. Najafi, E. Bellos, Effects of size and volume fraction of alumina nanoparticles on the performance of a solar organic Rankine cycle, *Energy Convers. Manag.* 182 (2019) 398–411.
- [25] J.A. Duffie, W.A. Beckman, *Solar Engineering of Thermal Processes*. 3rd ed. Hoboken (New Jersey): John Wiley and Sons Inc., 2006.
- [26] M.J. Montes, A. Abánades, J.M. Martínez-Val, M. Valdés, Solar multiple optimization for a solar-only thermal power plant, using oil as heat transfer fluid in the parabolic trough collectors, *Sol. Energy* 83 (12) (2009) 2165–2176.
- [27] E. Bellos, C. Tzivanidis, K.A. Antonopoulos, Exergetic, energetic and financial evaluation of a solar driven absorption cooling system with various collector types, *Appl. Therm. Eng.* 102 (2016) 749–759.
- [28] E. Bellos, C. Tzivanidis, V. Belessiotis, Daily performance of parabolic trough solar collectors, *Sol. Energy* 158 (2017) 663–678.
- [29] C. Mata-Torres, R.A. Escobar, J.M. Cardemil, Y. Simsek, J.A. Matute, Solar polygeneration for electricity production and desalination: Case studies in Venezuela and northern Chile, *Renew. Energy* 101 (2017) 387–398.
- [30] O. Brunin, M. Feidt, B. Hivet, Comparison of the working domains of some compression heat pumps and a compression-absorption heat pump, *Int. J. Refrig.* 20 (5) (1997) 308–318.
- [31] E. Bellos, I. Skaltsas, O. Pliakos, C. Tzivanidis, Energy and financial investigation of a cogeneration system based on linear Fresnel reflectors, *Energy Convers. Manag.* 198 (2019) 111821.
- [32] R. Petela, Exergy of undiluted thermal radiation, *Sol. Energy* 74 (6) (2003) 469–488.
- [33] E. Bellos, C. Tzivanidis, Multi-objective optimization of a solar driven trigeneration system, *Energy* 149 (2018) 47–62.
- [34] C. Tzivanidis, E. Bellos, K.A. Antonopoulos, Energetic and financial investigation of a stand-alone solar-thermal Organic Rankine Cycle power plant, *Energy Convers. Manag.* 126 (2016) 421–433.
- [35] <https://www.theheatexchangercompany.co.uk>.
- [36] E. Bellos, C. Tzivanidis, Parametric Investigation of a Trigeneration System with an Organic Rankine Cycle and Absorption Heat Pump Driven by Parabolic Trough Collectors for the Building Sector, *Energies* 13 (7) (2020) 1800.
- [37] E. Bellos, C. Tzivanidis, Assessment of linear solar concentrating technologies for Greek climate, *Energy Convers. Manag.* 171 (2018) 1502–1513.



## Drivers and barriers to energy-efficient technologies (EETs) in EU residential buildings

Clara Camarasa\*, Lokesh Kumar Kalahasthi, Leonardo Rosado

Sustainable Building Group, Chalmers University of Technology, Gothenburg, Sweden

### ARTICLE INFO

#### Keywords:

Energy efficiency  
Technology diffusion  
Technology selection  
Residential building stock  
Drivers  
Barriers

### ABSTRACT

To achieve carbon targets, the European Union (EU) aims to promote nearly zero-energy buildings (nZEB). To enable the necessary transition, technical solutions need to converge with socio-economic factors, such values and awareness of stakeholders involved in the decision-making process. In this light, the aim of this paper is to characterise perceived drivers and barriers to nine energy-efficient technologies (EET), according to key decision-makers' and persuaders of the technology selection in the EU residential building context. Results are collected across eight EU countries, i.e. Belgium (BE), Germany (DE), Spain (ES), France (FR), Italy (IT), Netherlands (NL), Poland (PL), and United Kingdom (UK). The stakeholders' selected are architects, construction companies, engineers, installers and demand-side actors. Data from a multi-country survey is analysed to calculate the share of 15 drivers and 21 barriers (aggregated to 5 groups), being selected for each EET and country. The 5 groups considered to analyse drivers and barriers are environmental, technical, economic, social, legal. The perceived barriers and drivers were further studied for their association across the countries using the Pearson's Chi2 and a Cramer's V tests. The results demonstrate that across all EETs and countries, the technical and economic driver groups are perceived to have the highest potential to increase the implementation rate of EET. In terms of barriers, economic aspects are seen as the foremost reason that EET are not scaling faster. In both drivers and barriers legal aspects are the least often selected. In overall the barrier groups show significant variation across countries compared to driver groups. These findings provide an evidence-basis to better understand arguments in favour and against specific EETs and, in this way, support policy makers and other interested parties to increase the market share of the selected solutions.

## 1. Introduction

### 1.1. Motivation

In the European Union (EU), buildings are currently the single biggest contributor of GHG emissions, responsible for approximately 40% of energy consumption and 36% CO<sub>2</sub> emissions. Furthermore, about 35% of the building stock is over 50 years old and more than 75% is considered to be energy inefficient [1]. In view of these facts, the EU aims to promote nearly zero-energy buildings (nZEB) [2]. In line with requirements from the European Commission, EU countries had to develop and submit nearly zero-energy buildings national plans, describing how they intended to increase the number of nZEBs in their respective country to comply with the directive [3]. Although technology options to decrease building's energy demand to nZEB standards are readily available and, in many cases, economically viable [4–9], average annual construction and retrofit rates in the residential sector are still around 1% [10]. Of these, less than 5% are reaching these standards

[11]. This implies that, despite their availability and economic viability, energy efficient technology solutions are not deployed at the required rate to meet EU's carbon reduction targets.

The discrepancy between the techno-economic potential and actual market behaviour has been coined as the 'energy efficiency gap' and implies that non-technical hurdles are preventing the large-scale diffusion of these solutions [12]. Any factor slowing the large-scale deployment of these technologies or limiting market success for cost-effective technology is referred to as a market barrier [13]. In this way, to foster the adoption of energy-efficient technologies, a pan-EU knowledge about the market-specific barriers and drivers is needed. This information can be particularly meaningful if it is based on evidence from the stakeholders involved in the technology selection, such as technology adopters, architects, engineers, constructors, and installers [14].

Against this background, the goal of the present study is to better understand what is impeding the large-scale deployment of these solutions. More specifically it focuses on gathering empirical evidence on the drivers and barriers for the available technology solutions allowing for differences across (1) stakeholders (potential adopters of the

\* Corresponding author.

E-mail address: [camarasa@chalmers.se](mailto:camarasa@chalmers.se) (C. Camarasa).

technologies, architects, engineers, constructors and installers), (2) EE technologies, and (3) EU countries. Findings can be used as evidence-basis to support policy makers further develop instruments and strategies, and companies or industry associations aiming to increase their market share of energy-efficient solutions.

1.2. Literature overview: drivers and barriers to energy efficient technologies in buildings

There is a broad literature on the drivers and barriers to energy efficiency in buildings. Several of these contributions discuss the situation in EU countries.

The reviewed scientific papers focus on empirical evidence on household’s adoption of energy efficient systems, more particularly those which have collected the perception of key stakeholders involved in building projects within the last two decades (years 2000–2020). Most retrieved studies focus on a single country or stakeholder (Table 1). Persson and colleagues investigated the existence and significance of barriers and driving forces for the implementation of energy-efficient houses in Sweden, interviewing construction companies to gather this information. They concluded that there is a need to demonstrate to both construction companies and potential customers the viability of building passive houses and that future building regulations from the European Union are identified as a regulatory driver [15]. Cagno and colleagues conducted an exploratory investigation analyses to a set of Dutch manufacturing enterprises and other agencies to map the views of stakeholders in the decision-making cycle. Their findings lead them to conclude that much greater attention should be paid to issues, such as extending policies from industrial final users to all companies supplying enterprises with capital, technologies, services, information, and competences [16]. Likewise, the purpose of the paper developed by Beillan and colleagues was to analyse the weight of socio-economic factors in the decision-making process of multiple energy efficiency technologies across various European countries. For this they selected case studies in Germany, Switzerland, Italy, Spain and France. For each case on-site surveys were conducted, including qualitative interviews with the owners, the residents and the involved professionals. Results from their study showed that (1) people getting involved in projects of energy-efficient refurbishment aren’t mainly and exclusively motivated by energy savings; (2) there’s a lack of skilled work force able to meet the requirements of energy-efficient retrofitting; (3) public support schemes for retrofitting measures play a crucial role; (4) the local embedding of projects is important [17]. Cooke and colleagues reported on the results of a qualitative study about building project stakeholders in the UK—their experience of alternative energy technologies (AETs), the factors that influence assessments and their views on how to improve the chances of using AETs in future projects. Among other conclusions, they highlighted the lack of experience of installing AETs in buildings in the UK, and the understanding of these technologies is variables - in line with the results from Persson and colleagues. Also, that there were a number of drivers and barriers to the use of AETs in buildings at the time of the study, and that the relevance of each of these varied between projects, with time and with the technology [18]. Achtmicht and colleagues identified key drivers and barriers for the adoption of building energy retrofits in Germany by analysing data from a 2009 survey of more than 400 owner- occupiers of single-family detached, semidetached, and row houses. They found that private owners who are able to afford it financially, for whom it is profitable, and for whom there is a favourable opportunity were more likely to undertake energy retrofit activities [19]. Stieß and colleagues offered a comparison of homeowners applying low and zero carbon technologies versus those carrying out standard refurbishment measures. They concluded that the dissemination of information and transfer of knowledge played a key role in achieving energy-efficient refurbishment measures [20]. Likewise, Pelenur and colleagues link demographics with barriers to energy efficiency measures adoption in residential sector in the UK [21]. Michelsen

Table 1 Quota for drivers and barriers, per stakeholder groups and countries.

#	Stakeholder groups	Quota										TOTAL
		BE	DE	ES	FR	IT	NL	PL	UK	Drivers	Barriers	
1.1	Architect	11	13	29	28	23	19	24	8	155	156	
1.2	Engineer	16	16	19	16	18	12	34	9	150	153	
1.3.	Construction companies	14	20	26	16	37	28	28	70	239	236	
1.4	Installers	19	19	26	25	31	22	6	6	155	147	
1.5	Demand-side actors	31	34	114	67	110	85	88	66	627	673	
<b>TOTAL</b>		<b>91</b>	<b>135</b>	<b>223</b>	<b>152</b>	<b>220</b>	<b>166</b>	<b>180</b>	<b>159</b>	<b>1326</b>	<b>1365</b>	

and Madlener explored the multi-dimensionality of the homeowners' motivation to decide between competing residential heating systems in Germany, concluding that adoption motivations can be grouped around six dimensions: (1) cost aspects, (2) general attitude towards the technologies, (3) government grant, (4) reactions to external threats (i.e., environmental or energy supply security considerations), (5) comfort considerations, and (6) influence of peers [22]. In Germany too, Kesterich and colleagues derived factors that increase the willingness to pay (WTP) of homeowners for energy efficiency in the specific case of an upcoming move. Their estimation results suggested that the WTP is not determined by socioeconomic attributes like household income or formal education, but rather by environmental concerns and energy awareness [23]. Likewise, Caird and colleagues surveyed consumers' (i.e. technology adopters) to study the reasons behind adoption of energy efficiency measures and renewable energy systems, including drivers and barriers. The reasons for considering but rejecting these technologies include the familiar price barriers, as well as other obstacles that varied according to the technology concerned [24]. Finally, Heiskanen offered a literature review on renewable energy technology deployment in residential buildings, in which concluded that a research gap exists because building owners across Europe are quite diverse, and the European markets exhibit different stages of maturity [25].

This literature overview shows a body of knowledge covering household-level factors influencing the adoption of building-scale energy efficiency solutions. Yet, each study addresses a distinct country, technology solution(s) and stakeholder's perspective. The only cross-country analysis of household adoption of energy efficient technologies and behavioural practices we are aware of is the OECD report "Assessing the Impacts of Climate Change" (2011) [26]. Results across the selected OECD countries included in the study were found to vary considerably with respect to appliance stock, investments in energy-savings equipment, energy savings behaviour, government support received for installations of energy-efficient technologies, environmental concerns and attitudes, or motivations to reduce energy consumption. For example, Dutch households are most likely to turn off their electronic appliances and devices. In comparison, households in Australia, the Czech Republic and South Korea are the least likely to switch off appliance in stand-by mode, while households in Sweden and Norway are the least likely to turn off lights when leaving a room. The June 2011 Eurobarometer survey also hints at differences across EU Members in terms of environmental concerns and actions [27]. For instance, in Luxembourg and Denmark 34% and 31% of the population, respectively, considers climate change to be the single most serious problem facing the world. In Portugal and Ireland, this share is only 7% and 13%, respectively. In the 6 months prior to the survey, about three quarters of Swedes, Slovenes and Luxembourgian report to have taken personal actions to fight climate change, but less than a third of Poles, Romanians or Estonians report the same. However, given the diversity of local and national contexts, studies from one country or specific technology cannot be readily generalized to other region or technology, even within the EU. Thus, comparing findings across studies and countries is not possible, as these differ in terms of technologies selected, behavioural practices, explanatory variables, and methods.

## 2. Materials and methods

This section describes the survey instrument used to retrieve the data as well as the analysis applied. The data collected from a large-scale multi-country survey are displayed and analysed for the percentage of respondents across the countries stating the relevance of various drivers and barriers for EETs. The perceived barriers and drivers were further studied for their association across the countries using the Pearson's Chi2 and a Cramer's V tests. The lower the p-value for Pearson's Chi2, the higher the level of association, i.e. how the preference towards a driver or barrier varies across the selected countries. Similarly,

the higher value of Cramer's V (between 0 and 1), the higher the level of association.

### 2.1. Data collection: a multi country online survey

The empirical analysis is based on data collected from a multi-country online survey distributed in 2019 across 8 European countries: Belgium (BE), Germany (DE), Spain (ES), France (FR), Italy (IT), Netherlands (NL), Poland (PL), and United Kingdom (UK). To enable cross-country comparability of the results, all countries used a common survey instrument translated into the local language and jargon with the support of a market expert team and stakeholder representatives from each country. The overall sample contains 7231 responses [28–30]. Since the population of interest (i.e. residential building projects in the EU) is significantly large and heterogeneous, and there was a need to represent even small subgroups of the population (e.g. stakeholder groups, comprehensive refurbishment projects, etc.), a stratified sample approach was considered as the most appropriate. To characterise the population of interest, the sample was then divided into three stratification axes, as of the main elements building projects are composed of: (I) stakeholder group, (II) building typology, and (III) project type. Based on the stratified approach, there was no maximum number of responses stipulated but rather a minimum quota for the three axes of stratification (Annex II, Table A2). One stratification axis is controlled ex-ante (i.e. stakeholder group) and two are controlled for during the survey or ex-post (i.e. building typology and project type). A number of steps were followed to control the ex-ante axis in the survey distribution. The first step was to study the structure of the axis in each country, which was done in terms of number of companies and sizes (i.e. number of employees). This information was collected from Eurostat [31]. This source was chosen because it ensured the cross-comparability of the statistics. This information was then transferred to a market research institute, commissioned for the distribution of the survey across the selected countries. The market research institute was then responsible for collecting the contacts for the selected stakeholder groups according to the number of companies and sizes specified by the Eurostat database for each country. The contact directory for each stakeholder group and country was constructed from different sources, namely: yellow pages, online lists, purchase of list from different suppliers (e.g. green book) or even sometimes from random telephone selection [32].

The original survey contained responses from seven stakeholder groups: (1) Conceiving, planning, and consulting services; (2) Material and technology supply; (3) Construction & installation; (4) Enabling services; (5) Operation and maintenance services; (6) Institutional demand side, and (7) Private demand side. However, the present study focuses on collecting the perspective of key decision-makers in the technology selection. Therefore, some stakeholder groups had to be excluded from the analysis. To select what stakeholder groups were included in the analysis, a literature review was performed. In this, several sources identified demand-side actors, (e.g. institutional and private demand side) are key decision-makers in the technology selection [33,34]. Nevertheless, recent findings demonstrate that in the technology selection process in EU residential buildings, many other stakeholders are involved and interconnected in these decisions, some of which can have the same or even more power and communication than the demand-side actors, namely architects, engineers, construction companies and installers [14]. These findings substantiate some earlier results from Beillan and colleagues, which had identified that architects played a key role for orienting homeowners towards comprehensive energy-efficient retrofitting. [17]. This supports the investigations from Heiskanen that indicated that installers are often the main source of information for building owners, and their recommendations have significant weight in the choice of several building systems or components [23]. On this basis, the barriers and drivers are based on the following perspective: architects (1.1), engineers (1.2), construction companies (1.3), installers (1.4), and demand-side actors, including institutional demand side, such as housing compa-

**Table A2**  
Minimum quota defined in the survey. Breakdown per stratification axis.

Stakeholder		Project type						Sub-total		Grand-total
		New built		Deep refurbishment		All other measures (including maintenance, refurbishment)				
Group	Sub-groups	SDB	MDB	SDB	MDB	SDB	MDB	SDB	MDB	SDB + MDB
<b>1. Conceiving, planning, and consulting services</b>	<i>Architects and engineers</i>	9	9	9	9	9	9	27	27	<b>54</b>
<b>2. Material and technology supply</b>	<i>Material or technology manufacturer or retailer</i>	9	9	9	9	9	9	27	27	<b>54</b>
<b>3. Construction &amp; installation</b>	<i>Construction companies and installers</i>	10	10	10	10	10	10	30	30	<b>60</b>
<b>4. Enabling services</b>	<i>Local authorities, banks and other financial services</i>	9	9	9	9	9	9	27	27	<b>54</b>
<b>5. Operation and maintenance services</b>	<i>Energy supply/utility and ESCO, facility managers: commercial, administrative, technical, maintenance, etc.</i>	10	10	10	10	10	10	30	30	<b>60</b>
<b>6. Institutional demand side</b>	<i>Investors, developers, housing companies for profit, public/part</i>	15	15	15	15	15	15	15	45	<b>60</b>
<b>7. Private demand side</b>	<i>Governmental/non-profit Private house owners, flats rented out or self-owned</i>	26	26	26	26	26	26	78	78	<b>156</b>
<b>Total</b>	<b>88</b>	<b>88</b>	<b>88</b>	<b>88</b>	<b>88</b>	<b>88</b>	<b>234</b>	<b>264</b>	<b>498</b>	

nies (for profit), housing company or housing association, cooperative (public/part governmental/non-profit) and private demand side, including: private owner (1.5).

In order to collect the information to identify the respondent's role in the building value chain, the respondents were asked: "Are you working professionally in one of the following companies or organisation types?" followed by a list of 21 options, including "Other company or organisation type in the building or construction sector" and "No, I do not work professionally in any company or organisation type related to the building and construction sector". To encompass all demand-side actors including private owners, for those interviewees who had indicated not to be working professionally in an organization from the building sector, there was the follow-up question "Do you privately own one or more residential home(s) or flat(s)?"

Since the analysis focused on a specific stakeholder groups (i.e. architects, engineers, construction companies, installers and demand-side actors), a subset of the complete database was used. Subsequently, the final sample used for this study consists of 1782 responses, with the following distribution across countries: BE = 115, DE = 181, ES = 317, FR = 209, IT = 329, NL = 216, PL = 204, UK = 211. The subset obtained for the above-mentioned stakeholder groups are further divided into two parts, one each for drivers and barriers. Based on the contact collection approach, it is reasonable to assume that these subsets are randomly collected. Because the scope of this study is limited to provide a basic analysis on the choice of drivers and barriers by country, stakeholder and technology separately. The inclusion of sample weights would be appropriate for performing an aggregated analysis where all three strata (country, stakeholders, and building typology) are studied together. In this way, the response to the above questions on drivers and barriers was another dimension defining the sample size. The parts are based on the valid responses to analyse the driver or barrier groups (i.e. at least one of the answer options in the question checked). This division is necessary as the respondents were given the freedom to answer either barriers or drivers or both based on their level of experience and knowledge. The complete list of stakeholders and their respective quotas in the final dataset with valid observations for driver and barrier groups are described in Table 1. The datasets for driver and barrier groups have 1326 and 1365 responses respectively. Among the stakeholders, nearly 50% quota belongs to the demand-side actors (1.5), followed by the construction companies (1.3). The architects (1.1), engineers (1.2), installers (1.4) have almost equal quota. Among the countries, the highest

quota belongs to the IT and lowest is for the BE. The lower sample size for the architects (1.1), engineers (1.2), and installers (1.4) in the UK, also for the installers (1.4) in the PL, does not affect the analysis, as all these stakeholders are treated as a single entity. The combined sample size matters in case of estimating the shares for drivers and barriers for various EETs. The fact that the number of responses is not exactly matching is because the respondents could answer either of the driver or barrier or both. The selection of drivers and barriers as well as the main categories were extracted from the literature study [22,35,36]. The questions related to drivers and barriers can be found in the Appendix I. For the entire questionnaire refer to [32].

To collect the information on the drivers for the EETs, interviewees were asked "What should happen to scale%tech% in%country%?" for a randomly selected technology. They were offered 15 answer options, grouped into the same 5 categories: environmental, technical, economic, social and legal. Again, they also had the option to select "Other" and "I don't know". We also included the option "I don't want this technology to be scaled". The valid observations shown in Table 1 exclude the respondents who answered, "I don't know" and "I don't want this technology to be scaled" for the drivers. The complete list of drivers and driver groups are shown in Table 2.

As a follow-up question, to identify perceived barriers, they were asked: "What are the key barriers for %tech% in the current%country% market?" for the same technology and were provided with 21 answer options, clustered into the same 5 categories as the drivers: environmental, technical, economic, social and legal. Along with the choice "Other" and "I don't know". The complete list of barriers and barrier groups are shown in Table 3. The valid observations shown in Table 1 exclude the respondents who answered, "I don't know" for barriers.

The final sample sizes for drivers was (1326) and (1365) for barriers respectively. The fact that the numbers of responses are not exactly matching is since the respondents could answer either of the driver or barrier or both. The selection of drivers and barriers as well as the main categories were extracted from the literature study [22,35,36]. The questions above can be found in the Appendix I. For the entire questionnaire refer to [32].

The format of the survey allowed participants to choose more than one answer option out of 15 drivers and 21 barriers displayed in Tables 2 and 3. Based on this, Table 4 shows the number of observations making 1 or more number of choices in both drivers and barriers. For example, in IT and for building automation, 7 observations choose

**Table 2**  
Breakdown of drivers and groups.

Driver Group	Driver	Definition
Environmental	1	Improvement of the technology's environmental performance (e.g. less energy consumption or carbon emissions)
	2	Energy input such as electricity, district heat, gas, oil should be produced more from renewable energy sources
Technical	3	Improvement of the reliability and functionality
	4	Easier installation process
	5	Improved user-friendly
	6	Better design
	7	Improving Advertising / Technical Information Technology
Economic	8	Price decrease and shorter payback time
	9	Energy cost saving and low running costs
Social	10	Better marketing of technology
	11	Improved consideration of demands by tenants and building owners
Legal	12	Improved communication in project teams
	13	Enforcement of building codes or by other legal requirements
	14	Promotion of energy-efficiency, low-carbon or sustainability labels for buildings
	15	Information campaign of authorities

**Table 3**  
Breakdown of barriers and groups.

Barrier Group	#	Definition	
Environmental	1	Lack of ambitious and clear political environmental targets	
	2	Lack of environmental awareness	
Technical	3	Lack of reliable technologies	
	4	Lack of high-performance technologies	
	5	Lack of simple production process	
	6	Lack of comprehensive information about alternatives and advantages/disadvantages	
	7	Lack of affordable products	
Economic	8	Low energy prices	
	9	Lack of subsidies	
	10	Lack of tax incentives	
	11	Lack of trust / awareness of lower life cycle / running costs	
	12	Lack of comprehensive financing models	
	13	Lack of qualified organizations / employees (e.g. for installation, construction)	
	Social	14	Lack of trust / awareness in higher acoustic comfort
		15	Lack of trust / awareness in heat comfort
16		Lack of interest in attractive design	
17		Lack of short or easy installation or maintenance	
Legal	18	Lack of education	
	19	Lack of a comprehensive legal framework	
	20	Lack of a comprehensive building standards	
	21	Lack of implementation of legal standards	

just one driver, and 6 observations choose just one barrier. The data shows that there is nearly an equal number of respondents making 1 to 5 choices in both drivers and barriers, in each EET. The distribution also varies among technologies and countries. For instance, in Building automation & smart metering IT, NL and UK have a higher number of responses between 1 and 2 choices than BE, DE, ES and FR, where the highest number of responses have selected between 3 and 5 drivers or barriers. Based on the numbers from Table 4, the authors decided to carry out the analysis at the level of group of driver and barriers, due to two major reasons. One of the reasons is, there are too many options for both drivers and barriers to make a cogent analysis. Also, most of the arguments can be correlated. For instance, a respondent may select “lack of affordable products” an argument which can be linked to “lack of subsidies”. In such cases, calculating the shares (probabilities) at the individual driver or barrier level to estimate the aggregate share for the groups will lead to an underestimation of the shares. Thus, the shares estimated at the group level does not include the number of drivers or barriers selected in that group. For instance, any respondent choosing at least one of the barriers from 3 to 6 in Table 3 is considered as an observation selecting the Technical barrier group.

2.2. Data analysis: overview of methodology

The data analysis is comprised of two parts. The first part estimates the probability of selecting each driver and barrier group for each EET and country combination. As shown in Eq. (1), the probabilities are the

ratio between the number of respondents thought a driver/barrier is significant ( $r_i$ ) and the total number of respondents that answered the survey ( $N_i$ ). These  $P_i$  are presented as percentages of respondents selecting the drivers and barriers in Sections 3.1 and 3.2.

$$P_i = \frac{r_i}{N_i} \tag{1}$$

In the second part, the level of two-way association between these probabilities and the eight countries is estimated using the Pearson's Chi2 and Cramer's V test. These statistics measure the two-way dependency between the probabilities of drivers/barriers among the countries. The Pearson's Chi2 is estimated from the number of observations in the matrix ( $n_{ij}$ ) as shown in the Eq. (2) below where,  $i$  is country (rows), and  $j$  is if a driver/barrier is selected or not selected (columns) for an EET and country [37]. Hence, there are eight rows ( $i = 1, 2, 3 \dots, 8$ ) representing the countries and two columns ( $j = 0,1$ ) where  $j = 1$  if a driver or barrier is selected for a given EET, and  $j = 0$  if not selected.

$$Chi2 = \sum_i \sum_j \frac{(n_{ij} - m_{ij})^2}{m_{ij}}; \text{ where } m_{ij} = \frac{(\sum_i n_{ij})(\sum_j n_{ij})}{\sum_i \sum_j n_{ij}} \tag{2}$$

Since there are eight countries and two options (a driver/barrier selected or not selected), the Chi2 obtained above has a total degree of freedom equal to seven i.e.,  $(8-1) * (2-1)$ . The Cramer's V is defined as given in Eq. (3) below where,  $n$  is the sample size and  $t$  is the minimum of number rows minus and number of columns minus one,  $t = 1$  in current paper as the number of rows equal to eight (countries) and the

**Table 4**  
Number of choices per EET, across selected countries for drivers and barriers.

		1. Building automation & smart metering							2. District heating							3. Electric storage									
		1	2	3	4	5	6	7	>7	1	2	3	4	5	6	7	>7	1	2	3	4	5	6	7	>7
BE	Drivers	1	1	3	0	1	1	0	2	0	4	4	1	2	0	2	1	1	0	2	1	2	1	0	1
	Barriers	0	1	3	0	2	0	0	3	0	2	5	3	2	0	1	3	2	1	3	1	1	0	0	2
DE	Drivers	1	2	0	2	4	2	1	1	2	2	0	3	5	0	0	0	4	3	2	0	2	0	0	2
	Barriers	1	1	2	2	3	2	2	0	4	3	2	2	4	0	1	0	4	4	2	0	2	0	1	1
ES	Drivers	0	4	4	6	2	3	1	0	2	1	5	4	3	6	2	1	2	6	6	5	6	3	1	2
	Barriers	1	4	4	5	5	2	2	0	2	7	2	5	8	1	3	1	2	2	6	4	5	5	1	3
FR	Drivers	0	2	7	3	3	0	1	3	2	1	1	3	3	1	2	2	2	3	1	1	7	2	1	0
	Barriers	0	3	4	3	3	2	0	2	0	5	2	1	2	2	1	3	1	1	2	3	4	1	1	3
IT	Drivers	7	3	7	3	2	1	0	0	6	6	5	3	1	2	0	1	4	10	5	2	0	1	0	0
	Barriers	6	7	4	3	5	0	0	1	6	11	7	1	2	0	0	1	8	10	5	1	0	0	0	0
NL	Drivers	5	1	7	2	2	2	1	0	1	7	6	2	4	0	0	0	8	1	2	1	2	0	0	0
	Barriers	6	3	3	0	4	0	2	1	0	7	6	1	3	1	1	0	8	3	0	0	3	0	0	0
PL	Drivers	1	0	1	4	4	2	2	4	3	2	1	0	6	4	1	1	2	5	3	3	5	1	0	0
	Barriers	1	0	1	2	7	1	2	4	1	2	2	1	4	3	3	1	1	3	4	1	4	2	1	2
UK	Drivers	4	6	0	2	5	1	1	3	5	0	1	2	4	1	0	2	3	3	3	1	3	1	1	0
	Barriers	4	4	2	2	5	1	0	3	3	2	4	2	1	0	0	4	4	2	3	0	5	0	0	1
Total	Drivers	19	19	29	22	23	12	7	13	21	23	23	18	28	14	7	8	26	31	24	14	27	9	3	5
	Barriers	19	23	23	17	34	8	8	14	16	39	30	16	26	7	10	13	30	26	25	10	24	8	4	12
		4. Heat Pumps							5. High-performance windows							6. Insulation									
		1	2	3	4	5	6	7	>7	1	2	3	4	5	6	7	>7	1	2	3	4	5	6	7	>7
BE	Drivers	2	1	3	1	0	0	0	2	1	3	3	2	1	0	0	1	1	3	6	2	0	0	0	0
	Barriers	2	0	3	1	0	2	0	2	1	4	3	1	0	2	0	1	1	4	6	1	1	0	0	0
DE	Drivers	3	2	0	2	4	1	1	1	1	6	2	2	3	0	0	0	2	1	2	0	2	1	1	1
	Barriers	4	2	0	1	5	2	0	2	4	1	3	1	4	0	1	0	2	2	1	1	1	0	0	4
ES	Drivers	3	3	7	2	2	5	0	2	4	1	7	7	2	1	1	0	5	5	10	5	0	3	0	0
	Barriers	0	6	6	3	5	2	1	1	1	2	6	4	4	3	3	0	4	4	6	4	8	3	0	1
FR	Drivers	2	6	0	1	4	1	2	1	5	3	3	2	5	0	1	2	0	1	5	0	5	1	2	0
	Barriers	3	2	1	2	2	0	0	4	3	4	2	4	6	1	0	3	2	1	3	0	4	2	2	2
IT	Drivers	12	9	3	3	1	0	0	1	10	7	2	5	1	0	0	0	8	6	3	3	1	1	0	1
	Barriers	11	4	8	3	1	0	0	1	11	6	4	1	3	0	0	0	8	7	2	3	1	2	0	0
NL	Drivers	10	6	3	0	1	0	0	0	1	3	3	3	3	0	1	0	4	6	2	1	3	0	0	0
	Barriers	2	6	3	1	3	0	0	1	2	1	1	4	3	1	0	0	10	0	2	1	2	0	0	0
PL	Drivers	7	1	3	4	2	1	0	0	2	3	4	2	6	3	3	2	2	3	2	3	6	3	1	5
	Barriers	4	0	4	4	3	1	0	2	0	3	3	1	7	1	3	6	2	1	1	4	6	2	2	7
UK	Drivers	2	3	1	1	3	1	1	2	2	2	4	2	2	2	2	2	4	4	4	5	3	1	0	3
	Barriers	1	2	4	1	3	1	0	2	2	3	3	2	1	1	3	2	5	3	5	1	8	1	1	1
Total	Drivers	41	31	20	14	17	9	4	9	26	28	28	25	23	6	8	7	26	29	34	19	20	10	4	10
	Barriers	27	22	29	16	22	8	1	15	24	24	25	18	28	9	10	12	34	22	26	15	31	10	5	15
		7. Photovoltaic systems							8. Solar thermal systems							9. Ventilation (with heat recovery)									
		1	2	3	4	5	6	7	>7	1	2	3	4	5	6	7	>7	1	2	3	4	5	6	7	>7
BE	Drivers	0	5	4	1	1	1	0	1	2	0	1	1	1	0	0	2	0	1	5	1	0	1	0	0
	Barriers	1	1	5	2	1	1	1	1	0	1	2	2	0	0	1	1	0	3	2	0	2	0	0	1
DE	Drivers	2	2	4	3	4	2	1	3	3	6	0	2	6	6	0	1	2	0	1	2	5	2	0	2
	Barriers	2	2	2	5	4	6	1	1	6	3	5	0	4	3	0	3	2	0	1	2	6	2	0	2
ES	Drivers	4	3	5	4	5	3	0	0	6	4	3	4	7	1	0	2	2	5	5	4	4	0	1	1
	Barriers	4	5	3	5	4	1	2	1	3	4	6	7	3	2	1	0	4	6	2	4	1	5	0	2
FR	Drivers	0	0	4	2	3	4	2	2	2	4	1	2	4	2	0	1	4	2	3	1	2	4	0	0
	Barriers	0	2	4	3	2	0	1	6	2	2	3	3	3	3	0	2	4	2	0	2	5	1	0	2
IT	Drivers	3	7	5	7	3	0	0	0	4	13	3	2	2	0	1	0	7	8	2	4	3	0	0	0
	Barriers	7	7	4	1	5	1	1	0	6	7	7	6	1	1	0	0	4	14	5	3	2	0	1	0
NL	Drivers	9	4	4	2	3	1	1	1	3	5	5	1	3	2	0	0	6	6	2	1	1	1	1	0
	Barriers	10	5	4	1	2	0	0	3	5	3	4	3	4	2	0	1	8	5	0	2	1	2	0	1
PL	Drivers	2	5	5	1	3	0	2	3	1	1	3	3	5	2	2	1	0	1	1	6	0	2	6	6
	Barriers	3	1	5	1	7	2	2	1	1	0	2	1	9	2	2	2	0	0	1	2	5	1	1	8
UK	Drivers	2	4	2	2	6	1	2	1	0	3	6	0	5	1	0	1	3	1	6	2	1	1	0	1
	Barriers	5	3	0	3	3	0	3	1	2	5	1	2	0	0	2	0	5	5	1	3	0	1	1	1
Total	Drivers	22	30	33	22	28	12	8	11	21	36	22	15	33	14	3	9	25	23	25	16	22	9	4	10
	Barriers	32	23	30	18	28	14	8	16	24	22	34	23	26	13	4	11	22	35	16	16	25	11	3	17

number columns is equal to two (if a driver or barrier selected or not). The value of Cramer’s V varies between zero and one, one showing the high correlation [38].

$$Cramer's\ V = \sqrt{\frac{Chi2}{nt}} \tag{3}$$

The Pearson’s Chi2 and Cramer’s V test evaluates the following hypotheses ( $H_0$ ,  $H_A$ ):

- Null Hypothesis ( $H_0$ ): There is no change in the influence of a driver or barrier for an EET (j) across the countries (i).
- Alternative Hypothesis ( $H_A$ ): There is a change in the influence a driver or barrier for an EET (j) across the countries (i).

The test statistic for Pearson’s Chi2 estimated in Eq. (2) is compared with the Chi2 distribution with degrees of freedom seven and the significance level 5% (i.e., absolute value of Pr in Table 5 is less than or equal to 0.05). If the test statistic is significant the  $H_0$  could be rejected,

**Table 5**  
Pearsons Chi2 and Cramers V, across selected EET for drivers and barriers.

EET	Category	Drivers				Barriers			
		Obs.	Pearson Chi2	Pr	Cramér's V	Obs.	Pearson Chi2	Pr	Cramér's V
<b>1. Building automation and smart metering</b>	<b>Environmental</b>	144	13.01	0.07	0.30	146	10.63	0.16	0.27
	<b>Technical***</b>		<b>16.56</b>	<b>0.02</b>	<b>0.34</b>		17.28	0.02	0.34
	<b>Economic***</b>		<b>10.91</b>	<b>0.14</b>	<b>0.28</b>		14.28	0.05	0.31
	<b>Social</b>		12.51	0.09	0.30		12.24	0.09	0.29
<b>2. District heating</b>	<b>Legal**</b>	142	18.13	0.01	0.36	157	<b>10.08</b>	<b>0.18</b>	<b>0.26</b>
	<b>Environmental***</b>		<b>12.01</b>	<b>0.10</b>	<b>0.29</b>		20.59	0.00	0.36
	<b>Technical***</b>		<b>9.88</b>	<b>0.20</b>	<b>0.26</b>		15.44	0.03	0.31
	<b>Economic**</b>		14.58	0.04	0.32		<b>3.16</b>	<b>0.87</b>	<b>0.14</b>
<b>3. Electric storage</b>	<b>Social</b>	139	11.72	0.11	0.29	139	12.55	0.08	0.28
	<b>Legal*</b>		<b>23.48</b>	<b>0.00</b>	<b>0.41</b>		<b>19.32</b>	<b>0.01</b>	<b>0.35</b>
	<b>Environmental</b>		8.21	0.32	0.24		12.03	0.10	0.29
	<b>Technical*</b>		<b>25.35</b>	<b>0.00</b>	<b>0.43</b>		<b>27.89</b>	<b>0.00</b>	<b>0.45</b>
<b>4. Heat pumps</b>	<b>Economic***</b>	145	<b>7.90</b>	<b>0.34</b>	<b>0.24</b>	140	20.77	0.00	0.39
	<b>Social</b>		9.02	0.25	0.26		13.23	0.07	0.31
	<b>Legal*</b>		<b>24.42</b>	<b>0.00</b>	<b>0.42</b>		<b>21.81</b>	<b>0.00</b>	<b>0.40</b>
	<b>Environmental**</b>		23.12	0.00	0.40		<b>7.81</b>	<b>0.35</b>	<b>0.24</b>
<b>5. High-performance windows</b>	<b>Technical***</b>	151	<b>9.18</b>	<b>0.24</b>	<b>0.25</b>	150	16.13	0.02	0.34
	<b>Economic</b>		8.88	0.26	0.25		7.52	0.38	0.23
	<b>Social</b>		12.43	0.09	0.29		11.61	0.11	0.29
	<b>Legal**</b>		37.16	0.00	0.51		12.47	0.09	0.30
<b>6. Insulation</b>	<b>Environmental***</b>	152	<b>5.36</b>	<b>0.62</b>	<b>0.19</b>	158	21.72	0.00	0.38
	<b>Technical***</b>		11.41	0.12	0.28		19.54	0.01	0.36
	<b>Economic*</b>		<b>22.45</b>	<b>0.00</b>	<b>0.39</b>		<b>17.76</b>	<b>0.01</b>	<b>0.34</b>
	<b>Social*</b>		<b>25.04</b>	<b>0.00</b>	<b>0.41</b>		<b>26.60</b>	<b>0.00</b>	<b>0.42</b>
<b>7. Photovoltaic systems</b>	<b>Legal*</b>	166	<b>19.93</b>	<b>0.01</b>	<b>0.36</b>	173	<b>15.56</b>	<b>0.03</b>	<b>0.32</b>
	<b>Environmental***</b>		<b>13.97</b>	<b>0.05</b>	<b>0.30</b>		16.09	0.02	0.32
	<b>Technical***</b>		<b>8.28</b>	<b>0.31</b>	<b>0.23</b>		17.25	0.02	0.33
	<b>Economic**</b>		17.13	0.02	0.34		<b>13.25</b>	<b>0.07</b>	<b>0.29</b>
<b>8. Solar-thermal systems</b>	<b>Social*</b>	153	<b>30.85</b>	<b>0.00</b>	<b>0.45</b>	157	<b>16.72</b>	<b>0.02</b>	<b>0.33</b>
	<b>Legal*</b>		<b>24.37</b>	<b>0.00</b>	<b>0.40</b>		<b>25.51</b>	<b>0.00</b>	<b>0.40</b>
	<b>Environmental</b>		13.08	0.07	0.28		10.92	0.14	0.25
	<b>Technical*</b>		<b>22.44</b>	<b>0.00</b>	<b>0.37</b>		<b>21.88</b>	<b>0.00</b>	<b>0.36</b>
<b>9. Ventilation (with heat recovery)</b>	<b>Economic</b>	166	6.69	0.46	0.20	173	12.78	0.08	0.27
	<b>Social**</b>		17.25	0.02	0.32		<b>7.32</b>	<b>0.40</b>	<b>0.21</b>
	<b>Legal***</b>		<b>11.70</b>	<b>0.11</b>	<b>0.27</b>		21.87	0.00	0.36
	<b>Environmental</b>		7.46	0.38	0.22		10.01	0.19	0.25
<b>9. Ventilation (with heat recovery)</b>	<b>Technical***</b>	153	<b>10.28</b>	<b>0.17</b>	<b>0.26</b>	157	19.33	0.01	0.35
	<b>Economic</b>		11.68	0.11	0.28		5.10	0.65	0.18
	<b>Social*</b>		<b>15.77</b>	<b>0.03</b>	<b>0.32</b>		<b>15.08</b>	<b>0.04</b>	<b>0.31</b>
	<b>Legal*</b>		<b>32.81</b>	<b>0.00</b>	<b>0.46</b>		<b>14.80</b>	<b>0.04</b>	<b>0.31</b>
<b>9. Ventilation (with heat recovery)</b>	<b>Environmental***</b>	134	<b>12.56</b>	<b>0.08</b>	<b>0.31</b>	145	19.75	0.01	0.37
	<b>Technical*</b>		<b>21.30</b>	<b>0.00</b>	<b>0.40</b>		<b>20.68</b>	<b>0.00</b>	<b>0.38</b>
	<b>Economic*</b>		<b>21.43</b>	<b>0.00</b>	<b>0.40</b>		<b>14.36</b>	<b>0.05</b>	<b>0.32</b>
	<b>Social*</b>		<b>16.61</b>	<b>0.02</b>	<b>0.35</b>		<b>24.24</b>	<b>0.00</b>	<b>0.41</b>
<b>9. Ventilation (with heat recovery)</b>	<b>Legal*</b>	134	<b>28.97</b>	<b>0.00</b>	<b>0.47</b>	145	<b>38.91</b>	<b>0.00</b>	<b>0.52</b>

Note: Significant at 5% level: 1. Drivers (\*\*\*), 2. Barriers (\*\*), and 3. Both drivers and barriers (\*).

proving a significant change in the influence a driver or barrier across countries.

### 3. Results

#### 3.1. Drivers for EET adoption

Key drivers vary across EET as well as across countries. Across all of the selected EETs, the technical and economic drivers have the highest share, except for IT and NL, where technical arguments are not so predominant. In the case of BE, another key group is the social. The technical driver group has a major share in the UK across all EETs with 100% in electric storage. The social driver is less selected in countries like ES across all technologies, being technical and environmental conditions the strongest motives. The least often selected driver across all countries are legal related matters. In BE, main arguments in favour of EETs vary substantially across the solutions. For instance, for building automation and smart metering, as well as for electric storage, social and/or environmental arguments are the most common. Whereas in district heating, heat pumps, insulation and solar thermal, it is related to technical concerns. It is noteworthy that across all technologies except photovoltaic

systems, economic drivers are among the least often selected. In DE, the most often selected driver across all EETs is technical-related matters, except for district heating which is led by environmental concerns. Again, across all technologies, the least often selected argument are legal ones. This is quite the opposite picture to ES, where legal-related arguments are the most often selected ones across all EETs, except photovoltaic systems where economic aspects are identified to lead their uptake. In FR, driver groups vary substantially across the various EETs. In building automation and smart metering, district heating, photovoltaic and solar thermal systems, and ventilation (with heat recovery) technical drivers are the first or second most selected driver. Whereas for electric storage, heat pumps, high-performance windows and, insulation it is economic parameters. These results can also be seen in IT, where techno-economic arguments are the most predominant across all technology solutions, except electric storage and ventilation (with heat recovery), where the technical aspects are among the least relevant. In NL, across all technologies except ventilation (with heat recovery), the most often selected drivers are the economic-related ones. Whereas the least often selected ones are on environmental and legal matters. In PL, techno-economic matters are always among the most predominant, except in photovoltaic systems and solar thermal systems where the tech-

nical aspects are not so relevant. Finally, in the UK, driver groups vary across EETs. For instance, for building automation and smart metering, district heating, electric storage, and ventilation with heat recovery technical and environmental aspects are the most relevant. While for heat pumps and high-performance windows it is the techno-economic related ones. It should also be noted that given the respondent was able to cross more than one driver, it could be that in some countries, the percentages for some groups are high. This does not necessarily mean that it is much more relevant than others, but simply that they could select more than one options in that same group.

### 3.2. Barriers for EET adoption

As in the case of the drivers, barriers to EET vary across the sampled solution and countries and the economic barrier group has the highest share (except electric storage EET in the DE). Economic arguments are followed mainly by technical aspects. As in the case of the drivers, legal arguments have the least number of responses across countries and technologies. When looking at each of the examined countries it can be depicted that in BE, main arguments impeding the large-scale deployment of the selected technologies are economic-related. These are followed by social-related barriers. When it comes to the least often identified arguments in BE across all EETs, it is legal and environmental matters. In DE, technical and economic aspects are the most often selected. Against legal matters which are the least often. In ES, economic aspects are also identified across all EETs as the most important, whereas, as in the other cases, legal aspects are the least relevant. Once again, in FR economic aspects are of most relevance, followed by technological impediments. The results for IT are quite similar to the ones portrayed in ES, where economic-related arguments are perceived as crucial in the drawback of their implementation in residential building projects, closely followed by technical and social. In the case of the NL, economic matters are clearly the most relevant hurdle impeding the uptake of all of the selected EETs, whereas legal matters play a minor role in their restriction. In the case of high-performing windows, social aspects are also identified as quite relevant in their limitation. In PL, key impediments are related to technical or economic aspects, with the only exception of high-performance windows and insulation, where the environmental are much more predominant than technical. In the case of ventilation (with heat recovery), economic and social have the same crucial weight in their blockage. Finally, in the UK, across all technologies technical and/or economic related matters are of utmost importance when it comes to barriers to EETs. In this way, in overall, BE and PL show the most distinct results of all countries. Again, given the respondent was able to cross more than one choice, it could be that in some countries, the percentages for some groups are high. This does not necessarily mean that it is much more relevant than others, but simply that they could select more than one options in that same group.

### 3.3. Pearson's Chi2 and Cramers V test

Table 5 shows the Pearson's Chi2 and Cramer's V test statistics between various EETs and driver or barrier groups. There are 45 combinations (number of rows in Table 5), 9 EETs and 5 groups for each driver and barrier groups. Overall, out of these 45 combinations, the Chi2 are significant at 5% level for 15 EET and driver or barrier group combinations (\*), 6 for EET and driver group combinations (\*\*); and 13 for EET and barrier group combinations (\*\*\*). Table 5 also highlights the groups for which the Chi2 is not significant at 5% for both driver and barrier groups. It is worthy to note that the choice of legal driver and barrier groups in seven out of nine EETs is found to vary significantly at 5% level across the countries, except the building automation and heat pumps (which is significant in driver groups but not in barrier groups). This shows that the legal aspects vary from country to country considerably. Also, Cramer's V for legal driver and barrier group vary between

0.3–0.5, proving the strong association between the stakeholder choices and country.

Comparing Table 5 with the above Figs. 3.1.1–3.1.9 for drivers, and Figs. 3.2.1–3.2.9 for barriers, the ventilation EET and legal group has the highest significance, at 1% level for Chi2 with Cramer's V close to 0.5 in both driver (25% in IT to 94% in PL) and barrier (10% in IT to 73% in DE). In case of driver groups, the legal drivers for heat pumps show the most significant variation across countries i.e., the choice having highest association with countries (10% NL to 78% in BE). In case of barrier groups, environmental barriers for ventilation show the most significant variation (38% in FR to 87% in DE) (Figs. 3.2.1–3.2.9).

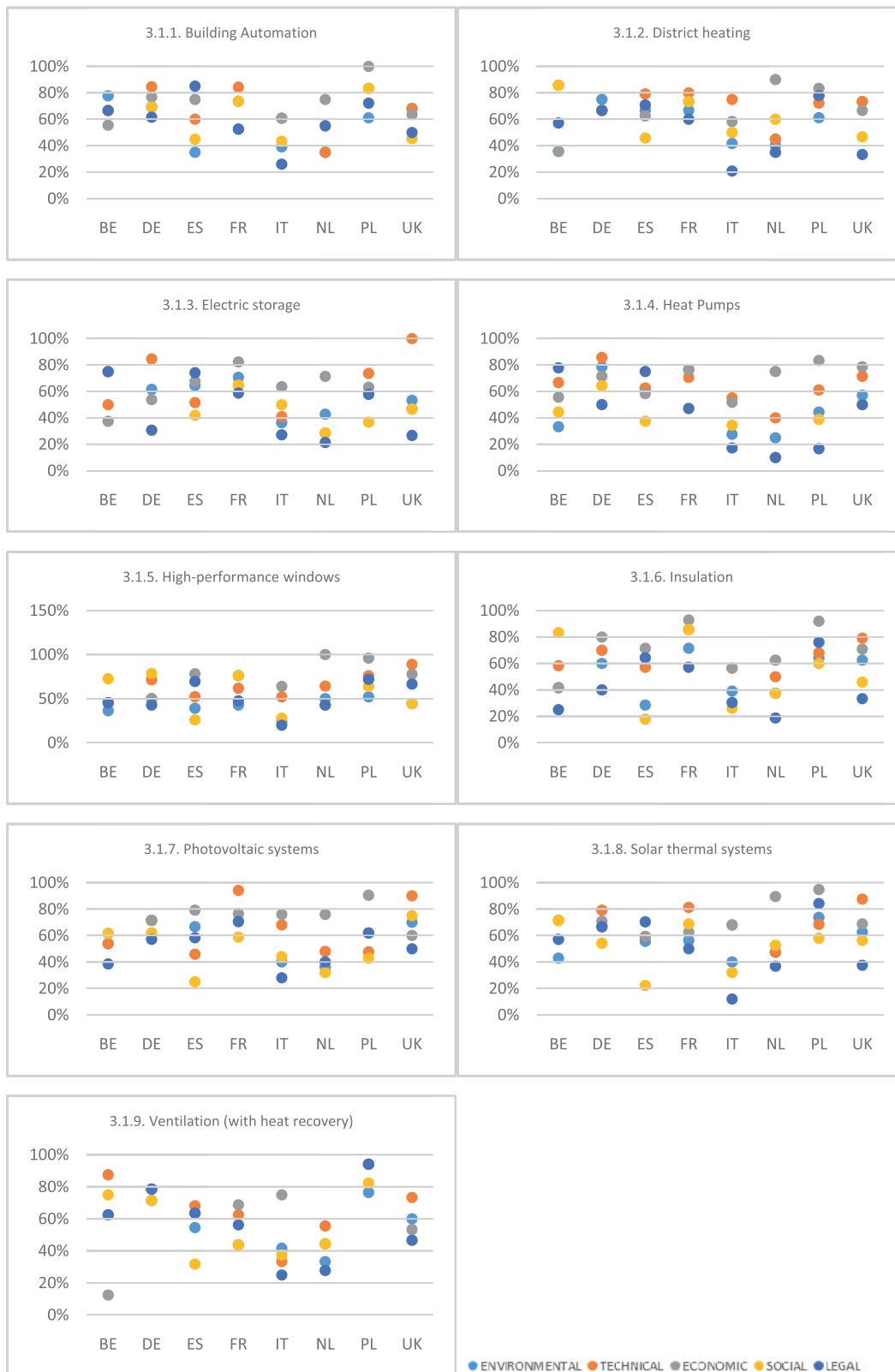
## 4. Discussion and conclusions

The goal of this study was to characterise perceived drivers and barriers to EETs adoption according to key decision-makers and persuaders in the technology selection. The selected solutions were building automation and smart metering, district heating, electric storage, heat pumps, high-performance windows, insulation, photovoltaic systems, solar thermal systems, and ventilation (with heat recovery). To this end, results from a multi-country survey were collected and assessed in order to better understand the market similarities and differences across these countries.

Findings show that drivers and barriers to EETs adoption differ depending on the specific solution and country. Yet, some general conclusions can be extracted. When it comes to potential drivers for the implementation of EETs, key decision-makers and persuaders identified economic and technical aspects as being the most relevant, especially among district heating, heat pumps, photovoltaic, solar thermal, and ventilation (with heat recovery). When it comes to barriers impeding the selection of these technologies, it is economic-related arguments, such as "Lack of trust / awareness of lower life cycle / running costs", the most often selected ones.

This outcome indicates that the assumed economic viability of these solutions is not sufficiently acknowledged or appealing to foster their large-scale deployment in the selected countries. This coincides with some of the findings from previous studies [39], which try to monetize other impacts of the energy efficiency measures in order to make these actions more appealing to the decision-makers [39,40]. In turn, it strengthens the results of the study by Stieß and colleagues, highlighting the critical role that the dissemination of information and transfer of knowledge play in achieving energy-efficient refurbishment measures. Likewise, the fact that environmental aspects are not the most often selected ones, also supports the findings from Beillan and colleagues indicating that people getting involved in projects of energy-efficient refurbishment aren't mainly and exclusively motivated by energy savings. Results of this study further compliment the findings from Michelsen and colleagues, concluding that adoption motivations for can be grouped around the various dimensions [22]. This study also suggest that inasmuch these various dimensions exist, they do not entail the same weight across technologies and countries. Finally, the results from this paper shed light to the findings from Caird and colleagues, which identified that obstacles for energy efficiency that varied according to the technology concerned [24], by providing an overview on how these barriers (and drivers) might vary across solutions and geographies. In terms of geographies, is worth noting that within this study, results vary across countries even within the same EU climatic zone (e.g. IT and ES). This emphasises the presence of values and awareness in the adoption of EET technologies at a national level, along with the importance of developing policy measures that address this matter at a country-scale.

Future research should focus on extending the findings of this study to the remaining EU countries, as well as non-residential buildings. Likewise, advancing the understanding on how the various arguments vary across the specific stakeholder groups. Findings from this study could be used to develop evidence-base policy instruments (national and pan-



Figs. 3.1.1–3.1.9. The percentage of respondents choosing a driver group across the selected EETs and countries.



Figs. 3.2.1–3.2.9. The percentage of respondents choosing a barrier group across the selected EETs and countries.

EU) aiming to foster the large-scale diffusion of energy-efficient technologies. In particular, findings from this paper could support the identification of key barriers and drivers per technology solutions, as well as the linkage of these to the particular stakeholder groups.

### Acknowledgments

This work has been financed by Climate-KIC, supported by the EIT – a body of the European Union TC\_2.7.8\_190515\_P183–1B under the h2020 framework. The authors would like to thank Lena Hennes, Katrin Bienge and Justus von Geibler for their support in the development of the survey and collection of the data used in this paper.

### Appendix A. Survey Questions

#### **Are you working professionally in one of the following company or organisation types?**

Please tick the most relevant (work more than 30% of your working hours).

##### **MATERIAL AND TECHNOLOGY SUPPLIER**

- Raw resource provider
- Technology or component manufacturer (e.g. HVAC, PV)
- Material or technology trader

##### **SERVICE PROVIDER AND ENABLER**

- Architect office
- Engineer office
- Consulting company
- Installer company
- Construction company
- Public authority
- Bank / other financial service company
- Facility management office - administrative
- Facility management office - technical
- Energy supply/utility or Energy service company (ESCO)
- Research institute
- Non-governmental organisation (NGO)
- Business association, agency
- Media company

##### **DEMAND-SIDE ACTOR (demanding materials, technologies and services)**

- Investment or development company
- Housing company (for profit)
- Housing company or housing association, cooperative (public/ part governmental/ non-profit)

##### **OTHER company or organisation type in the building or construction sector:**

Please insert text

- No, I do not work professionally in any company or organisation type related to the building and construction sector

##### **Do you privately own one or more residential home(s) or flat(s)?**

- Yes
- No

##### **What are the key barriers for%tech% in the current%countryadj% market?**

*The technology is randomly selected and assigned to you.*

- Environmental
  - Lack of ambitious and clear political environmental targets
  - Lack of environmental awareness
- Technical
  - Lack of reliable technologies

- Lack of high-performance technologies
- Lack of simple production process
- Lack of comprehensive information about alternatives and advantages/disadvantages

##### • Economic

- Lack of affordable products
- Low energy prices
- Lack of subsidies
- Lack of tax incentives
- Lack of trust / awareness of lower life cycle / running costs
- Lack of comprehensive financing models
- Lack of qualified organizations/ employees (e.g. for installation, construction)

##### • Social

- Lack of trust / awareness in higher acoustic comfort
- Lack of trust / awareness in heat comfort
- Lack of interest in attractive design
- Lack of short or easy installation or maintenance
- Lack of education

##### • Legal

- Lack of a comprehensive legal framework
- Lack of a comprehensive building standards
- Lack of implementation of legal standards

##### • Other: Please describe

##### • I do not know

#### **What should happen to scale%tech% in%country%?**

*The technology is randomly selected and assigned to you.*

##### • Environmental

- Improvement of the technology's environmental performance (e.g. less energy consumption or carbon emissions)
- Energy input such as electricity, district heat, gas, oil should be produced more from renewable energy sources

##### • Technical

- Improvement of the reliability and functionality
- Easier installation process
- Improved user-friendliness
- Better design

##### • Economic

- Price decrease and shorter payback time
- Energy cost saving and low running costs

##### • Social

- Better marketing of technology
- Improved consideration of demands by tenants and building owners
- Improved communication in project teams

##### • Legal, standards and labels

- Enforcement of building codes or by other legal requirements
- Promotion of energy-efficiency, low-carbon or sustainability labels for buildings
- Information campaign of authorities

##### • Other: Please describe

##### • I do not think this technology should scale up

##### • I do not know

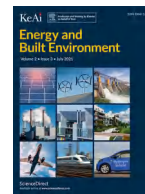
The complete questionnaire can be accessed through the link: <https://chalmersuniversity.box.com/v/SurveyQuestionnaire>.

### Appendix B. Survey minimum quota

#### References

- [1] ENldings, (2019). <https://ec.europa.eu/energy/en/topics/energy-efficiency/buildings> (Accessed 28 November 2018).
- [2] European Commission, Nearly Zero-Energy Buildings - European Commission, (n.d.). <https://ec.europa.eu/energy/en/topics/energy-efficiency/buildings/nearly-zero-energy-buildings> (Accessed 18 December 2018).

- [3] P. Zangheri, R. Armani, M. Pietrobon, L. Pagliano, Identification of Cost-Optimal and NZEB Refurbishment Levels for Representative Climates and Building Typologies Across Europe, (2016). doi:10.1007/s12053-017-9566-8.
- [4] McKinsey&Company, Pathways to a Low-Carbon Economy: Version 2 of the Global Greenhouse Gas Abatement Cost Curve, (2010). <http://www.mckinsey.com/business-functions/sustainability-and-resource-productivity/our-insights/pathways-to-a-low-carbon-economy> (accessed May 16, 2017).
- [5] IPCC, IPCC 5 (2014). Full report, 2014. [https://www.ipcc.ch/pdf/assessment-report/ar5/wg3/ipcc\\_wg3\\_ar5\\_full.pdf](https://www.ipcc.ch/pdf/assessment-report/ar5/wg3/ipcc_wg3_ar5_full.pdf) (accessed April 8, 2016).
- [6] C. Camarasa, C. Nägeli, C. Salzer, S. Saraf, Y. Ostermeyer, Specific Barriers to Massive Scale Energetic Refurbishment for Sample Markets in Europe, in: 2015.
- [7] BPIE, Nearly Zero Energy Buildings Definitions Across Europe, Brussels, 2015. [http://episcope.eu/fileadmin/episcope/public/docs/reports/EPISCOPE\\_SR1\\_NewBuildingsInTypologies.pdf](http://episcope.eu/fileadmin/episcope/public/docs/reports/EPISCOPE_SR1_NewBuildingsInTypologies.pdf) (accessed December 18, 2018).
- [8] L. Kranzl, A. Müller, M. Hummel, E. Heiskanen, C. Rohde, J. Steinbach, M. Pietrobon, R.A. Veit, B. Öko-Institut, T. Kenkmann, Z. Georgiev, B.A. Cosmina, M. Bruno, L. Enerdata, C. Sebi, P.Z. Seven, J. Karasek, ENTRANZE, 2014. [http://www.entranze.eu/files/downloads/D6\\_11/entranze\\_report\\_final.pdf](http://www.entranze.eu/files/downloads/D6_11/entranze_report_final.pdf) (Accessed December 18, 2018).
- [9] A. Hermelink, S. Schimschar, T. Boermans, P. Di Milano, L. Pagliano, P. Zangheri, R. Armani, K. Voss, E. Musall, Towards Nearly Zero-Energy Buildings Definition of Common Principles Under the EPBD, 2013. [www.ecofys.com](http://www.ecofys.com) (accessed April 10, 2019).
- [10] Buildings - European Commission, (n.d.). <https://ec.europa.eu/energy/en/topics/energy-efficiency/buildings> (Accessed 28 November 2018).
- [11] J. Groezinger, T. Boermans, A. John, J. Seehusen, F. Wehringer, M. Scherberich, Overview of Member States information on NZEBs, 2014. [www.ecofys.com](http://www.ecofys.com) (Accessed 21 December 2018).
- [12] M. Jakob, The Drivers of And Barriers to Energy Efficiency in Renovation Decisions of Single-Family Home-Owners, 2007. [www.cepe.ethz.ch](http://www.cepe.ethz.ch) (Accessed 21 December 2018).
- [13] A.B. Jaffe, R.N. Stavins, The energy-efficiency gap What does it mean? *Energy Policy* 22 (1994) 804–810, doi:10.1016/0301-4215(94)90138-4.
- [14] C. Camarasa, R. Heiberger, L. Hennes, M. Jakob, Y. Ostermeyer, L. Rosado, Key Decision-Makers and Persuaders in the Selection of Energy-Efficient Technologies in EU Residential Buildings, (2020) 1–32. doi:10.3390/buildings10040070.
- [15] J. Persson, S. Gr, E. Onkvist, Drivers for and Barriers to Low-Energy Buildings in Sweden, (2015). doi:10.1016/j.jclepro.2014.09.094.
- [16] E. Cagno, A. Trianni, E. Worrell, F. Miggiano, Barriers and Drivers for Energy Efficiency: Different Perspectives from an Exploratory Study in the Netherlands, *Energy Proc.* 61 (2014) 1256–1260, doi:10.1016/j.egypro.2014.11.1073.
- [17] V. Beillan, E. Battaglini, A. Goater, A. Huber, Barriers and drivers to energy-efficient renovation in the residential sector: empirical findings from five European countries, *ECEEE Rep* (2011) 1083–1093.
- [18] R. Cooke, A. Cripps, A. Irwin, M. Kolokotroni, Alternative energy technologies in buildings: stakeholder perceptions, *Renew. Energy* 32 (2007) 2320–2333, doi:10.1016/j.renene.2006.12.004.
- [19] M. Achtmicht, R. Madlener, Factors influencing German house owners preferences on energy retrofits, *Energy Policy* 68 (2014) 254–263, doi:10.1016/j.enpol.2014.01.006.
- [20] I. Stieß, E. Dunkelberg, Objectives, barriers and occasions for energy efficient refurbishment by private homeowners, *J. Clean. Prod.* 48 (2013) 250–259, doi:10.1016/j.jclepro.2012.09.041.
- [21] M.J. Pelenur, H.J. Cruickshank, Closing the Energy Efficiency Gap: A Study Linking Demographics with Barriers to Adopting Energy Efficiency Measures in the Home, (2012). doi:10.1016/j.energy.2012.09.058.
- [22] C.C. Michelsen, R. Madlener, Motivational Factors Influencing the Homeowners; Decisions Between Residential Heating Systems\_ An Empirical Analysis for Germany, (2013). doi:10.1016/j.enpol.2013.01.045.
- [23] M. Kesternich, What Drives WTP for Energy Efficiency When Moving? Evidence from a Germany-wide Household Survey, 2010. <http://ftp.zew.de/pub/zew-docs/dp/dp11004.pdf> (Accessed 2 August 2019).
- [24] S. Caird, R. Roy, H. Herring, Improving the energy Performance of UK Households: Results from Surveys of Consumer Adoption and Use of Low-and Zero-Carbon Technologies, (n.d.). doi:10.1007/s12053-008-9013-y.
- [25] E. Heiskanen, K. Matschoss, Understanding the uneven diffusion of building-scale renewable energy systems: a review of household, local and country level factors in diverse European countries, *Renew. Sustain. Energy Rev.* 75 (2017) 580–591, doi:10.1016/j.rser.2016.11.027.
- [26] S. Jamet, J. Corfee-Morlot, Assessing the impacts of climate change, *OECD Econ.* (2009) 5–36 Dep. Work. Pap.0\_1,2, doi:10.1787/224864018517.
- [27] PublicOpinion - European Commission, (n.d.). <https://ec.europa.eu/commfrontoffice/publicopinion/index.cfm/Chart/getChart/themeKy/24/groupKy/136> (Accessed 3 May 2020).
- [28] L. Ostermeyer, Y. Camarasa, C. Saraf, S. Naegli, C. Jakob, M. Von Geibler, J. Bienge, K. Hennes, Building Market Brief Germany Climate Innovation Experience Edition, n.d. <http://cuesanalytics.eu/wp-content/uploads/2018/10/181023-CK-BMB-BMB-GERMANY-DEF-CIE-Edition.pdf> (Accessed 18 December 2018).
- [29] G.L.D. Ostermeyer, Y. Camarasa, C. Saraf, S. Naegli, C. Jakob, M. Palacios, A. Catenazzi, Building Market Brief France Climate Innovation Experience Edition, n.d. <http://cuesanalytics.eu/wp-content/uploads/2018/10/181023-CK-BMB-BMB-FRANCE-DEF-CIE-Edition.pdf> (Accessed 18 December 2018).
- [30] A. Ostermeyer, Y. Camarasa, C. Saraf, S. Naegli, C. Jakob, M. Visscher, H. Meijer, Building Market Brief The Netherlands Climate Innovation Experience Edition, n.d. <http://cuesanalytics.eu/wp-content/uploads/2018/10/181023-CK-BMB-BMB-NETHERLANDS-DEF-CIE-Edition.pdf> (Accessed 18 December 2018).
- [31] E.-S. survey- Eurostat, Distribution of Population by Tenure Status, Type of Household and Income Group, (n.d.). [https://ec.europa.eu/eurostat/web/products-datasets/-/ILC\\_LVHO02](https://ec.europa.eu/eurostat/web/products-datasets/-/ILC_LVHO02) (Accessed 16 January 2020).
- [32] C. Camarasa, On the Uptake of Energy Efficiency Technologies in European Residential Buildings Licentiate Thesis, Göteborg, Sweden, 2019.
- [33] M. Hecher, S. Hatzl, C. Knoeri, A. Posch, The Trigger Matters: The Decision-Making Process for Heating Systems in the Residential Building Sector, (2017). doi:10.1016/j.enpol.2016.12.004.
- [34] J. Friege, E. Chappin, Modelling Decisions on Energy-Efficient Renovations: a Review, *Renew. Sustain. Energy Rev.* 39 (2014) 196–208, doi:10.1016/j.rser.2014.07.091.
- [35] M.I. Abreu, R. Oliveira, J. Lopes, Attitudes and practices of homeowners in the decision-making process for building energy renovation, *Proc. Eng.* 172 (2017) 52–59, doi:10.1016/j.proeng.2017.02.016.
- [36] J. Busch, K. Roelich, C.S.E. Bale, C. Knoeri, Scaling up local energy infrastructure; An agent-based model of the emergence of district heating networks, *Energy Policy* 100 (2017) 170–180, doi:10.1016/j.enpol.2016.10.011.
- [37] K. Pearson, On the criterion that a given system of deviations from the probable in the case of a correlated system of variables is such that it can be reasonably supposed to have arisen from random sampling, *J. Sci.* 50 (1900) 157–175, doi:10.1080/14786440009463897.
- [38] H. Cramér, A contribution to the theory of statistical estimation, *Scand. Actuar. J.* (1946) 85–94, doi:10.1080/03461238.1946.10419631.
- [39] D. Popescu, S. Bienert, C. Schützenhofer, R. Boazu, Impact of Energy Efficiency Measures on the Economic Value of Buildings, (2012). doi:10.1016/j.apenergy.2011.08.015.
- [40] F. Fuerst, E. Oikarinen, O. Harjunen, Green Signalling Effects in the Market for Energy-Efficient Residential Buildings \*\*\* City of Helsinki Urban Facts, (n.d.). [https://www.repository.cam.ac.uk/bitstream/handle/1810/260169/Fuerst\\_et\\_al-2016-Applied\\_Energy-AM.pdf?sequence=1](https://www.repository.cam.ac.uk/bitstream/handle/1810/260169/Fuerst_et_al-2016-Applied_Energy-AM.pdf?sequence=1) (accessed April 16, 2018).



## Indoor environmental quality (IEQ) assessment of Nigerian university libraries: A pilot study

Williams P Akanmu<sup>a</sup>, Sunday S Nunayon<sup>b,\*</sup>, Uche C Eboson<sup>a</sup>

<sup>a</sup> Department of Building, School of Environmental Technology, Federal University of Technology, Minna, P.M.B 65, Minna, Niger State, Nigeria

<sup>b</sup> Department of Architecture and Civil Engineering, City University of Hong Kong, Tat Chee Avenue, Kowloon, Hong Kong

### ARTICLE INFO

#### Keywords:

Comfort conditions  
Illuminance  
Indoor environmental quality  
Nigerian university libraries  
Noise level  
Thermal comfort

### ABSTRACT

An indoor environmental quality (IEQ) assessment of academic libraries in Nigeria was conducted through objective measurements. The selected university libraries were Abubakar Gimba Library; Awwal Ibrahim Library; and Ibrahim Badamosi Babangida Library Complex. The libraries were evaluated under operating conditions and during their peak usage periods. Measurements of the main descriptors of good IEQ, including the acoustical, visual, and thermal comfort conditions were performed using portable IEQ meters. The methodology employed for the assessment of these IEQ descriptors followed prescriptions of international standards ASHRAE standard 55 and ISO 7730. To determine the time of the day in which the library buildings can achieve optimum IEQ, measurements were taken in the morning and afternoon. The results obtained were compared with reference values found in the international Standard CIBSE Guide A for adequate IEQ compliance of academic libraries. The findings of this study are expected to help in improving the IEQ of academic libraries in Nigeria and other parts of the world.

### 1. Introduction

Academic libraries are at the forefront of the purposes of establishing universities. Personal, and private studies from wide-ranging sources are carried out in libraries, requiring set standard interior conditions if the purposes will be optimally achieved. The quality of a library's indoor environment is, therefore, important. Good and acceptable indoor environmental quality (IEQ) can greatly influence the learning capacity of users of any academic library. For example, proper IEQ conditions can improve the effectiveness of comprehension and assimilation, the advancement of skills, and the quality of activities such as reading.

Indoor environmental quality (IEQ) refers to the quality of thermal comfort, health, and well-being that a building's indoor environment can offer to the occupants and/or users. The level of IEQ depends on many complex interconnected parameters [1]. These parameters have been reported to include the design and operation of building systems that control thermal comfort, indoor air quality (IAQ), acoustics, and illuminance [2-4]. The assessment of the overall comfort of the indoor environment places foremost attention to human health. The negative impact of the built environment on the health of users is a matter of concern, which points to some design or technical flaws in the building.

Studies have shown evidence that there is a direct and consistent connection between the indoor environment and human well-being. This relationship usually presents both short-term and long-term effects on people [5]. For example, De Giuli et al. [6] reported that poor IEQ of a building can affect the comfort, health, and productivity of the occupants. Alike, poor IEQ has been implicated in psychological and other building-related illnesses that are not immediately obvious [7,8]. Understanding the sources of indoor environmental discomfort and their adequate handling can often help prevent many problems ahead of time, during a design process [9].

The topic of IEQ of buildings has received tremendous attention from researchers over the years. However, some of these studies are deficient. For instance, Wong and Jan [10] evaluated the total building performance of academic buildings in Singapore using a combination of the walkthrough, simple instrumentation, and occupancy and use analysis approaches. While the findings are important, the scope of the study limits its generalization for policy formulation. Recently, some authors utilized subjective and/or objective methods to assess IEQ parameters in libraries. Different widely studied thematic areas of IEQ (i.e., environmental factors that define IEQ) include acoustic, visual, and thermal comforts. The forth IEQ thematic area is IAQ, however, it is not the focus of discussion in the present study. Hutchinson [11] conducted a clinical

\* Corresponding author.

E-mail address: [ssnunayon2-c@my.cityu.edu.hk](mailto:ssnunayon2-c@my.cityu.edu.hk) (S.S. Nunayon).

review on learning and teaching in the educational environment, showing that background noise levels, visual distractions, and room temperature can influence the learning processes due to their effects on concentration and inspiration.

From the acoustic theme, Ntui [12] determined levels of environmental noise and identified noise sources, which cause discomfort to users of the University of Calabar Library. The study found that noise levels in the university library were high, exceeding the acceptable threshold of noise level established by the World Health Organization (WHO). Aremu et al. [13] assessed indoor noise at the University of Ilorin Main Library in Nigeria. Different issues reported include subjective rating, extent of noise disruption, and ambient daytime and nighttime noise levels. From this study, noise rating and extent of disruptions were divergent. Also, most of the noise level measurements exceeded the recommended maximum limit of 45 Decibels (dB). Franks and Asher [14] studied the utilization of universities' limited space to satisfy both separate and collective study needs of students across four university libraries. Permeation of sound between floors was reported due to the inability of floors with open level designs to uphold sound insulation. Castro-Martínez et al. [15] examined the effect of noise, reverberation, and acoustical barriers on the level of attention of 141 students from a Columbian private university. The study revealed that the students' attention processes were affected by noise levels. However, Castro-Martínez and colleagues found that decreasing reverberation time increased the levels of attention and performance of the students. In an explorative study of acoustic comfort in the library of Birmingham, Xiao and Aletta [16] presented various sources of sound profiles for each floor in the library. These include verbal individual sounds, non-verbal individual sounds, mechanical sounds, crowds of people, and environmental noise.

Another important thematic area of IEQ widely reported is the visual/lighting comfort. The provision and maintenance of a visually comfortable environment in university libraries is a critical issue for users to concurrently maintain wellbeing and good productivity [17,18]. Most of the tasks that library users perform require visual sensation rather than physical labor, which implies that the library environment should be visually comfortable. Illuminance levels had been reported to have a significant impact on visual performance. For example, Yoshida and Yamamoto [19] and Tseng et al. [20] observed that under different illuminance, the capability of discerning color differs. Lin and Huang [21] also found that the time of visual perception was shorter when the illuminance was 500 lx than for other conditions. Lee et al. [22] and Lin and Huang [23] have also reported better and improved performance for letter searching and text comprehension with higher illuminance intensity.

Moreover, thermal comfort is a key parameter of IEQ. Thermal comfort is a complex IEQ criterion and may be influenced by both environmental and personal factors. The various parameters that can influence thermal comfort need to be well thought of and carefully considered at the design stage of library buildings [24]. These factors include air temperature, mean radiant temperature, air relative humidity (RH), air velocity (environmental factors), metabolic rates, and clothing insulation (personal factors) [25]. Other non-quantifiable elements of comfort that can vary the level of tolerance toward certain thermal conditions include culture, habits and traditions, mental states, and expectations [26]. Among these factors, air temperature and relative humidity are considered very important. In six Australian field studies, de Dear and Auliciems [27] found that in air-conditioned and free-running buildings, the neutral temperature was 23.8 °C and 25.5 °C, respectively. Kwok and Chun [28] found out that students in naturally ventilated classrooms were thermally comfortable than their counterparts in the air-conditioned classroom, even though the naturally ventilated classrooms were 3 °C warmer than the air-conditioned classrooms. Furthermore, humidity can cause discomfort due to an uncomfortably increased level of skin humidity and insufficient cooling of the mucous membranes in the upper respiratory tract by inhalation of humid, or warm air [29].

Several studies have investigated the effects of relative humidity (RH) on thermal comfort. Klein and Schlenger [30] conveyed that the exposure of the human body to low RH can cause skin dryness and irritation due to the rapid evaporation of moisture from the skin surface. However, only a modest effect can be observed on thermal comfort within an acceptable temperature during sedentary activities such as may be obtainable in the library. Arens et al. [31] investigated the effect of high RH on thermal comfort for sedentary functions and found that for the temperature range of 20–26 °C, there were no significant psychological or physiological differences in human response to the exposure of between 60% and 90% RH. The human body feels discomfort when it is wet because high friction occurs between the clothing and the skin [32].

As the literature review above demonstrates, however, only a few studies have been conducted on the IEQ of university libraries in developing countries whereas there are many studies on this subject in the developed world. The few studies from developing countries centered on the acoustic parameter of IEQ. An exhaustive literature search showed that no known studies have been conducted in any academic library in Nigeria to assess the IEQ, despite the comparatively old age of library buildings, their usage and study techniques employed since the buildings were designed and built. A major factor is a token available for funding environmental research, lack of qualified researchers, and the perception that the indoor environment does not play any significant role in the health, learning performance, and academic achievements of students. Although there have been library-related studies in Nigeria [12,13], to the best of our knowledge, this is the first systematic study that objectively assessed the IEQ of Nigerian university libraries. The present study is significant because there is a directly proportional relationship between the level of indoor environmental conditions and the level of knowledge acquisition and work efficiency of library users. Also, this study focuses on artificial design conditions that can significantly affect these three indoor environmental conditions (i.e., acoustic, visual, and thermal) that future university library designs must take into account to achieve optimum performance. Furthermore, the outcome of the current assessment will assist in evaluating the kind and degree of corrections that must be introduced to the current university libraries under study if they will fulfill their purposes. Finally, the findings will also emphasize the merits of utilizing standardized monitoring methods; identifying current problems, and raising awareness of indoor environmental issues among administrators of university libraries and policymakers both on local and regional scales.

## 2. Methodology

The purpose of assessing the indoor environmental quality of the university library buildings being studied was to collect quantitative data about the current comfort conditions of the buildings, indoor and outdoor environmental parameters. The detailed experimental procedures are described in the following sections.

### 2.1. Description of selected university libraries and measurement procedures

Measurements of IEQ parameters were carried out in three different academic libraries: Abubakar Gimba Library in IBB University, Lapai; Awwal Ibrahim Library in the Federal University of Technology annex library; and Ibrahim Badamosi Babangida Library Complex in the Federal University of Technology, Minna. The essence was to understand how to improve the IEQ of the university libraries to increase the performance, health, and well-being of users. The selection of the libraries was based on the sophistication of design, construction materials, and population of users. Photos of various functional units/sections of the three libraries are shown in Figs. 1-3.



(a) Façade - AGL

(b) e-library – AGL



(c) Reading Room 1 - AGL

(d) Reading Room 2 – AGL



(e) Reference Unit - AGL

(f) Serial Unit - AGL

Fig. 1. Different units assessed in the AGL.

For the sake of brevity, the phrases Abubakar Gimba Library; Awwal Ibrahim Library; and Ibrahim Badamosi Babangida Library Complex will hereafter be abbreviated as AGL, AIL, and IBBLC, respectively in this article. The measurements occurred between July and September between the hours of 9 am and 4 pm. The measurements were carried out in July and September because they are the peak usage periods of the three libraries. These are the periods when most users patronize the libraries. Semester tests are usually conducted in July while exams are conducted in September, hence, students are engaged in many studies. The measuring probes were fitted and made ready from 8:00 am, and the collection of data commenced by 9:00 am, to permit the environmental adaptation of each measuring device. All the data collections were performed repeatedly until 4 pm every day. The level of illuminance,  $E$  of the outdoor environment ranged from 800 lux to 14,500 lux. The outdoor tempera-

ture was between 30 °C and 32 °C. The cooling system was in operation in the library buildings. The details of the measurement procedures for lighting, acoustic, and thermal comfort conditions are given in the following sections.

## 2.2. Lighting comfort measurements

Several sampling points were chosen in the reading plane in each library. The spaces considered in each library were first divided into a few equal areas that were as nearly square as possible. The number of measurement positions was evaluated based on the room index, expressed as Eq. (1) [33].

$$i = \frac{w.l}{h_m.(w + l)} \quad (1)$$



(a) Façade - AIL

(b) Circulation Unit – AIL



(c) Reference Unit - AIL

(d) System Unit - AIL

where:  $w$  is the room width (m);  $l$  is the room length (m); and  $h_m$  is the distance of the lighting source from the reading desk (m). Using the value of the room index,  $i$ , the number of the grid points was 4 if the room index value was less than 1, and 9 if the room index value was between 1 and 2 [33]. The measurement of the illuminance was taken at the center of each square to (i) justify whether the lighting provision in each space was evenly distributed or not; (ii) determine the average value of illuminance,  $E$  (lux) for the whole reading area by averaging the value of these measurements. Likewise, another three-point measurement was also taken for the lighting level directly on the reading plane. A portable light lux meter (model E75CC, Precision Gold) was used for measuring illuminance  $E$  (the SI unit is lux) to check the light intensity of illuminated library spaces, to fit valid standards. The lux meter consisted of a basic measuring device and a measuring sensor. The measuring sensor comprised one silicon photodiode and spectral response filter. The lux meter was factory calibrated before the measurement and the sensor was covered to calibrate the lux meter to a zero-reading before each measurement. Data were recorded when the lux meter showed a stable reading. The measured values of the lux meter could be seen in the 4-digit liquid crystal display (LCD). Besides, the lux meter was suitable for measuring low illumination intensities and correcting the spectral sensitivity of the eye. The equipment could operate within a temperature range of 0 °C up to 50 °C and at a maximum relative humidity of 80%. Also, its accuracy was  $\pm 5\%$  of reading and its capacity ranged between 0 and 50,000 lux. The average value of illuminance for the whole period of measurements was compared with the threshold provided in the CIBSE Guide A for environmental design [34], to assess whether a suitable level of illuminance was offered for reading purposes by the lighting provisions of each space.

### 2.3. Acoustic comfort measurements

Following the ISO 3382 recommendations [35], several measurement points were chosen in each space sampled in the libraries. The number of measured points ranged from 4 to 6, depending on the area of the room. The noise levels were measured in the middle of each space, for a measurement time of 10 min, and all measurements were averaged and compared with the provisions of the standard. The equipment used to measure noise levels was the 210 (L) x 55 (W) x 32 (H) mm Digital Sound Level Meter (model NO5CC, Precision Gold). This sound meter was a high-quality device, which delivered objective, reproducible levels of sound in decibels (dB). Furthermore, the equipment satisfied the requirements of the International Electrotechnical Commission's IEC 401 Type 2 standards. The equipment could monitor sound pressure levels (SPL) from 30 dB to 130 dB in high and low measurement level ranges. Generally, for low noise settings, the meter is adjusted to the 30 to 100 dB scale, while for high noise settings, it is adjusted to the 80 to 130 dB scale. The sensor of the sound level meter had a 12.77 mm electric condenser microphone, which was located at the top of the meter. The accuracy of the sensing microphone was  $\pm 1.5$  dB. The front-located 4-digit LCD readings taken by the meter for easy viewing at 0.1 dB resolution were updated every 0.5 s. Moreover, the sound level meter used in this study had a dynamic feature or time weighting that performed a small degree of averaging on the instantaneous sound pressures. These time weightings are generally recognized as “slow”, “fast”, or “max” response. The “max” function is self-explanatory and is rarely used for most noise measurement. The “fast” response averages over a 125 ms period; while the “slow” response averages for 1 s. Certain measurement types specify the use of “fast” or “slow” response, but the “fast” response



(a) Façade - IBBLC

(b) Circulation Unit – IBBLC



(c) Serial Unit - IBBLC

(d) System Unit – IBBLC

is usually recommended for general purpose applications because the meter follows the noise contours very closely and the captured maximum levels are not subject to excessive smoothing.

#### 2.4. Thermal comfort measurements

The methodology of measurement employed in our experiment was similar to those used in previous works of Ricciardi and Buratti [33] and Nematchoua et al. [36], and prescriptions of existing standards such as ISO 7730 [37] and ASHRAE standard 55 [38]. In every room assessed, the air temperature at three different points was measured. The first point was at the occupancy area near the outer wall, the second point was in the occupancy area near the wall adjacent to another room and the third point was between the first and the second points. The indoor air temperature was measured using a compact auto-ranging digital psychrometer (EX330) manufactured by Extech® Instruments Corporation, Waltham, MA, U.S.A. The attainable basic uncertainty in temperature measurements was  $\pm 0.5\%$ . Various components of the psychrometer included an extra-large 4000 count LCD allowing for large, easily readable 1" display digits, test leads, and a built-in non-contact AC voltage (NCV) detector with an LED indicator and a beeper. The measuring sensor was a Type K temperature probe – thermocouple ( $^{\circ}\text{F}/^{\circ}\text{C}$  switchable) and could measure between a temperature range of  $-50$  to  $1000^{\circ}\text{C}$ . The digital psychrometer was set in various positions within the various library spaces, by subdividing the space and the readings on the measuring probes were taken every 30 min. For each experiment, measurements were taken at 1.1 m height above the floor level to assess the spatial regularity of thermal conditions in the same environment. All measurements taken for the entire period of measurement were av-

eraged and compared with international standards. The measurement conditions for the three IEQ factors investigated are shown in Table 1.

##### 2.4.1. Brief description of the cooling system in the libraries

The cooling systems of the three libraries were similar. Spaces with at least one exterior wall and a net usable floor area less than  $160\text{ m}^2$  were cooled using either the window- or split-type air conditioners while spaces greater than  $160\text{ m}^2$  such as the reading areas were cooled using packaged air-conditioning units. These package units consisted of water chillers which were located at the rooftop of the library buildings. Chilled water was pumped from the chillers through insulated pipe networks to the various Air handling units (AHU) before it was supplied through supply ductwork into the concerned spaces. The refrigerating load in the libraries throughout the year was fundamentally cooling. Exhaust fans with air recirculation potential as well as fresh air to balance up the temperature regulating control of these spaces were engaged.

#### 2.5. Statistical analysis

The mean and standard deviation values were used to estimate the variability arising from different sets of experimental measurements. The standard deviation was determined using the following relationship:

$$s = \sqrt{\frac{\sum_{i=1}^n (x_i - \bar{x})^2}{n-1}} \quad (2)$$

where, at  $i = 1$  to  $n$ ,  $x_1, x_2 \dots x_n$  are the measured data and  $\bar{x}$  is their mean value, and  $n$  is the total number of data for each IEQ descriptor.

**Table 1**  
Measurement conditions for the three IEQ parameters.

IEQ Parameters	Measurement Conditions
Thermal comfort measurements	Period of sampling: every 30 min interval. Duration of measurement: 7 h daily.
Acoustic measurements	Sound intensity level: every 30 min interval from 9 am to 4 pm daily.
Lighting measurements	Duration of measurements: 7 h daily. Artificial lighting system: turned on during measurement. Natural lighting condition: bright sky.

In this study, the authors hypothesized about the difference between the various groups of experimental conditions to draw conclusions based on statistical testing of data. As a convention, the null hypothesis,  $H_0$  was used to describe a lack of variance between these groups, that is, the mean values of IEQ parameters from one experimental condition and another experimental condition were equal ( $H_0: \mu_1 = \mu_2$ ). For the alternative hypothesis, the authors described the existence of variance, that is, the estimated mean values of the IEQ descriptors were not equal ( $H_1: \mu_1 \neq \mu_2$ ). The conditions tested were twofold. First, the differences between IEQ descriptors during morning and afternoon periods. In this case, an independent sample *t*-test (two-tailed) was conducted to assess if the null or alternative hypothesis was true. Second, differences among the three libraries in terms of IEQ descriptors were also tested using the one-way analysis of variance (ANOVA) test. To find out the group of university libraries where IEQ parameters were statistically significantly different, a Tukey–Kramer Honest Significance Difference (HSD) Post Hoc test was conducted. The estimated *p*-value from the various statistical tests conducted was exploited for taking decisions on these differences. To ensure a 95% certainty that the differences did not occur by chance, the  $\alpha = 0.05$  setting was employed with the probability of rejecting the null hypothesis when  $p < 0.05$ .

### 3. Results

#### 3.1. Lighting assessment

Clearly from Fig. 4, the illuminance levels fell below the recommended level of 500 lux, which can have a significant effect on the users of the libraries. The average illuminance level in each library unit in AGL during morning and afternoon periods was  $128.33 \pm 16.07$  &  $245.00 \pm 30.00$  lux for the reference unit,  $95.00 \pm 5.00$  &  $176.67 \pm 55.08$  lux for the reading room–1,  $91.67 \pm 18.93$  &  $180.00 \pm 0.10$  lux for the reading room–2,  $40.00 \pm 0.15$  &  $120.00 \pm 0.18$  lux for the serial unit, and  $130.00 \pm 62.45$  &  $248.33 \pm 12.58$  lux for the E-library section, respectively. The average morning and afternoon illuminance for AIL was  $73.33 \pm 27.54$  &  $163.33 \pm 50.08$  lux for the reference unit,  $82.00 \pm 38.69$  &  $217.33 \pm 55.64$  lux for the circulation unit, and  $50.00 \pm 20.00$  &  $113.33 \pm 35.47$  lux for the system unit, respectively. Whereas, for IBBLC, the average illuminance during morning and afternoon periods was  $30.00 \pm 10.00$  &  $68.33 \pm 7.64$  lux for the reference unit,  $60.00 \pm 17.32$  &  $136.67 \pm 20.21$  lux for the circulation unit,  $20.00 \pm 5.00$  &  $65.00 \pm 13.23$  lux for the system unit,  $89.50 \pm 26.19$  &  $125.00 \pm 21.79$  lux for the serial unit–1,  $62.67 \pm 31.01$  &  $115.00 \pm 31.22$  lux for the serial unit–2, and  $33.33 \pm 23.09$  &  $91.67 \pm 16.07$  lux for the postgraduate unit, respectively. With the readings falling below the acceptable value of 500 lux, turning off the artificial lighting at any point in time is not feasible. An independent *t*-test ( $\alpha = 0.05$ , 2-tailed) showed that in most of the library units, there was a significant difference ( $p < .05$ ) between the illuminance levels during morning and afternoon periods except for the reading room-1 in AGL ( $p = .06$ ), system ( $p = .05$ ) and reference ( $p = .05$ ) units in AIL, and serial unit-1 ( $p = .15$ ) and serial unit-2 ( $p = .11$ ) in IBBLC.

The box and whisker plots (Fig. 5) showed that there were no outliers among the measured values of illuminance levels for each university

**Table 2**  
Daylighting factors of the indoor spaces.

Location	Space Description	Daylight Factor
AGL	Reference Unit	2.6
	Reading Room 1	3.5
	Reading Room 2	3.4
	Serial Unit	3.9
	E-Library	1.8
AIL	Reference Unit	1.8
	Circulation Unit	1.6
	System Unit	1.5
IBBLC	Reference Unit	2.1
	Circulation Unit	2.3
	System Unit	2.6
	Serial Unit 1	2.3
	Serial Unit 2	1.8
	Postgraduate Unit	2.1

library. The Shapiro-Wilk’s test for normality suggested that the data were normally distributed at  $p = .36$  for AGL,  $p = .91$  for AIL, and  $p = .45$  for IBBLC. The homogeneity of variances was satisfied, as assessed by Lavene’s test of Homogeneity of variances ( $p = .74$ , median). The one-way ANOVA test on these illuminance level scores yielded statistically significant variation among university libraries,  $F(2, 11) = 5.43$ ,  $p = .02$ . A Tukey HSD-Kramer’s post hoc test indicated that the levels of illuminance in AGL and IBBLC differed significantly at  $p = .02$ ; while the illuminance levels in AIL were not statistically significantly different from those in AGL ( $p = .53$ ) and IBBLC ( $p = .27$ ), lying somewhere in the middle.

Apart from the assessment of the artificial lighting in the selected academic libraries, the daylight factor was also estimated as the ratio of the indoor illuminance to the outdoor illuminance, expressed as a percentage. The average daylight factor in all units of the three libraries was less than 5 as shown in Table 2.

#### 3.2. Acoustic assessment

From the acoustics results in Fig. 6, the mean dB levels obtained indicated that noise levels varied at various locations of the academic libraries and were way beyond the recommended value of 45 dB. The average noise levels for morning and afternoon periods in AGL were  $49.67 \pm 16.92$  &  $66.33 \pm 19.09$  dB for the reference unit,  $53.67 \pm 9.75$  &  $64.83 \pm 13.90$  dB for the reading room–1,  $46.83 \pm 10.54$  &  $53.00 \pm 7.00$  dB for the reading room–2,  $56.17 \pm 8.25$  &  $68.00 \pm 7.94$  dB for the serial unit, and  $48.67 \pm 18.06$  &  $65.50 \pm 16.30$  dB for the E-library unit, respectively. In AIL, the average noise levels for morning and afternoon periods were  $47.33 \pm 14.50$  &  $58.83 \pm 20.83$  dB for the reference unit,  $48.67 \pm 10.12$  &  $59.00 \pm 8.72$  dB for the circulation unit, and  $52.33 \pm 8.96$  &  $67.50 \pm 15.26$  dB for the system unit, respectively. The morning and afternoon average noise levels found in IBBLC were  $49.00 \pm 19.05$  &  $57.33 \pm 27.00$  dB for the reference unit,  $46.50 \pm 13.81$  &  $63.17 \pm 25.36$  dB for the circulation unit,  $47.50 \pm 18.63$  &  $64.00 \pm 27.78$  dB for the system unit,  $52.33 \pm 6.25$  &  $72.17 \pm 15.75$  dB for the serial unit–1,  $50.83 \pm 12.85$  &  $59.00 \pm 21.28$  dB for the serial unit–2, and  $50.17 \pm 15.33$

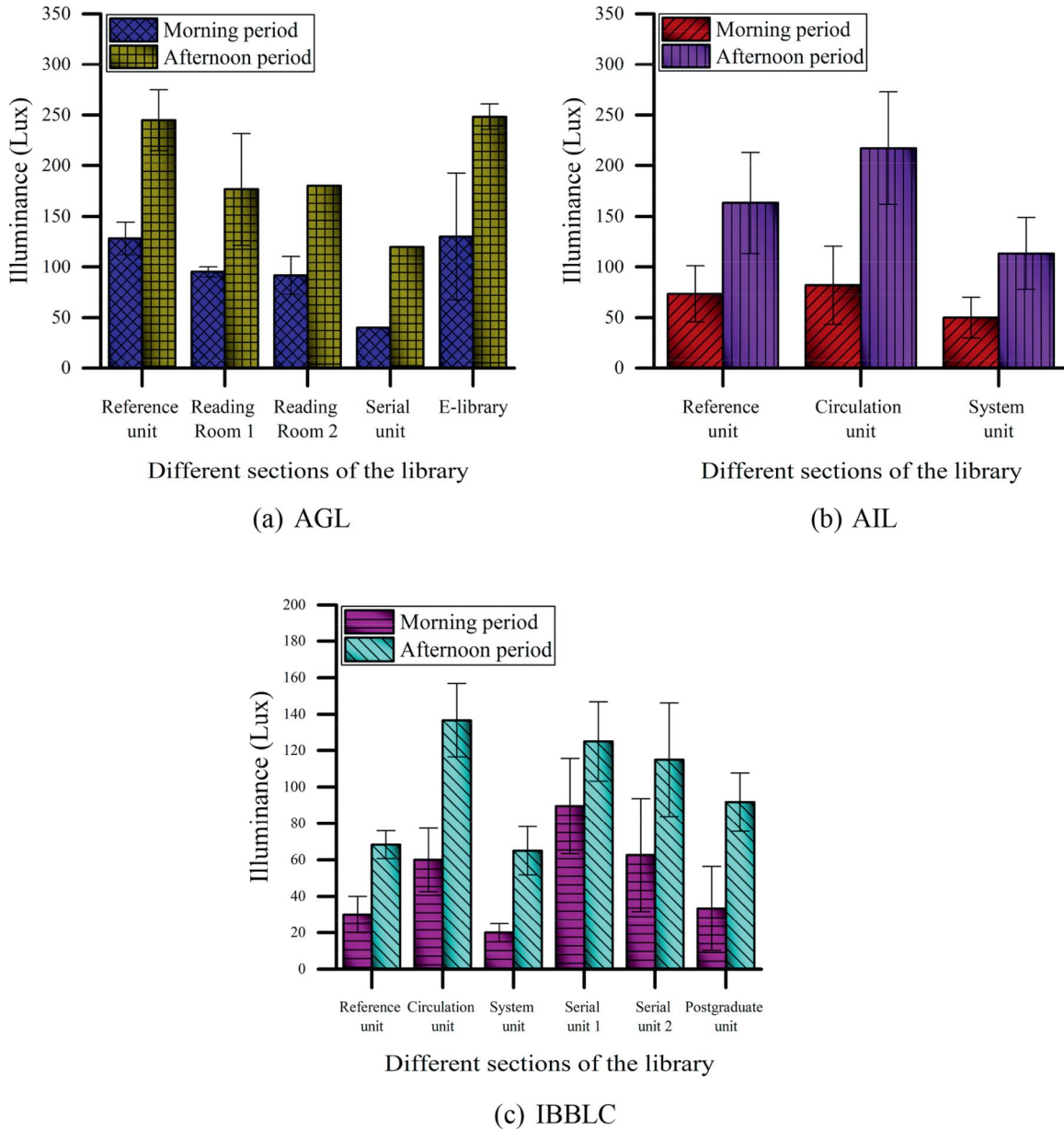


Fig. 4. Measured illuminance of different academic libraries.

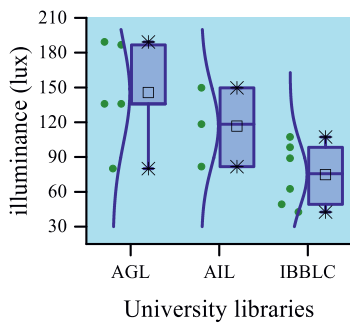


Fig. 5. The box and whisker plots for illuminance levels in the university libraries.

&  $61.33 \pm 22.85$  dB for the postgraduate unit, respectively. In comparison, the noise levels observed during the afternoon period were higher than those observed in the morning period, suggesting that most users patronize the library during the afternoon period. Although the noise

levels in all the assessed units of the three libraries were relatively higher in the afternoon than in the morning, the differences were not statistically significant ( $p > .05$ ).

The assessment of the noise levels using the box and whisker plots (Fig. 7) showed the presence of outliers in the measured data for AGL and IBBLC. After conducting a sensitivity analysis, one outlier that could affect the normal distribution of data and influence the overall result was excluded. The Shapiro–Wilk’s test revealed that the remaining data were normally distributed at  $p = .45$  for AGL,  $p = .19$  for AIL, and  $p = .18$  for IBBLC. The homogeneity of variances was satisfied, as assessed by Lavene’s test ( $p = .43$ , median). The one-way ANOVA test indicated that there was no statistically significant difference in the noise levels of the three libraries,  $F(2, 10) = 0.64$ ,  $p = .55$ .

### 3.3. Thermal assessment

Fig. 8 presents the average room temperature in different units of the libraries investigated. During the morning and afternoon periods, the average indoor temperature values observed in AGL

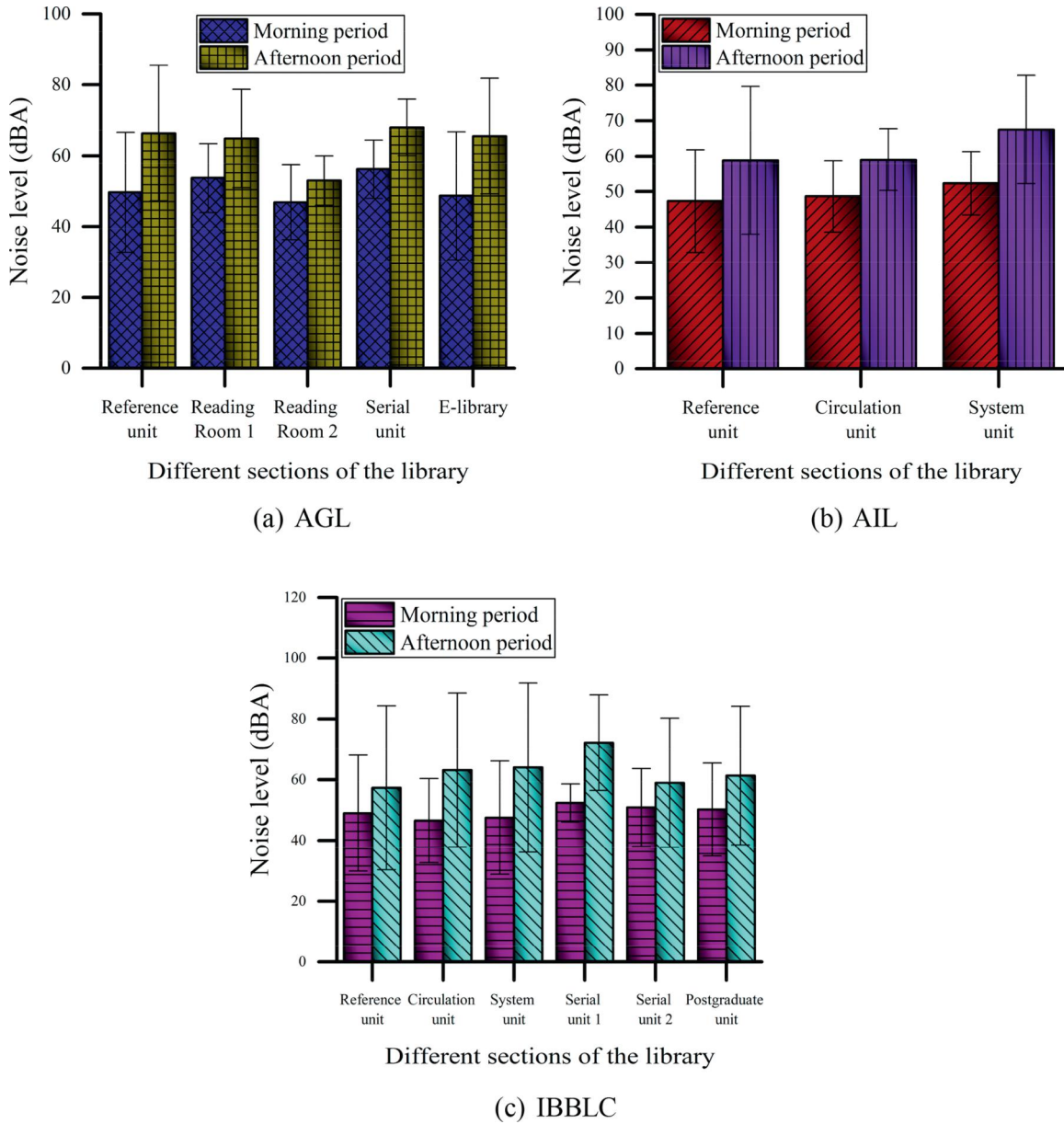


Fig. 6. The level of noise in various functioning spaces of academic libraries.

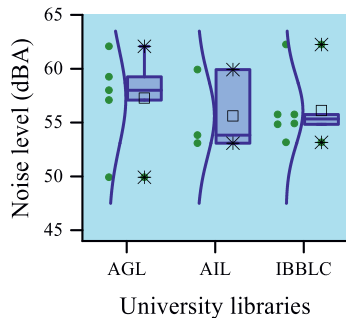
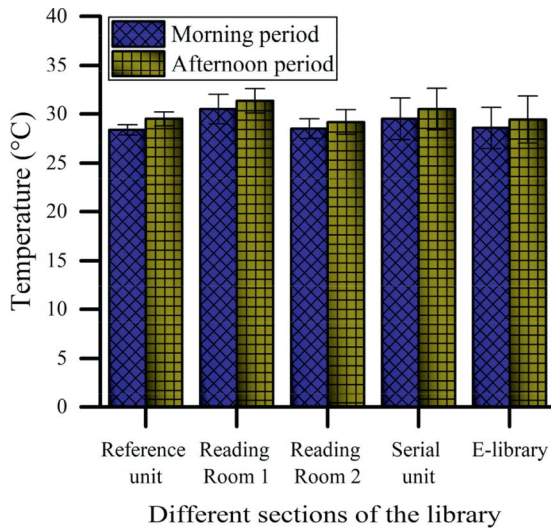


Fig. 7. The box and whisker plots for noise levels in the university libraries.

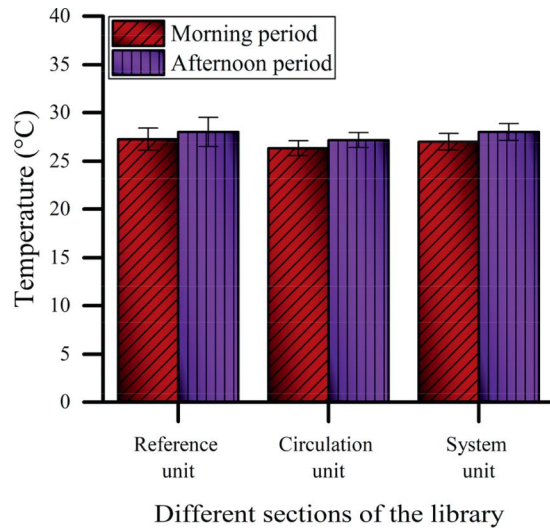
were  $28.38 \pm 0.53$  &  $29.50 \pm 0.71$  °C,  $30.50 \pm 1.50$  &  $31.33 \pm 1.26$  °C,  $28.50 \pm 1.00$  &  $29.17 \pm 1.26$  °C,  $29.50 \pm 2.12$  &  $30.50 \pm 2.12$  °C,  $28.57 \pm 2.10$  &  $29.43 \pm 2.40$  °C for the reference unit, reading room-1, reading room-2, serial unit, and E-library section, respectively. Similarly,

the morning and afternoon indoor temperature values in AIL were  $27.25 \pm 1.15$  &  $28.00 \pm 1.50$  °C for the reference unit,  $26.33 \pm 0.76$  &  $27.17 \pm 0.76$  °C for the circulation unit, and  $27.00 \pm 0.87$  &  $28.00 \pm 0.87$  °C for the system unit. In the case of IBBLC, the morning and afternoon indoor temperature values were  $26.33 \pm 0.58$  &  $27.00 \pm 0.50$  °C,  $27.00 \pm 0.87$  &  $28.07 \pm 0.81$  °C,  $26.53 \pm 0.92$  &  $27.00 \pm 0.87$  °C,  $27.50 \pm 1.80$  &  $28.50 \pm 1.80$  °C,  $27.42 \pm 1.42$  &  $28.17 \pm 1.76$  °C,  $26.00 \pm 0.87$  &  $26.50 \pm 0.87$  °C for the reference unit, circulation unit, system unit, serial unit-1, serial unit-2, and the postgraduate unit, respectively. The results revealed that the units in AGL exhibited higher room temperature values compared to the units in AIL and IBBLC. Generally, the room temperature in the libraries was about 2–6 °C higher than the recommended or reference value. An independent *t*-test ( $\alpha = 0.05$ , 2-tailed) confirmed that there was no significant difference between indoor temperature for morning and afternoon periods in all units of the university libraries ( $p > .05$ ).

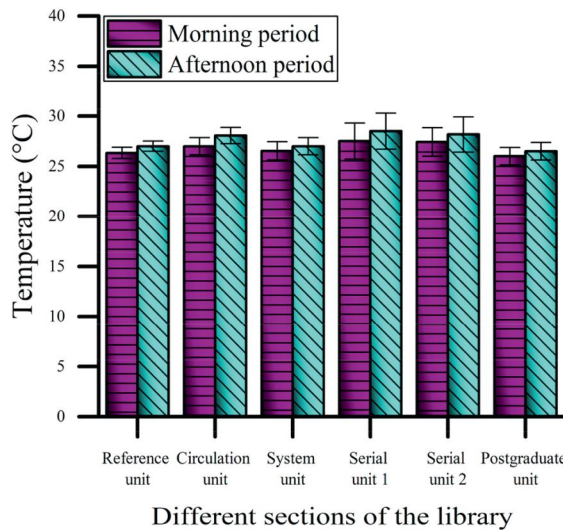
It was observed that there were no outliers in the indoor temperature data, which were normally distributed for each university library, as depicted by the box and whisker plots (Fig. 9) and the Shapiro-Wilk’s test



(a) AGL



(b) AIL



(c) IBBLC

Fig. 8. Sectional thermal conditions of different academic libraries.

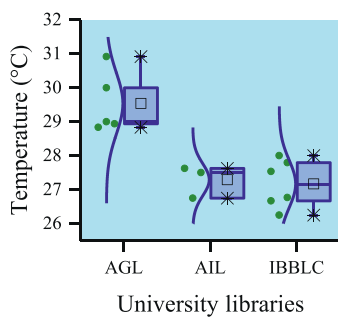


Fig. 9. The box and whisker plots for indoor temperature in the university libraries.

for normality ( $p = .36$  for AGL,  $p = .91$  for AIL, and  $p = .45$  for IBBLC), respectively. The Lavene’s test showed that the homogeneity of variances was not violated ( $p = .67$ , median). The one-way ANOVA test indicated

a statistically significant difference in indoor temperature among university libraries,  $F(2, 11) = 15.54, p < .01$ . A Tukey HSD-Kramer’s post hoc test revealed that the indoor temperature was statistically significantly lower in AIL ( $27.29 \pm 0.90$  °C,  $p < .01$ ) and IBBLC ( $27.17 \pm 0.47$  °C,  $p < .01$ ) compared to AGL ( $29.54 \pm 0.70$  °C). There was no statistically significant difference between the AIL and IBBLC ( $p = .97$ ).

Similarly, Fig. 10 shows that very few sections of the libraries had relative humidity (RH) within the provisions of the standard. The average RH values for morning and afternoon measurements in AGL were  $70.83 \pm 5.11$  &  $69.77 \pm 4.37\%$ ,  $70.43 \pm 2.21$  &  $69.50 \pm 1.80\%$ ,  $72.00 \pm 3.28$  &  $71.19 \pm 3.01\%$ ,  $73.33 \pm 0.58$  &  $71.83 \pm 0.29\%$ ,  $64.00 \pm 7.94$  &  $62.83 \pm 7.65\%$  for the reference unit, reading room–1, reading room–2, serial unit, and E-library section, respectively. The average morning and afternoon RH values in AIL were  $73.83 \pm 1.04$  &  $73.00 \pm 1.00\%$  for the reference unit,  $75.83 \pm 1.76$  &  $74.83 \pm 1.61\%$  for the circulation unit, and  $74.33 \pm 1.15$  &  $73.67 \pm 1.04\%$  for the system unit. Whereas, the average morning and afternoon RH values in IB-

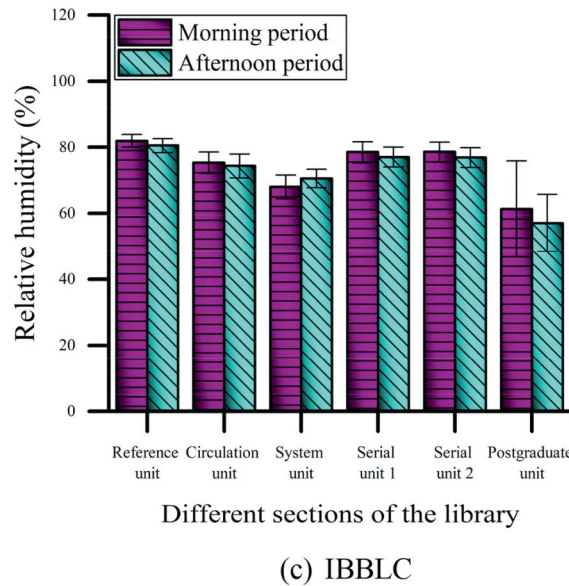
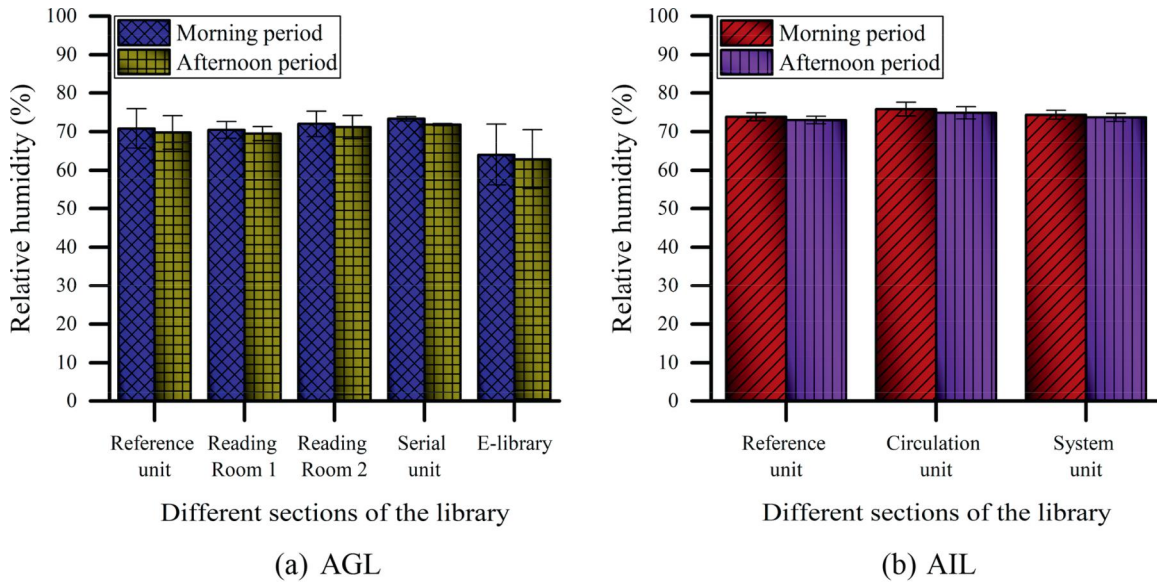


Fig. 10. The level of relative humidity in different units of university libraries.

BLC were  $82.00 \pm 2.00$  &  $80.50 \pm 2.18\%$ ,  $75.33 \pm 3.21$  &  $74.33 \pm 3.62\%$ ,  $68.00 \pm 3.61$  &  $70.50 \pm 2.78\%$ ,  $78.50 \pm 3.28$  &  $77.00 \pm 3.00\%$ ,  $78.60 \pm 3.08$  &  $76.83 \pm 3.01\%$ ,  $61.33 \pm 14.47$  &  $57.07 \pm 8.67\%$  for the reference unit, circulation unit, system unit, serial unit-1, serial unit-2 and the post-graduate unit, respectively. The RH values in most of the units exceeded the recommended value of 70%. This threshold was exceeded by 1–3% in AGL, 3–6% in AIL, and 1–12% in IBBLC. The above results also showed that more than two-thirds of the library spaces had RH values exceeding the limits specified by international standards. The lowest value ( $57.07 \pm 8.67\%$ ) of RH occurred in the afternoon in the Postgraduate unit of IBBLC while the highest value ( $82.00 \pm 2.00\%$ ) of RH was observed in the reference section of IBBLC. An independent *t*-test ( $\alpha = 0.05$ , 2-tailed) showed that there was no significant difference between the level of RH during morning and afternoon periods for all units in the three libraries ( $p > .05$ ) except for the serial unit in AGL ( $p = .02$ ).

While the box and whisker plots (Fig. 11) showed that there was an outlier in the RH data for AGL, the sensitivity analysis conducted indicated that the outlier did not influence the results. The data were nor-

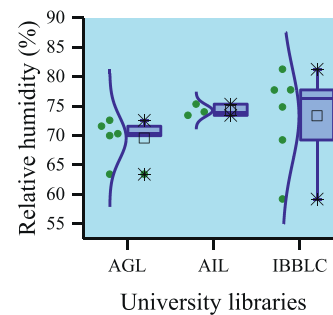


Fig. 11. The box and whisker plots for relative humidity in the university libraries.

mally distributed, as assessed by the Shapiro-Wilk’s test for normality in which  $p = .10$  for AGL,  $p = .58$  for AIL, and  $p = .29$  for IBBLC. The homogeneity of variances was satisfied, as assessed by Lavene’s test ( $p = .27$ , median). The one-way ANOVA test showed that there was no statisti-

cally significant difference in the level of indoor RH among university libraries,  $F(2, 11) = 0.81, p = .47$ .

#### 4. Discussions

The academic library, which is an integral part of a university campus, is ‘an innovation intermediary that plays an active role in knowledge and value co-creation throughout the various roles and functions provided by its services’ [39]. A library is an indispensable part of the university education. Beyond simple collections of books and erudite periodicals as well as the general role of affording access to written art and information, modern university libraries play a key role in contemporary campuses by providing a wide range of academic services in the education of students. In many ways, university libraries had increasingly grown in usage as they have advanced into adaptable facilities, acclimatizing to vicissitudes in technology and education [40]. Therefore, more than any common library, the efficiency of university libraries is considered very important. However, many university libraries lack good environmental quality and consequently may dampen the interest for their use by students and faculty (staff). Due to the regular improvement of academic libraries, additional physical facilities are frequently provided to meet the needs of library users, which had resulted in poor IEQ levels [12]. Nevertheless, the provision of study and reading areas with good IEQ have remained important for focussed learning and knowledge acquisition. Besides, with so many varied services in the contemporary university libraries, and to attain these ample functions, the IEQ requirements of its indoor environment are paramount and must be satisfied. Therefore, effective design and progressive management are indispensable to achieving good IEQ performance in university libraries.

In this study, the authors assessed three different IEQ parameters including visual, acoustic, and thermal comforts of various units in three Nigerian university libraries. The illuminance levels in the three library spaces varied significantly and was also found to be non-uniformly distributed despite the provision of daylight in the library buildings. This could be attributed to the presence or not of near windows. The system unit in IBBLC, characterized by a small expanse of windows, had the lowest light intensity of about 20 lux. These windows were also covered with blinds for most of the time, which could lead to the observed poor lighting condition and cause the forfeiture of light intensity enhancement by daylight in this space. However, effective and desirable protections can correct and eliminate the reflective glare that could penetrate the room from the natural daylight and its effect on readers as well as prevent library collections from overheating, ultraviolet radiation, and decay. The maximum intensities of light were obtained in the reference unit (247 lux) and the e-library unit (260 lux) of the AGL, both characterized by the smallest room width and proper position of windows to receive adequate daylight. In the remaining spaces of the libraries, the illuminance was not enough to carry out visual tasks ( $< 250$  lux) and this was due to the fact that some of the lighting points had stopped functioning. The weak indoor daylight causes serious fall-off of illumination. Due to the meager illuminance level in the three libraries, the users would suffer various visual related discomforts such as eyestrain, irritation of the eyes, blurred vision, headache, and others. Consequently, some of the most common readers’ activities inside the library buildings such as book-searching and reading would be hugely impacted. Given the significant correlation between lighting and library users’ performance, rational and scientific lighting design, to optimize the efficiency of users’ activities is urgently required. To achieve this, three potential improvement approaches are proffered. Firstly, the power and illuminance of artificial light fixtures could be amplified as a compensatory way to provide a more comfortable visual environment for library users and other library activities. Choosing the appropriate light sources, adjusting the approaches to task lighting, and, even more, considering readers’ expectations and perception during the design of libraries’ lighting systems, will immensely contribute to the optimization of library illumination and increase the efficiency of users. Secondly, a large area of

glass windows could be provided to deliver adequate daylight to ensure a better lighting space, without any additional adverse effects on readers or library collections, especially when the lamps cannot meet the lighting requirements of readers. Thirdly, the hybrid approach could be another option. Because it is typical for windows to exhibit high daylight transmittance and display oblique lighting strategy in contrast with the design of high-color-temperature artificial lighting (such as fluorescent lamps), the combination of suspended low-color-temperature fluorescent lamps and low-transmittance windows can reduce the supposed discomfort of readers and enhance their efficiency and accuracy.

On the average, all the fourteen studied spaces in the libraries presented background noise levels greater than 45 dB, and the highest value (72 dB) was reached in the afternoon in the serial unit of the IBBLC while a minimum noise level of 46.54 dB was found in the circulation unit of the IBBLC during the morning period. The excessive noise level observed in these library spaces could be credited to the combined effect of noise from the HVAC system, standing fans, lamps, and other equipment operations. Another likely source of noise includes those generated from traffic. More so, the library users contributed to the increased noise level due to additional sources of noise, which could be either verbal individual sounds, non-verbal individual sounds such as those from footsteps on hard floor finishes, mobile phones, and noise from the crowd of people [16]. This demonstrates that users of academic libraries often display certain disturbances or behaviors that are inimical to the noise policies of such libraries. One cardinal policy of academic libraries is to ensure a conducive environment for all library clientele to study. Therefore, to maintain a high degree of silence or quietness in academic libraries, every library user must respect the rights of other library users by ensuring that noise is minimized when using the library. As well, the reflection of sound reaching the wall surface due to the hardness of the wall materials could be implicated in raising the noise level in the libraries, although a proportion of the reflected sound may be absorbed by the human body [41]. It appears that the problem of high noise levels in academic libraries is not peculiar to Nigerian universities alone. For example, Nafez et al. [42] in a study assessing the noise levels in libraries of Kermanshah University of Medical Sciences in Iran reported that about 41% of reading rooms had their noise levels above 45 dB. Lange et al. [43] performed an objective measurement of the Humanities and Social Sciences Library and the Schulich Library of Science and Engineering, which were the two largest branches in the McGill University Library system. The mean dB levels recorded by these measurements revealed that noise levels ranged from 46.54 to 48.88 dB. In September 2018, Pierard and Baca [44] conducted a noise level measurement within the Learning Commons of the Zimmerman Library at the University of New Mexico (UNM). The results of the study indicated that the average noise levels were high and reached 56.45 dB in the morning, 58.11 dB in the afternoon, and 50.91 dB in the evening, suggesting that the library environment was not conducive for study. Generally, the elevated level of noise observed can be a constant source of concern for library users and administrators. Indeed, it is one of the most common and topmost complaints that students present to library administrators [45,46]. Although these university libraries have had to provide different measures for controlling high noise levels for many years, this burden has not reduced. Given that quiet space is becoming more important to library users coupled with the fact that dissatisfaction with noise in many university libraries is common, it is crucial for more effective noise control measures to be considered in university libraries. In the literature, common strategies to combat the prevalence of noise in academic libraries have been established [14,46,47]. Some of the most effective and worthwhile evidence-based noise reduction interventions for libraries to consider when faced with noise problems include rearrangement of furniture [48], the designation of spaces, and monitoring of personnel [49]. Likewise, Rajagopalan et al. [50] recommended the application of absorptive materials for the floors and walls and appropriate noise insulation for façades. However, strategies such as changing lighting [51], and the development of noise policies [46,47,52] have been reported

to yield unquantifiable effects. More recently, many library users have also begun to advocate for quietness in the library, including noiseless floors, reading rooms, and more customary use of a library space [53]. Considering the significance of university libraries for students vis-à-vis the divergent needs of academic library users, various library administrators need to consider more rigorously the solutions on which to base their noise reduction decisions. One plausible way is to perform a delicate harmonizing act in the provision of both quiet and collaborative spaces. It is anticipated that the results presented in this paper will assist library administrators and space planners to select effective interventions for satisfactory noise reduction.

Temperature and humidity are adjudged the critical parameters in the study of thermal comfort [54]. The CIBSE standard 2006 [34] states that the comfort zone conditions for a library space need the air temperature to be between 24 °C and 25 °C and relative humidity between 40% and 70%. It is important to point out that at temperatures above 25 °C and RH above 70%, the users' dissatisfaction begins as a result of the high air enthalpy (stiffness, shortness of breath). However, the three libraries investigated were not within the comfort range (but much higher) even though they were mechanically ventilated. The average temperature distribution in the three libraries ranged from 26 to 32 °C. These values were against the set point of 23 °C suggested by Andersen and Gyntelberg [55] and between 20 °C and 22 °C suggested by Salthammer et al. [56] for typical academic settings. Most importantly, it was noted that the temperature of the studied library spaces increased as the outdoor temperature increased, with only marginal lower temperatures measured indoors. One major reason for this could be the introduction of warm unconditioned outdoor air through the opening of windows and doors. In temperate or mixed climates, other than discomfort, higher temperatures can reduce performance and learning outcomes [57,58]. However, due to the paucity of investigations in tropical climates, the effects of higher temperature on learning outcomes remain unclear. Nevertheless, the indoor temperature of university libraries should be within the range of thermal comfort standards.

The average indoor RH of the three libraries evaluated in this study was usually above the often-recommended maximum threshold of 70%. It is worth noting that this generally acceptable limit of indoor RH takes care of the risks related to dampness and mold growth. Besides, it was shown that there was no significant difference between the values of reported descriptors of thermal comfort for the morning period and those measured for the afternoon period. It was also noted that the slight increase in temperature in the afternoon had little or no impact on the RH. The elevated levels of temperature and humidity were not unexpected because Nigeria is a tropical climate and has high daytime temperatures of 25–44 °C and relative humidity of 50–90% throughout the year.

Thermal conditions (RH and temperature) within the universities' library buildings must be considered carefully mainly because of their high occupant densities and because of the negative influence that an unsatisfactory thermal environment has on library users and collections, especially in the hot and humid climate of tropical regions like Nigeria. Because of the importance of thermal comfort in academic libraries, there is also a need to investigate the factors that influence thermal comfort. Besides, thermal comfort is highly associated with the effectiveness of the ventilation system [59,60] particularly in crowded indoor environments, such as university libraries. Therefore, the mechanical cooling systems of these libraries could be improved in this regard. Assessing the ventilation parameters of the air distribution system, such as the amount of outside air provided into the library space (air exchange rates), the length of the time that fresh air remains in the library (age of air), and the effectiveness of air exchange are critical in establishing the extent to which air is distributed inside the library buildings. Although mechanical systems are more expensive, they have an all-round better IEQ [61] and are being used in some offices in Nigeria. Other than improving the mechanical cooling systems, the adoption of passive cooling systems is another option that could be considered in achieving educational thermal comfort in university libraries. This could be a more feasible and

sustainable method on a large scale, however, there is a need for more alternative methods to determine the best approach that could be applied in university libraries in hot climates.

Finally, a cursory look at the issues highlighted above from a design point of view suggests that it is significant for building managers and engineers to consider IEQ indices such as thermal, visual, and acoustic comfort at the design stage. More specific and in-depth attention on library users' well-being is essential in addition to the efficiency and sustainability of university library buildings. It is also not sufficient to design a library with the potential to offer comforts, the proper monitoring and assessment of the library buildings as well as library users' performance are equally important.

## 5. Limitations of the study

The authors acknowledge a few limitations in this study that could be addressed in future research. First, the IAQ assessment of the three academic libraries was not conducted in this study. It is strongly recognized that IAQ is also an important parameter of IEQ, but because of its wide coverage, the authors intend to report its comprehensive assessment in future studies. The second limitation is that this study did not account for the Predicted Mean Vote (PMV) index and the Predicted Percentage Dissatisfied (PPD) index. While the PMV index predicts the mean comfort response of a larger group of people according to the ASHRAE thermal sensation scale, the PPD index is a quantitative measure of the thermal comfort of a group of people in any thermal environment. These two parameters would be considered and estimated in our subsequent studies.

## 6. Conclusions

In this study, the results of an objective assessment of the IEQ of three university library buildings located in Minna, Nigeria have been presented. The various IEQ factors measured were, the sound intensity, thermal (temperature and relative humidity), and lighting conditions. The results showed that the average measured illuminance has higher values in the reference and e-library units of the AGL at 247 and 260 lux, respectively. All the fourteen studied spaces in the libraries had background noise levels exceeding the recommended threshold limit value (TLV) of 45 dB, the highest value reaching up to 72 dB in the serial unit of IBBLC during an afternoon period. On the other hand, the indoor temperature was above the reference value for thermal comfort in all library units. The minimum value of the indoor temperature was 26 °C in the Postgraduate unit of IBBLC while the maximum value reached 32 °C in the reading room-1 of AGL. Overall, the IEQ parameters did not conform with well-established standards such as the CIBSE Guide A (2006) and CIBSE TM57 (2015). The evidence from this current assessment revealed that the quality of the indoor environment of these libraries was poor, pointing to the need for interventions. It is also evident from this study that the key issues affecting IEQ in the studied university libraries include inadequate lighting, excessive noise levels, and thermal discomfort. Because the observed poor IEQ can have negative consequences on library users, it is believed that this paper will help library administrators to pay adequate and/or greater attention to IEQ improvement of university libraries.

## Funding

The authors received no external financial support for this research. This research was completely funded by the authors.

## Declaration of Competing Interest

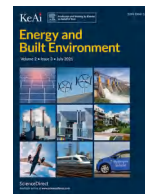
The authors declare no known or expected conflict of interest related to the research, authorship, or publication of this article.

## CRedit authorship contribution statement

**Williams P Akanmu:** Conceptualization, Supervision, Resources, Writing - review & editing. **Sunday S Nunayon:** Methodology, Resources, Data curation, Formal analysis, Visualization, Writing - original draft, Writing - review & editing. **Uche C Ebozon:** Conceptualization, Investigation, Resources.

## References

- [1] T. Catalina, V Iordache, IEQ assessment on schools in the design stage, *Build. Environ.* 49 (2012) 129–140.
- [2] M.J. Jantunen, O. Hanninen, K. Katsouyanni, H. Knoppel, N. Kuenzli, E. Lebrecht, M. Maroni, K. Saarela, R. Sram, D. Zmirou, Air pollution exposure in European cities: the “EXPOLIS” study, *J. Expo. Anal. Environ. Epidemiol.* 8 (1998) 495–518.
- [3] M.G. Apte, W.J. Fisk, J.M. Daisey, Associations between indoor CO<sub>2</sub> concentrations and sick building syndrome symptoms in U. S. office buildings: an analysis of the 1994–1996 BASE study data, *Indoor Air* 10 (2000) 246–257.
- [4] M. Neube, S. Riffat, Developing an indoor environment quality tool for assessment of mechanically ventilated office buildings in the UK – A preliminary study, *Build. Environ.* 53 (2012) 26–33.
- [5] Y. Al Horr, M. Arif, M. Katayfgyiotou, A. Mazroei, A. Kaushik, E. Elsarrag, Impact of indoor environmental quality on occupant well-being and comfort: a review of the literature, *Int. J. Sustain. Built Environ.* 5 (2016) 1–11.
- [6] V. De Giuli, O. Da Pos, M. De Carli, Indoor environmental quality and pupil perception in Italian primary schools, *Build. Environ.* 56 (2012) 335–345.
- [7] Houtman I., Douwes M., de Jong T., Meeuwse J.M., Jongen M., Brekelmans F., Nieboer-Op de Weegh M., et al. New Forms of Physical and Psychosocial Health Risks at Work. Policy Department Economic and Scientific Policy, available at <http://www.europarl.europa.eu/document/activities/cont/201107/20110718ATT24294/20110718ATT24294EN.pdf>; accessed on 20/02/2018.
- [8] M.S. Jaakkola, R. Quansah, T.T. Hugg, S.A. Heikkinen, J.J. Jaakkola, Association of indoor dampness and molds with rhinitis risk: a systematic review and meta-analysis, *J. Allergy Clin. Immunol.* 132 (2013) 1099–1110.
- [9] M. Piasecki, K. Kostyrko, S. Pykacz, Indoor environmental quality assessment: part 1: choice of the indoor environmental quality sub-component models, *J. Build. Phys.* 41 (2017) 264–289.
- [10] N.H. Wong, W.L.S. Jan, Total building performance evaluation of academic institutions in Singapore, *Build. Environ.* 38 (2003) 161–176.
- [11] L. Hutchinson, Educational environment, *Br Med J* 326 (7393) (2003) 810–812.
- [12] A.I. Ntui, Noise sources and levels at the university of calabar library, Calabar, Nigeria, *Afr. J. Lib., Arch. Inform. Sci.* 19 (1) (2009) 53–63.
- [13] A.S. Aremu, J.O. Omoniyi, T. Saka, Indoor noise in academic libraries: a case study of university of ilorin main library, Nigeria, *Afr. J. Lib. Arch. Inf. Sci.* 25 (2015) 5–14.
- [14] J.E. Franks, D.C. Asher, Noise management in twenty-first century libraries: case studies of four US academic institutions, *New Rev. Acad. Libr.* 20 (2014) 320–331.
- [15] J.A. Castro-Martínez, J.C. ROA, A.P. Benítez, S. Gonzalez, The effect of classroom acoustic change on the attention level of university students, *Interdisciplinaria* 33 (2016) 201–214.
- [16] J. Xiao, F. Aletta, A soundscape approach to exploring design strategies for acoustic comfort in modern public libraries: a case study of the Library of Birmingham, *Noise Mapp.* 3 (2016) 264–27.
- [17] J.A. Leech, W.C. Nelson, R.T. Burnett, S. Aaron, M.E. Raizenne, It’s about time: a comparison of Canadian and American time-activity patterns, *J. Expo. Anal. Environ. Epidemiol.* 12 (2002) 427–432.
- [18] D. Serghides, C. Chatziniola, M. Katayfgyiotou, Comparative studies of the occupants’ behaviour in a university building during winter and summer time, *Int. J. Sustain. Energy.* 34 (2015) 528–551.
- [19] Y. Yoshida, Y. Yamamoto, Color management of liquid crystal display placed under light environment, *Electron Commun.* 86 (2003) 1–14.
- [20] F.Y. Tseng, C.J. Chao, W.Y. Feng, S.L. Hwang, Assessment of human color discrimination based on illuminant color, ambient illumination and screen background color for visual display terminal workers, *Ind. Health* 48 (2010) 438–446.
- [21] C.C. Lin, K.C. Huang, Effects of color combination and ambient illumination on visual perception time with TFT-LCD, *Percept. Mot. Skills* 109 (2009) 607–625.
- [22] D.S. Lee, Y.H. Ko, I.H. Shen, C.Y. Chao, Effect of light source, ambient illumination, character size and interline spacing on visual performance and visual fatigue with electronic paper displays, *Displays* 32 (2011) 1–7.
- [23] C.C. Lin, K.C. Huang, Effects of ambient illumination conditions and background color on visual performance with TFT-LCD screens, *Displays* 34 (2013) 276–282.
- [24] T. Steemers, J.O. Lewis, J.R. Goulding, Energy in Architecture: the European Passive Solar Handbook BT Batsford for the Commission of the European Communities, Directorate General XII for Science, Research, and Development, 1992.
- [25] M. Katayfgyiotou, D. Serghides, Bioclimatic chart analysis in three climate zones in Cyprus, *Indoor Built Environ.* 24 (2015) 746–760.
- [26] A. Tablada, A.M. De la Peña, F. De Troyer, Thermal Comfort of Naturally Ventilated Buildings in Warm-Humid Climates: Field Survey, 2005.
- [27] R.J. de Dear, Auliciems A Validation of the predicted mean vote model of thermal comfort in six Australian field studies, *ASHRAE Trans.* 91 (1985) 452–468.
- [28] A.G. Kwok, C. Chun, Thermal comfort in Japanese schools, *Sol. Energy* 74 (2003) 245–252.
- [29] J. Toftum, A.S. Jorgensen, P.O. Fanger, Upper limits for indoor air humidity to avoid uncomfortably humid skin, *Energy Build.* 28 (1998) 1–13.
- [30] O. Klein, J. Schlenger, Basics: Room Conditioning, Birkhauser Verlag, Berlin, 2008.
- [31] E. Arens, F. Bauman, C. Huizenga, ASHRAE Investigation of Thermal Comfort At High Humidity, Building Science at University of California at Berkeley, 2002 <http://www.arch.ced.berkeley.edu/resources/bldgsci/research/thermalcomf.html>.
- [32] J. Appah-Dankyi, C. Koranteng, An assessment of thermal comfort in a warm and humid school building at Accra, Ghana, *Adv. Appl. Sci. Res.* 3 (2012) 535–547.
- [33] P. Ricciardi, C. Buratti, Environmental quality of university classrooms: subjective and objective evaluation of the thermal, acoustic, and lighting comfort conditions, *Build. Environ.* 127 (2018) 23–36.
- [34] CIBSE Environmental Design, CIBSE Guide A, the Chartered Institution of Building Services Engineers, London, 2006.
- [35] ISO 3382 Acoustics – Measurement of Room Acoustic Parameters – Part 1: Performance spaces, 2009.
- [36] M.K. Nematshou, R. Tchinda, P. Ricciardi, N. Djongyang, A field study on thermal comfort in a naturally ventilated building located in the equatorial climatic region of Cameroon, *Renew. Sustain. Energy Rev.* 39 (2014) 381–393.
- [37] ISO 7730 Moderate Thermal Environment – Determination of PMV and PPD Indices and Specifications of the Conditions For Thermal Comfort, International Organization for Standardization, Geneva, Switzerland, 2005.
- [38] ASHRAE Standard 55/2004 Thermal Environment Conditions For Human Occupancy, 2004 Atlanta, GA, USA.
- [39] G.L. Casali, M. Perano, T. Abbate, Understanding roles and functions of academic libraries as innovation intermediaries within the service-dominant logic perspective: an Australian case study, *J. Libr. Adm.* 57 (2017) 135–150.
- [40] B. Edwards, Libraries and Learning Resource Centre, 2nd ed., Elsevier, Burlington, 2009.
- [41] F. Asdrubali, F. D’Alessandro, S. Schiavoni, A review of unconventional sustainable building insulation materials, *Sustain. Mater. Technol.* 4 (2015) 1–17.
- [42] A.H. Nafez, S. Lofti, R. Rostami, R. Saeedi, Lofti Shahla, Assessment of the noise levels in libraries and dormitories of Kermanshah University of Medical Sciences in 2016 (Kermanshah, Iran), *Presenium Environ. Bull.* 6 (2017) 4890–4893.
- [43] J. Lange, A. Miller-Nesbitt, S. Severson, Reducing noise in the academic library: the effectiveness of installing noise meters, *Library Hi Tech* 34 (1) (2016) 45–63.
- [44] Cindy Pierard & Olivia Baca, Finding the sonic sweet spot: implementing a noise management program in a library learning commons, *J. Access Serv.* 16 (4) (2019) 125–150.
- [45] K. Yelinek, D. Bressler, The perfect storm: a review of the literature on increased noise levels in academic libraries, *Coll. Undergr. Libr.* 20 (2013) 40–51.
- [46] S. Heaton, Master, N. No phone zone, *Public Serv. Q.* 2 (4) (2007) 69–80.
- [47] K.M. Lever, J.E. Katz, Cell phones in campus libraries: an analysis of policy responses to an invasive mobile technology, *Inf. Process. Manag.* 43 (4) (2007) 1133–1139.
- [48] P.D. Luyben, L. Cohen, R. Conger, S.U. Gratton, Reducing noise in a college library, *Coll. Res. Libr.* 42 (5) (1981) 470–481.
- [49] C.P. Bird, D.D. Puglisi, Noise reduction in an undergraduate library, *J. Acad. Librarian.* 10 (5) (1984) 272–277.
- [50] P. Rajagopalan, H.T.H. Nguyen, A. Carre, Acoustic performance of contemporary public libraries: an evaluation of public libraries in Melbourne, Australia, *Archit. Sci. Rev.* (2016).
- [51] B. Hronek, Using lighting levels to control sound levels in a college library, *Coll. Undergr. Libr.* 4 (2) (1997) 25–28.
- [52] E. Clement, P.A. Scott, No food, no drink, no noise, *Coll. Res. Lib. News* 55 (2) (1994) 81–83.
- [53] J. Howard, At libraries, Quiet Makes a comeback. The Chronicle of Higher Education, 2012 available at <http://chronicle.com/article/At-Libraries-Quiet-Makes-a/132885/> (accessed March 26, 2015).
- [54] J. Palonen, O. Seppanen, J.J.K. Jaakkola, The effects of air temperature and relative humidity on thermal comfort in the office environment, *Indoor Air* 3 (1993) 391–397.
- [55] I. Andersen, F. Gyntelberg, Modern indoor climate research in Denmark from 1962 to the early 1990s: an eyewitness report, *Indoor Air* 21 (3) (2011) 182–190.
- [56] T. Salthammer, E. Uhde, T. Schripp, et al., Children’s well-being at schools: impact of climatic conditions and air pollution, *Environ. Int.* 94 (Supplement C) (2016) 196–210.
- [57] P. Wargocki, D.P. Wyon, The effects of moderately raised classroom temperatures and classroom ventilation rate on the performance of schoolwork by children (RP-1257), *HVAC&R Res.* 13 (2) (2007) 193–220.
- [58] U. Haverinen-Shaughnessy, R.J. Shaughnessy, Effects of classroom ventilation rate and temperature on students’ test scores, *PLoS One* 10 (8) (2015) e0136165.
- [59] W. Yang, J.S. Bradley, Effects of room acoustics on the intelligibility of speech in classroom for young children, *J. Acoust. Soc. Am.* 12 (2010) 225–234.
- [60] D. Wrightson, J.M. Wrightson, Acoustical considerations in planning and design of library facilities, *Library Hitech* 17 (1999) 349–357.
- [61] S. Heidari, S. Sharples, A comparative analysis of short-term and long-term thermal comfort surveys in Iran, *Energy Build.* 34 (2002) 607–614.



## Empirical investigation to explore potential gains from the amalgamation of phase changing materials (PCMs) and wood shavings

Adham M. Mohammed<sup>a,\*</sup>, Amira Elnokaly<sup>b</sup>, Abdel Monteleb M. Aly<sup>a</sup>

<sup>a</sup> Department of Architecture, Faculty of Engineering, University of Assiut, Egypt

<sup>b</sup> School of Architecture and the Built Environment, University of Lincoln, UK

### ARTICLE INFO

#### Keywords:

PCMs  
Heat peak  
Heat peak shift  
Thermal performance  
Wood shavings  
By-products

### ABSTRACT

The reduction of gained heat, heat peak shifting, and the mitigation of air temperature fluctuations are some desirable properties that are sought after in any thermal insulation system. It cannot be overstated that these factors, in addition to others, govern the performance of such systems thus their effect on indoor ambient conditions. The effect of such systems extends also to Heating, Ventilation and Air-conditioning (HVAC) systems that are set up to operate optimally in certain conditions. Where literature shows that PCMs and natural materials such as wood-shavings can provide efficient passive insulation for buildings, it is evident that such approaches utilise methods that are of a degree of intricacy which require specialist knowledge and complex techniques, such as micro-encapsulation for instance. With technical and economic aspects in mind, an amalgam of PCM and wood-shavings has been created to be utilised as a feasible thermal insulation. The amalgamation was performed in the simplest of methods, through submerging the wood shavings in PCM. An experimental procedure was devised to test the thermal performance of the amalgam and compare this to the performance of the same un-amalgamated materials. Comparative analysis revealed that no significant thermal gains would be expected from such amalgamation. However, a significant reduction in the total weight of the insulation system would be achieved that, in this case, shown to be up to 20.94%. Thus, further reducing possible strains on structural elements due to the application of insulation on buildings. This can be especially beneficial in vernacular architectural approaches where considerably large amounts and thicknesses of insulations are used. In addition, cost reduction could be attained as wood shavings are significantly cheaper compared to the cost of PCMs.

### 1. Introduction

To achieve higher comfort levels of occupants, traditional architecture incorporated varied aspects such as natural ventilation, shading, thermal mass and passive cooling techniques as some of the most important passive design features of traditional architecture [1,2]. In hot-arid climate regions, 70–80% of total energy consumption is used to operate active cooling systems [3], and consequently, reducing the reliance on those will have a drastic impact on energy consumption. An optimized envelope design can improve the thermal performance through passive solar techniques [4–7]. Some of the other variables that influence indoor thermal comfort includes thermos-physical properties of the building's envelope material [8]; the roof optical properties, namely the albedo, thermal emissivity and building insulation [5,9–11] that play an important role in the energy balance of buildings. Indoor air temperature is one of the important factors that contribute to achieving the thermal comfort of occupants inside buildings [12,13–16]. The outdoor heat loads that a building is exposed to may affect the indoor air tem-

peratures as heat is conducted through the building's envelope. Many passive attempts to limit the effect of exterior heat on interior temperatures have been, to a good extent, successful [17–20]. This results in a lowered indoor temperature which increases thermal comfort in hot climates and reduces strain on HVAC systems caused due to heat overload on these devices [13,21–24].

In the last couple of years, PCMs have been extensively researched as a possible part of passive thermal control methods. Many researchers have attempted to utilize them in different ways [25–31], which have shown good potential. The innovative manner in which PCMs have been utilised has been miscellaneous. Methods such as using a layer of paraffin wax on brick walls and inside building envelopes which have shown to be successful in reducing indoor air temperatures and related cooling electricity consumption of up to 75% [32–41]. Other studies have attempted utilise "PCM immersion" of building elements such as PCMs infused wallboards [42–45,39], PCM-mortar [46–51], PCM infused bricks [52–54], PCM-concrete [55–66] and PCM-enhanced plaster [67–69]. Such methods have reported the ability to reduce indoor temperatures by up to 5 °C. Similarly, the combination of PCMs and other materials

\* Corresponding author.

E-mail address: [adham@aun.edu.eg](mailto:adham@aun.edu.eg) (A.M. Mohammed).

such as Silica, Graphene and Gypsum has also been investigated with promising results as to the thermal performance [70–78]. Also, the incipient field of Nano-technology has allowed for much progress in this regard by adding certain types of Nano-particles to enhance PCM mixtures [31,79–83]. In terms of methods of utilising PCMs, encapsulation of PCMs seems to provide a good potential as a passive thermal control technique [84–92]. The encapsulated PCM is used also in various manners. Macro-encapsulated PCMs can be used to fill a void in brick walls which show a possible reduction in temperature of up to 6.31 °C or 25% of peak temperatures [29,93–95]. Similarly, macro-encapsulated PCMs can be placed in bags which also show a decrease in peak indoor temperatures, reported to be around 12.04–17.26% [96–98].

Traditional methods have also shown good thermal performance, in many cases comparable to modern passive thermal control methods [99–102]. Such methods involve using copious natural materials such as stone, mud, fabrics, plant segments and wood, utilised in various ways [101]. With the abundance of suitable natural materials, wood shavings have been the focus of investigation as it has shown good thermal behaviour. In addition, wood shavings are commonly found as a by-product in wood workshops and through industrial process. In many cases, it is disposed of with no significant use [103], which consequently results in it being of low cost, thus, further expanding the feasibility of usage. Furthermore, wood shavings are low in density compared to materials such as PCMs, resulting in lower weights. Also, utilization of wood-waste in, particular, is seen to be of desirable environmental impacts [102,104], which includes many forms such as cork, wood fibre and hemp. It is further explained that the advantageous thermal properties are a result of certain characteristics such as lower embodied energy, moisture buffering capacity compared to other inorganic materials [104]. In addition to its low thermal conductivity that ranges from 0.048 to 0.055 W/mK, which is comparable to other commercial insulation materials [102,104–106]. Furthermore, waste wood can be formed into a panel-like shape that can act as effective thermal insulation with a density of around 315 kg/m<sup>3</sup> and thermal conductivity of around 0.08 W/mK [106,107]. It is worthy to note that many segments of various types of plants are considered to be composed of wood-fibres, especially plants stalks and stems. Under certain conditions, these segments can be utilized to act as actual wood-fibres, which have been found to provide good thermal behaviour, be cost-effective and have less environmental impact [15,99,103,107–112]. Such plant segments can include cotton-stalk [113–117], date palm branches [118], tomato-stalks [119], sunflower [120], corn cob [121], straw-bale [122–125], bamboo [41] and poppy husk [126]. Such materials have been utilised in various ways, which has shown thermal conductivities ranging between 0.051 and 0.053 W/(m K) [122] and as low as 0.040 W/mK [125,127,128] in some cases, with heat dampening of 93.6% and a heat time lag of 9.12 h [123]. Combined wood particles of different sizes, into boards, are also a viable approach that has shown efficient performance with thermal conductivities of between 0.1078 W/mK and 0.0742 W/mK [129,130]. It is evident from the previously discussed literature that using wood-related materials as a form of natural insulation is advantageous, with thermal performances similar to this of commercial synthetic materials, in addition to having better environmental impacts.

The mentioned earlier refers to successful attempts to utilise both wood-based materials and PCMs. However, most of these attempts were made through mechanisms that require substantial technical effort such as impregnation of PCMs into the micro structure of fibrous materials, including wood, through the use of vacuum pressure [131–133]. In the present study, wood shavings were amalgamated with PCMs through submerging. This particular method was utilised as it requires little intricacies thus eliminating cost, effort and technical issues. Hence, the novelty of the present study lays in the experimental investigation of the effectiveness of a simplified amalgamation approach as an alternative to common complex PCM utilisation methods that require intricate technologies to conduct, such as these mentioned earlier. Furthermore, the experimental approach carried out, in this case, differs from simi-

lar studies in terms of the purpose of using wood-shaving. Where most studies perceive such material as an encapsulation medium for the PCM particles as a macro encapsulation [134–138], the present study uses wood-shavings as a supplement to PCM, intending to enhance its thermal performance as thermal insulation. The aim of the mentioned earlier is to explore possible advantageous gains that may be achieved from such simple a method, weather gain of a thermal nature or otherwise. To achieve this, the amalgamated mixture is investigated for many features. Aspects such as heat peak reduction are important and heat peak shift are investigated as they describe the potential of a thermal insulator to impede conduction of heat through facades and the influence of the latent heat storage of such materials [40,41,54,66,97,139–142]. Also, the ability to reduce fluctuations in indoor air temperature has been investigated in this article. This is of significance as outdoor air temperature may fluctuate un-uniformly [20,143,144] causing analogous fluctuations in indoor air temperatures [145,146], which can cause thermal discomfort to inhabitants and affect the performance of HVAC systems exposed to this.

## 2. Thermal performance of PCM panels

As determined, the tested panel is placed between two controlled environments. To apply the required heat variations on one of the sides of the panel, a climatic chamber was used. To control the initial temperature of the other side, a confinement holding the panel was created. As the temperature would vary on the side of the panel that is exposed to the chamber, the other side would gradually be thermally influenced by this variation. Through measuring the air temperature on both sides and comparing them, the effect of the PCM/ PCM-wood shavings could be assessed. The same process was repeated for the control panel (panel with 1 sheet of Plexi-glass) and the 1 cm air gap panel (panel with 2 sheets of Plexi-glass). Fig. 1 shows a schematic representation describing the position of the tested panel in relation to the controlled environments applied.

To choose an appropriate type of PCM for this study several factors were considered. It was considered that the chosen type of PCM is applicable in building applications, thus, having a melting/freezing temperature that is within range of the prevailing temperatures found in some hot climates. It is important to note that literature has pointed out that applications relying on PCMs can fail due to inappropriate melting/solidification temperatures [147]. In addition to being durable and having congruent melting to ensure that it retains its original structure throughout numerous cycles of phase change [148,149]. In addition, aspects such as 1) chemical stability; 2) complete reversible freeze/melt cycle; 3) limited degradation; 4) non-toxicity, 5) non-flammability and 6) non-explosiveness and non-corrosiveness were taken into account [150]. Paraffin waxes can provide most of the required criteria described earlier [151]. The PCM initially chosen to be used is Paraffin wax 43/46 obtained from a UK based chemical company (Scientific laboratory supplies SLS) product No. CHE2750, shown in Fig. 2 (A&B). Table 1 shows some of the physical and chemical properties of the PCM as provided by the supplier.

### 2.1. Experimental rig

To conduct the experimental condition described earlier, a rig consisting of several elements was designed. An appropriate container was required to encapsulate the tested material without affecting test results. Factors such as leakage, chemical compatibility and expansion properties of the PCM were taken into account as literature shows that they may be of importance in PCM testing [148,152]. The container used for this experiment was created using sheets of MDF wood that were cut using an epilogue Fusion M2™ Laser cutter and engraver for precise cutting. The container is constructed of a frame of MDF wood with a thickness of 10 mm, with a width of 18 mm. The inner dimensions were 20 \* 24 cm to accommodate the PCM panel (20 \* 20 cm) and provide

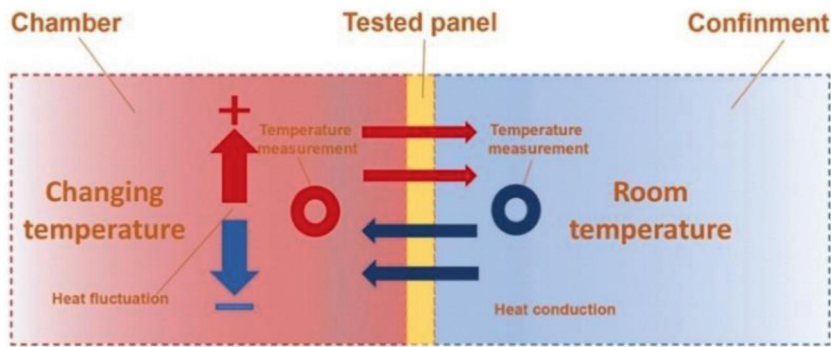


Fig. 1. Schematic representation of the experimental procedures carried out on the tested panels (Authors' own).

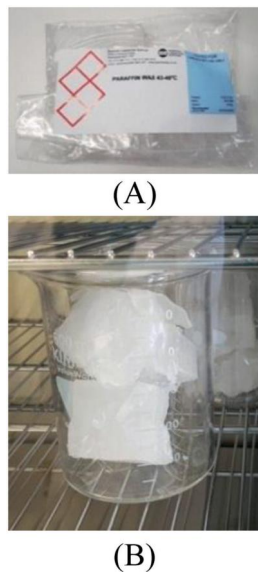


Fig. 2. (A) Packaging of Paraffin wax as provided by supplier. (B) Appearance of paraffin wax in the solid phase.

**Table 1**  
physical and chemical properties of the paraffin wax as provided by the supplier.

Appearance	White waxy solid
Odour	Nectareous.
pH	Not applicable
Boiling Point	350 °C
Melting Point	43 °C
Flash Point	300 °C (Closed cup)
Upper Flammable Limit	Not applicable
Lower Flammable Limit	Not applicable
Auto Ignition	Not applicable
Explosive Properties	No.
Oxidising Properties	No.
Vapour Pressure	Not applicable
Relative Density	0.9550
Water Solubility	Insoluble in water.

a 20% of the PCM volume as void for expansion (4 cm). Four layers of water-sealing varnish coating are applied to ensure that no absorption of the PCM would occur when it is in the liquid phase. The top side of the frame was removable to allow for the materials to be inserted into the container. Both sides of the frame were covered with sheets of Plexi-glass of 2 mm thickness using glue. The container after assembly is shown in Fig. 3(A). For comparison purposes, two more panels were created. One of them, a panel that consisted of a single 2 mm layer of Plexi-glass and a wooden frame with the same dimensions as the PCM

encapsulation panel, was used as a reference control panel. The other panel was identical to the previously mentioned, however, no materials were placed inside. The purpose of this panel is to test the thermal performance of the two layers of Plexi-glass with an intermediate air gap of 1 cm width.

As mentioned earlier, a five-sided box-like confinement was constructed of isolating materials. The 6th side remained as a void to accommodate the panel under investigation. This allowed the side of the panel that is facing the inner part of the confinement to be exposed (initially) to room temperature while the other side is exposed to the pre-set temperatures. Fig. 3(B) shows the confinement after final assembly, including fibre-wood insulation. The box-like confinement was made of 18 mm thick sheets of medium density fibre wood (MDF) that were cut and assembled with inner dimensions of 20 cm\*20 cm\*35 cm. To hold the PCM encapsulation panel at the front of the confinement as required, a platform with the same inner dimensions as the panel was created from the same materials. Insulated was made by covering all sides with four layers of wood-fibre sheets (Diall™ Fibre wood underlay) with a total thickness of 20 mm, shown in Fig. 3(C). An epilogue Fusion M2™ Laser cutter and engraver, shown in Fig. 3(D), was used to ensure accuracy of the cut parts. To subject the PCM panels that are under investigation to environment-like conditions, the panels and the insulated confinement were placed inside an environmental chamber during the testing process. The environmental chamber used was a Panasonic™ versatile environmental test chamber model MLR-352 as shown in Fig. 3 (E&F). The chamber can be programmed to manipulate the temperature of the inner environment to change from 0 °C to 60 °C. To monitor the change in air temperature of both sides of the encapsulation panel throughout the duration of the experiment in which heat was applied, two HOBO® MX Temp/RH Data Loggers model-(MX1101) shown in Fig. 3(G) below are used. The data loggers had built-in thermal sensors with a range of -20° to 70 °C with an accuracy of ±0.21 °C in addition to humidity sensors. The loggers are capable of logging up to one reading per second. Control and setup of the data loggers can be done through an iOS or Android™ device through a Bluetooth® connection. Logged data is also downloaded through the wireless connection mentioned earlier through HOBO mobile® app.

## 2.2. Experimental procedures

The following depicts details regarding the creation of the three panels in addition to a control panel and an empty panel created for further comparison purposes. A description of the heat profiles applied to the panels with various details is also provided.

### 2.2.1. PCM panel testing

To create a PCM panel, 382 gs of the PCM were weighed (the PCM had a density of 0.9550, and the required panel was with dimensions of 20×20×1 cm). This was the amount required to create a panel with the desired dimensions. The PCM was then placed in a steel container then

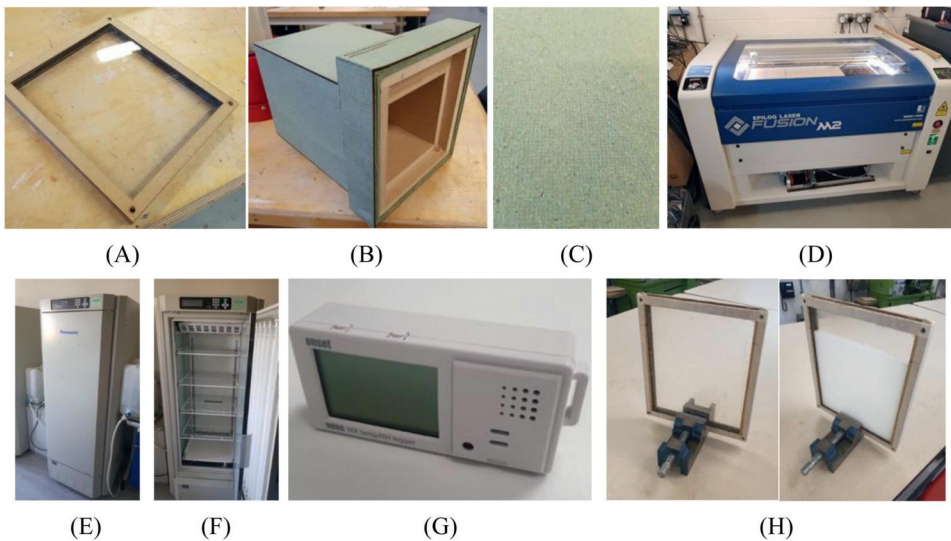


**Fig. 3.** (A) Material container after assembly. (B) The Box-like confinement, with the platform end. (C) Diall™ Fibre wood underlay sheets. (D) epilogue Fusion M2™ Laser cutter and engraver. (E) Exterior of environmental chamber. (F) Interior of chamber, (G) HOBO® MX Temp/RH Data Logger model-(MX1101). (H) Encapsulation panel secured upright using a holder, PCM had been poured in and left to cool, photographed after approximately 10 min.

**Table 2**  
Pre-set heat profiles.

Heat profile	Minimum temp. °C	Maximum temp. °C	Cycles	Cycle duration (hours)	Total duration(hours)
1	15	57	1	24	24
2	15	55	1	12	12
3	35	55	2	6	12
4	35	55	3	4	8
5	35	55	3	2	6
6	35	55	3	1	3

liquefied using an electric hotplate to a temperature of 65 °C approximately. The liquefied PCM was poured into the encapsulation panel. The encapsulation panel was held upright using a holder shown in Fig. 3(H) above as the liquefied PCM was poured-in till 200 mm were filled to leave 40 mm for expansion as mentioned earlier. The PCM was poured slowly so that to ensure that no air pockets (air-bubbles) had been formed. The panel was left over-night in a relatively cool environment to allow for the PCM to solidify. Both the encapsulation and the confinement were then placed inside the environmental chamber, which was then sealed. A series of tests were performed on the panel. In each test, a different heat profile was used. The aim of this is to monitor the performance of the tested materials under different modes of heat loads. It is important to note that two of the heat profiles are used to simulate natural day/night cycles were as the rest was used to simulate different fluctuations in temperatures that may occur in certain environmental conditions. Table 2 depicts the temperatures and durations that the chamber was pre-set to. A difference is identified between the pre-set and actual measured temperatures, due to capabilities. Measurements were set to be logged every 10 seconds.

In heat profile 1, a gradually increasing/decreasing profile was used. The profile was an attempt to simulate the natural gradual increase of temperature that would occur in a hot environment during day time and the decrease of temperature during night time. The heat profile ranged from 15 °C to 57 °C in a duration of 24 h. Fig. 4(A) shows the temperature inside the chamber during testing. To achieve a gradually changing temperatures as required, twelve steps of temperatures had to be set. Each step was for a duration of 1 h and increased in temperature by 7 °C. Likewise, Profiles 2–6 were conducted with varying cycles of heat and different durations. Fig. 4 (B, C, D, E & F) show the change in temperature according to the setting of each profile.

**2.2.2. Wood shavings filled panel (Ws)**

Wood shavings obtained from a local provider were used. The utilized wood shavings were chipping of plywood obtained as a by-product

of wood manufacturing processes. The approximate calculated bulk density of the shaving in their loose form was 0.1 g/cm<sup>3</sup>. An amount of 40 g of wood shavings was placed inside the panel (with dimensions of 20×20×1 cm). This amount was sufficient for the panel to be filled with wood shavings without any form of compression. Fig. 5 (A) shows the panel filled with the amount of wood shavings.

**2.2.3. PCM/Wood-shavings (PCM/Ws) panel testing**

The same locally obtained wood-shavings, mentioned earlier, were used. To create the mixture of wood-shavings and Paraffin wax, 40 g of wood-shavings were weighed on a scale (as 14% of the total weight of the mixture). An amount of 260 g of Paraffin wax (86% of the total weight of the mixture) was melted on a magnetic stirrer (set to 60 °C) which was used to stir the wood-shavings in the mixture. The wood-shavings were added gradually to the wax while being stirred. This is to ensure that all particles of the wood-shavings have been engulfed with the wax. Once the entire amount of wood-shavings was added to the wax, it was important to manually stir the mixture as it had created a paste-like substance that demanded manual stirring to ensure that the mixture is completely homogenous. It should be noted that the stirring was performed at a constant temperature of 60 °C so that to ensure that the wax would remain in a liquefied form throughout the entire process. After being stirred, the mixture left to slightly cool (to around 43 °C) to facilitate placing it into the panel for testing. Fig. 5 (B) shows the slightly cooled mixture. Initial trials have shown that it may be hard to place the mixture in the panel in a liquefied form as it is of high density which makes it difficult to manage placement in a relatively small opening such as this of the panel. Similar to previous tests performed on the PCM panel (described in Section 2.2.1), the panel was filled with the created mixture, as shown in Fig. 5 (C). The panel was cooled to room temperature before any testing to ensure that no latent heat would affect testing, which was repeated prior to all tests. Then, the filled panel was placed in its analogues section in the testing confinement which is

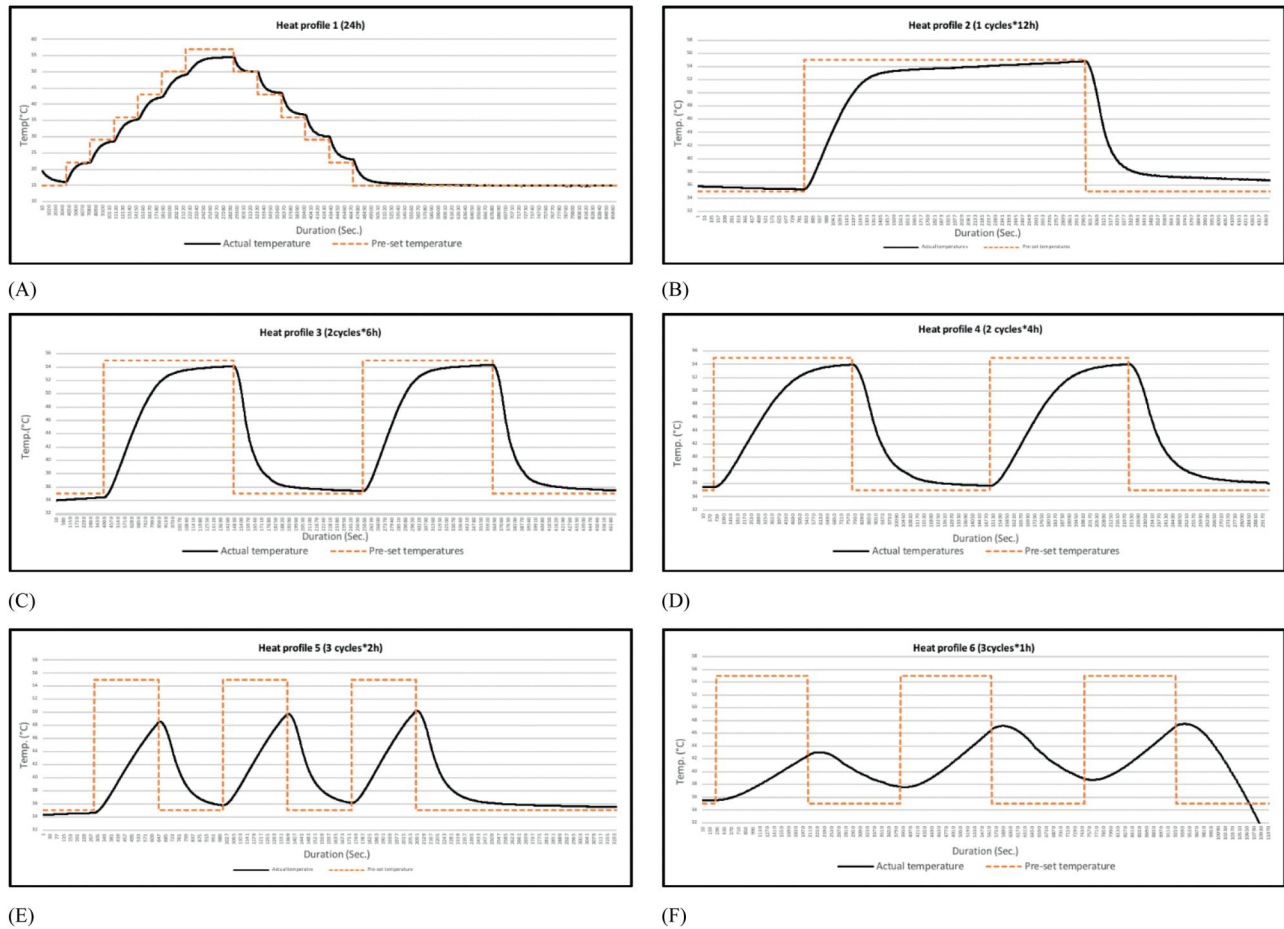


**Fig. 4.** Pre-set and actual temperature inside the environmental chamber for: (A) Heat profile 1, (B) Heat profile 2, (C) Heat profile 3, (D) Heat profile 4, (E) Heat profile 5, (f) Heat profile 6.

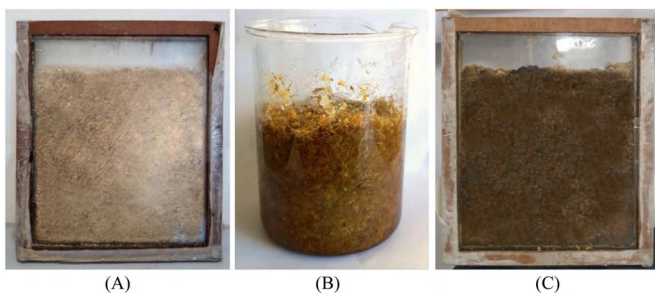


**Fig. 5.** (A) Panel filled with 40 g of wood shavings. (B) Mixture of 20% wood-shavings and 80%paraffin wax cooled to a temperature of around 43 °C. (C) Panel filled with mixture ready to be placed inside environmental chamber.

then placed inside the environmental chamber in the same manner as described earlier in the previously mentioned thermal tests.

**2.2.4. Control panel and air gap panel test**

As explained earlier, the same tests using the mentioned heat profiles were carried out on the control panel and the air gap panel for comparison purposes.

**2.2.5. Verification of measurements**

It should be noted that to verify the accuracy of the measurements obtained, several steps were taken. In addition to the measurements mentioned earlier, for profile 2 and profile 6, the measurements were repeated once with the same data logger mentioned earlier and twice

with another data logger of the same type. In total, the mentioned tests were carried out four times using two different loggers. These profiles were specifically selected for the verification process as they represent both a short and long-term duration cycle of heat. The results showed that all of the verification tests were in alignment and the deviations in temperature readings were less than (0.05 °C) thus suggesting the validity of measurements. In addition to this, all of the profiles were also repeated with an alternate logger (in total two repetitions for each profile). The results of this also showed an alignment with a deviation in measurements less than (0.03 °C). Hence, it is be verified that the measurements are accurate.

**2.3. Results and analysis**

Table 3 shows the results for all the tested panels under the influence of various heat profiles. In the mentioned table, a comparison is presented between the results of the panel created with a single sheet of Plexi-glass which simulates a single-panel window referred to as the control panel in this study. Results for the panel consisting of two panels of plexiglass is referred to as the “1 cm” air gap panel, the PCM filled panel is referred to as “PCM panel” and the panel filled with the PCM/wood-shavings mixture is referred to as “PCM/Ws panel”. In Table 3, the column named “Chamber temperature ranges” presents the actual temperatures measured inside the chamber during each heat profile. Also, for each panel, the table presents the actual measured temperature ranges (maximum and minimum temperatures) that have occurred inside the confinement (shown in the column named “Temperature range”). The maximum temperature inside the confinement compared to the actual

**Table 3**  
Thermal measurement of panels under heat profiles.

Heat profile No.	Chamber temp. ranges (°C)	Control panel				1 cm Air gap panel				Wood shavings			
		Temp. range (°C)	Fluctuation (%)	Peak temp. shift (Min.)	Peak temp. reduction (°C)	Temp. range (°C)	Fluctuation (%)	Peak temp. shift (Min.)	Peak temp. reduction (°C)	Temp. range (°C)	Fluctuation (%)	Peak temp. shift (Min.)	Peak temp. reduction (°C)
1	15 - 52.5	15 - 49.8	92.8	60.3	2.7	15 - 48.1	88.2	66.7	4.4	15 - 48.4	89.1	78.8	4.1
2	35 - 53.8	35 - 53.04	96	9.83	0.76	35 - 52.5	93	19.7	1.3	35 - 52.9	95.2	23.3	0.9
3	35 - 52.6	35 - 49.1	80.1	11.5	3.5	40.8 - 48.7	44.9	23.7	3.9	38.7 - 49	58.5	25.8	3.6
4	35 - 52.3	35 - 46.6	67	9.6	5.7	37.2 - 46.5	53.6	15.7	5.8	40.1 - 46.6	37.6	30	5.7
5	35 - 49.6	35 - 42.4	50.7	18.5	7.2	35 - 42.7	52.7	30.7	6.9	35 - 42.2	49.3	39	7.4
6	35 - 46	35 - 39.9	44.5	7	6.1	35 - 39.9	44.5	18	6.1	35 - 39.8	43.6	44.8	6.2
PCM													
PCM/Ws													
1	15 - 52.5	15 - 46.9	85	74.8	5.6	15 - 46.7	84.5	72.2	5.8				
2	35 - 53.8	35 - 51.6	88	24.8	2.2	35 - 52.5	93	23.7	1.3				
3	35 - 52.6	38.7 - 46.9	46.6	27.1	5.7	39.7 - 48.8	51.7	28.3	3.8				
4	35 - 52.3	37.2 - 45.6	48.5	32.5	6.7	40 - 45.7	32.9	34	6.6				
5	35 - 49.6	35 - 42.0	47.9	36.1	7.6	38.8 - 42	21.9	41.1	7.6				
6	35 - 46	35 - 39.3	39	21.7	6.7	35 - 39.4	40	40.5	6.6				

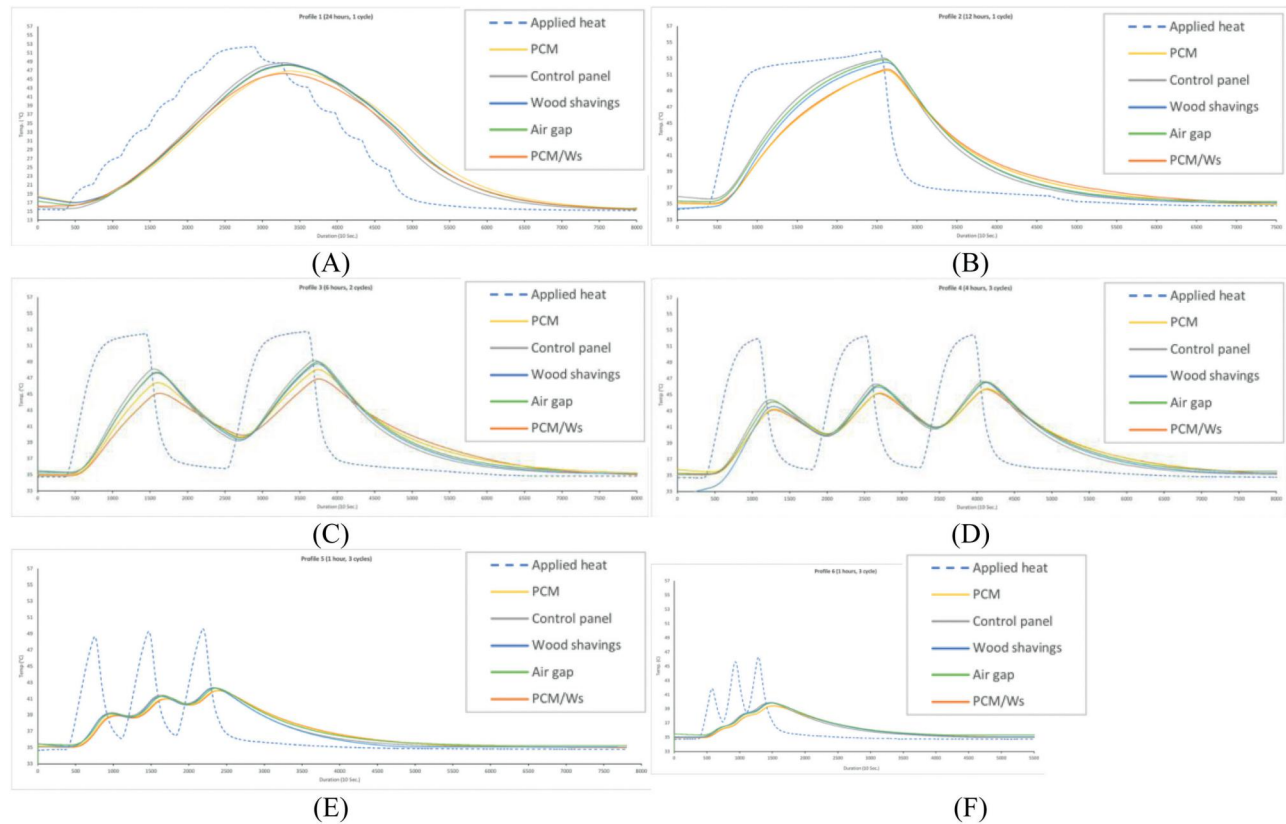


Fig. 6. Temperatures of all panels during testing. (A) Profile 1. (B) Profile 2. (C) Profile 3. (D) Profile 4. (E) Profile 5. (F) Profile 6.

maximum applied heat shows the potential in reduction of heat gain in the event of using a certain panel (referred to in the table as “Peak temperature reduction”). The reduction in peak temperatures is calculated as (the Max temp. of the chamber – Max. temp. inside the confinement). The table also shows the variation in temperature fluctuation which was calculated as a percentage based on the difference of temperatures measured inside and outside the confinement (“Max. temp. inside the confinement – Min temp. inside the confinement” / “Max. temp. in the chamber - Min. Temp. in the chamber” \* 100%), thus, showing the potential of using such panels to mitigate heat fluctuations. This also shows the influence of the duration of exposure to heat has on the ability to mitigate fluctuations. The results additionally show the shift in the peak temperature time due to the presence of each panel, which is a property that could be utilised in many applications such as heat storage devices.

In heat profile 1, shown in Fig. 6 (A), there was a reduction in the peak air temperature and a shift in the peak temperature time for all panels. As expected, the control panel has shown the least influence on the temperatures as it only consists of a 2 mm Plexi-glass panel. The “1 cm” air gap panel showed more influence as it resulted in decreased temperatures in comparison with the control panel. This is due to the effect of the air gap which acts as thermal insulation to an extent [153–157]. The Ws panel has shown a reduction in temperature close to this of the “1 cm” air gap panel. The most thermal influence was observed in both the PCM and the PCM/Ws panel. A negligible difference in temperature reduction was present between both mentioned panels. As for temperature fluctuation, similar results can be observed in all panels. The PCM and the PCM/Ws panel have shown the least fluctuation percentage in comparison with the other panels. This is also true for the peak heat shift durations. It is noted also that heat profile 1 showed the largest heat peak time shift in comparison with other heat profiles. Although the increase of temperatures was almost identical in all panels, the pace at which temperatures dropped inside the confinement is not

as identical. The control panel was the fastest to cool down. The “1 cm” air gap panel was slower to cool. The PCM and the PCM/Ws however, were the last to cool. This is possibly due to the latent heat effect of the PCM [158–160].

In heat profile 2, shown in Fig. 6 (B), similar results as heat profile 1 can be seen. However, it is noted that the peak temperatures of panels were higher than those of heat profile 1. This is possibly due to the applied heat increasing rapidly to 54 °C within 1.5 h of the test then stabilizing for the rest of the duration of the test. This implies that the fluctuation of temperatures may be less reduced if the temperature change is slow as this would allow for the heat to be further conducted through the panels thus causing further increasing and decreasing in the temperature inside the confinement. Similar results are shown in the rest of the heat profiles in regards to the performance of the panels shown in Fig. 6 (C, D, E & F). The results show that there is a strong correlation between the duration of the cycle and the performance of the panels. In cycles with longer durations such as in heat profiles 3 and 4, the temperatures inside the confinement were found to be fluctuating relatively higher. Whereas in heat profiles with shorter cycles such as heat profiles 5 and 6, the fluctuations were found to be lower. It is important to note that this is the case for all the tested panels although the PCM/Ws was seen to have the least fluctuation in all heat profiles regardless of the duration of the cycle. Fig. 7 (A) shows the relationship between cycle duration and the percentage of fluctuation in the tested panels based on the logged measurements of this investigation.

As for the heat peak time shift which represents the duration elapsed from the point that the maximum air temperature occurs inside the chamber and the point that the maximum air temperature is reached inside the confinement, it is evident that there is a minor correlation between the duration of heat application and shift in peak temperature, as seen in Fig. 7 (B). To elucidate, despite several inconsistencies, the shift seems to increase as the duration of exposure to heat is decreased. An exception to this is profile 1, in which, the largest shifts have been

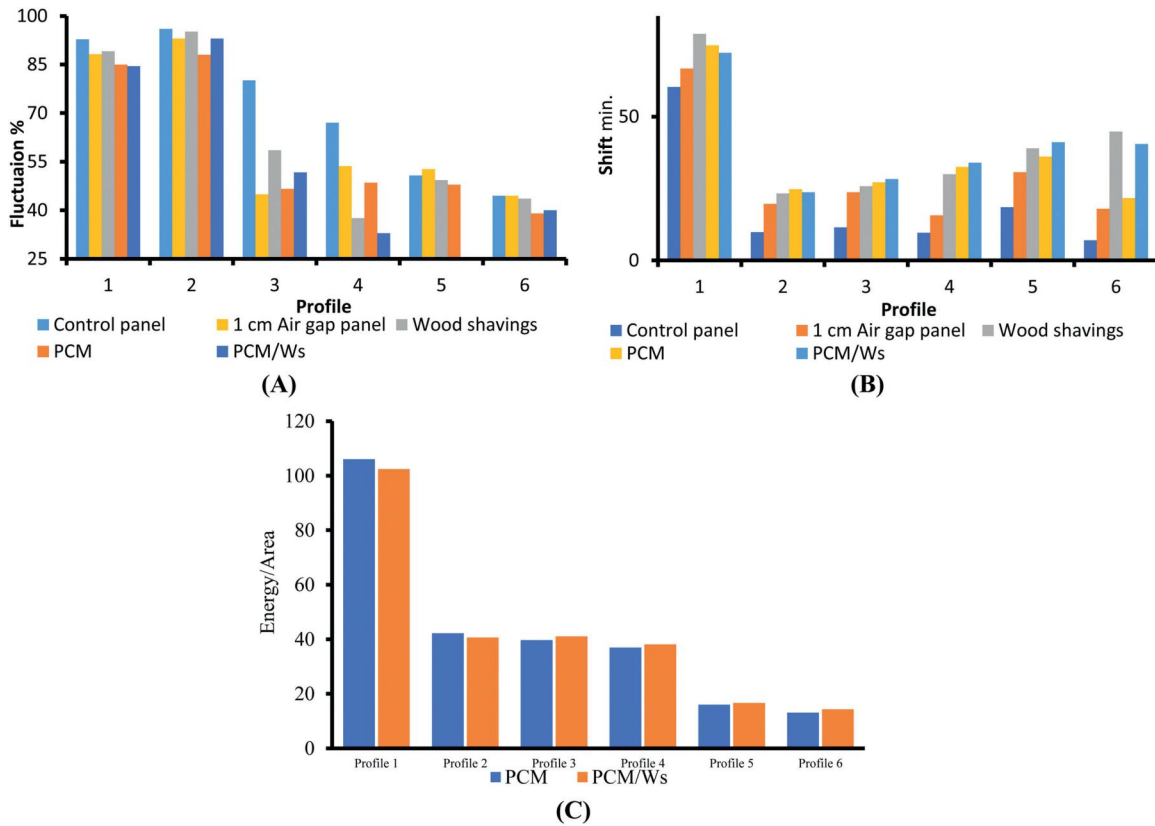


Fig. 7. (A) Relation between observed temperature fluctuations in all panels and duration of heat profile cycles. (B) Relation between shift in peak temperatures in all panels and duration of heat profile cycles. (C) Comparison of area under curves for panels.

observed despite exerting the most duration of exposure to heat. This may be explained as a result of the highly gradual mode of increase and decrease of heat. The gradual increase in heat allows for the PCM to reach its melting point after a longer duration without being affected by the heat before this point. It is worthy to note that the Ws, PCM and PCM/Ws panels have shown the most shift duration, with the PCM and PCM/Ws performing most efficiently in this regard in most of the heat profiles. It is important to point out that the type of PCM will influence its latent heat capacity thus affecting its capability to shift the heat peak [161], other types of PCMs can cause an extended heat peak shift as observed in the work of Chung and Park [96], Piselli et al. [97] and Principi and Fioretti [162] discussed earlier. This is true also for the reduction in the peak temperature. All panels have resulted in a reduction that ranged from an insignificant reduction (such as 0.76 °C in the control panel) to very significant reductions (such as 7.6 °C in the PCM panel). The study shows that both the PCM and PCM/WS panels have resulted in the highest highest reduction in all heat profiles due to the melting properties of the PCM as discussed earlier in literature. However, it can be seen also that the reduction is at its greatest the shorter the heat cycle is. This can be elucidated as due to the lack of sufficient duration that allows the tested panel to gain heat so as to raise its temperature. Hence, it can be inferred that heat profile 1 and profile 2 represent a more accurate assessment of the temperature reduction capabilities of the tested panels as they have longer cycle durations (24 h and 12 h). Whereas, heat profiles 3,4,5 and 6 may represent temperature reduction of these panels in conditions where rapid changes in temperature are occurring.

It can be seen that the thermal performance of the PCM and the PCM/Ws amalgam are similar to a large extent. For further comparison, the area encompassed under the curves of the mentioned earlier panels, represented earlier, are compared. Such areas can be indicative of the energy exerted inside the confinement during testing the mentioned panels. A trapezoidal approximation is used to calculate the mentioned areas. Fig. 7 (C) shows a comparison between the mentioned panels

for all heat profiles. It can be seen that the performance of the panels in terms of energy is similar to a large extent. It may be worthy to note that the area under profile 1 curves are clearly much larger, which is consistent with the duration of applied heat for that profile. The areas for Profiles 5 and 6, however, are seen to particularly small a result of the applied heat fluctuating. This is to imply that the effect of heat fluctuation on the applied heat is similar to the effect of reducing the maximum applied temperature in terms of exerted energy. Most importantly, it can be observed from the measurements discussed earlier that although both PCMs and wood shavings have significant thermal performance, the amalgamation of both materials has not resulted in a significant thermal enhancement in the thermal performance of the panels. The measured data shows that the performance of the PCM panel and the PCM/Ws panel is almost identical. Thus, it can be inferred that adding wood shavings to PCMs would not result in enhancing the thermal performance. The values of thermal conductivities of PCM and wood-shaving can explain this fact. Studies show that the thermal conductivity of paraffin waxes, like PCM, of similar melting points to this used in the present study to be around 0.20 to 0.22 W/(m•K) [163–170]. Whereas, the thermal conductivity of MDF/plywood wood-shavings can be as low as 0.11 to 0.17 W/(m•K) [171–177] and in some cases as low as 0.03 W/(m•K) [178,179]. The inherent low thermal conductivity of wood-shavings, compared to this of PCM, can explain the fact that replacing an amount of PCM with a similar volume of wood-shavings will not negatively impact the overall thermal insulation performance. Meaning that, within the amalgam panels, a portion of the denser PCM content is replaced with a material of a lower thermal conductivity, wood-shavings, which increases its overall insulation capabilities and reduces weight due to its relatively lightweight.

From a constructional perspective, the amalgamation of these two materials can be of good use. As thermal insulation is applied to the exterior of buildings, this presents a structural load that is taken into consideration during the construction process. Heavier loads would result

in more strain on structural elements which require further structural support thus increasing cost. However, having a density of  $0.1 \text{ g/cm}^3$ , the addition of wood shavings to PCM would result in a significantly lower weight with the same, if not improved, thermal performance. For example, the PCM panel mentioned earlier was filled with 380 g of PCMs (with a density of  $9.95 \text{ g/cm}^3$ ). The thermal performance of the mentioned panel was matched and improved in some cases with the usage of the PCM/Ws which contained 260 g of PCMs and 40 g of wood shavings with a total weight of 300 g. This constitutes a weight reduction of 80 g (20.94% of total weight). It is important to note that such a reduction in weight can be of significant influence in certain areas in the world where traditional architecture prevails. In such buildings, considerably thick insulation may be applied to counter extreme weather conditions, such as rural Egyptian architecture built in hot-arid desert climates for instance [180], where insulations can reach a thickness of over 50 cm. In fact, many countries around the world still utilise such vernacular building approaches to the present day, such as India [11181,182], Yamen [183], Macedonia [184], Myanmar [185], Nepal [186], Spain [187], Romania [188] and Japan [189]. Such buildings carry a large potential to benefit from insulation solutions such as this presented in the present study, where a saving in weight can be highly advantageous.

### 3. Conclusions

The appraisal of literature presented in this work identified that the use of PCMs, wood shavings and other natural materials as an innovative approach for passive thermal control is highly promising at low cost. However, attempts to combine these materials to gain enhanced thermal performance, although promising, have been performed using complex techniques that may be unsuitable where high-tech is not widely available. Little or no attempts have been carried out to investigate possible gains through the simple amalgamation of PCMs and wood shavings. In the context of this article, this was investigated with regards to not only thermal aspects but possible other gains. Comparison of the tested materials shows the following:

- PCMs and PCMs submerged in wood shaving have shown to have better thermal performance compared to wood shavings (in the Ws panel). However, measurements have shown that both PCMs and PCMs/wood shavings have very similar thermal performance, with PCM/wood shavings demonstrating a slightly better performance. This implies that adding amounts of wood shavings to PCMs would not result in any significant enhancement in the thermal performance.
- Although no or little thermal gain can be achieved from submerging wood shavings in PCM, from a construction perspective, advantageous gains may be achieved. Namely, a reduction in weight of 22.94% may be achieved when using a mixture of PCMs and wood shavings rather than using PCMs, with almost identical thermal performance. This is also economically advantageous as wood shavings are typically of low cost as a by-product of industrial processes. Hence, replacing amounts of PCM, in PCM related applications, with wood-shavings will certainly reduce thermal insulation costs.
- PCMs and wood shavings submerged in PCMs can mitigate heat gain significantly. In cases of long heat cycles, the peak temperature was reduced by up to  $5.8 \text{ }^\circ\text{C}$ . In cycles that have shorter durations, the heat peak reduction was up to  $7.6 \text{ }^\circ\text{C}$ . It should be noted that this reduction was achieved using 1 cm thick panels. Similar panels with larger thicknesses can have a significantly better reduction in temperatures. This highlights the advantageous attribute of weight reduction by using wood-shavings.
- The experimental study shows that PCMs and wood shavings submerged in PCMs have good potential to reduce air temperature fluctuations. For example, the PCM/Ws panel has shown a notable reduction in air temperature fluctuations (by 15.5% to 60%) compared to the thermal performance of the control panel (reduced fluctua-

tions by 7.2% to 55.5%) and the 1 cm air gap panel (reduced fluctuations by 11.8% to 55.5%). This is true for all of the tested heat profiles which have different cycles of high/low temperatures with various cycle durations. The reduction in fluctuations is evidently affected by its duration and intensity.

- A shift in the peak temperature can be achieved using thermal insulation systems, depending on the system's latent heat properties and the duration of the applied heat cycles. However, adding wood shavings to PCM in an insulation system will not have a significant effect on the duration of the heat peak shift.

The results of this investigation have shown that, in addition to PCMs having the capability to reduce heat conduction through building walls, they can play a good role in mitigating air temperature fluctuations and cause a shift in the heat peak which may in certain cases be beneficial. More importantly, the data has shown that adding wood shaving to PCMs on a thermal insulation system in a simple submerged manner would not negatively affect the performance of this system, and, would result in a reduction of weight and cost. This reduction is of high significance in terms of construction requirements and cost. Other materials have such qualities which is a good area for future research. It is evident that further studies are needed to comprehend possible gains of amalgamating PCMs with natural low-cost substances to further improve thermal, technical and economic aspects of thermal insulation systems.

### Declaration of Competing Interest

The authors declare that they have no known competing financial interests or personal relationships that could have appeared to influence the work reported in the article entitled " Potential gains from the amalgamation of Phase Changing Materials (PCMs) and wood shavings".

### CRedit authorship contribution statement

**Adham M. Mohammed:** Conceptualization, Methodology, Validation, Formal analysis, Investigation, Resources, Writing - original draft, Visualization. **Amira Elnokaly:** Methodology, Validation, Writing - review & editing, Supervision, Project administration. **Abdel Monteleb M. Aly:** Writing - review & editing, Supervision, Project administration.

### Acknowledgments

This article has been funded by the Egyptian ministry of higher education as a part of a PhD joint supervision scholarship programme. The authors would like to thank the Joseph Bank laboratories (JBL), University of Lincoln, UK for their support through providing experimental equipment essential for this article. The authors also thank Dr. Francesca Gherardi for facilitating and providing technical support.

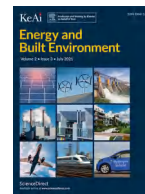
### References

- [1] Amira Elnokaly, Ahmed Elseragy, Sustainable heritage development: learning from urban conservation of heritage projects in non-western contexts European, J. Sustainable. Dev. 2 (2013).
- [2] Hassan Fathy, Natural Energy and Vernacular Architecture, Hassan Fathy, 1986.
- [3] H. Koch-Nielsen, Stay Cool : A Design Guide for the Built Environment in Hot Climates, Routledge, 2013.
- [4] M. Ayoub, A. Elseragy, Parameterization of traditional domed-roofs insulation in hot-arid climates in Aswan, Egypt Energy Environ. 29 (2018) 109–130.
- [5] A. Elnokaly, M. Ayoub, A. Elseragy, Parametric investigation of traditional vaulted roofs in hot-arid climates, Renew. Energy 138 (2019) 250–262.
- [6] A. Elnokaly, A. Elseragy, What impedes the development of renewable energy technology, Egypt MCEET 2007 Sustainable Energy: Technologies, Materials and Environmental Issues, MCEET, Cairo, Egypt, 2007.
- [7] M. Fahmy, M. Mahdy M, M. Nikolopoulou, Prediction of future energy consumption reduction using GRC envelope optimization for residential buildings in Egypt, Energy Build. 70 (2014) 186–193.
- [8] R. Zeng, X. Wang, H. Di, F. Jiang, Y. Zhang, New concepts and approach for developing energy efficient buildings: ideal specific heat for building internal thermal mass, Energy Build. 43 (2011) 1081–1090.

- [9] K. Meyn S, Heat Fluxes Through Roofs and their Relevance to Estimates of Urban Heat Storage, University of British Columbia, 2000.
- [10] P. Ramamurthy, T. Sun, K. Rule, E. Bou-Zeid, The joint influence of albedo and insulation on roof performance: an observational study, *Energy Build.* 93 (2015) 249–258.
- [11] Santamouris M., Synnefa A. and T. Karlessi 2011 Using advanced cool materials in the urban built environment to mitigate heat islands and improve thermal comfort conditions - Dimensions.
- [12] M. Frontczak, P. Wargocki, Literature survey on how different factors influence human comfort in indoor environments, *Build. Environ.* 46 (2011) 922–937.
- [13] A. Qadi S, B. Sodagar, A. Elnokaly, Estimating the heating energy consumption of the residential buildings in Hebron, Palest. *J. Clean. Prod.* 196 (2018) 1292–1305.
- [14] F. Asdrubali, F. D'Alessandro, G. Baldinelli, F. Bianchi, Evaluating in situ thermal transmittance of green buildings masonries—A case study *Case Studies in Construction, Materials 1* (2014) 53–59.
- [15] A. Korjenic, V. Petránek, J. Zach, J. Hroudová, Development and performance evaluation of natural thermal-insulation materials composed of renewable resources, *Energy Build.* 43 (2011) 2518–2523.
- [16] J. Zach, J. Hroudová, J. Brožovský, Z. Krejza, A. Gailius, Development of thermal insulating materials on natural base for thermal insulation systems, *Proc. Eng.* 57 (2013) 1288–1294.
- [17] W. Feist, J. Schnieders, V. Dorer, A. Haas, Re-inventing air heating: convenient and comfortable within the frame of the Passive House concept, *Energy Build.* 11 (2005) 1186–1203.
- [18] J. Holmes M, N. Hacker J, Climate change, thermal comfort and energy: meeting the design challenges of the 21st century, *Energy Build.* 39 (2007) 802–814.
- [19] A. Elnokaly, I. Keeling, An empirical study investigating the impact of micro-algal technologies and their application within intelligent building fabrics, *Proc. - Soc. Behav. Sci.* 216 (2016) 712–723.
- [20] A. Elnokaly, CFD analysis of tensile conical membrane structures as microclimate modifiers in hot arid regions, *Civil Eng. Archit. Hrpub 2* (2014) 92–102.
- [21] D. Burillo, V. Chester M, S. Pincetl, D. Fournier E, J. Reyna, Forecasting peak electricity demand for Los Angeles considering higher air temperatures due to climate change, *Appl. Energy* 236 (2019) 1–9.
- [22] S. Jovanović, S. Savić, M. Bojić, Z. Djordjević, D. Nikolić, The impact of the mean daily air temperature change on electricity consumption, *Energy* 88 (2015) 604–609.
- [23] G. Özbalta T, A. Sezer, Y. Yıldız, Models for prediction of daily mean indoor temperature and relative humidity: education building in Izmir, Turkey *Indoor Built Environ.* 21 (2012) 772–781.
- [24] S. Zhang, Y. Cheng, Z. Fang, C. Huan, Z. Lin, Optimization of room air temperature in stratum-ventilated rooms for both thermal comfort and energy saving, *Appl. Energy* 204 (2017) 420–431.
- [25] D. Li, Y. Wu, B. Wang, C. Liu, M. Arici, Optical and thermal performance of glazing units containing PCM in buildings: a review, *Constr. Build. Mater.* 233 (2020) 117327.
- [26] K. Singh Rathore P, K. Shukla S, K. Gupta N, Potential of microencapsulated PCM for energy savings in buildings: a critical review, *Sustain. Cities Soc.* 53 (2020) 101884.
- [27] K. Kant, A. Shukla, A. Sharma, Heat transfer studies of building brick containing phase change materials, *Sol. Energy* 155 (2017) 1233–1242.
- [28] R. Vicente, T. Silva, Brick masonry walls with PCM macrocapsules: an experimental approach, *Appl. Thermal Eng.* 67 (2014) 24–34.
- [29] T. Silva, R. Vicente, N. Soares, V. Ferreira, Experimental testing and numerical modelling of masonry wall solution with PCM incorporation: a passive construction solution, *Energy Build.* 49 (2012) 235–245.
- [30] L. da Cunha S R, B. de Aguiar J L, Phase change materials and energy efficiency of buildings: a review of knowledge, *J. Energy Storage* 27 (2020) 101083.
- [31] L. Yang, J. Huang, F. Zhou, Thermophysical properties and applications of nano-enhanced PCMs: an update review, *Energy Convers. Manag.* 214 (2020) 112876.
- [32] S. Álvarez, F. Cabeza L, A. Ruiz-Pardo, A. Castell, J.A. Tenorio, Building integration of PCM for natural cooling of buildings, *Appl. Energy* 109 (2013) 514–522.
- [33] D. Cao V, S. Pilehvar, C. Salas-Bringas, A.M. Szczotok, T.Q. Bui, M. Carmona, J.F. Rodriguez, A.-L. Kjøniksen, Thermal analysis of geopolymer concrete walls containing microencapsulated phase change materials for building applications, *Sol. Energy* 178 (2019) 295–307.
- [34] A. de Gracia, Dynamic building envelope with PCM for cooling purposes – Proof of concept, *Appl. Energy* 235 (2019) 1245–1253.
- [35] J. Lei, J. Yang, E.-H. Yang, Energy performance of building envelopes integrated with phase change materials for cooling load reduction in tropical Singapore, *Appl. Energy* 162 (2016) 207–217.
- [36] H.-M. Chou, C.-R. Chen, V.-L. Nguyen, A new design of metal-sheet cool roof using PCM, *Energy Build.* 57 (2013) 42–50.
- [37] M. Ahangari, M. Maerefat, An innovative PCM system for thermal comfort improvement and energy demand reduction in building under different climate conditions, *Sustain. Cities Soc.* 44 (2019) 120–129.
- [38] A. Izquierdo-Barrientos M, J.F. Belmonte, D. Rodríguez-Sánchez, A.E. Molina, J.A. Almendros-Ibáñez, A numerical study of external building walls containing phase change materials (PCM), *Appl. Thermal Eng.* 47 (2012) 73–85.
- [39] J. Xie, W. Wang, J. Liu, S. Pan, Thermal performance analysis of PCM wallboards for building application based on numerical simulation, *Sol. Energy* 162 (2018) 533–540.
- [40] K. Biswas, Y. Shukla, A. Desjarlais, R. Rawal, Thermal characterization of full-scale PCM products and numerical simulations, including hysteresis, to evaluate energy impacts in an envelope application, *Appl. Thermal Eng.* 138 (2018) 501–512.
- [41] Q. Wang, R. Wu, Y. Wu, Y. Zhao C, Parametric analysis of using PCM walls for heating loads reduction, *Energy Build.* 172 (2018) 328–336.
- [42] A. Buonomano, F. Guarino, The impact of thermophysical properties and hysteresis effects on the energy performance simulation of PCM wallboards: experimental studies, modelling, and validation, *Renew. Sustain. Energy Rev.* 126 (2020) 109807.
- [43] H. Wang, W. Lu, Z. Wu, G. Zhang, Parametric analysis of applying PCM wallboards for energy saving in high-rise lightweight buildings in Shanghai, *Renew. Energy* 145 (2020) 52–64.
- [44] C. Li, H. Yu, Y. Song, Y. Tang, P. Chen, H. Hu, M. Wang, Z. Liu, Experimental thermal performance of wallboard with hybrid microencapsulated phase change materials for building application, *J. Build. Eng.* 28 (2020) 101051.
- [45] S. Wi, J. Chang S, S. Kim, Improvement of thermal inertia effect in buildings using shape stabilized PCM wallboard based on the enthalpy-temperature function, *Sustain. Cities Soc.* 56 (2020) 102067.
- [46] H. Yeon J, Thermal behavior of cement mortar embedded with low-phase transition temperature PCM, *Constr. Build. Mater.* 252 (2020) 119168.
- [47] C. Costa J A, A.E. Martinelli, R.M. do Nascimento, A.M. Mendes, Microstructural design and thermal characterization of composite diatomite-vermiculite paraffin-based form-stable PCM for cementitious mortars, *Constr. Build. Mater.* 232 (2020) 117167.
- [48] M. Frigione, M. Lettieri, A. Sarcinella, J. Barroso de Aguiar, Sustainable polymer-based phase change materials for energy efficiency in buildings and their application in aerial lime mortars, *Constr. Build. Mater.* 231 (2020) 117149.
- [49] L. Li, H. Yu, R. Liu, Research on composite-phase change materials (PCMs)-bricks in the west wall of room-scale cubicle: mid-season and summer day cases, *Build. Environ.* 123 (2017) 494–503.
- [50] L. Olivieri, A. Tenorio J, D. Revuelta, L. Navarro, F. Cabeza L, Developing a PCM-enhanced mortar for thermally active precast walls, *Constr. Build. Mater.* 181 (2018) 638–649.
- [51] V. Rao V, R. Parameshwaran, V. Ram V, PCM-mortar based construction materials for energy efficient buildings: a review on research trends, *Energy Build.* 158 (2018) 95–122.
- [52] R. Saxena, D. Rakshit, C. Kaushik S, Experimental assessment of Phase Change Material (PCM) embedded bricks for passive conditioning in buildings, *Renew. Energy* 149 (2020) 587–599.
- [53] Y. Gao, F. He, X. Meng, Z. Wang, M. Zhang, H. Yu, W. Gao, Thermal behavior analysis of hollow bricks filled with phase-change material (PCM), *J. Build. Eng.* 31 (2020) 101447.
- [54] S. Dabiri, M. Mehrpooya, G. Nezhad E, Latent and sensible heat analysis of PCM incorporated in a brick for cold and hot climatic conditions, utilizing computational fluid dynamics, *Energy* 159 (2018) 160–171.
- [55] V. Vinayaka Ram, R. Singhal, R. Parameshwaran, Energy efficient pumpable cement concrete with nanomaterials embedded PCM for passive cooling application in buildings, *Mater. Today: Proc.* (2020).
- [56] F. Cabeza L, L. Navarro, A.L. Pisello, L. Olivieri, C. Bartolomé, J. Sánchez, S. Álvarez, J.A. Tenorio, Behaviour of a concrete wall containing micro-encapsulated PCM after a decade of its construction, *Sol. Energy* 200 (2020) 108–113.
- [57] E. Mohseni, W. Tang, H. Khayat K, H. Cui, Thermal performance and corrosion resistance of structural-functional concrete made with inorganic PCM, *Constr. Build. Mater.* 249 (2020) 118768.
- [58] A. Benkaddour, M. Faraji, H. Faraji, Numerical study of the thermal energy storage behaviour of a novel composite PCM/Concrete wall integrated solar collector, *Mater. Today: Proc.* (2020).
- [59] R. Arivazhagan, S. Arun Prakash, P. Kumaran, S. Sankar, B. Loganathan G, A. Arivaranan, Performance analysis of concrete block integrated with PCM for thermal management, *Mater. Today: Proc.* 22 (2020) 370–374.
- [60] L. Erlbeck, P. Schreiner, K. Schlachter, P. Dörnhofer, F. Fasel, F.-J. Methner, M. Rädle, Adjustment of thermal behavior by changing the shape of PCM inclusions in concrete blocks, *Energy Convers. Manag.* 158 (2018) 256–265.
- [61] R. Guo, Y. Pan, L. Cai, S. Hino, Bonding behavior of CFRP grid-concrete with PCM shotcrete, *Eng. Struct.* 168 (2018) 333–345.
- [62] U. Berardi, A. Gallardo A, Properties of concretes enhanced with phase change materials for building applications, *Energy Build.* 199 (2019) 402–414.
- [63] R. Arivazhagan, S. Arun Prakash, P. Kumaran, S. Sankar, B. Loganathan G, A. Arivaranan, Performance analysis of concrete block integrated with PCM for thermal management, *Mater. Today: Proc.* (2019).
- [64] N. Essid, A. Loulizi, J. Neji, Compressive strength and hygric properties of concretes incorporating microencapsulated phase change material, *Constr. Build. Mater.* 222 (2019) 254–262.
- [65] A. D'Alessandro, A.L. Pisello, C. Fabiani, F. Ubertini, L.F. Cabeza, F. Cotana, Multifunctional smart concretes with novel phase change materials: mechanical and thermo-energy investigation, *Appl. Energy* 212 (2018) 1448–1461.
- [66] D. Cao V, S. Pilehvar, C. Salas-Bringas, A.M. Szczotok, L. Valentini, M. Carmona, J.F. Rodriguez, A.-L. Kjøniksen, Influence of microcapsule size and shell polarity on thermal and mechanical properties of thermoregulating geopolymer concrete for passive building applications, *Energy Convers. Manag.* 164 (2018) 198–209.
- [67] S. Wi, S. Yang, J. Lee, J. Chang S, S. Kim, Dynamic heat transfer and thermal performance evaluation of PCM-doped hybrid hollow plaster panels for buildings, *J. Hazard. Mater.* 374 (2019) 428–436.
- [68] N. Mekaddem, B. Ali S, M. Fois, A. Hannachi, Paraffin/ expanded perlite/plaster as thermal energy storage composite, *Energy Proc.* 157 (2019) 1118–1129.
- [69] Z. Pavlík, J. Fořt, M. Pavlíková, J. Pokorný, A. Trník, R. Černý, Modified lime-cement plasters with enhanced thermal and hygric storage capacity for moderation of interior climate, *Energy Build.* 126 (2016) 113–127.

- [70] K. Asimakopoulou E, I. Kolaitis D, A. Founti M, Fire safety aspects of PCM-enhanced gypsum plasterboards: an experimental and numerical investigation, *Fire Saf. J.* 72 (2015) 50–58.
- [71] O. Chung, S.-G. Jeong, S. Yu, S. Kim, Thermal performance of organic PCMs/micronized silica composite for latent heat thermal energy storage, *Energy Build.* 70 (2014) 180–185.
- [72] T. Feczko, L. Trif, D. Horák, Latent heat storage by silica-coated polymer beads containing organic phase change materials, *Sol. Energy* 132 (2016) 405–414.
- [73] S.-G. Jeong, J. Jeon, J. Cha, J. Kim, S. Kim, Preparation and evaluation of thermal enhanced silica fume by incorporating organic PCM, for application to concrete, *Energy Build.* 62 (2013) 190–195.
- [74] L. Liu, K. Zheng, Y. Yan, Z. Cai, S. Lin, X. Hu, Graphene aerogels enhanced phase change materials prepared by one-pot method with high thermal conductivity and large latent energy storage, *Sol. Energy Mater. Sol. Cells* 185 (2018) 487–493.
- [75] S. Serrano, C. Barreneche, A. Navarro, L. Haurie, A.I. Fernandez, L.F. Cabeza, Use of multi-layered PCM gypsums to improve fire response. Physical, thermal and mechanical characterization, *Energy Build.* 127 (2016) 1–9.
- [76] J. Yang, G.-Q. Qi, R.-Y. Bao, K. Yi, M. Li, L. Peng, Z. Cai, M.-B. Yang, D. Wei, W. Yang, Hybridizing graphene aerogel into three-dimensional graphene foam for high-performance composite phase change materials, *Energy Storage Mater.* 13 (2018) 88–95.
- [77] D. Zou, X. Ma, X. Liu, P. Zheng, Y. Hu, Thermal performance enhancement of composite phase change materials (PCM) using graphene and carbon nanotubes as additives for the potential application in lithium-ion power battery, *Int. J. Heat Mass Transf.* 120 (2018) 33–41.
- [78] Y. Zhu, Y. Qin, S. Liang, K. Chen, C. Tian, J. Wang, X. Luo, L. Zhang, Graphene/SiO<sub>2</sub>/n-octadecane nanoencapsulated phase change material with flower like morphology, high thermal conductivity, and suppressed supercooling, *Appl. Energy* 250 (2019) 98–108.
- [79] B. Eanest Jebasingh, A. Valan Arasu, A detailed review on heat transfer rate, supercooling, thermal stability and reliability of nanoparticle dispersed organic phase change material for low-temperature applications, *Mater. Today Energy* 16 (2020) 100408.
- [80] B. Eanest Jebasingh, A. Valan Arasu, A comprehensive review on latent heat and thermal conductivity of nanoparticle dispersed phase change material for low-temperature applications, *Energy Storage Mater.* 24 (2020) 52–74.
- [81] S. Laraib Tariq, H. Muhammad Ali, M. Ammar Akram, M. Mansoor Janjua, M. Ahmadlouydarab, Nanoparticles enhanced phase change materials (NePCMs)-a recent review, *Appl. Therm. Eng.* (2020) 115305.
- [82] L.-S. Wong-Pinto, Y. Milian, S. Ushak, Progress on use of nanoparticles in salt hydrates as phase change materials, *Renew. Sustain. Energy Rev.* 122 (2020) 109727.
- [83] M. Sheikhholeslami, A.N. Keshteli, H. Babazadeh, Nanoparticles favorable effects on performance of thermal storage units, *J. Mol. Liquids* 300 (2020) 112329.
- [84] X. Huang, X. Chen, A. Li, D. Atinafu, H. Gao, W. Dong, G. Wang, Shape-stabilized phase change materials based on porous supports for thermal energy storage applications, *Chem. Eng. J.* 356 (2019) 641–661.
- [85] M. Li, B. Mu, Effect of different dimensional carbon materials on the properties and application of phase change materials: a review, *Appl. Energy* 242 (2019) 695–715.
- [86] S. Rathore P K, K. Shukla S, Potential of macroencapsulated PCM for thermal energy storage in buildings: a comprehensive review, *Constr. Build. Mater.* 225 (2019) 723–744.
- [87] F. Rodríguez-Cumplido, E. Pabón-Gelves, F. Chejne-Jana, Recent developments in the synthesis of microencapsulated and nanoencapsulated phase change materials, *J. Energy Storage* 24 (2019) 100821.
- [88] T. Santos, M. Kolokotroni, N. Hopper, K. Yearley, Experimental study on the performance of a new encapsulation panel for PCM's to be used in the PCM-Air heat exchanger, *Energy Proc.* 161 (2019) 352–359.
- [89] T. Yan, J. Gao, X. Xu, T. Xu, Z. Ling, J. Yu, Dynamic simplified PCM models for the pipe-encapsulated PCM wall system for self-activated heat removal, *Int. J. Thermal Sci.* 144 (2019) 27–41.
- [90] M. Alawadhi E, Woodhead Publishing, Oxford, 2015, pp. 231–248.
- [91] T. Yan, Z. Sun, J. Gao, X. Xu, J. Yu, W. Gang, Simulation study of a pipe-encapsulated PCM wall system with self-activated heat removal by nocturnal sky radiation, *Renew. Energy* 146 (2020) 1451–1464.
- [92] W.-M. Yan, J. Ho C, Y.-T. Tseng, C. Qin, S. Rashidi, Numerical study on convective heat transfer of nanofluid in a minichannel heat sink with micro-encapsulated PCM-cooled ceiling, *Int. J. Heat Mass Transf.* 153 (2020) 119589.
- [93] N. Hichem, S. Noureddine, S. Nadia, D. Djamilia, Experimental and numerical study of a usual brick filled with PCM to improve the thermal inertia of buildings, *Energy Proc.* 36 (2013) 766–775.
- [94] S. Rathore P K, K. Shukla S, An experimental evaluation of thermal behavior of the building envelope using macroencapsulated PCM for energy savings, *Renew. Energy* 149 (2020) 1300–1313.
- [95] R. Hirmiz, M. Teamah H, F. Lightstone M, S. Cotton J, Analytical and numerical sizing of phase change material thickness for rectangular encapsulations in hybrid thermal storage tanks for residential heat pump systems, *Appl. Thermal Eng.* 170 (2020) 114978.
- [96] M. Chung, J. Park, An experimental study on the thermal performance of phase-change material and wood-plastic composites for building roofs, *Energies* 10 (2017) 195.
- [97] C. Piselli, V.L. Castaldo, A.L. Pisello, How to enhance thermal energy storage effect of PCM in roofs with varying solar reflectance: experimental and numerical assessment of a new roof system for passive cooling in different climate conditions, *Sol. Energy* (2018).
- [98] J. Alqallaf H, M. Alawadhi E, Concrete roof with cylindrical holes containing PCM to reduce the heat gain, *Energy Build. Compl.* (2013) 73–80.
- [99] F. Asdrubali, F. D'Alessandro, S. Schiavoni, A review of unconventional sustainable building insulation materials, *Sustain. Mater. Technol.* 4 (2015) 1–17.
- [100] S. Schiavoni, F. D'Alessandro, F. Bianchi, F. Asdrubali, Insulation materials for the building sector: a review and comparative analysis, *Renew. Sustain. Energy Rev.* 62 (2016) 988–1011.
- [101] S. Sheweka, A. Elnokaly, Waste management and material recycle as a potential of sustainable building envelope for low income housing Sustainability and Innovation for the future, 41st IAHS World Congress (Albufeira, Algarve, Portugal), 2016.
- [102] Z. Pásztor, I. Ronyecz Mohácsiné, Z. Börcsök, Investigation of thermal insulation panels made of black locust tree bark, *Constr. Build. Mater.* 147 (2017) 733–735.
- [103] B. Abu-Jdayil, A.-H. Mourad, W. Hittini, M. Hassan, S. Hameedi, Traditional, state-of-the-art and renewable thermal building insulation materials: an overview, *Constr. Build. Mater.* 214 (2019) 709–735.
- [104] I. Cetiner, D. Shea A, Wood waste as an alternative thermal insulation for buildings, *Energy Build.* 168 (2018) 374–384.
- [105] M. Jerman, I. Palomar, V. Kočí, R. Černý, Thermal and hygric properties of biomaterials suitable for interior thermal insulation systems in historical and traditional buildings, *Build. Environ.* 154 (2019) 81–88.
- [106] C. Lacoste, R. El Hage, A. Bergeret, S. Corn, P. Lacroix, Sodium alginate adhesives as binders in wood fibers/textile waste fibers biocomposites for building insulation, *Carbohydr. Polym.* 184 (2018) 1–8.
- [107] H. Binici, O. Aksogan, Eco-friendly insulation material production with waste olive seeds, ground PVC and wood chips, *J. Build. Eng.* 5 (2016) 260–266.
- [108] H.-R. Kymäläinen, A.-M. Sjöberg, Flax and hemp fibres as raw materials for thermal insulations, *Build. Environ.* 43 (2008) 1261–1269.
- [109] J. Khedari, S. Charoenvai, J. Hirunlabh, New insulating particleboards from durian peel and coconut coir, *Build. Environ.* 38 (2003) 435–441.
- [110] H. Binici, M. Eken, M. Dolaz, O. Aksogan, M. Kara, An environmentally friendly thermal insulation material from sunflower stalk, textile waste and stubble fibres, *Constr. Build. Mater.* 51 (2014) 24–33.
- [111] H. Benkreira, A. Khan, K.V. Horoshenkov, Sustainable acoustic and thermal insulation materials from elastomeric waste residues, *Chem. Eng. Sci.* 66 (2011) 4157–4171.
- [112] M. Chikhi, B. Agoudjil, A. Boudenne, A. Gherabli, Experimental investigation of new biocomposite with low cost for thermal insulation, *Energy Build.* 66 (2013) 267–273.
- [113] O. Akaranta, Production of particle boards from bioresources, *Bioresource Technol.* 75 (2000) 87–89.
- [114] B. Akinyemi A, J.O. Afolayan, E. Ogunji Oluwatobi, Some properties of composite corn cob and sawdust particle boards, *Constr. Build. Mater.* 127 (2016) 436–441.
- [115] M. Nasir, P. Khali D, M. Jawaid, M. Tahir P, R. Siakeng, M. Asim, A. Khan T, Recent development in binderless fiber-board fabrication from agricultural residues: a review, *Constr. Build. Mater.* 211 (2019) 502–516.
- [116] R. Pedieu, B. Riedl, A. Pichette, Physical and mechanical properties of panel based on outer bark particles of white birch: mixed panels with wood particles versus wood fibres Maderas, *Ciencia y Tecnol.* 12 (2008).
- [117] S. Sam-Brew, D. Smith G, Flax and Hemp fiber-reinforced particleboard, *Ind. Crops Prod.* 77 (2015) 940–948.
- [118] M. Ghofrani, A. Ashori, R. Mehrabi, Mechanical and acoustical properties of particleboards made with date palm branches and vermiculite, *Polym. Test.* 60 (2017) 153–159.
- [119] I. Taha, S. Elkafafy M, H. El Mously, Potential of utilizing tomato stalk as raw material for particleboards, *Ain Shams Eng. J.* 9 (2018) 1457–1464.
- [120] P. Klímek, P. Meinschmidt, R. Wimmer, B. Plinke, A. Schirp, Using sunflower (*Helianthus annuus L.*), topinambour (*Helianthus tuberosus L.*) and cup-plant (*Silphium perfoliatum L.*) stalks as alternative raw materials for particleboards, *Ind. Crops Prod.* 92 (2016) 157–164.
- [121] M. Viel, F. Collet, C. Lanos, Development and characterization of thermal insulation materials from renewable resources, *Constr. Build. Mater.* 214 (2019) 685–697.
- [122] K. Wei, C. Lv, M. Chen, X. Zhou, Z. Dai, D. Shen, Development and performance evaluation of a new thermal insulation material from rice straw using high frequency hot-pressing, *Energy Build.* 87 (2015) 116–122.
- [123] R. Gallegos-Ortega, T. Magaña-Guzmán, J.A. Reyes-López, M.S. Romero-Hernández, Thermal behavior of a straw bale building from data obtained in situ. A case in Northwestern México, *Build. Environ.* 124 (2017) 336–341.
- [124] M. Pruteanu, Investigations regarding the thermal conductivity of straw bulletin of the polytechnic institute of Iasi, *Constr. Archit. Sect.* 8 (2010).
- [125] C. Rojas, M. Cea, A. Iriarte, G. Valdés, R. Navia, P. Cárdenas-R J, Thermal insulation materials based on agricultural residual wheat straw and corn husk biomass, for application in sustainable buildings, *Sustain. Mater. Technol.* 20 (2019) e00102.
- [126] H. Keskin, M. Kucuktuvek, M. Guru, The potential of poppy (*Papaver somniferum Linnaeus*) husk for manufacturing wood-based particleboards, *Constr. Build. Mater.* 95 (2015) 224–231.
- [127] A. Sabapathy K, S. Gedupudi, Straw bale based constructions: measurement of effective thermal transport properties, *Constr. Build. Mater.* 198 (2019) 182–194.
- [128] Y. Brouard, N. Belayachi, D. Hoxha, N. Ranganathan, S. Méo, Mechanical and hygrothermal behavior of clay + Sunflower (*Helianthus annuus*) and rape straw (*Brassica napus*) plaster bio-composites for building insulation, *Constr. Build. Mater.* 161 (2018) 196–207.
- [129] H. Park J, Y. Kang, J. Lee, J. Chang S, S. Wi, S. Kim, Development of wood-lime boards as building materials improving thermal and moisture performance based on hygrothermal behavior evaluation, *Constr. Build. Mater.* 204 (2019) 576–585.
- [130] H. Park S, J. Lee P, Effects of floor impact noise on psychophysiological responses, *Build. Environ.* 116 (2017) 173–181.
- [131] J. Chang S, S. Wi, J. Lee, S. Kim, Development of vacuum impregnation equipment

- and preparation of mass/uniform shape-stabilized phase change materials, *Int. J. Heat Mass Transf.* 132 (2019) 817–824.
- [132] J. Lee, S. Wi, Y. Yun B, J. Chang S, S. Kim, Thermal and characteristic analysis of shape-stabilization phase change materials by advanced vacuum impregnation method using carbon-based materials, *J. Ind. Eng. Chem.* 70 (2019) 281–289.
- [133] J. Lee, S. Wi, S.-G. Jeong, J. Chang S, S. Kim, Development of thermal enhanced n-octadecane/porous nano carbon-based materials using 3-step filtered vacuum impregnation method, *Thermochim. Acta* 655 (2017) 194–201.
- [134] B. Liang, X. Lu, R. Li, W. Tu, Z. Yang, T. Yuan, Solvent-free preparation of bio-based polyethylene glycol/wood flour composites as novel shape-stabilized phase change materials for solar thermal energy storage, *Sol. Energy Mater. Sol. Cells* 200 (2019) 110037.
- [135] J. Liang, L. Zhiming, Y. Ye, W. Yanjun, L. Jingxin, Z. Changlin, Fabrication and characterization of fatty acid/wood-flour composites as novel form-stable phase change materials for thermal energy storage, *Energy Build.* 171 (2018) 88–99.
- [136] Z. Liu, Z.J. Yu, T. Yang, D. Qin, S. Li, G. Zhang, F. Haghghat, M.M. Joybari, A review on macro-encapsulated phase change material for building envelope applications, *Build. Environ.* 144 (2018) 281–294.
- [137] H. Yang, Y. Wang, Q. Yu, G. Cao, R. Yang, J. Ke, X. Di, F. Liu, W. Zhang, C. Wang, Composite phase change materials with good reversible thermochromic ability in delignified wood substrate for thermal energy storage, *Appl. Energy* 212 (2018) 455–464.
- [138] H. Yang, Y. Wang, Q. Yu, G. Cao, X. Sun, R. Yang, Q. Zhang, F. Liu, X. Di, J. Li, C. Wang, G. Li, Low-cost, three-dimension, high thermal conductivity, carbonized wood-based composite phase change materials for thermal energy storage, *Energy* 159 (2018) 929–936.
- [139] X. Li Z, A. Al-Rashed, M. Rostamzadeh, R. Kalbasi, A. Shahsavari, M. Afrand, Heat transfer reduction in buildings by embedding phase change material in multi-layer walls: effects of repositioning, thermophysical properties and thickness of PCM, *Energy Convers. Manag.* 195 (2019) 43–56.
- [140] M. Rym, E. Klugmann-Radziemska, Possibilities and benefits of a new method of modifying conventional building materials with phase-change materials (PCMs), *Constr. Build. Mater.* 211 (2019) 1013–1024.
- [141] A. Zondag H, R. de Boer, S.F. Smeding, J. van der Kamp, Performance analysis of industrial PCM heat storage lab prototype, *J. Energy Storage* 18 (2018) 402–413.
- [142] C. Wickramaratne, S. Dhau J, R. Kamal, P. Myers, Y. Goswami D, E. Stefanakos, Macro-encapsulation and characterization of chloride based inorganic phase change materials for high temperature thermal energy storage systems, *Appl. Energy* 221 (2018) 587–596.
- [143] Roux J.-J., Hubert J.-L., Virgone J., Rodler A. and Kim E.-J. 2013 Are 3D heat transfer formulations with short time step and sun patch evolution unnecessary for building simulation?
- [144] F. Zebende G, A.A. Brito, A.M. Silva Filho, A.P. Castro,  $\rho$ DCCA applied between air temperature and relative humidity: an hour/hour view, *Phys. A: Stat. Mech. Appl.* 494 (2018) 17–26.
- [145] L. Mba, P. Meukam, A. Kemajou, Application of artificial neural network for predicting hourly indoor air temperature and relative humidity in modern building in humid region, *Energy Build.* 121 (2016) 32–42.
- [146] K. Melikov A, U. Krüger, G. Zhou, T.L. Madsen, G. Langkilde, Air temperature fluctuations in rooms, *Build. Environ.* 32 (1997) 101–114.
- [147] V. Soni, A. Kumar, V.K. Jain, Modeling of PCM melting: analysis of discrepancy between numerical and experimental results and energy storage performance, *Energy* 150 (2018) 190–204.
- [148] V. Butala, U. Strith, Experimental investigation of PCM cold storage, *Energy Build.* 41 (2009) 354–359.
- [149] P. Majumdar, A. Saidbakhsh, A heat transfer model for phase change thermal energy storage, *Heat Recov. Syst. CHP* 10 (1990) 457–468.
- [150] P. Venkataraj K, S. Suresh, Experimental study on thermal and chemical stability of pentaerythritol blended with low melting alloy as possible PCM for latent heat storage, *Exp. Thermal Fluid Sci.* 88 (2017) 73–87.
- [151] V. Konstantinidis C, Integration of Thermal Energy Storage in Buildings Thesis, 2010.
- [152] M. Hasnain S, Review on sustainable thermal energy storage technologies, Part I: heat storage materials and techniques, *Energy Convers. Manag.* 39 (1998) 1127–1138.
- [153] M. Arici, H. Karabay, M. Kan, Flow and heat transfer in double, triple and quadruple pane windows, *Energy Build.* 86 (2015) 394–402.
- [154] M. Arici, M. Kan, An investigation of flow and conjugate heat transfer in multiple pane windows with respect to gap width, emissivity and gas filling, *Renew. Energy* 75 (2015) 249–256.
- [155] O. Aydin, Determination of optimum air-layer thickness in double-pane windows, *Energy Build.* 32 (2000) 303–308.
- [156] H. Karabay, M. Arici, Multiple pane window applications in various climatic regions of Turkey, *Energy Build.* 45 (2012) 67–71.
- [157] J. Xamán, C. Pérez-Nucamendi, J. Arce, J. Hinojosa, G. Álvarez, I. Zavala-Guillén, Thermal analysis for a double pane window with a solar control film for using in cold and warm climates, *Energy Build.* 76 (2014) 429–439.
- [158] K. Du, J. Calautit, Z. Wang, Y. Wu, H. Liu, A review of the applications of phase change materials in cooling, heating and power generation in different temperature ranges, *Appl. Energy* 220 (2018) 242–273.
- [159] V. Tyagi V, D. Buddhi, PCM thermal storage in buildings: a state of art, *Renew. Sustain. Energy Rev.* 11 (2007) 1146–1166.
- [160] M. Umair M, Y. Zhang, K. Iqbal, S. Zhang, B. Tang, Novel strategies and supporting materials applied to shape-stabilize organic phase change materials for thermal energy storage—A review, *Appl. Energy* 235 (2019) 846–873.
- [161] J. Pereira da Cunha, P. Eames, Thermal energy storage for low and medium temperature applications using phase change materials – A review, *Appl. Energy* 177 (2016) 227–238.
- [162] P. Principi, R. Fioretti, Thermal analysis of the application of PCM and low emissivity coating in hollow bricks, *Energy Build.* 51 (2012) 131–142.
- [163] Hussein H., Abed A. and Abdulmunem A. 2018 An experimental investigation of using aluminum foam matrix integrated with paraffin wax as a thermal storage material in a solar heater.
- [164] M. Sadrameli S, F. Motaharnejad, M. Mohammadpour, F. Dorkoosh, An experimental investigation to the thermal conductivity enhancement of paraffin wax as a phase change material using diamond nanoparticles as a promoting factor, *Heat Mass Transf.* 55 (2019) 1801–1808.
- [165] G. Murali, K. Mayilsamy, A. T V, An experimental study of PCM-incorporated thermosiphon solar water heating system, *Int. J. Green Energy Vol.* 12 (2014) 978–986.
- [166] M. Kenisarin, K. Mahkamov, F. Kahwash, I. Makhkamova, Enhancing thermal conductivity of paraffin wax 53–57 °C using expanded graphite, *Sol. Energy Mater. Sol. Cells* 200 (2019) 110026.
- [167] M. George, A.K. Pandey, N. Abd Rahim, V.V. Tyagi, S. Shahabuddin, R. Saidur, A novel polyaniline (PANI)/ paraffin wax nano composite phase change material: superior transition heat storage capacity, thermal conductivity and thermal reliability, *Sol. Energy* 204 (2020) 448–458.
- [168] N. Wang, R. Zhang X, S. Zhu D, W. Gao J, The investigation of thermal conductivity and energy storage properties of graphite/paraffin composites, *J. Therm. Anal. Calorim.* 107 (2012) 949–954.
- [169] L. Wang X, B. Li, G. Qu Z, F. Zhang J, G. Jin Z, Effects of graphite microstructure evolution on the anisotropic thermal conductivity of expanded graphite/paraffin phase change materials and their thermal energy storage performance, *Int. J. Heat Mass Transf.* 155 (2020) 119853.
- [170] B. Buonomo, D. Ercole, O. Manca, S. Nardini, Numerical investigation on thermal behaviors of two-dimensional latent thermal energy storage with PCM and aluminum foam, *J. Phys.: Conf. Ser.* 796 (2017) 012031.
- [171] F. Yapici, A. Ozcifici, R. Esen, S. Kurt, The effect of grain angle and species on thermal conductivity of some selected wood species, *BioResources* 6 (2011) 2757–2762.
- [172] X. Yi, D. Zhao, R. Ou, J. Ma, Y. Chen, Q. Wang, A comparative study of the performance of wood-plastic composites and typical substrates as heating floor, *BioResources* 12 (2017) 2565–2578.
- [173] Y. Li K, M. Fleischmann C, J. Spearpoint M, Determining thermal physical properties of pyrolyzing New Zealand medium density fibreboard (MDF), *Chem. Eng. Sci.* 95 (2013) 211–220.
- [174] C. Qi, F. Zhang, J. Mu, Y. Zhang, Z. Yu, Enhanced mechanical and thermal properties of hollow wood composites filled with phase-change material, *J. Clean. Prod.* 256 (2020) 120373.
- [175] X. Lu, B. Liang, X. Sheng, T. Yuan, J. Qu, Enhanced thermal conductivity of polyurethane/wood powder composite phase change materials via incorporating low loading of graphene oxide nanosheets for solar thermal energy storage, *Sol. Energy Mater. Sol. Cells* 208 (2020) 110391.
- [176] V. Kočí, M. Jerman, Z. Pavlík, J. Maděra, J. Žák, R. Černý, Interior thermal insulation systems based on wood fiberboards: experimental analysis and computational assessment of hygrothermal and energy performance in the Central European climate, *Energy Build.* 222 (2020) 110093.
- [177] H. Ikei, C. Song, Y. Miyazaki, Physiological effects of touching coated wood international, *J. Environ. Res. Public Health* 14 (2017) 773.
- [178] J. Kotlarewski N, B. Ozarska, K. Gusamo B, Thermal conductivity of papua new guinea balsa wood measured using the needle probe procedure, *BioResources* 9 (2014) 5784–5793.
- [179] S. Tangjuank, S. Kumfu, Particle Boards from Papyrus Fibers as Thermal Insulation, *J. Appl. Sci. Vol.* 11 (14) (2011).
- [180] A. Farouk Mohamed, Comparative study of traditional and modern building techniques in Siwa Oasis, Egypt: case study: affordable residential building using appropriate building technique, *Case Stud. Constr. Mater.* 12 (2020) e00311.
- [181] Y. Kulshreshtha, J.A. Mota Nelson, K.S. Jagadish, J. Bredenoord, P.J. Vardon, M.C.M. van Loosdrecht, H.M. Jonkers, The potential and current status of earthen material for low-cost housing in rural India, *Constr. Build. Mater.* 247 (2020) 118615.
- [182] A. Chel, N. Tiwari G, A. Chandra, A model for estimation of daylight factor for skylight: an experimental validation using pyramid shape skylight over vault roof mud-house in New Delhi (India), *Appl. Energy* 86 (2009) 2507–2519.
- [183] S. Attia A, Traditional multi-story house (Tower House) in Sana'a City, Yemen. An example of sustainable architecture, *Alex. Eng. J.* 59 (2020) 381–387.
- [184] R. Tomovska, A. Radivojević, Tracing sustainable design strategies in the example of the traditional Ohrid house, *J. Clean. Prod.* 147 (2017) 10–24.
- [185] M. Zune, C.A.J. Pantua, L. Rodrigues, M. Gillott, A review of traditional multistage roofs design and performance in vernacular buildings in Myanmar, *Sustain. Cities Soc.* (2020) 102240.
- [186] B. Khadka, Mud masonry houses in Nepal: a detailed study based on entire reconstruction scenario in 31 earthquake-affected districts, *Structures* 25 (2020) 816–838.
- [187] J. Delgado M C, C. Guerrero I, Earth building in Spain, *Constr. Build. Mater.* 20 (2006) 679–690.
- [188] A. Dutu, M. Niste, I. Spatarelu, I. Dima D, S. Kishiki, Seismic evaluation of Romanian traditional buildings with timber frame and mud masonry infills by in-plane static cyclic tests, *Eng. Struct.* 167 (2018) 655–670.
- [189] I. Hassel B, A. Kitamori, J. Kiho, K. Komatsu, Prefabricated mud wall units based on a traditional Japanese building system: lateral in-plane performance in terms of connection, and crack development using digital speckle photography, *Int. J. Sustain. Built Environ.* 2 (2013) 1–9.



## Study of the automotive aerodynamic performance affected by entrance structure of forecabin

Yuqi Huang, Shun Wang, Yuan Ji, Zhentao Liu\*

Power Machinery & Vehicular Engineering Institute, Zhejiang University, Hangzhou 310027, China

### ARTICLE INFO

#### Keyword:

Ahmed body  
Forecabin  
Drag coefficient  
CFD

### ABSTRACT

Recently, the requirement for cooling capacity decreased when the driving energy changed from liquid fuel to lithium batteries. Therefore, the structure and location of the forecabin could be adjusted based on the aerodynamic performance. The current study conducted a significant number of simulations in order to find out the effects of the internal flow through forecabin in an Ahmed body. The following conclusions have been identified: 1, The flow through the forecabin would always increase the resistance of the entire body, and the drag coefficient increases, on average, by approximately 85%. 2, When the aspect ratio is higher or the position of the inlet opening is lower, the total drag coefficient is lower due to a weaker vortex strength, a simpler vortex structure and a relatively simple flow. 3, The existence of the forecabin will largely increase the oscillation frequency of the flow field by approximately 15 times compared to the original Ahmed model. Finally, the high drag coefficient moment always appears to be due to the formation of more complex or intense vortex motion. These conclusions can offer useful results and references for the structural design of the front cabin for new energy vehicles.

### 1. Introduction

A vehicle's air resistance is directly proportional to its speed squared once it reaches above 60 km/h the air resistance rises steeply. The outer shape of an automobile has a substantial impact on the vehicle's aerodynamic performance [1]. Therefore, it is critically important in order to achieve a reduction in drag coefficient, thereby saving energy and reducing emissions.

In general, research into automotive aerodynamics has typically favored simple bodies over detailed car geometries [2]. A generic car ensures that conclusions are unlikely to be geometry specific and research findings will likely relate to common aerodynamic characteristics which are widely applicable [3]. Although many different types of simplified ground vehicle models have been historically investigated, the Ahmed vehicle model, which makes it possible for us to identify the main pressure drag sources and their contribution to the overall aerodynamics, is still the most preferred simplified ground vehicle model. It has been employed in quite a few experimental studies and computational studies [4]. The external flow field of the model can simulate the basic characteristics of the real vehicle's flow condition with the exception of the rotating wheels, the forecabin and protrusions on the bottom and surface of the vehicle body. It is a bluff body with separated boundary layers, recirculating flows and complex three-dimensional wake structures [5].

Recently, academic research has been conducted on the influence of both the front grille shape and the coverage area on the resistance of the car. To optimize the losses generated by the flow through the vehicle, both experimental and numerical simulations are commonly used in the automotive environment by Wittmeier and Kuthada [6], and this research demonstrates that grille shutters result in a smaller contribution by the cooling airflow to overall drag. Liu et al. [7] performed a numerical simulation on a full-scale CAD automobile model with different grille shapes, including straight, convex, concave, and M and W-shaped, and the results show that the straight grille has the best effect with smaller  $C_d$  by 0.05% as well as the least amount of materials consumption in the manufacture of the grille. However, this study did not discuss the influence on the internal cooling performance through this covering method. Zhang et al. [8] have demonstrated that the underhood airflow in the forecabin can be optimized by introducing an air-duct and modified grille openings. At both highway speeds and idle conditions, reducing the excessive airflow that does not contribute to the cooling purpose, a notable improvement in the underhood airflow management can be achieved by using a combination of side-grille sealing with a wide air-duct.

As well as researching the opening area of the forecabin front grille, the influence of the airflow area inside the forecabin and inlet blade inclination on the cooling performance and the cooling resistance co-

\* Corresponding author.

## Nomenclature

### Geometry

A	width of the air intake [m]
B	height of the air intake [m]
c	clearance between the model and floor [m]
W	width of Ahmed Model [m]
H	height of Ahmed Model [m]
L	characteristic length [m]
$\beta$	ratio of width and height of air intake
$\Delta x$	grid length in the direction of velocity [m]
$\Delta y$	near wall height [m]
x	Cartesian x-axis direction
y	Cartesian y-axis direction
z	Cartesian z-axis direction

### Fluid flow characteristics

f	frequency of periodic motion [Hz]
$C_d$	drag coefficient
y+	a empirical parameter of turbulent boundary layer
$u_t$	friction velocity [m/s]
$\nu$	kinematical viscosity [m <sup>2</sup> /s]
$Re_H$	Reynolds number based on the model height
$St_H$	Strouhal number based on the model height
Co	relative relationship between time step and space step
U	inflow velocity magnitude [m/s]
$U_x$	velocity in x direction [m/s]
$U_{oa}$	average airflow velocity magnitudes at the exit of the forecabin [m/s]
$\Delta t$	time step [s]
U	the size of the velocity vector within a cell [m/s]
$Q_{in}$	forecabin inlet mass flow rates [kg/s]
$\omega_x$	vorticity in x direction [s <sup>-1</sup> ]
$\omega_y$	vorticity in y direction [s <sup>-1</sup> ]

### Numerical simulation

p	pressure [pa]
$u_i$	velocity component in the i direction [m/s]
$\tau_{ij}$	subgrid-scale stress tensor [N•m <sup>-2</sup> ]
$\mu_t$	subgrid-scale turbulent viscosity [m <sup>2</sup> s <sup>-1</sup> ]
$\tau_{kk}$	isotropic part of the subgrid-scale stresses [N•m <sup>-2</sup> ]
$S_{ij}$	rate-of-strain tensor [s <sup>-1</sup> ]
$L_s$	mixing length for subgrid scales [m]
k	Von Kármán constant
$C_w$	WALE constant
Q	dimensionless Q-criterion value
$\Omega$	vorticity tensor [s <sup>-1</sup> ]

efficient have been researched. D'Hondt et al. [9] explored the effect of air tightness on engine cooling performance and drag coefficient by placing solid walls in the upper and lower parts of the heat exchanger, and concluded that the sealing implementation results in an important increase in the flow rate through the porous media with limited impact on the drag coefficient. Pambianco et al. [10] studied the influence of the inlet blade inclination on the drag of the whole vehicle. He stated that the evolution trends of the cooling drag coefficient varied little with the inlet blade inclination. However, drag levels were lower when the inlet blade inclination increased and suggested a decrease in the cooling flow rate.

The position of the front air intake of a vehicle is also an important factor which affects the air resistance. Khaled et al. [11] investigated the effect on the aerodynamic torsor of the lateral and vertical (vehicle height) positioning of the air inlet opening in the vehicle's front end. This research indicated that the central position in vertical direction of the air-inlet opening, which reduced the drag coefficient by 1.3%,

the cooling drag coefficient by 56.4%, the lift coefficient by 4.9% and the pitching momentum coefficient by 3.6%, was the best position for aerodynamic torsor reduction.

By using parametric study, key geometric parameters to design a grille opening configuration were represented by Kim et al. [12]. The article explores the effects of vertical height, horizontal width, size, linear deformation, position and blockage on the total drag of the base model, and it shows that decreasing the base model horizontal width or implementing a higher opening inlet of the grille would help to reduce the total drag coefficient. It should be noted that the flow simulations are performed at the velocity of 110 km/h inflow condition with a small passenger vehicle model.

With the development of new energy vehicles, the driving force can be derived from Lithium-battery, fuel-cell battery or even solar energy. A varied energy type offers the opportunity to innovatively design the structure of the automobile. In particular, for some conditions, the forecabin is not a necessarily an important aspect nor does it need be large in size or in any particular position. As mentioned above, the air drag reduction design of the external flow field in the automobile is now fairly mature [13]. "Forecabin" flow resistance optimization, to reduce the vehicle air resistance, has become an important method reduce fuel consumption, and preliminary effects have been achieved when applied to low carbon vehicles [14].

Much research has been undertaken regarding the influence of grille shapes [6-8], positions [11-12] and active control strategies [15] on the total drag coefficient, but existing studies do not fully consider the underlying mechanism of resistance reduction. Thus, in this study, a series of simulations were carried to determine the flow pattern around the forecabin. The Ahmed model was chosen in this study but a different position and aspect ratio of an area-constant air entrance was utilized in order to fully investigate the steady and transient influence of intake opening characteristic on total drag coefficient of the model. Some relative optimum arrangement of the air entrance position is obtained through the analysis, which may be beneficial when designing the vehicles' structure.

## 2. Methodology

### 2.1. Modelling of Ahmed model with forecabin

In this study, some adjustments have been applied to the original Ahmed model shown, as shown in Fig. 1. A cavity with several different but simple inlet structures is designed to simulate the vehicular forecabin. Thus, the influence of different forecabins on the car model resistance can be easily considered without excessively increasing model complexity, and the internal flow field and vorticity field are straightforward to obtain. Three different positions (UP, MIDDLE and DOWN) and five different aspect ratios ( $\beta=2, 2.5, 3, 3.5$  and  $4$ ) are designed to investigate different aerodynamics performances considering bilateral symmetry of the models. The inlet openings are rectangular and in each case, the area is constant. The distances between the centreline of the inlet opening and the top of the forecabin are 52 mm, 72 mm and 92 mm for the UP, MIDDLE and DOWN case, respectively.  $\beta$  represents the ratio of inlet opening width (A) to height (B) as shown in Fig. 1. The length, width, and height (H) of the whole model are 1045.8 mm, 389 mm and 288 mm, respectively, and more detailed dimensions are also shown in Fig. 1.

The computational domain is shown in Fig. 2. In order to minimize the influence of the boundaries on the flow field around the car model, with the exception of the bottom surface, the distance between the other boundaries and the model should be sufficient in size [16]. The distance from the entrance to the inlet openings is 7.25 times the height H of the car model, and the distance from the model's rear surface to the domain exit is 18.125H. The width and height of the domain are both 5H respectively, and the ground clearance between the model and floor is calculated as c/H which in this case is found to equal to 0.174.

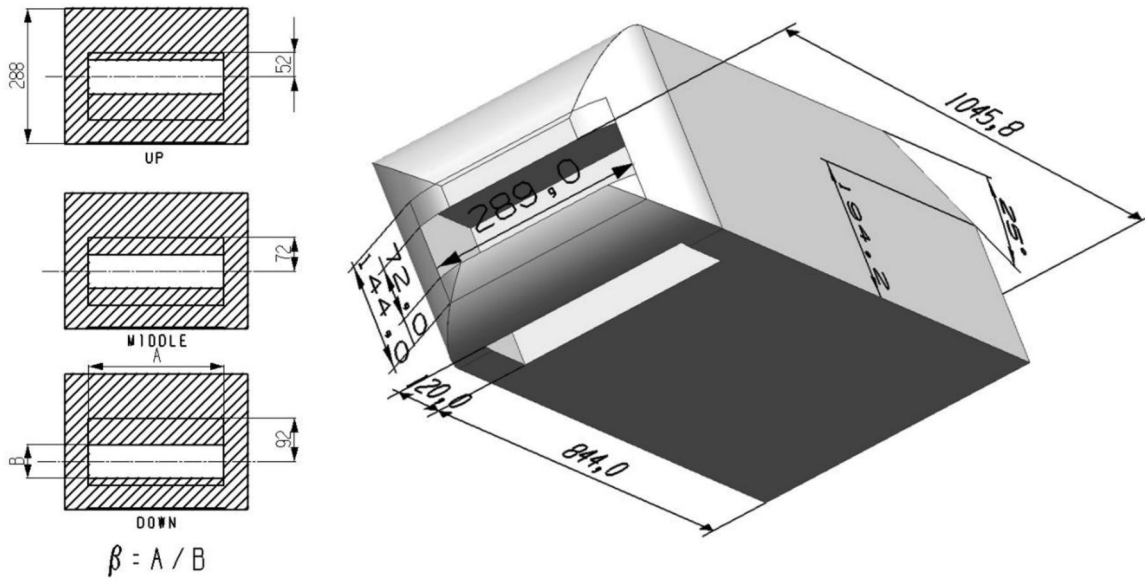


Fig. 1. Dimensions of different models.

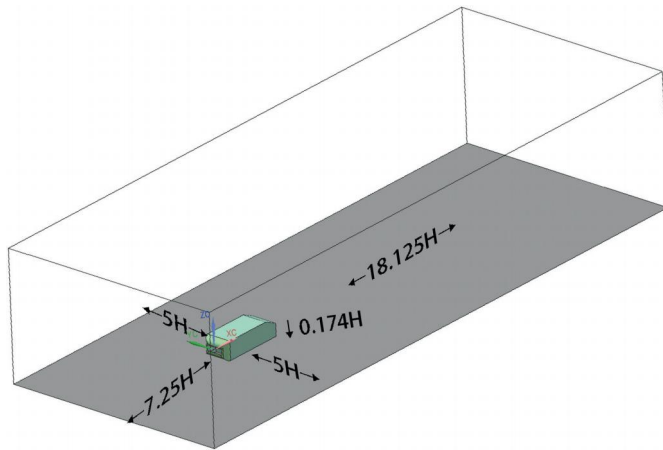


Fig. 2. View of the computational domain.

2.2. Mesh generation

Based on the DOWN\_4 case as shown in Fig. 1, two sets of grids were designed to verify the effect of grid resolution on numerical results. MESH\_1 and MESH\_2 have 5.27 million and 9.65 million grids, respectively. The quantitative effect of mesh resolution was investigated through the x-component velocity comparisons at the horizontal centerline of model opening (dotted line), as shown in Fig. 3. Obviously, there are some minor differences in speed distribution however the biggest difference is no greater than 5%. It is decided that MESH\_1 would provide a good compromise between rather high accuracy and drastically reduced numerical calculation time. Hence MESH\_1 was used in this study.

The mesh details are shown in Fig. 4. Fig. 4(a) displays the surface mesh of the car body whilst the volume mesh adjacent to the car body is shown in Fig. 4(b). The unstructured mesh adjacent to the wall is encrypted with several layers of growing tetrahedron grid, and the size of the first layer of the tetrahedron grid is about 1 mm. A hybrid grid scheme is adopted, and a structural grid is arranged on the outside of the cuboid zone filled with unstructured grid to ensure grid quality.

In general, we use the wall  $y^+$  value to measure the relative importance of the viscous process and the turbulent process. (wall  $y^+$  value

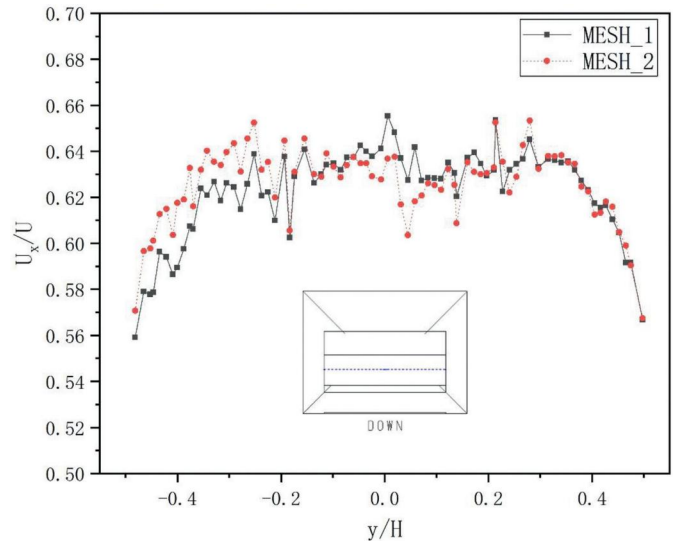


Fig. 3. The x-velocity comparisons at horizontal centerline in model opening for the grid-resolution.

is defined as:  $y^+ = \frac{u_t \Delta y}{\nu}$ , similar to Reynolds number where  $u_t = \sqrt{\frac{\tau_w}{\rho}}$  represents the friction velocity,  $\Delta y$  represents the near wall height, and  $\nu$  represents kinematical viscosity). The wall  $y^+$  values for this mesh (MESH\_1) are less than 3, which meets the calculation requirements.

2.3. Numerical methods and boundary conditions

Large Eddy Simulation (LES) method is applied in this study, which can directly simulate large-scale turbulent motion, and meanwhile also adopt a sub-grid model to process the effect of small-scale turbulent motion. Thus, it is also called “filtered” Navier-Stokes equations. The computational time by LES model is less than the time taken by Direct Numerical Simulation, and its simulating accuracy is higher than the Reynolds Average Navier-Stokes method. When simulating the three-dimensional bluff body flow field, the large eddy simulation can obtain a more accurate vortex structure. The basic governing equations con-

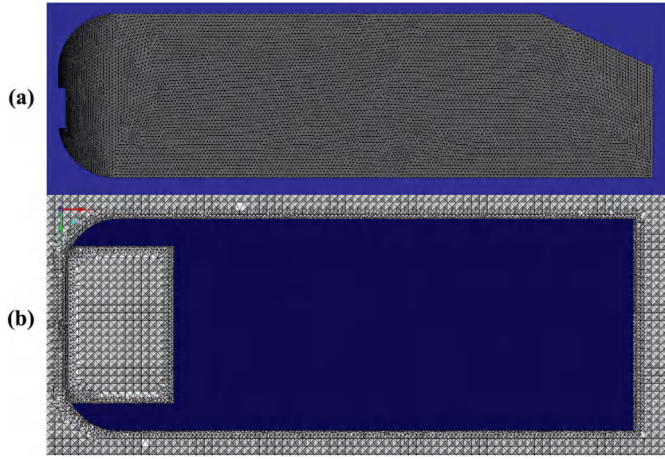


Fig. 4. Mesh detail of the Ahmed body with a cavity, (a)surface mesh of the car body (b)near wall volume mesh at the surface parallel to the ground.

sisting of the conservation of mass and momentum for incompressible flow are listed as follows:

$$\frac{\partial \bar{u}_i}{\partial x_i} = 0 \tag{1}$$

$$\frac{\partial \bar{u}_i}{\partial t} + \frac{\partial (\bar{u}_i \bar{u}_j)}{\partial x_j} = -\frac{1}{\rho} \frac{\partial \bar{p}}{\partial x_i} + \nu \frac{\partial^2 \bar{u}_i}{\partial x_j \partial x_j} - \frac{\partial \tau_{ij}}{\partial x_j} \tag{2}$$

where  $p$  is the pressure,  $u_i$  is the velocity component in the  $i$  direction, and  $\nu$  is the kinematic viscosity. The subgrid-scale stress (SGS)  $\tau_{ij}$  is defined by:

$$\tau_{ij} = \rho \bar{u}_i \bar{u}_j - \rho \bar{u}_i \bar{u}_j \tag{3}$$

And the subgrid-scale stresses modelling as:

$$\tau_{ij} - \frac{1}{3} \tau_{kk} \delta_{ij} = -2\mu_t \bar{s}_{ij} \tag{4}$$

where  $\mu_t$  is the subgrid-scale turbulent viscosity. The isotropic part of the subgrid-scale stresses  $\tau_{kk}$  is not modelled, but added to the filtered static pressure term. The rate-of-strain tensor is defined by:

$$\bar{s}_{ij} = \frac{1}{2} \left( \frac{\partial \bar{u}_i}{\partial \bar{x}_j} + \frac{\partial \bar{u}_j}{\partial \bar{x}_i} \right) \tag{5}$$

In this study, the Wall-Adapting Local Eddy-Viscosity (WALE) model was employed. The eddy viscosity is modelled as:

$$\mu_t = \rho L_s^2 \frac{\left( S_{ij}^d S_{ij}^d \right)^{3/2}}{\left( \bar{S}_{ij} \bar{S}_{ij} \right)^{5/2} + \left( S_{ij}^d S_{ij}^d \right)^{5/4}} \tag{6}$$

where  $L_s$ , which is representing the mixing length for subgrid scales, and  $S_{ij}^d$  in the WALE model are defined, respectively, as

$$L_s = \min(kd, C_w V^{1/3}) \tag{7}$$

$$S_{ij}^d = \frac{1}{2} \left( \bar{g}_{ij}^2 + \bar{g}_{ji}^2 \right) - \frac{1}{3} \delta_{ij} \bar{g}_{kk}^2, \bar{g}_{ij} = \frac{\partial \bar{u}_i}{\partial x_j} \tag{8}$$

where  $k$  is the von Kármán constant, WALE constant  $C_w=0.325$ ,  $d$  is the distance to the closest wall, and  $V$  is the volume of the computational cell.

Iso-surface of the dimensionless Q-criterion is adopted in the current study to compare the differences of vortex structures, which is defined as

$$Q = \frac{1}{2} \cdot (|\Omega|^2 - |S|^2) \tag{9}$$

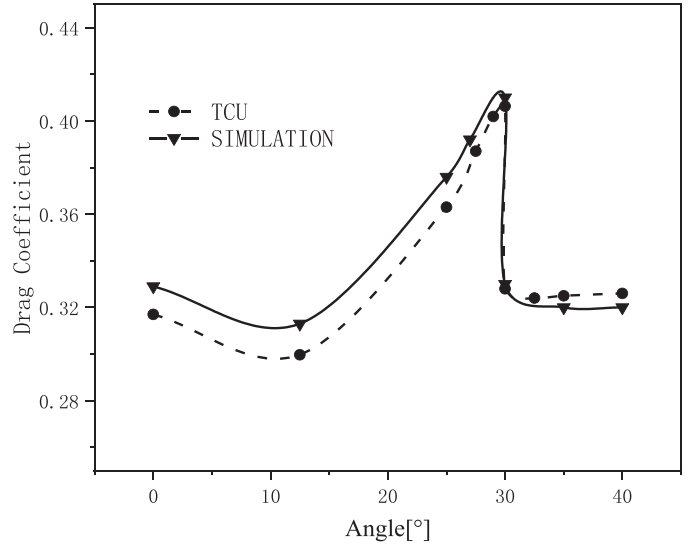


Fig. 5.  $C_d$  comparison between TCU wind tunnel and simulation.

where  $\Omega$  is the vorticity tensor, and  $S$  is the rate-of-strain tensor.

In these simulations, the velocity of the inlet is set as 25 m/s, therefore the Reynolds number based on the model height  $Re_H$  is approximately  $4.86 \times 10^5 (Re = UL/\nu, U$  is inflow velocity magnitude,  $L$  is characteristic length. It represents a ratio of inertial force to viscous force). ANSYS FLUENT 19.0 is selected as the model solving software. The ground in the numerical model is treated as a moving wall boundary condition with the same speed as air inlet flow. Upper and lateral surfaces of the channel are treated as slip surfaces using symmetry boundary condition. The velocity inlet boundary condition and the pressure outlet boundary condition are chosen to improve the convergence of the solution process.

A total of 0.5 s of unsteady simulation by LES method is performed, and the time step  $\Delta t$  is set to 0.00005 according to the Courant number criterion  $(Co = (\Delta t^* |U|) / \Delta x, \text{ where } |U| \text{ is the size of the velocity vector within a cell, } \Delta x \text{ is the grid length in the direction of velocity. To ensure that the Courant number is less than 1, the Courant number was calculated based on the maximum speed and the minimum mesh size). Semi-Implicit Method for Pressure Linked Equations algorithm is adopted for pressure-velocity coupling, and Bounded Central Differencing scheme is adopted for momentum discretization.$

### 3. Validation of numerical models

The validation of this study was conducted in our previous work [17] based on scaled down Ahmed models to improve the computational efficiency according to Kohri et al. [4]. Ahmed models with different rear angles were modelled, and these models are the same as the experiment models conducted in small wind tunnel with Particle Image Velocimetry (PIV) method at Tokyo City University (TCU). The simulation boundary conditions were consistent with the experiments, and the drag coefficient curves of simulation and TCU results, shown in Fig. 5, demonstrates that the deviation between simulation and experiment is insignificant, with a maximum deviation less than 5%, which means that the numerical models and simulation methods are suitable and precise.

## 4. Results and analysis

### 4.1. Effects of the entrance at different heights

Fig. 6 displays the flow state of  $y/H = 0$  section in a different vertical position (DOWN\_4, MID\_4 and UP\_4). It can be clearly seen that all these cases have corner vortices in the upper-right of this profile when

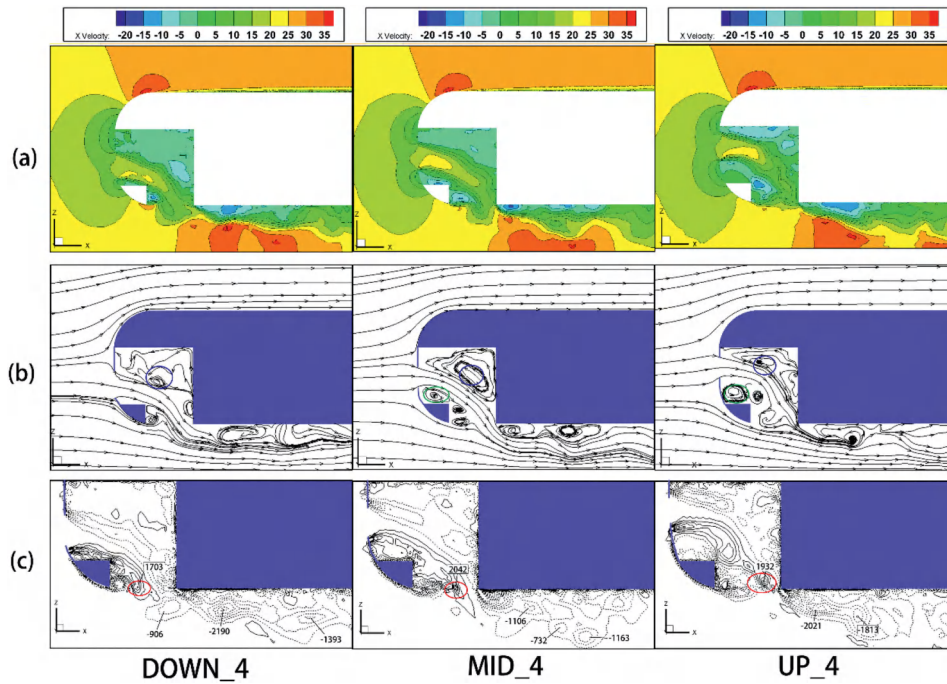


Fig. 6. Flow state of  $y/H = 0$  section in different vertical position, (a)velocity contours (b)streamline (c) vorticity contours ( $\omega_y$ ).

the air passes through the forecabin (marked by blue circles). In the UP\_4 and MID\_4 cases, small vortexes occurred because of the height discrepancy between the inlet and bottom of cavity (marked by green circles). When the height decreased, such as in the DOWN\_4 case, the size of this vortex reduced accordingly. Additionally, in the DOWN\_4 case, the streamlines indicate that the flows pass the cavity smoothly, avoiding impact with the rear wall of cavity. All these occurrences in DOWN\_4 case contribute to a better aerodynamics performance than occurs in the UP\_4 and MID\_4 case. It indicates that, with the vertical position of the air intake moving upwards, it is easier for the air flow to be blocked by the inner wall of the forecabin, causing confusion in both the forecabin and the separating bubbles beneath the bottom surface of the model.

In Fig. 6(c), the vortex contour shows this kind of confusion. When the airflow flows out of the forecabin, a vortex is formed in the middle of the exit (marked by red circles). As the position of the air intake increases, not only does the vortex have a tendency to develop backwards, but also the vortex intensity generally increases. And these phenomena are the most likely cause of the vortex scale and the vortex strength at the bottom of the Ahmed model increasing with the rising position of the air intake.

The average airflow velocity magnitudes at the exit of the forecabin are recorded in Fig. 7. It can be seen that at different opening positions, the DOWN\_4 case has the highest average exit velocity, followed by the MID\_4 case and finally the UP\_4 case. This phenomenon is probably due to the presence of a simpler flow field and vorticity field in the forecabin when the opening position is relatively low. In addition, a larger velocity magnitude means a larger mass flow entering the forecabin, so the DOWN\_4 case will be cooled more quickly.

#### 4.2. The effect of the aspect ratio $\beta$

When the height of the opening position is constant and the aspect ratio  $\beta$  becomes smaller, the situation changes and the differences are shown in Fig. 8. As can be seen from the 3D streamline diagram in Fig. 8(a), the flow in the forecabin in the case of  $\beta=2$  is more complicated, compared to the case of  $\beta=4$ , because two corner vortexes appeared in both sides of the main flow. This may be the reason why, with a smaller aspect ratio, the airflow entering the forecabin is more eas-

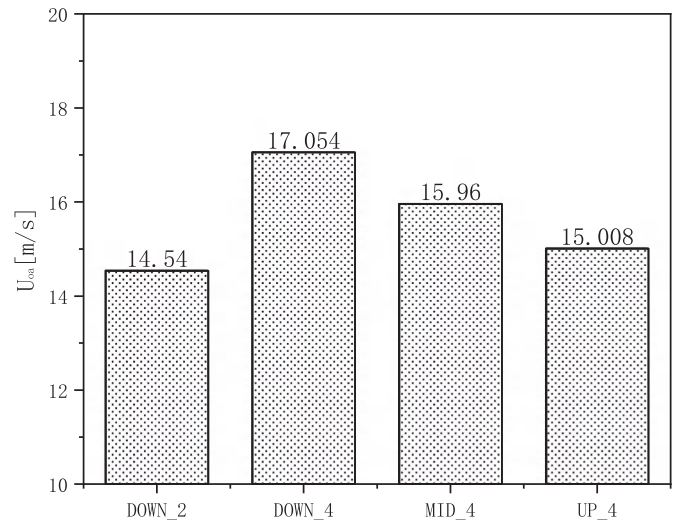
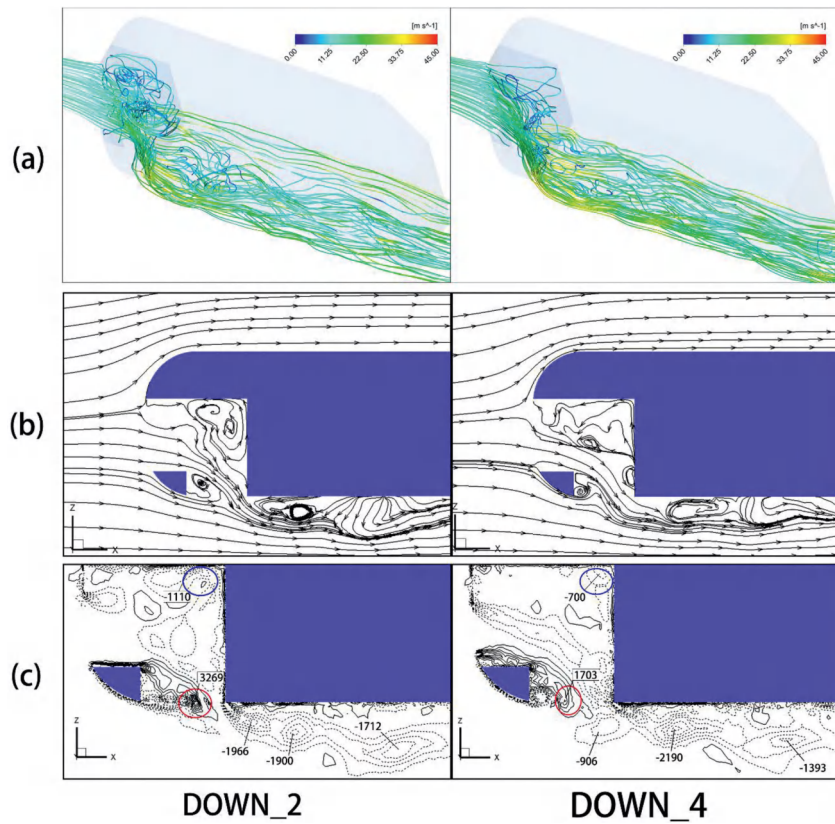


Fig. 7. The average velocity magnitude at the exit surface of the forecabin.

ily blocked by the surrounding wall of the cabin to produce a stronger vortex structure near the wall. The streamline and vorticity contours at  $y/H = 0$  section is shown in Fig. 8(b) and (c). It can be seen that the intensity of the corner vortex in the upper-right in the forecabin at  $\beta=2$  case is stronger than the  $\beta=4$  case. And the same regulation can be seen at the vortexes in the middle of the exit. These phenomena indicate that when the aspect ratio  $\beta$  is reducing, the vortex structure will be more complicated and the vortex intensity will be stronger in the forecabin flow, which could lead to a higher drag coefficient of the whole body.

Additionally, the average airflow velocity magnitudes, shown in Fig. 7 at different  $\beta$  values (2 and 4), confirm the conclusion above, because the average velocity magnitude in the  $\beta=2$  case is significantly lower compared to the  $\beta=4$  case, which indicates a more complicated flow in the forecabin in that case. Moreover, there may be an opposite trend between the average velocity magnitude at the exit of the forecabin and the total drag coefficient.



**Fig. 8.** Flow state at different  $\beta$  values, (a)3D streamline, coloured with velocity magnitude (b)streamline at  $y/H = 0$  section (c) vorticity contours ( $\omega_y$ ) at  $y/H = 0$  section.

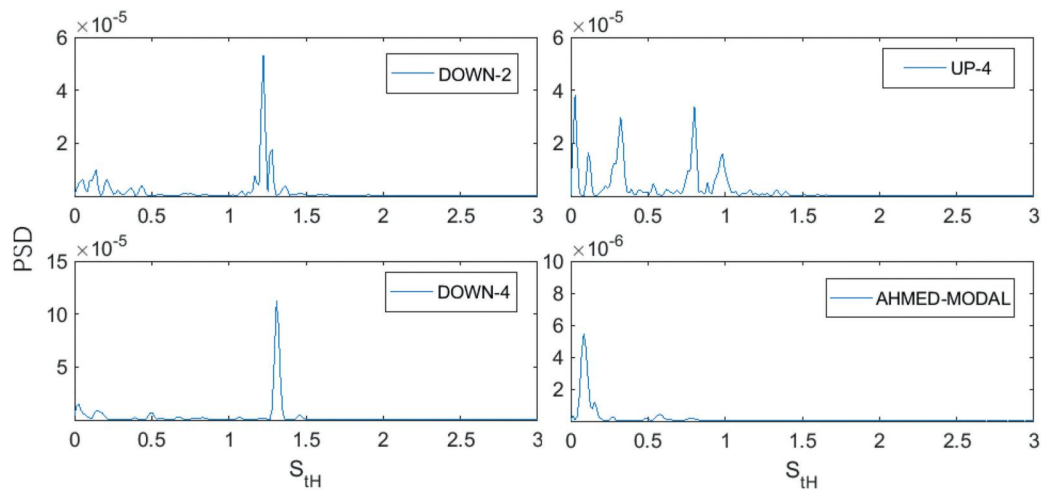


**Fig. 9.** The power spectral density of drag traces in different model.

4.3. Instantaneous analysis

Power Spectral Densities (PSD) associated with the measured  $C_d$  are reported in Fig. 9. Results are shown in a non-dimensional form introducing the Strouhal number  $S_{tH} = f \cdot H/U$  (where  $f$  represent the frequency,  $H$  is the height of the Ahmed Model). In DOWN\_4 case, the predominant Strouhal number  $S_{tH}$  is 1.35 and the equivalent frequency is 117 Hz, which is in agreement with the results of Thacker et al. [18]. The DOWN\_4 case has a higher predominant  $S_{tH}$  number than the DOWN\_2 case. In light of the work by Ho and Huerre et al. [19], those fluctuations can then be associated with the roll-up of the shear layer due to the Kelvin–Helmholtz instability mechanism.

The original Ahmed Model is also traced by its drag in PSD as shown in Fig. 9. With a predominant peak at  $S_{tH}=0.085$ , which is in agreement with the results of Tunay et al. [20], it is remarkable that the frequency is much lower than other cases with air intake and forecabin. The UP\_4 case and the DOWN\_2 case have many narrow peaks in power spectral densities compared to the DOWN\_4 case and the original Ahmed Model case, and this could be the reason that with  $\beta$  glows small or the vertical position glows the corner vortex emerged, the complicated separating bubbles or the intricate vortex structure near the inside wall of the forecabin will disturb the flow field. In other words, the fluctuation with a more concentrated predominant peak in PSD means a simpler flow, so the drag coefficient will be smaller. It is known that

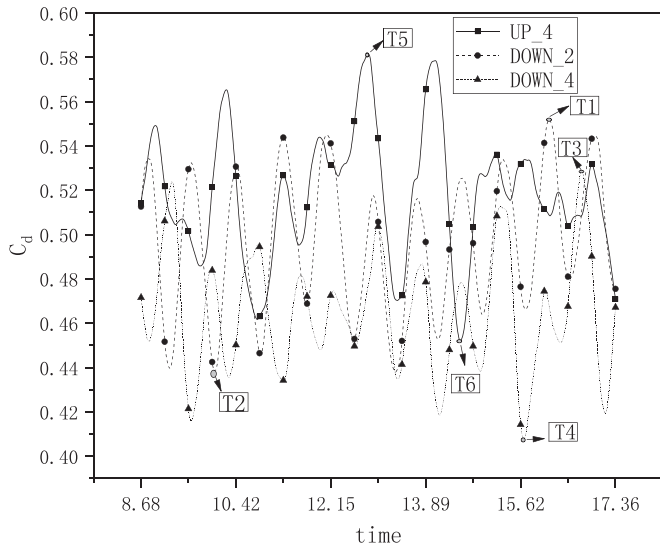


Fig. 10. Drag coefficient fluctuation in dimensionless time from 8.68 to 17.36.

a specific unsteady organization could be characterized by a constant value of Strouhal number. Therefore, it is concluded that the influence of the forecabin section on the Ahmed Model will allow the entire flow field to evolve from low-frequency organization to high-frequency organization.

In order to better reveal the cause of the drag coefficient fluctuation, the varieties of the drag coefficient in each case in a period of dimensionless time from 8.68 to 17.36 (corresponding real time range is from 0.1 s to 0.2 s) is integrated and shown in Fig. 10. On each fluctuation curve, the two extreme points with the highest and lowest drag coefficient are selected. For example, for the DOWN\_2 case, the moments of the highest and lowest drag coefficients are named T1 and T2, respectively, and a similar naming systems is used for DOWN\_4 and UP\_4. Three specific cross sections ( $x/H = 0.49, x/H = 1.01$  and  $x/H = 1.53$ , respectively) are shown in Fig. 11, and the vorticity contours ( $\omega_x$ ) are drawn. For an obvious comparison, in each case, the left half of the cloud shows the high drag coefficient moment, and the right half of the cloud shows the low drag coefficient moment.

First, in a number of cross sections, it is found that as the cross section extends along the flow direction, the vortex intensity begins to decrease gradually, and finally they reach almost the same level. This means that the effect of the differences in the position of the air intake and the aspect ratio will gradually weaken and disappear as the

flow moves downstream. Then, the position of the air intake is investigated, thus, DOWN\_4 and UP\_4 case is compared. It is obvious that in different cross section, UP\_4 case almost always has a larger vortex scale and higher vortex intensity than DOWN\_4 case. However, the high drag moment shows the same law above than the low drag moment, and this may illustrate that a larger vortex scale and higher vortex intensity could be a key reason for high drag coefficient. Finally, there is no clear, regular pattern between DOWN\_2 and DOWN\_4 case in Fig. 11 at some special cross section ( $x/H = 0.49, 1.01$  and  $1.53$ ). However, inspired by the results in the time-averaged analytical method, the flow inside the forecabin may be a key factor affecting the drag coefficient when aspect ratio  $\beta$  changes. Therefore, for a more detailed understanding of the effect of internal flow on resistance at different resistance moments and times, the Q-criteria isosurface diagram for different resistance moments from T1 to T4 in the forecabin for different aspect ratios is given in Fig. 12.

As mentioned above, Fig. 12 indicates that when the aspect ratio  $\beta$  is smaller, the vortex structures near the wall and the corner vortices are more intensive, and that results in a higher drag coefficient in the whole model. Additionally, high drag coefficient moment (T1 and T3) shows a stronger vortex structure than low drag coefficient moment (T2 and T4). At some large geometric corners, the difference in the strength of corner vortices is obvious. It indicates that the formation of high-strength vortices is an important factor affecting instantaneous drag. The formation and disappearance of the vortex near the Ahmed model is a continuous and periodic process, thus causing the overall resistance to fluctuate continuously in a small range, as shown in Fig. 10.

4.4. Overall effect of the aspect ratio and the position

In general, considering the effect of aspect ratio and position with relative data in our previous work [17], it can be seen clearly from Fig. 13 that the drag declines as the  $\beta$  grows in each vertical position, and the drag also declines as the vertical position declines at each  $\beta$  value, which closely agrees with the previous explanation. This means that a flatter and lower air entrance would lead to a lower total drag coefficient with an area-constant intake opening. Moreover, according to the experiment data of Ahmed et al. [21], the drag coefficient is approximately 0.28 using original Ahmed model. Therefore, it seems that forecabin together with rectangular air inlet window will increase vehicle drag coefficient to a large extent, by nearly 85%. The forecabin inlet mass flow rates  $Q_{in}$  in DOWN\_2, DOWN\_4, MID\_4 and UP\_4 cases are also indicated in Fig. 13. However, it seems the MID\_4 case has the maximum mass flow rate which results in a stronger cooling performance of the forecabin.

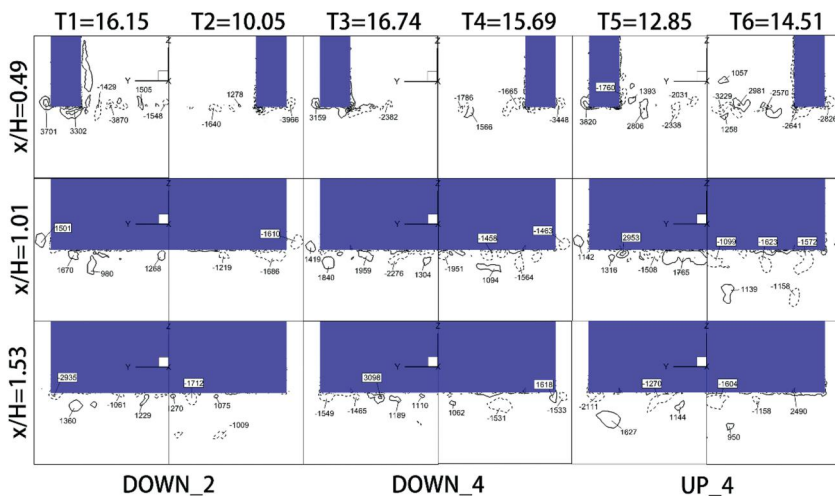


Fig. 11. Vorticity contours ( $\omega_x$ ) at different times in some specific cross section.

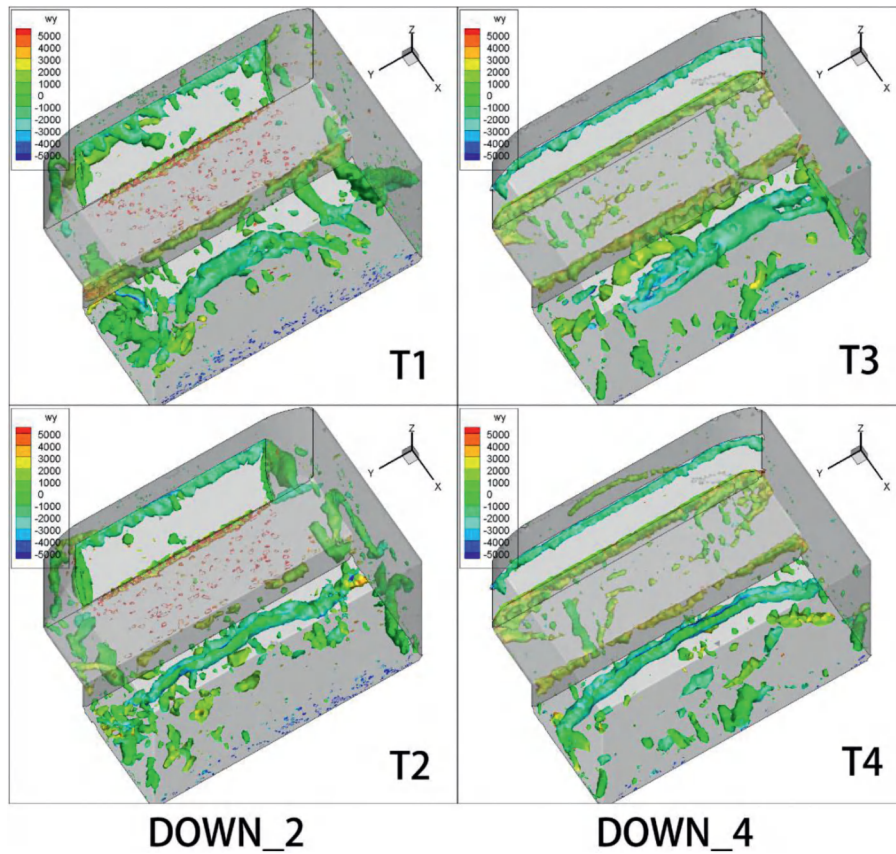


Fig. 12. Iso-surfaces of second invariant of the velocity gradient of DOWN\_2 and DOWN\_4 case at different drag coefficient time in the forecabin, coloured with  $\omega_y$ .

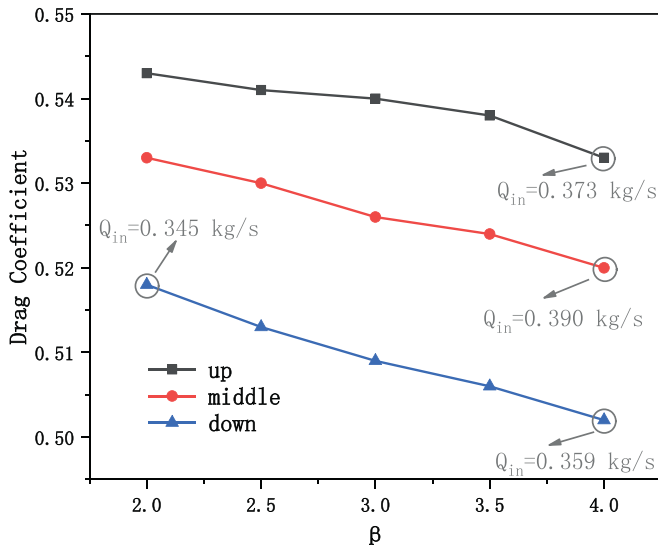


Fig. 13. Drag coefficient with different  $\beta$  in UP, MIDDLE, and DOWN position.

### 5. Conclusion

As the internal combustion engine is no longer the only power source for vehicles, there is now an opportunity to consider different structures for automobile compartments. In this study, the effect of the forecabin on vehicular aerodynamics was studied through simulations on revised Ahmed models. The numerical simulating methodology with LES model was firstly validated by PIV experiments, then different aspect ratios

and inlet locations of forcabin were considered in detail. The following conclusions could be drawn as a result of this study:

- 1 When the opening of the forecabin is flatter or the position of it is lower, either a simpler vortex structure or a lower vorticity intensity is achieved, as well as a more straightforward streamline. These phenomena are manifested as a reduction in vehicle air resistance, and are validated by the simulation results.
- 2 Using PSD method, it can be concluded that the influence of the forecabin section on the Ahmed model will allow the entire flow field to evolve from low-frequency organization to high-frequency organization. The high drag coefficient moments are due to its instantaneous high-strength vortices. Not surprisingly, this is consistent with the time-averaged conclusions above.
- 3 An entrance with flatter shape and lower position can reduce the air resistance, but the MIDDLE design achieves an improved cooling performance. In general, the forecabin will largely increase the drag coefficient of a car by 85%.

Using all the numerical simulation work, an analysis regarding the influence of the front air entrance arrangement on the drag coefficient of the Ahmed model was conducted. When applied to new energy vehicles, which do not need such a large area of front grille, the study conclusions are useful when re-designing the front grille shape in order to save energy. However, these simulation results still need to be further verified through future experiments. Due to the limitations of time and condition, simulation examples need further refinement. In addition, this air resistance study inside the forecabin currently is not fully combined with the operation of cooling system. Therefore, it is anticipated that further research is required on the aerodynamic study and automobile design.

## Declaration of Competing Interest

The authors declare that there is no conflicts of interest.

## Acknowledgement

The authors would like to acknowledge the support from NSFC 91741203 which allowed the research project to be conducted. The authors also would like to acknowledge the support from NSFC-RS Joint Project under the grant number no. 5151101443 and IE/ 151256.

## References

- [1] K.S. Song, S.O. Kang, S.O. Jun, et al., Aerodynamic design optimization of rear body shapes of a sedan for drag reduction, *Int. J. Autom. Technol.* 13 (6) (2012) 905–914.
- [2] Huminic A., Huminic G. Numerical flow Simulation for a Generic Vehicle Body on wheels with variable underbody diffuser. SAE Technical Paper, 2012.
- [3] A. Huminic, G. Huminic, Aerodynamic study of a generic car model with wheels and underbody diffuser, *Int. J. Autom. Technol.* 18 (3) (2017) 397–404.
- [4] I. Kohri, T. Yamanashi, T. Nasu, et al., Study on the transient behaviour of the vortex structure behind Ahmed body, *SAE Int. J. Passenger Cars-Mech. Syst.* 7 (2014–01–0597) (2014) 586–602.
- [5] Krastev, V.K.; Bella, G., On the steady and unsteady turbulence modeling in ground vehicle aerodynamic design and optimization. SAE Technical Papers, 2011.
- [6] F. Wittmeier, T. Kuthada, Open grille DrivAer model-first results, *SAE Int. J. Passenger Cars-Mech. Syst.* 8 (2015–01–1553) (2015) 252–260.
- [7] L. Liu, C. Jing, X Hu, Numerical simulation of the influence of intake grille shape on the aerodynamic performance of a passenger car, in: Proceedings of the International Power, Electronics and Materials Engineering Conference, Atlantis Press, 2015.
- [8] C. Zhang, M. Uddin, C. Robinson, et al., Full vehicle CFD investigations on the influence of front-end configuration on radiator performance and cooling drag, *Appl. Therm. Eng.* (2017) S1359431117352985.
- [9] M. D'Hondt, P. Gillieron, P. Devinant, Aerodynamic drag and flow rate through fore-cabins of motor vehicles, in: Proceedings of the Aiaa Applied Aerodynamics Conference, 2013.
- [10] Y. Liu, S. Wang, Distribution of gas-liquid two-phase slug flow in parallel micro-channels with different branch spacing, *Int. J. Heat Mass Transf* 132 (2019) 606–617.
- [11] M. Khaled, H.E. Hage, F. Harambat, et al., Some innovative concepts for car drag reduction: a parametric analysis of aerodynamic forces on a simplified body, *J. Wind Eng. Ind. Aerodyn.* (2012) 107–108 (none).
- [12] J.M. Kim, K.M. Kim, S.J. Ha, et al., Grille design for passenger car to improve aerodynamic and cooling performance using CFD technique, *Int. J. Autom. Technol.* 17 (6) (2016) 967–976.
- [13] S. Vignesh, V.S. Gangad, V. Jishnu, et al., Windscreen angle and Hood inclination optimization for drag reduction in cars, *Procedia Manuf.* 30 (2019) 685–692.
- [14] J.P. Howell, Aerodynamic drag reduction for low carbon vehicles, in: Sustainable Vehicle Technologies, 2012, pp. 14–15.
- [15] J.C. Li, Y.D. Deng, Y.P. Wang, et al., CFD-Based research on control strategy of the opening of Active Grille Shutter on automobile, *Case Stud. Therm. Eng.* 12 (2018) 390–395.
- [16] E. Gunpinar, U.C. Coskun, M. Ozsipahi, et al., A generative design and drag coefficient prediction system for sedan car side silhouettes based on computational fluid dynamics, *Comput.-Aided Des.* 111 (2019) 65–79.
- [17] Ji Y., Cheng J., Xing J., et al. A computational fluid dynamics study of air entrance influence on the air resistance of ahmed reference body. 2017.
- [18] A. Thacker, S. Aubrun, A. Leroy, et al., Experimental characterization of flow unsteadiness in the centerline plane of an Ahmed body rear slant, *Exp. Fluids* 54 (3) (2013) 1–16.
- [19] P. Huerre, Perturbed free shear layers, *Ann. Rev. Fluid Mech.* 16 (1984) 365–424.
- [20] T. Tunay, B. Yaniktepe, B. Sahin, Computational and Experimental Investigations of the Vortical Flow Structures in the Near Wake Region Downstream of the Ahmed Vehicle Model, *J. Wind Eng. Ind. Aerodyn.* 159 (2016) 48–64.
- [21] S.R. Ahmed, G. Ramm, G. Faltin, Some Salient Features of the Time-Averaged Ground Vehicle Wake, SAE World Congress, 1984 Paper No 840300.

